WOODHEAD PUBLISHING
IN MECHANICAL ENGINEERING

Spacecraft thermal control

J. Meseguer, I. Pérez-Grande and
A. Sanz-Andrés

WP
WOODHEAD
PUBLISHING

Spacecraft thermal control

Related titles:

Dynamics of tethered satellite systems
(ISBN 978-0-85709-156-7)
Aimed at engineering students and professionals working in the field of mechanics of space flight, this book examines space tether systems – one of the most forward thinking directions of modern astronautics. The main advantage of this technology is the simplicity, profitability and ecological compatibility: space tethers allow the execution of various manoeuvres in orbit without costs of jet fuel due to the use of gravitational and electromagnetic fields of the Earth. This book will acquaint the reader with the modern state of the space tether's dynamics, with specific attention to the research projects of the nearest decades. The book presents the most effective mathematical models and the methods used for the analysis and prediction of space tether systems' motion; attention is also given on the influence of the tether on spacecraft's motion, to emergencies and chaotic modes.

Introduction to aerospace materials
(ISBN 978-1-85573-946-8)
The structural materials used in airframe and propulsion systems influence the cost, performance and safety of aircraft, and an understanding of the wide range of materials used and the issues surrounding them is essential for the student of aerospace engineering. *Introduction to aerospace materials* reviews the main structural and engine materials used in aircraft, helicopters and spacecraft in terms of their production, properties, performance and applications. The first three chapters of the book introduce the reader to the range of aerospace materials, focusing on recent developments and requirements. The book then discusses the properties and production of metals for aerospace structures, including chapters covering strengthening of metal alloys, mechanical testing, and casting, processing and machining of aerospace metals. The next ten chapters look in depth at individual metals including aluminium, titanium, magnesium, steel and superalloys, as well as the properties and processing of polymers, composites and wood. Chapters on performance issues such as fracture, fatigue and corrison precede a chapter focusing on inspection and structural health monitoring of aerospace materials. Disposal/recycling and materials selection are covered in the final two chapters.

MEMS for automotive and aerospace applications
(ISBN 978-0-85709-118-5)
Micro-Electro-Mechanical-Systems (MEMS) are miniature devices or machines which integrate elements such as actuators, sensors and a processor to form microsystems. The automotive sector is currently the biggest consumer of MEMS and this market is expected to grow, driven by safety legislation. Emerging applications in the aerospace field will face unique challenges related to harsh environmental conditions and reliability requirements. Part One covers MEMS in automotive applications, including safety systems, stability control and engine management. Part Two describes MEMS in aircraft such as navigation systems, devices for health monitoring and drag reduction. MEMS thrusters for nano and pico satellites are also covered.

Details of these and other Woodhead Publishing books can be obtained by:

- visiting our web site at www.woodheadpublishing.com
- contacting Consumer Services (e-mail: sales@woodheadpublishing.com; fax:+44(0) 1223 832819; tel: +44(0) 1123 499140; address: Woodhead Publishing Limited, 80 High Street, Sawston, Cambridge CB22 3HJ, UK)

If you would like to receive information on forthcoming titles, please send your address details to Customer Services, at the address above. Please confirm which subject areas you are interested in.

Spacecraft thermal control

José Meseguer, Isabel Pérez-Grande and Angel Sanz-Andrés

Oxford Cambridge Philadelphia New Delhi

Published by Woodhead Publishing Limited, 80 High Street, Sawston,
Cambridge CB22 3HJ, UK
www.woodheadpublishing.com
www.woodheadpublishingonline.com

Woodhead Publishing, 1518 Walnut Street, Suite 1100, Philadelphia, PA 19102–3406, USA

Woodhead Publishing India Private Limited, G-2, Vardaan House, 7/28 Ansari Road,
Daryaganj, New Delhi – 11002, India
www.woodheadpublishingindia.com

First published in 2012, Woodhead Publishing Limited

Cover image courtesy of ESA/AOES.

British Library Cataloguing in Publication Data
A catalogue record for this book is available from the British Library.

Library of Congress Control Number 2012934934

Woodhead Publishing ISBN 978-1-84569-996-3 (print)
ISBN 978-0-85709-608-1 (online)

Typeset by RefineCatch Limited, Bungay, Suffolk
Printed in the UK and USA

Contents

List of figures

List of tables

Foreword

When the challenge of writing a book on the thermal control of space systems was proposed to us, and we accepted, we were aware of the large amount of work that this task involved, and also of the limited scope of the final result, due to the wide-ranging nature of the subject. In the last few decades, there has been an explosive growth of technical and scientific information in almost all fields of knowledge, and obviously, the space technology field is no exception.

Focusing our attention on the thermal control subsystem of a spacecraft, the information that can be gathered in one's office (books, specialized journal papers, congresses, technical reports, etc.) and online is so great that one cannot be familiar with or assimilate all the relevant information that has been published. This can all too easily give rise to a feeling of anguish.

Due to the above reasons, our objective has been to gather and concentrate in a text of reasonable length, the basic knowledge needed to understand how the thermal control subsystem of a spacecraft works. In so doing, our intention is to offer a book that can be employed as a basic guide for aerospace engineering graduate students; as a reference book for engineers starting their professional careers in the spacecraft thermal control design field; and for engineers or specialists of other subsystems that want to know more about thermal control. It can also be of interest to scientists participating in the definition phase of space experiments.

This book is divided into four parts, of varying length. The first part, Chapters 1–3, is devoted to the presentation of the basic and specific concepts of a space mission, its development phases, the environment it must withstand, the orbits and trajectories needed to accomplish the mission, and the subsystems that help to achieve this. The fundamentals of heat transfer are presented in the second part (Chapters 4 and 5). As a number of excellent books containing the relevant information can be found in this field, we have decided to present the concepts involved in a summary way, considering that the interested reader has easy access to the recommended literature.

In the third part (Chapters 6–17), by far the largest, the numerous technologies that can be employed in the thermal control subsystem are outlined. The fourth and last part (Chapters 18–20) is devoted to the formal aspects of spacecraft development, needed to ensure the suitability of a given thermal control project, namely the design, analysis, and testing of a spacecraft system or subsystem.

As in all professional activity, people working in a specific field end up inventing a private language which becomes difficult and sometimes incomprehensible to people outside the field. We are not talking about the case where some words can have a meaning different for a professional and for a layman, but about the development of an exclusive nomenclature that can even lead these texts to be unintelligible to the non-initiated. In the aerospace field there is often a widespread use of acronyms, which at times can be considered excessive, and which adds yet more difficulty to the comprehension of the texts, which are challenging to begin with. In some technical reports one can get the impression that one can get rid of some chapters except the list of acronyms. Leaving ironies aside, and coming back to a more formal discourse, in this text we have tried to avoid the

overuse of acronyms, with the aim that a non-specialized reader, opening the book at random, will not need frequent visits to a list of acronyms to understand the text.

The authors want to thank all those people that have helped, to some degree, in the preparation of this book, especially to Mr. Trevor O'Leary and Ms. Lidia Antón.

About the authors

José Meseguer is Full Professor of Aerospace Engineering at the Universidad Politécnica de Madrid (UPM), and is the Director of the Instituto Universitario de Microgravedad 'Ignacio Da Riva' (IDR/UPM), an Institute of UPM for Aerospace R&D activities. Since 1974, he has worked in the compilation and updating of a handbook on spacecraft thermal control under several European Space Agency/ European Space and Technology Centre ESA/ESTEC contracts (*Spacecraft Thermal Control Design Data Handbook*).

He has worked in design, manufacturing and launching of the satellite UPM-Sat 1 (1991–1996). He has been a member of the ESA Fluid Physics and Materials Working Group, member of the Council of Scientists of INTAS (International Association for the Promotion of Cooperation with Scientists from the Independent States of the Former Soviet Union), member of the Spanish Delegation at the Space Advisory Group of the European Commission of the European Union, Member of the Central Technology Advisory Committee of the European Space Agency, and head of the Spanish Programme for Space Research of the Secretaría General del Plan Nacional de I+D, Comisión Interministerial de Ciencia y Tecnología (CICYT).

Dr. Isabel Pérez Grande, Aerospace Engineer and PhD in Aerospace Engineering, is Associate Professor of Thermodynamics and Spacecraft Thermal Control at Escuela Técnica Superior de Ingenieros Aeronáuticos of Universidad Politécnica de Madrid. She is the Head of the

Thermal Control Group of the research Institute IDR/UPM. From the beginning of her professional career, she has been involved in the thermal control design of space instrumentation, and has participated in several research projects related to thermal subjects (thermal modelling of the heating of samples in furnaces for crystal growth processes in microgravity, thermal feasibility study of Aldebaran launcher upper stage, etc.). She was responsible for the thermal control design of the micro satellite UPM-Sat 1, and the thermal control of the balloon-borne solar telescope SUNRISE. Currently, she is responsible for thermal control of the instrument PHI of the ESA mission Solar Orbiter. She is co-author of 18 international refereed publications and more than 25 communications in conferences.

Angel Sanz-Andres was born in Guadalajara (Spain), in 1956. He obtained an Aeronautical Engineer Degree (Universidad Politécnica de Madrid, UPM, Spain) in 1978, and a PhD degree in Aeronautical Engineering in 1983. He held an assistant professor position at UPM from 1978 to 1986, and a full professor position since then. He has taught Aerodynamics since 1978, and simultaneously Spacecraft Technology (postgraduate course of the UPM) since 1991. He also served as Vice-director for research at Escuela Técnica Superior de Ingenieros Aeronáuticos (Aeronautical Faculty of UPM) for a four-year term.

His main activities in R&D during these years have been focused in the space technology and aerodynamics fields.

In the space technology field, he served as technical director of the small satellite programme of the UPM, including the development of the UPM-Sat 1 satellite, launched on 7 July 1995 with the European launcher Ariane 4, totally developed in the UPM with co-operation of several institutions and firms of the Spanish space industry (CASA, INTA, CRISA,

IBM, etc.), and now he is in a similar position in the development of UPM-Sat 2. He has also contributed as thermal and structural advisor in the development of OSIRIS instruments for the ROSETTA mission, and other space programmes such as DESAT, FUEGO, SUNRISE, PHI instrument in Solar Orbiter, etc. He was also in charge of the development of the CPLM payload for the qualification flight of MINISAT-01 platform, and participated in the compilation of the ESA Handbook of Spacecraft Thermal Control Design Data. Some time ago, he also participated in a research programme devoted to the study of fluid dynamics in microgravity conditions (theoretical and experimental contributions to space experiments on board SPACELAB, TEXUS sounding rockets, etc., including the design for ESA of equipment for combustion research in microgravity).

In the aerodynamics field, he is engaged in theoretical and experimental aerodynamics mainly in relation to industrial applications, including the development of an accredited laboratory for anemometer calibration.

He has participated in more than 22 research programmes, and published the results obtained in 67 international publications, 17 national publications, 68 proceedings and 76 technical reports, and directed 13 PhD theses related to the above-mentioned lines.

He has been actively involved in the organization of several courses and meetings. He is also a member of several associations and a referee of several scientific journals (e.g., *Journal of Fluid Mechanics*, *Physics of Fluids A*). He has participated as an independent expert in some evaluations of INTAS and served as an expert for the European Commission for Brite-EuRam Programmes, and several scientific advisory committees of ESA (European Space Agency). He also served as president of the Spanish Association of Wind Engineering (Asociación Nacional de Ingeniería del Viento, ANIV).

1

The space mission

Abstract: The aim of this chapter is to explain some basic concepts widely employed in spacecraft design, such as the space missions, the phases of space programme development and the sharing of responsibilities among the different organizations involved in a space programme. The conceptualization of the design of such big projects, or mission architecture, in terms of mission elements is considered. The main types of space missions, and the spacecraft division into payload and platform or bus (and its subsystems), are also described.

Key words: space mission, development phases, mission types, subsystems.

1.1 Introduction

Generally speaking, it can be said that a large amount of the space activities which have taken place over the last 50 years have been focused on performing services to the community in terms of scientific and commercial aims that could not have been performed by any other means.

Since the launch of Sputnik-I in 1957, space technology has been rapidly evolving, reaching a degree of complexity that could not have been imagined in its early years.

One of the problems that needs to be solved in order to successfully achieve these aims is to assure suitable thermal

behaviour for all the spacecraft subsystems. This may not seem critical or problematic in the case of Earth-based equipment, but it is crucial in the space environment. The physical and technical bases for thermal control design of spacecraft are the main subject of this book.

The set of activities needed to achieve a given objective is designated as a 'mission'. A space mission, therefore, is focused on achieving a given objective by using a space system, because, even in spite of its difficulty and complexity, it is the only feasible or suitable method.

Due to the large cost and effort needed to perform space missions, the design disciplines involved in space mission development have attained a high degree of sophistication and complexity over the years. As a first step in this complex design process, the classical approach recommends trying to define the aim of the mission in a clear but generic way.

Some examples of this 'clear and generic' definition are: to provide communications between two continents, TV coverage, weather forecast, global positioning services, Earth's resources determination, crop inventory, space observation (concerning space sciences), or experimentation in microgravity conditions. In the second step these objectives should be specified to some degree, and in this way the space mission is defined by one or more broad objectives as well as the existing restrictions and limitations. These are the bases from which to start the definition of a space system which can satisfy these objectives under the established restrictions (for instance, time, cost, and performances).

It is extremely important not to substitute these generic objectives by detailed numerical requirements, because, although the objectives remain fixed over time, the numerical requirements can change depending on the state of the technology and on the way the problem is formulated and understood, which evolve with time.

1.2 Mission analysis and design

To achieve the declared mission objectives a design and analysis process is established. This process is composed of several phases which are given different names depending on the organization responsible, although the differences are not substantial.

The design and development phases of a space programme, according to ESA standards, are summarized in Table 1.1.

In a more general approach the space mission life can be split into five main stages:

1. *Concept development*. The initial phase aimed at obtaining a definition of the space mission and of its main elements.

Table 1.1 **The design and development phases of a space programme, according to ESA standards (ECSS-E-ST-10C, 2009)**

Phase	Name	Associate milestones
0	Mission Analysis	MDR Mission Definition Review
A	Feasibility	PRR Preliminary Requirements Review
B	Preliminary Definition	SRR System Requirements Review PDR Preliminary Design Review
C	Detailed Definition	CDR Critical Design Review
D	Production/ Qualification	QR Qualification Review AR Acceptance Review ORR Operational Readiness Review
E	Utilization	FRR Flight Readiness Review LRR Launch Readiness Review CRR Commissioning Result Review ELR End of Life Review
F	Disposal	MCR Mission Close-out Review

2. *Detailed design*. This is the phase where the real design is performed, and at the end a detailed definition of all the space mission components is obtained. In some cases it can also include the development of hardware or software for testing.
3. *Manufacturing and qualification*. In this phase, parts are manufactured, equipment is assembled to form the systems (both flight and ground), the software is developed, and the whole system verified.
4. *Launch*. It includes the launch campaign and the system deployment.
5. *Commissioning and operations*. Once the flight systems have been launched, a test and calibration phase is performed, before passing control to the organization exploiting the system.

The areas of responsibility of the key organizations that intervene in the development of a space system are:

- Space system operator, which controls and maintains the space and ground facilities and resources.
- End users (in scientific or governmental missions) or customers (in commercial missions), who lead the definition of the requirements (astrophysics, meteorological, etc.).
- Developers, who set up the whole system (buying, organizing, testing, etc.).
- Sponsors, who are responsible for financially supporting the project, performing the planning, developing the programme structure, estimating the budget and available funding.

Space system operators and users should generate reasonable technical and economical requirements, while the developer organization should provide the final product on time, taking

into account the changes that may take place in the political and financial situation.

The aim of the initial phases is to assess the need for the specific space mission and to study alternative valid concepts that satisfy the requirements coming from the operator and end user (or customers).

In this regard, operators and end users develop their requirements building on considerations such as the following: mission objectives, operations concept, schedule, life cycle costs and affordability, market situation, research needs, national and international space policy, technology developments, or commercial objectives.

The developer should consider different methods to satisfy the needs defined by the end users/operators/customers, which include developing and assessing different concepts for the mission architecture and components for the mission operations, considering factors as performance, life cycle costs, time schedule, risks, supportability, producibility, financing sources, and return on investment.

If the result satisfies the mission needs at a reasonable cost, the Preliminary Requirements Review (PRR) milestone is successfully accomplished, and the mission design phase starts.

1.3 Elements of a space mission

The space mission is conceptually divided into elements that all together form the mission architecture (Figure 1.1). These mission elements are:

- the subject to be explored, studied, communicated . . .
- the trajectory (set of orbits)
- the space segment (spacecraft, bus or platform, payload)

Figure 1.1 **Mission architecture is defined in terms of the combination of the mission elements**

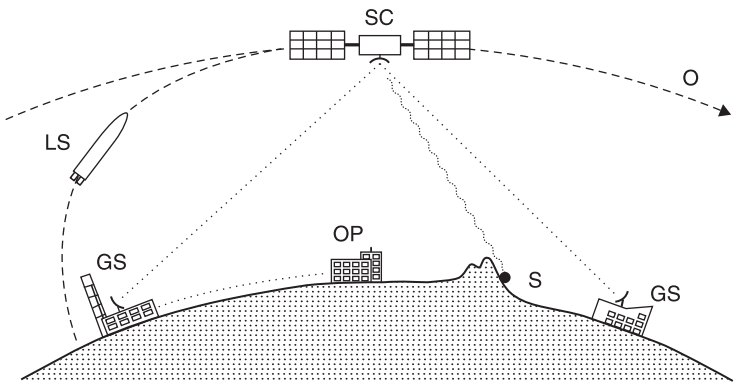

Key: S, subject; O, orbit; SC, spacecraft; LS, launch system; GS, ground station; OP, operations.

- the launch system
- the ground segment (ground stations)
- the mission operations
- the command, control and communications architecture.

For each mission a suitable mission architecture should be devised in order to fulfil the mission objectives at the lowest costs, and on schedule.

The subject of the mission refers to the things or physical phenomena which are studied with the instruments on board the spacecraft (the payload) responsible for the mission execution. For instance, the Earth's surface is the subject if the aim is to determine vegetation type and conditions, or geological formation, or the moisture content in the atmosphere; another type of subject can be the sea's surface to determine the water temperature. As the only possible way for the spacecraft to interact with the outside world is the electromagnetic field (in some cases also the gravitational

field), the first decision is to determine the part of the electromagnetic spectrum most suitable to accomplish the mission by interacting with the subject.

The payload is the set of instruments and software that is in charge of performing the interaction with the subject. In the case of a mission with complex requirements, as they are accomplished mainly through the adequate performance of the payload, it is what determines the cost, complexity and efficiency of the mission.

The spacecraft bus (or platform) provides the payload with the resources it needs to fulfil its mission (see Figure 1.2, p. 11). These resources are: trajectory (orbit) and attitude control, power, telemetry and telecommand, dimensional stability (structure) and thermal environmental conditions. The payload, together with the bus (or platform), constitutes the spacecraft or space segment.

The launch system includes the launch base and its facilities, the launch vehicle, the interfaces with the launch tower, and the required ground support equipment.

The trajectory, or orbit, is the path followed by the spacecraft. It is composed of trajectory sections, each one fulfilling a particular role, e.g.: initial parking orbit, transfer orbit, mission orbits and disposal orbit. The trajectory is one of the main mission elements due to its large influence on the other elements. For this reason, several alternatives should be studied in order to find the most satisfactory one.

The command, control, and communications architecture is the arrangement of the elements that are able to satisfy the mission requirements concerning communications, command and control. Its size and complexity depend on the quantity, speed and timing of the data to be transferred, and on the number and capacity of the ground and space resources, their availability and location.

The ground system is the set of fixed and mobile stations on the ground, connected through data links, which allows: the tracking of the spacecraft; the sending, receiving and processing of the data and the telemetry of the mission; and the sending of the information to the users and operations.

Mission operations is the organization (personnel, hardware, software) which executes the mission, the concept and policies of the mission, the established procedures and the data flow.

In this initial phase, the mission analysis and design process, several alternative concepts that give an appropriate answer to the declared objectives should be considered. The established way of describing these alternative concepts is by defining their architecture, which is composed of the above-mentioned elements. Each architecture can be evaluated in terms of cost, performance, and developing time. This evaluation supplies the information for an appropriate choice.

1.4 Types of space missions

There are many types of space missions; the most common can be classified as scientific, telecommunications or Earth observation missions. A summary of some recent space missions (mainly scientific and technological) with European leadership or participation is shown in Table 1.2.

1.5 Spacecraft design: subsystems and payloads

Since the beginning of space activities, a large number of spacecraft have been built, launched, and operated as part of different missions such as commercial, scientific, or military

Table 1.2 **Summary of some scientific and technological space missions with European leadership or participation**

Mission	Launch date	Orbit[A]	References
Cluster	16 July 2000	HELO	Escoubet et al. (2001), Credland (1995)
Double Star	29 December 2003 and 25 July 2004	HELO	Liu et al. (2005)
ERS-2 (European Remote Sensing Satellite)	21 April 1995	LEO, polar	Lecomte (1998), Francis et al. (1991), Francis et al. (1995)
Envisat	1 March 2002	LEO, polar	Louet (2001)
GIOVE-A (Galileo In-orbit Validation Element)	28 December 2005	MEO	Benedicto et al. (2006), Ebinuma & Unwin (2007)
HST (Hubble Space Telescope)	24 April 1990	LEO	Laurance (1990)
ISO (Infrared Space Observatory)	17 November 1995	HELO	Kessler et al. (1991), Kessler et al. (1996), Kessler et al. (2003)
Cassini-Huygens	15 October 1997	IPO	Lebreton & Matson (2002)
INTEGRAL (International Gamma Ray Astrophysics Laboratory)	17 October 2002	HELO	Clausen & Winkler (1994)
Mars Express	2 June 2003	IPO	Chicarro et al. (2004)
MeteoSat	[B]	GEO	Stuhlmann et al. (2005)
Rosetta	2 March 2004	IPO Comet	Glassmeier et al. (2007)
SMART-1 (Small Missions for Advanced Research in Technology)	27 September 2003	IPO Moon	Foing et al. (2006)

(Continued)

Table 1.2 **Summary of some scientific and technological space missions with European leadership or participation (*Continued*)**

Mission	Launch date	Orbit[A]	References
SOHO (Solar Heliospheric Observatory)	2 December 1995	L1	Huber et al. (1996), Bonnet & Felici (1997)
Ulysses	6 October 1990	IPO Sun	Marsden (2001)
Venus Express	9 November 2005	IPO Venus	Svedhem et al. (2007)
XMM-Newton (X-ray Multimirror Mission)	10 December 1999	HELO	Barré et al. (1999)

Notes
[A] HELO: highly eccentric elliptical Earth orbit; LEO: low Earth orbit; MEO: medium altitude Earth orbit; IPO: interplanetary orbit; GEO: geostationary orbit; L1: Lagrange point 1 (see Sections 3.3 and 3.5).
[B] Series of geostationary meteorological satellites.

ones. The spacecraft types employed to accomplish these missions have quite different configurations as a result of the need of fulfilling the strict requirements imposed during the design optimization process. Notwithstanding the difference in configurations, they can be classified in a general sense depending on the attitude control type (which is intimately related to the payload needs and therefore to the mission itself). Depending on the attitude control type, spacecraft can be spin stabilized, three axis stabilized, or others.

Each one of these types has quite different characteristics in terms of spacecraft configurations, internal equipment, and thermal control design approach.

Concerning the spacecraft, it can be considered as composed of two parts: bus (also platform or service module) and payload, as above mentioned. The payload is the part directly related to the mission objectives, and the bus or platform gives support to the payload, as for instance:

Figure 1.2 **Spacecraft subsystems, with indication of the support given to the payload**

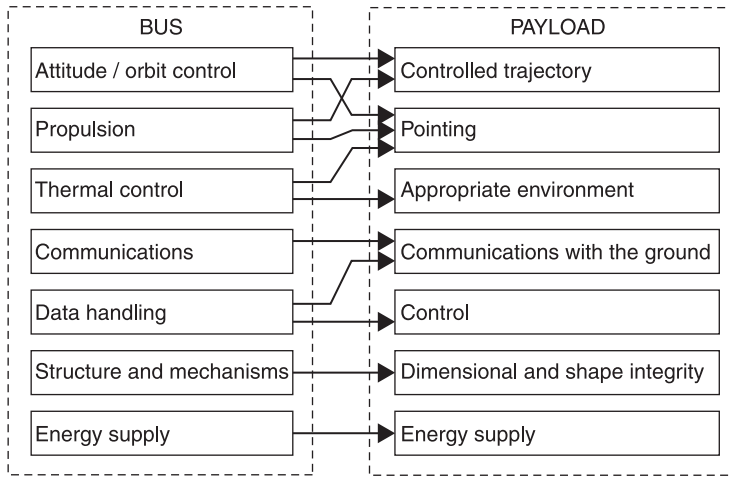

appropriate pointing, control, communications with the ground station, controlled trajectory, dimensional and shape integrity, appropriate environment and energy supply. These resources are provided by different parts of the spacecraft bus called subsystems. The relationship between the payload functions and the subsystems are displayed in Figure 1.2.

1.6 References

Barré, H., Nye, H. and Janin, G. (1999) An overview of the XMM Observatory System, *ESA Bulletin*, **100:** 15–20.

Benedicto, J., Gatti, G., Garutti, A., Paffet, J., Bradford, A. et al. (2006) The triumph of GIOVE-A – the first Galileo satellite, *ESA Bulletin*, **127**: 62–9.

Bonnet, R.M. and Felici, F. (1997) Overview of the SOHO Mission, *Advances in Space Research*, **20**: 2207–18.

Chicarro, A., Martin, P. and Trautner, R. (2004) The Mars Express Mission: an overview, ESA SP-1240, 3–13.

Clausen, K. and Winkler, C. (1994) 'Integral' – a challenging scientific mission, *ESA Bulletin*, **79**: 6–13.

Credland, J. (1995) The Cluster mission – ESA's space fleet to the magnetosphere, *ESA Bulletin*, **84**: 112–17.

Ebinuma, T. and Unwin, M. (2007) GPS receiver demonstration on a Galileo test bed satellite, *Journal of Navigation*, **60**: 349–62.

ECSS-E-ST-10C (2009) *Space engineering. System engineering general requirements*, ESA Requirements and Standards Division, ESTEC, Noordwijk, The Netherlands, March 2009.

Escoubet, C.P., Fehringer, M. and Goldstein, M. (2001) Introduction to the Cluster mission, *Annales Geophysicae*, **19**: 1197–200.

Foing, B.H., Racca, G.D., Marini, A., Evrard, E., Stagnaro, L. et al. (2006) SMART-1 mission to the Moon: Status, first results and goals, *Advances in Space Research*, **37**: 6–13.

Francis, C.R., Graf, G., Edwards, P.G., McCraig, M., McCarthy, C. et al. (1995) The ERS-2 spacecraft and its payload, *ESA Bulletin*, **83**: 13–31.

Francis, R., Graf, G., Edwards, P.G., McCraig. M. and McCarthy, C. (1991) The ERS-1 spacecraft and its payload, *ESA Bulletin*, **65**: 26–48.

Glassmeier, K.H., Boehnhardt, H., Koschny, D., Kührt, E. and Richter, I. (2007) The Rosetta Mission: Flying towards the origin of the solar system, *Space Science Reviews*, **128**: 1–21.

Huber, M.C.E., Domingo, V., Dale, D.C., Witcomb, G., Bonnet, R.M. et al. (1996) The history of the SOHO mission, *ESA Bulletin*, **86**: 25–35.

Kessler, M., Steinz, J., Anderegg, M., Clavel, J., Drechsel, G. et al. (1996) The Infrared Space Observatory (ISO) mission, *Astronomy & Astrophysics*, **315**: L27–L31.

Kessler, M.F., Heske, A., Metcalfe, L. and Salama, A. (1991) The ISO mission – a scientific overview, *ESA Bulletin*, **67**: 8–16.

Kessler, M.F., Müller, T.G., Leech, K., Arviset, C., García-Lario, P. et al. (2003) *The ISO Handbook, Volume I: ISO – Mission and Satellite Overview*, SAI-2000-035/Dc, Version 2.0, ESA, November 2003.

Laurance, R.J. (1990) The history of the Hubble Space Telescope and ESA's involvement, *ESA Bulletin*, **61**: 9–11.

Lebreton, J.P. and Matson, D.L. (2002) The Huygens Probe: science, payload and mission overview, *Space Science Reviews*, **104**: 59–100.

Lecomte, P. (1998) 'The ERS scatterometer instrument and the on-ground processing of its data', Joint ESA-Eumetsat Workshop on Emerging Scatterometer Applications – From Research to Operations, Noordwijk, The Netherlands, 5–7 October 1998.

Liu, Z.X., Escoubet, C.P., Pu, Z., Laakso, H., Shi, J.K. et al. (2005) The Double Star mission, *Annales Geophysicae*, **23**: 2707–12.

Louet, J. (2001) The Envisat mission and system, *ESA Bulletin*, **106**: 10–25.

Marsden, R.G. (2001) The heliosphere after Ulysses, *Astrophysics and Space Science*, **277**: 337–47.

Stuhlmann, R., Rodriguez, A., Tjemkes, S., Grandell, J., Arriaga, A. et al. (2005) Plans for EUMETSAT's Third Generation Meteosat geostationary satellite programme, *Advances in Space Research*, **36**: 975–81.

Svedhem, H., Titov, D.V., McCoy, D., Lebreton, J.P., Barabash, S. et al. (2007) Venus Express – the first European mission to Venus, *Planetary and Space Science*, **55**: 1636–52.

2

Space environment

Abstract: Space environment concerns all the environmental conditions affecting the development of a space mission, from the very beginning of the design phase to the end of life in orbit, taking into account all intermediate stages, such as production, integration, testing and launching. Particularly, the spacecraft has to survive to the extreme conditions of outer space under a wide variety of circumstances, and some of them have to fulfil their missions in other planetary atmospheres. In this chapter the main aspects of space environment are described, focusing the attention on those which are of relevance from the point of view of the thermal control design.

Key words: ground environment, launch thermal environment, in-orbit environment.

2.1 Introduction

A spacecraft is designed to fulfil all the requirements of a given space mission. Because of that, since the very beginning of the design phase the integrity of the spacecraft must be guaranteed, as well as the correct functioning of the spacecraft itself, the different subsystems, and, obviously, the payloads.

Keeping the above in mind, it is clear that the environmental conditions where the spacecraft has to develop its mission

are of paramount importance in the design process, from the first step of the design until the end of the spacecraft's operating life. These environmental conditions must include not only the extreme environment that the spacecraft will face in outer space, but also the potential sources of damage the vehicle can encounter on Earth, from the phase where the spacecraft is only a collection of materials and components to be integrated, until the launching and orbit insertion.

In general the effect of space medium can be grouped into five categories: (1) vacuum, (2) electrically neutral particles, (3) plasma, (4) radiation, and (5) micrometeoroids and orbital debris. The interactions associated with each one of these environmental conditions are summarized in Table 2.1.

This book is mainly devoted to the thermal control subsystem, the task of which is to maintain the temperature of all spacecraft components, subsystems, engineering equipment, payloads and the total flight system, at safe operating and survival levels throughout the entire lifespan of the spacecraft for all flight modes. Like any other subsystem, the spacecraft thermal control subsystem is essential to ensure the reliable operation and long-term survival of any spacecraft.

Environmental effects affect the different subsystems of the spacecraft. In the case of the thermal control subsystem, the environmental thermal loads are one of the main factors that drive the design of the subsystem. Furthermore, the environmental effects may affect the performance of the subsystem through the degradation of the thermo-optical properties of the spacecraft's external surfaces once in orbit. Since the target of the thermal control subsystem is to keep the different parts of the spacecraft within their operating temperature ranges, it usually requires the evacuation of heat from dissipating parts which are prone to overheating, or to

Table 2.1 Space environment effect

Environment	Effect
Vacuum	▪ Pressure differentials ▪ Surface degradation due to solar ultraviolet radiation ▪ Contamination
Electrically neutral particles	▪ Mechanical effects (aerodynamic drag, physical sputtering) ▪ Chemical effects (atomic oxygen attack, spacecraft glow)
Plasma	▪ Spacecraft charging (shift in electrical potential) ▪ Electrostatic discharge and dielectric breakdown ▪ Enhanced sputtering ▪ Re-attraction of contamination
Radiation	▪ Total dose effects (electronic degradation, crew safety hazards) ▪ Single event effects (upsets, latch-up, burnout)
Micrometeoroids and orbital debris	▪ Surface damage due to hypervelocity impacts

Source: After Tribble (2003).

heat those parts which are too cold. The thermal control process generally requires the transfer of heat between different parts of the spacecraft, as well as between the spacecraft and outer space. Obviously, this last heat exchange becomes seriously affected when the surface's optical properties (solar absorptance, α, and infrared emissivity, ε) are modified by environmental conditions. In general, environmental effects related to conditions such as vacuum, electrically neutral particles, radiation, and micrometeoroids and orbital debris, modify the absorptance to emissivity ratio

of the spacecraft's external surfaces, whereas those related to plasma affect the re-attraction of contamination.

Since the space environment can cause severe problems for space systems, great efforts have been devoted to characterize the space environment, in order to properly assess its potential effects on spacecraft. To this end, a considerable amount of technical publications on related topics dealing with space environment have been published. Furthermore, the different space agencies have developed space environment standards which aim to assist in the consistent application of space environment engineering to space products through the specification of required or recommended methods (ECSS-E-ST-10-04C, 2008).

In the next section, a brief review of the ground environment is presented. In Section 2.3 a summary of the launch environment is included. The following sections are devoted to the specific environmental aspects to be considered once the spacecraft is in orbit, including the determination of the external thermal loads on to a space vehicle.

2.2 Ground environment

On the ground, the spacecraft and all its components are subjected to a large variety of potentially aggressive environments, the Earth's atmosphere being the main source of the problems. The terrestrial atmosphere has water and oxygen, and is extremely corrosive for a large number of materials, including some of those used in spacecraft (such as light alloys for structural use).

Another source of problems associated with the terrestrial atmosphere is dust, which falls on the horizontal surfaces of the bodies. To avoid dust contamination, spacecraft and their different subsystems are assembled and integrated in

so-called clean rooms. Simply put, a clean room is a receptacle whose internal surfaces are made of materials which do not generate dust, and is equipped with an air-conditioning system with appropriate dust filters. In some specific cases, when a very clean environment is needed, a smooth air flow is established through the clean area to avoid the dust deposition on horizontal surfaces (even after filtration, dust remains in the air).

Therefore, spacecraft are subjected to particulate contamination. Particulate denotes those pieces of matter with micrometric sizes, which inevitably deposit on the spacecraft surfaces during manufacturing, integration, testing, and launching (this type of contamination is unusual once the spacecraft is in orbit). Particulate contamination becomes especially critical with regard to optical instruments, whose characteristics are related not only to the rate of transmission and reflectance, but also to the amount of scattering present in the optics.

The amount of particulates that deposit on a given surface is a function of the amount of particulate per unit volume existing in the surrounding air. Because of that, air quality is defined in terms of the maximum allowable number of particles per unit of volume of air (air class).

In the International System of units (abbreviated SI from the French *Système International d'unités*), the name of the air class is taken from the base 10 logarithm of the maximum allowable number of particles per cubic metre of air, having sizes of 0.5 μm or larger. In the Imperial System, the name of the class is taken from the maximum allowable number of particles 0.5 μm or larger, per cubic foot (Tribble, 2003).

The above classifications are those defined in the Federal Standard 209 E, and they are related through the expression $M = \log (k_v N)$, where M is the air class expressed in SI (rounded to one decimal digit), N the air class in Imperial

units, and k_v = 35.32 m^3/ft^3 the constant that relates cubic feet to cubic metres.

There is another airborne particulate cleanliness classification defined in ISO 14644-1 (ECSS-Q-ST-70-01C, 2008), which is based on a criterion similar to the above stated. If C_n is the maximum permitted concentration (in particles per cubic metre of air) of particles that are equal to or larger than the considered particle size (0.5 μm), the ISO classification number is $M_{ISO} = \log(k_{pd}C_n)$, where k_{pd} = 35.17 is a constant which depends on the assumed particle sizes distribution.

ISO class 7, equivalent to class M 5.5 (N = 10000), is typical of most spacecraft manufacturing clean rooms.

2.3 Launch thermal environment

The launch phase is critical in the spacecraft's life because, over a short period of time, the vehicle is under extreme stresses such as axial loads due to launcher acceleration, and lateral loads due to wind gusts. In addition, the spacecraft has to withstand a large amount of mechanical vibrations, as well as a considerable dose of acoustic energy (mainly just after lift-off), when the rocket noise is reflected on the ground, and of aerodynamic noise as the launcher passes through the aerodynamic transonic regime. Mechanical loads also include shock mechanical loads due to the processes involved in both launcher stages separation, and in spacecraft separation.

Furthermore, at the beginning of the launching phase, when the launcher increases its altitude, the atmospheric pressure varies from the atmospheric pressure at the launch site to the outer space vacuum, which can lead to depressurization loads if no provisions are taken into account

to properly evacuate the air trapped in the spacecraft, and in the fairing (Sanz-Andrés et al., 1997).

Thermal loads due to the aerodynamic heating of the fairing during the ascending step in the low levels of terrestrial atmosphere, and to the direct aerodynamic heating of the spacecraft after fairing jettisoning (because of the existing residual atmosphere at high altitudes), have to be considered.

In effect, another significant form of environmental heating is the molecular heating caused by molecular flow at the upper atmosphere, which can act after fairing jettisoning (it usually takes place close to 115 km of altitude) or at very low perigees at orbital velocities. Aerodynamic heating also occurs when aerobraking is used to modify the orbit of a spacecraft arriving at a planet with an atmosphere. This manoeuvre reduces the eccentricity of an elliptical orbit with less fuel than the direct use of a rocket engine, but with a direct impact on the thermal control subsystem.

Free molecular heating is due to the bombardment of the spacecraft by individual molecules (free molecular flow). This means that a residual atmosphere is needed for the appearance of this phenomenon. In most cases, this only occurs at the end of the launching phase, after fairing jettisoning. Although it would be desirable that fairing jettisoning occurs as soon as possible after lift-off (decreasing the mass to be carried), this requirement is in opposition to that of spacecraft heating due to free molecular flow caused if fairing jettisoning takes place where the density of the atmosphere is still significant. In a first approximation, the free molecular heating rate can be estimated by the expression $\dot{Q}_{fmh} = k_{fmh}\rho U^3/2$, where k_{fmh} is a factor between 0.6 and 0.8 (although in most cases the value $k_{fmh} = 1$ is considered for conservatism), ρ the air density, and U the magnitude of the velocity parallel to the heated surface. When the above

expression is applied, it must be taken into account that at very high altitudes the atmosphere's density is very variable, because the atmosphere expands and contracts depending on many parameters (the level of solar electromagnetic activity, the geomagnetic index, the longitude, the latitude and the day of the year, amongst others).

Available flight data indicate that, during launching, large heating variations between the different external parts of the spacecraft are encountered, the average heat load being 250 W/m^2, which is acceptable for most spacecraft components. It must be remembered, however, that the launch phase is only a very small fraction of the whole operational life of the spacecraft. There are satellite orbits with very low perigee altitudes, where the satellite can suffer free molecular heating, although generally, this phenomenon has to be considered for perigee altitudes below 200 km approximately.

2.4 In-orbit thermal environment

Once the spacecraft is placed in orbit, besides the thermal requirements of the different subsystems of the spacecraft, the thermal control subsystem has to guarantee the fulfilment of those requirements associated with the payloads. This point is critical in the case of scientific missions, where each device has its own operating temperature range.

The space environment depends on whether the particular mission is Earth-orbiting or deep space. For a spacecraft orbiting the Earth (or any other planet or moon), the main sources of environmental heating are solar radiation, both direct and reflected by the planet, and the infrared energy emitted by the planet itself (Figure 2.1).

Figure 2.1 Environmental heat fluxes for a planet-orbiting spacecraft

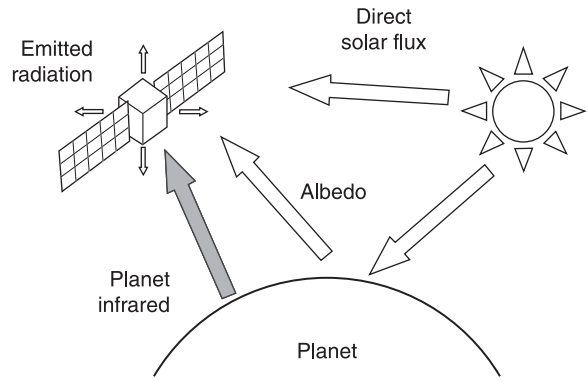

2.4.1 Solar radiation

The Sun is the main source of heating and power for a spacecraft close enough to the Sun (a limit could be 2 AU, Astronomical Unit). The spectral distribution of solar irradiation is approximated by a blackbody at 5762 K (ECSS-E-ST-10-04C, 2008); therefore its effects are primarily perceived as shortwave radiation. Close to the Earth (at 1 AU), the nominal value of the direct solar incident energy on a surface normal to a line from the Sun is the so-called solar constant, whose value is G_s = 1366.1 W/m^2, according to ISO 21348 (2007). The magnitude of the solar constant is not constant. The first reason for this variation is that, following the mean sunspot number, which varies with an 11-year solar cycle, the energy emitted by the Sun varies with the same cycle, although such a variation is only a small fraction of the average emitted energy (Anderson et al., 2001; Anderson and Smith, 1994). The second reason is associated with the Earth's orbit: because of the eccentricity of the elliptical orbit of the Earth, the mean distance between

the Earth and Sun varies approximately ±1.7% throughout the year. Therefore, direct solar irradiation values range from 1321.6 W/m^2 at aphelion to 1412.9 W/m^2 at perihelion (ECSS-E-ST-10-04C, 2008).

Although for thermal purposes the spectral distribution of the solar radiation can be approached by a blackbody at 5762 K, the study of its real spectral distribution is also of great interest. Thus, the real irradiation spectral distribution at 1 AU can be found in ASTM E-490 (2006) and ECSS-E-ST-10-04C (2008). This distribution is based on data from satellites, Space Shuttle missions, high-altitude aircraft, rocket soundings, and ground-based solar telescopes. The integrated spectral irradiance conforms to the value of the solar constant accepted by the space community of 1366.1 W/m^2, as mentioned above. A plot of this solar irradiation at 1 AU from the values given by ASTM E-490 (2006) can be seen in Figure 2.2. In this plot the spectral emissive power of the Sun, modelled as a blackbody at 5762 K, at the Earth's orbit is also represented. Note that this curve has been obtained assuming that the Sun's surface behaves like a blackbody at 5762 (see expression (5.4)), multiplying its emissive power by $(r_S/d_0)^2$, where r_S is the Sun's radius, and d_0 the distance from the Earth to the Sun.

Looking in detail at this distribution, one can see that 99% of solar radiation is between 0.15 and 10 μm. The visible part of the spectrum (0.4 to 0.8 μm) is included within this range, and it represents 46% of the total radiation; 47% is in the near infrared range (0.8 to 2.5 μm) and 7% is ultraviolet radiation (0.3 to 0.4 μm). The maximum takes place at 0.45 μm.

The angle of view of the Sun at 1 AU is 0.5°. This means that at Earth orbits, for thermal calculation purposes, solar radiation can be considered to be parallel rays. In the case of thermal analysis performed for closer distances to the Sun, as

Figure 2.2 **Spectral distribution of solar irradiation at 1 AU: spectral emissive power, E_λ, versus wavelength, λ (solid line). Spectral emissive power of the Sun as a blackbody at 5762 K at the Earth's orbit (dashed line)**

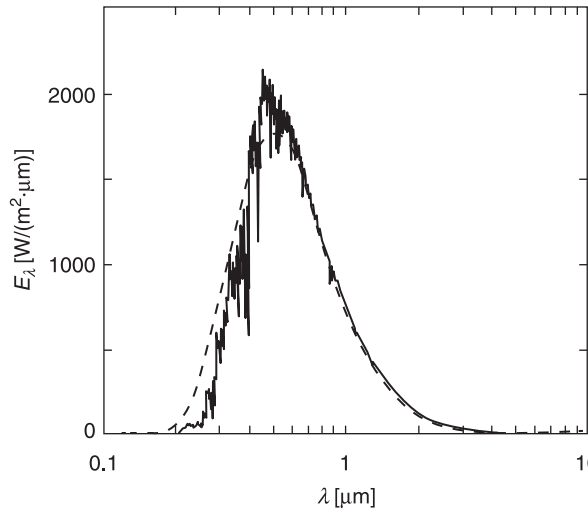

in the case of a thermal study of a Mercury orbiter, the effect of the solar angle might have to be taken into account, mainly for the design of optical devices.

The value of the solar constant at a distance between the body and the Sun, d, in astronomical units, can be written as $G_s(d) = G_s(d_0)\,(d_0/d)^2$, d_0 being the distance from the Earth to the Sun in astronomical units (d_0 = 1 AU). Values of the solar constant at different planetary orbits can be found in Table 2.2.

The calculation with a simple analytical expression of the solar radiation absorbed by a flat surface of area A, whose normal vector forms an angle θ with the solar rays is

$$\dot{Q}_{Sun} = \alpha G_s A \cos\theta, \tag{2.1}$$

Table 2.2 **Relevant data on the planets and the Moon (1 AU = 149.5 × 10^6 km)**

	d [AU]	R_P [km]	G_s [W/m^2]	T_P [K]	*a*
Mercury	0.387	2330	9034	442	0.106
Venus	0.723	6100	2588	231.7	0.65
Earth	1.0	6367.5	1366	255*	0.30
Mars	1.521	3415	585	210.1	0.15
Jupiter	5.173	71375	51	110.0	0.52
Saturn	9.536	60500	15	81.1	0.47
Uranus	19.269	24850	3.6	58.2	0.51
Neptune	30.034	25000	1.5	46.6	0.41
Pluto	39.076	2930	0.89	–	–
Moon	1.0	1738	1353	273	0.07

* Derived from a heat flux of 230 W/m^2 (see Subsection 2.4.3).

Note: Distance to the Sun in AU, *d*. Radius of the planet, R_P. Solar flux, G_s. Equivalent blackbody temperature of the planet, T_P. Average planetary albedo, *a*. Data concerning *d*, R_P, and G_s are from STCDD (1989), and data concerning T_p and *a* are from ECSS-E-ST-10-04C (2008).

where α is the solar absorptance of the surface (see Section 6.1).

An interesting exercise is the determination of the equilibrium temperature of an isothermal spacecraft with no internal heat generation, T_{sc}, that is orbiting the Earth. It can be obtained assuming that the spacecraft is in thermal balance, receiving energy only from the Sun and rejecting heat to space by radiation.

In this case, the heat balance equation states that the absorbed radiation from the Sun must equal the heat radiated to deep space, that is: $A_{pr}\alpha G_s = A\varepsilon\sigma T_{sc}^4$, where A_{pr} is the spacecraft area projected normal to the Sun direction, A the total area, G_s the solar flux per unit area at the spacecraft orbit, α the spacecraft surface absorptance in the solar band,

ε the infrared emissivity, and σ the Stefan-Boltzmann constant, $\sigma = 5.67 \times 10^{-8}$ W/(m^2·K^4). Note that in this expression it has been assumed that the spacecraft temperature is much greater than the surrounding space environment, so that radiation reaching the vehicle from sources other than the Sun can be neglected.

Therefore, $T_{sc} = [A_{pr} G_s \alpha/(A\sigma\varepsilon)]^{1/4}$. The equilibrium temperatures of a black ($\alpha/\varepsilon = 1$) sphere ($A_{pr}/A = 1/4$), $T_{bs} = T_{sc}$, at distances from the Sun equal to the corresponding distances to the Sun of the different planets is shown in Figure 2.3. Taking into account that just like living matter, equipment and mechanisms perform better close to room temperature, this plot highlights the important role that thermal control plays in spacecraft design. The influence of the parameter α/ε is shown in Figure 6.2.

Figure 2.3 **Temperature, T_{bs}, of a black sphere exposed to sunlight at the distance, d, of the different planets from the Sun, as given in Table 2.2**

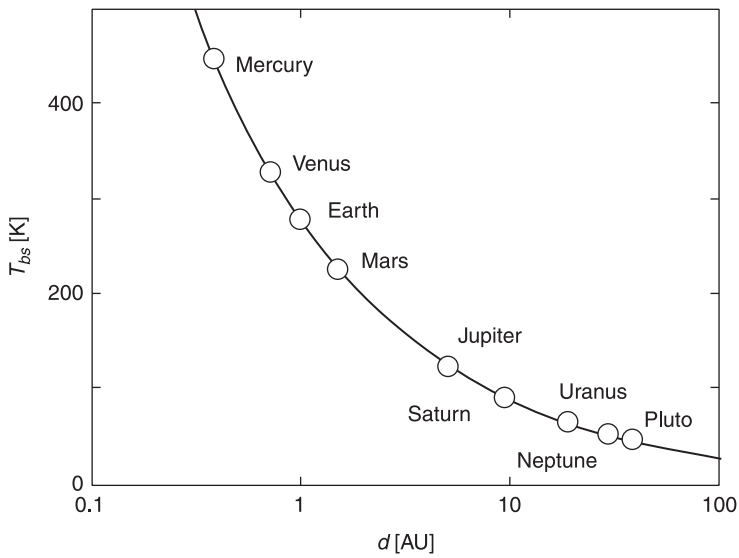

2.4.2 Albedo radiation

The next significant thermal environment contributor is albedo (from the Latin *albus*, for whiteness). Albedo is the part of the solar radiation incident upon the planet which is reflected or scattered by the planet surface and atmosphere (if any). The albedo coefficient, *a*, is defined as the fraction of incident solar radiation which is reflected off a planet. Therefore its influence as a thermal load for spacecraft design is higher for low-altitude orbits. Due to the roughness of a planet's surface, the albedo is assumed to be diffuse. As an approximation, the spectral distribution of the reflected light is considered to be the same as that of incident light, despite the fact that some surface materials can lead to the absorption of certain wavelength bands.

Albedo values for different planets or moons range from very low values (0.073 for the Moon) to relatively high (0.65 for Venus), as indicated in Table 2.2. The albedo coefficient, *a*, may be highly variable over the planet's surface, as happens with the Earth's surface. Thus, oceans absorb most of the incident radiation, the local albedo coefficient being between 0.05 and 0.10; whereas ice or snow, for example the Antarctic surface, reflects most of the solar radiation and the local albedo coefficient is about 0.95. In continental areas the albedo can range from small values over forests to higher values over desert areas. The presence of clouds, mainly the quantity and the type, is also an important factor that alters the local albedo. An albedo coefficient value of 0.8 is typical for cloudy areas. For a spacecraft in low Earth orbit (LEO), depending on the orbit inclination, the orbital average albedo varies between 24% in equatorial orbits to 42% in polar orbits, approximately (Gilmore, 1994). The mean value for the Earth is taken as 0.3 (ECSS-E-ST-10-04C, 2008).

When determining the thermal loads on a spacecraft, albedo loads are only applicable when the portion of the planet that is seen by the spacecraft is sunlit. The calculation is often a complex task usually carried out with the help of computer tools. As it applies only to the portion of the planet illuminated by the Sun, its value will depend on the solar zenith angle, that is, the angle between the Sun–Planet vector and the Planet–Spacecraft vector. The orbit angle, β, the minimum angle between the spacecraft's orbit plane and the Sun–Earth vector (Figure 3.7), also has to be taken into account. For Earth orbits, detailed information on data and the corrections that have to be applied to those angles to calculate the albedo coefficient is presented by Anderson et al. (2001), based on measurements of the NOAA (National Oceanic and Atmospheric Administration) and ERBE (Earth Radiation Budget Experiment) satellites.

For simplified analytical estimations, the albedo absorbed energy on a surface of area A can be calculated assuming that the planet behaves as a reflecting sphere as follows,

$$\dot{Q}_{alb} = aG_s AF_{SC-P}\cos\phi, \tag{2.2}$$

for $-\pi/2 \le \phi \le \pi/2$, where a is the planetary albedo coefficient, G_s the solar constant, ϕ the solar zenith angle, and F_{SC-P} the view factor between the surface and the planet. The angle ϕ takes into account the fact that the albedo is at a maximum at the sub-solar point and it becomes zero when the planet seen by the spacecraft is in eclipse. Other simple analytical models that take into account seasonal effects and latitude and longitude on the Earth's surface can be found in ECSS-E-ST-10-04C (2008).

In the case of Earth orbits, the albedo loads are relevant only for low Earth orbits. For telecommunications satellites in geostationary orbits (GEO), these loads are practically negligible.

2.4.3 Planetary radiation

Planetary radiation is the thermal radiation emitted by a planet. It is also called outgoing longwave radiation. It is a combination of the radiation emitted by the planet's surface and by atmospheric gases. It is diffuse radiation within the infrared part of the spectrum. As is the case with the albedo coefficient, the emission of a planet's surface varies from one point to another. For example, on Earth, it depends on the local time, on the presence of water (oceans), highly populated areas, desert areas, etc. Data on the variation with the latitude and with the orbit inclination of the mean infrared Earth radiation can be found in Gilmore (1994), and detailed information of these variations on the Earth's surface and correlations between the Earth's infrared radiation and the albedo coefficient are presented by Anderson et al. (2001).

Planets are not strictly in thermal balance. Nevertheless, the solar energy absorbed by the planet is almost balanced with the emitted radiation, a fact that can be used to determine a planet's radiative properties from the energy balance equation. For thermal purposes, the thermal energy emitted by planets can be characterized by means of the planet's blackbody equivalent temperature. If the albedo coefficient, a, is known, a first estimation of the planet's equivalent blackbody temperature, T_P, can be obtained by equating the solar energy absorbed by the planet to the emitted energy. Thus:

$$G_s \pi R_P^2 (1 - a) = 4\pi R_P^2 \sigma T_P^4, \tag{2.3}$$

where σ is the Stefan-Boltzmann constant, and R_P is the radius of the planet. Note that the resulting temperature is independent of the value of R_P, as can be seen in the equation. Interestingly, for planets like Mercury with a long day

compared to its year, the use of a single temperature to model the thermal behaviour of the planet may not work properly, and more complex models are necessary. In the case of the Earth, with a mean albedo coefficient $a = 0.3$, its blackbody equivalent temperature is about $T_P = T_E = 255\,\text{K}$. This corresponds to an average flux of 230 W/m^2 on the Earth's surface. For an orbiting spacecraft it can vary from 150 W/m^2 to 350 W/m^2. The blackbody equivalent temperatures for other solar system planets are given in Table 2.2.

From the blackbody temperature of the planet, T_P, the planetary infrared thermal load on a spacecraft surface of area A can be calculated from:

$$\dot{Q}_{planet} = \varepsilon A F_{SC-P} \sigma T_P^4, \tag{2.4}$$

where ε is the infrared emissivity of the spacecraft surface, and F_{SC-P} the view factor between the spacecraft surface and the planet.

The infrared radiation emitted by a planet is in the same wavelength band as the infrared radiation emitted by spacecraft. This implies that any surface treatment oriented to reflect planet-emitted radiation would also reduce, by the same proportion, the emission ability of the surface, which would reduce the radiation to outer space of the heat dissipated within the spacecraft. Due to these reasons infrared radiation emitted by a planet can present a heavy backload on spacecraft radiators in low-altitude orbits, which must be placed on the satellite surface with a view factor of the planet as low as possible.

As is the case with albedo loads, infrared planetary radiation is relevant for low-altitude orbits. However, its influence on satellites in geostationary orbits is negligible.

In addition to the main heat sources already described, there is another source of heating associated with charged

particles, such as that existing in van Allen's belts located at the geomagnetic equator plane of the Earth. Such a heat source is extremely weak when compared with other sources, and in most cases, when the operating temperature range of the components is close to room temperature, its effects are not considered. This is not the case of equipment that must operate at very low temperatures, because, for example, charged particle heating can significantly raise the equilibrium temperature of a cryogenic radiator.

2.5 Other in-orbit environmental aspects

There are other aspects related to space environment that have to be taken into account in the design of the thermal control subsystem, because, although they are not direct sources of heat loads, they can be considered as indirect sources of heating due to their effect on the degradation of the properties of the materials used in the spacecraft, mainly those used in external surfaces. There are two main indirect sources: radiative and micrometeoroids and orbital debris.

The compositions of the radiation fields outside the magnetic field of the Earth are spatially and temporally variable and the fields are commonly divided into four different sources and types (Borggräfe et al., 2009):

- Galactic cosmic radiation consists of fully ionized particles from outside the solar system (91% protons, 8% particles, 1% heavy nuclei), and includes nuclei of almost all known chemical elements and energies in the range of several tens up to 10^{12} MeV per nucleon (see Figure 2.4). Their distribution is assumed to be almost isotropic throughout space. Even though the number of high-charge and

energetic particles is relatively small, their contribution to the deployed dose is significant due to their highly ionizing character, and thus, hazardous biological effects.

- Solar particle events are temporal and sudden ejections of particles from the Sun's heliosphere, mainly protons, with a high flux density. These are widely accepted to be caused by coronal mass ejections, accelerating the particles to smaller kinetic energies in comparison to galactic cosmic radiation, but with much higher particle fluencies. The enormous flux ratios are the reason why solar particle events can deliver a very high dose in a short period of time since solar particle events typically last from several hours to a few days.

Figure 2.4 **Radiation environment concerning high-energy particle radiation**

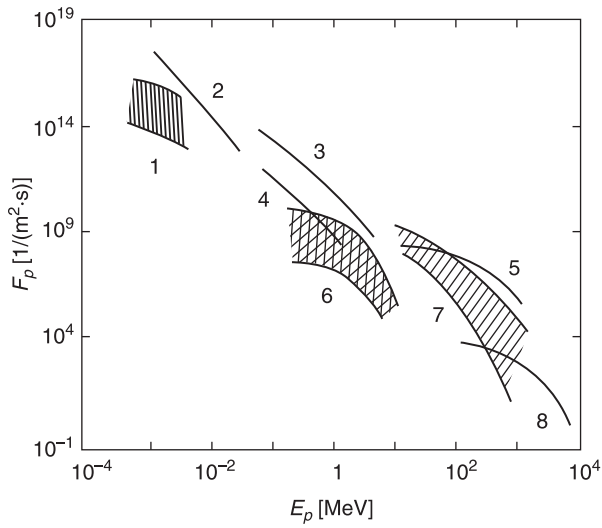

Key: Flux density of high-energy particles, F_p, versus particle energy, E_p. 1 – solar wind protons; 2 – auroral electrons; 3 – trapped electrons; 4 – trapped protons (outer zone); 5 – trapped protons (inner zone); 6 – solar storm protons; 7 – solar flare protons; 8 – galactic cosmic rays.

- Trapped radiation fields (van Allen's belts) consist of trapped cosmic radiation particles along the field lines of the terrestrial magnetic field, mainly protons and electrons.
- Secondary radiation occurs from planets, or spectrum interaction with planetary atmosphere or surface, mainly neutrons.

It must be added that in contrast to free space conditions, the radiation environment in planetary orbits and on a planet's surface will be reduced by up to 40% due to the shielding of the planet's mass, since solar and galactic radiation is essentially isotropic.

Over the last few decades, space environment international standards have been developed for physical phenomena of the natural environment such as galactic cosmic rays, solar energetic particles, the Earth's magnetic field, the ionosphere, the plasmasphere, etc. A survey of the current status of the international standards under development can be found in Panasyuk (2006), whereas details on the effect of radiation on spacecraft design are given in Tribble (2003).

Meteorites and micrometeoroids are solid bodies having densities close to 5000 kg/m^3, whose mass can span over several orders of magnitude. They move through interplanetary space at velocities of 20 km/s or even larger.

The concentration of meteorites and micrometeoroids increases close to large gravitational masses, such as that of the Earth, and they can be a danger to spacecraft. The amount of meteorites per unit of volume decreases as the meteorites' volume increases, in such a way that most of them are extremely small (a sheet of aluminium, 0.5 mm thick, is strong enough to withstand solid particles with sizes up to 1 μm). Therefore, in most spacecraft, the external shell and the thermal insulation (multilayer insulation) are sufficient to protect the spacecraft against the solid particles,

likely to be encountered. Of course, this may not be valid in the case of long or special missions, where additional safety provisions have to be undertaken.

However, close to Earth, meteorites and micrometeoroids are not the main source of dangerous impacts for spacecraft. The most dangerous are other spacecraft, or parts of spacecraft (so-called space debris), which are in orbit close to the Earth as a result of more than 50 years of space activity. Large efforts are devoted by space agencies to tracking these objects through radar and optical methods from ground-based tracking stations which are distributed all over the world. A statistical distribution of space debris across the various orbital regimes (low Earth orbit, LEO; mid Earth orbit, MEO; geostationary orbit, GEO) can be found in Bobrinsky and Del Monte (2009), and the time variation of the number of objects in Earth's orbit is presented in Lewis et al. (2009).

Close to the Earth, the amount of space debris produced by human activities is larger than the amount of micrometeoroids, mainly in low Earth orbits. Because of the magnitude of the problem for existing operational spacecraft, and for the future ones, some efforts are being made to study this problem and to provide mathematical models of it (Bradley and Wein, 2009; Li Yi-yong et al., 2009), as well as to introduce some limitations on the growth of the uncontrolled mass placed in orbit (Krag, 2009; Stokes and Davey, 2009; Crowther, 2009).

Available information (obtained from registered impacts on spacecraft sensors) demonstrate that there are billions of small micro-particles orbiting near the Earth, mainly particles eroded from rocket nozzles, with dimensions between 0.01 mm and 0.5 mm. Concerning large-mass body impacts, five accidental collisions in outer space have been identified, but the Iridium/Cosmos collision was the first to involve two intact satellites. This impact took place on 10 February 2009. Iridium 33, a US communications satellite, and

Cosmos 251, a decommissioned Russian satellite, collided as the two objects passed over northern Siberia. This intersection caused two distinct clouds of debris to extend through a substantial part of the low Earth orbit. It also raised public awareness of the issue of space debris more than any other collision and stimulated much media attention. The Iridium/Cosmos event is only the most recent collision involving traceable orbiting objects. The European Space Agency's Database and Information System Characterizing Objects in Space (DISCOS) describes the occurrence of five historical collisions since 1991: Cosmos 1934 (1992), Cerise (1996), Thor Burner IIA stage 2 (2005), Cosmos 3M stage 2 (2005), and Iridium 33 / Cosmos 2251 (2009), although another four additional collisions may have taken place (Lewis et al., 2009). An increase in the likelihood of collisions is expected.

Finally, microgravity is another effect to be considered within the space environment. The handling of liquid (and gases) in space is more difficult due to microgravity. From the point of view of thermal control, the main effect is the absence of natural thermal convection, which must be forced when it is needed (as happens in manned missions). Another aspect to be considered is the position of liquid–gas interfaces (for instance, in liquid propeller tanks).

2.6 References

Anderson, B.J., Justus, C.G. and Batts, G.W. (2001) *Guidelines for the Selection of Near-Earth Thermal Environment Parameters for Spacecraft Design*, NASA TM-2001-211221, October.

Anderson, B.J. and Smith, R.E. (1994) *Natural Orbital Environment Guidelines for Use in Aerospace Vehicle Development*, NASA TM-4527, June.

ASTM E-490–00a (2006) *Standard Solar Constant and Zero Air Mass Solar Spectral Irradiance Tables*, American Society for Testing and Materials (ASTM).

Bobrinsky, N. and Del Monte, L. (2009) 'ESA's Space Situational Awareness Programme', 2009 CEAS European Air and Space Conference, Manchester, UK, 26–29 October, 2009.

Borggräfe, A., Quatmann, M. and Nölke, D. (2009) Radiation protective structures on the base of a case study for a manned Mars mission, *Acta Astronautica*, **65**: 1292–1305.

Bradley, A.M. and Wein, L.M. (2009) Space debris: assessing risk and responsibility, *Advances in Space Research*, **43**: 1372–90.

Crowther, R. (2009) 'Addressing orbital debris through national regulation', 2009 CEAS European Air and Space Conference, Manchester, UK, 26–29 October 2009.

ECSS-E-ST-10-04C (2008) *Space engineering. Space environment*, ESA Requirements and Standards Division, ESTEC, Noordwijk, The Netherlands, November 2008.

ECSS-Q-ST-70-01C (2008) *Space product assurance. Cleanliness and contamination control, Space engineering, Space environment*, ESA Requirements and Standards Division, ESTEC, Noordwijk, The Netherlands, November 2008.

Gilmore, D.G., Ed. (1994) *Satellite Thermal Control Handbook*, The Aerospace Corporation Press, El Segundo, California, USA.

ISO 21348 (2007) Space environment (natural and artificial). Process for determining solar irradiances, International Organization for Standardization, May 2007.

Krag, H. (2009) 'The activities of ESA's Space Debris Office', 2009 CEAS European Air and Space Conference, Manchester, UK, 26–29 October 2009.

Lewis, H.G., Swinerd, G.G. and Newland, R.J. (2009) 'The space debris environment: future evolution,' 2009 CEAS

European Air and Space Conference, Manchester, UK, 26–29 October 2009.

Li Yi-yong, Shen Huai-rong and Li Zhi (2009) Faster algorithm of debris cloud orbital character from spacecraft collision breakup, *Advances in Space Research*, **43**: 1527–31.

Panasyuk, M.I. (2006) Working Group 4 of international standardization organization – experience of developing the standards of space environment, *Advances in Space Research*, **38**: 2583–6.

Sanz-Andrés, A., Santiago-Prowald, J., and Ayuso-Barea, A. (1997) Spacecraft launch depressurization loads, *Journal of Spacecraft and Rockets*, **34**: 805–10.

STCDD (1989) *Spacecraft Thermal Control Design Data Handbook*, ESA PSS-03-108, Issue 1.

Stokes, P.H. and Davey, J.R. (2009). 'The role of international standards in debris mitigation', 2009 CEAS European Air and Space Conference, Manchester, UK, 26–29 October 2009.

Tribble, A.C. (2003) *The Space Environment, Implications for Spacecraft Design*, Princeton University Press, Princeton, New Jersey, USA.

3

Keplerian orbits

Abstract: The basic concepts concerning spacecraft trajectory, or orbit, are described. The orbit transfers (co-planar or Hohmann, and orbit plane inclination change), the orbit in space, and the main orbit perturbations (non-gravitational forces, non-spherical mass distributions, interactions with third bodies) are also considered, as well as lighting conditions for spacecraft (eclipse, occultation, umbra) and the types of orbits, their relation with the mission, and their impact on the spacecraft subsystem design.

Key words: characteristic velocities, orbit transfers, orbit perturbations, lighting conditions, types of orbits.

3.1 One-body problem

The motion of a spacecraft travelling in the solar system, described in the simplest way, can be formulated as a rigid body attracted by a central force (gravitation attraction) generated by a much more massive body, the primary. It is the so-called one-body problem. The primary can be the Earth (or another planet) in the case of an orbiting spacecraft, or the Sun if the spacecraft is following an interplanetary orbit.

If the two bodies have similar masses, the problem is usually called the two-body problem, which can be reduced

to the one-body problem by performing a suitable parameter transformation. One example is the motion of the Earth–Moon system. In the case of an interplanetary probe, travelling from the Earth to Mars, the problem involves four bodies (the Sun, the Earth, Mars and the spacecraft). But, for a preliminary phase study, it can be split into three one-body problems, namely, the spacecraft–Earth problem, the spacecraft–Sun problem, and the spacecraft–Mars problem. Each one is applicable when the spacecraft is in the vicinity of one of the planets, or in interplanetary space, outside the sphere of influence of the planets.

In the case of the one-body problem, the trajectory of a spacecraft (whose mass is small compared to the primary mass) can be determined by using Newton's equations (expressed in a suitable inertial reference frame). Using vector notation, the velocity, **v**, acceleration, **a**, and the position of the spacecraft, **r**, defined in the above-mentioned reference frame, are related by the expression

$$\mathbf{a} = \frac{\mathrm{d}\mathbf{v}}{\mathrm{d}t} = \frac{\mathrm{d}^2\mathbf{r}}{\mathrm{d}t^2}, \tag{3.1}$$

and Newton's second law can be written as follows

$$\frac{\mathrm{d}(m\mathbf{v})}{\mathrm{d}t} = \mathbf{F}; \qquad m\frac{\mathrm{d}^2\mathbf{r}}{\mathrm{d}t^2} = \mathbf{F}, \tag{3.2}$$

where m is the mass of the spacecraft, t the time, and **F** the applied external force, in this case the gravitational force (Roy, 1988). The second expression is valid when the mass, m, is a constant.

In the case of the gravitational attraction, the force between two bodies is directly proportional to the product of the masses of the bodies, m_1 and m_2, and inversely proportional to the square of the distance between them, r,

$$F = G\frac{m_1 m_2}{r^2}, \tag{3.3}$$

where G is the universal gravitation constant ($G = 6.670 \times 10^{-11}$ Nm^2/kg^2). In this case, the mass of the primary is m_1, and the mass of the spacecraft is $m = m_2$, and therefore, in vector notation

$$\frac{\mathrm{d}^2\mathbf{r}}{\mathrm{d}t^2} = -Gm_1\frac{\mathbf{r}}{r^3} = -\mu\frac{\mathbf{r}}{r^3}, \tag{3.4}$$

where $\mu = Gm_1$. The integration of the vector product of (3.4) by **r** leads to

$$\mathbf{r} \wedge \frac{\mathrm{d}^2\mathbf{r}}{\mathrm{d}t^2} = 0, \qquad \mathbf{r} \wedge \frac{\mathrm{d}\mathbf{r}}{\mathrm{d}t} = \mathbf{h}, \tag{3.5}$$

where **h**, the constant of integration, is the angular momentum. Therefore, its direction is maintained fixed, always pointing in the same direction, which implies that the trajectory of the body always remains in the plane that is perpendicular to **h**, and contains both vectors, **r** and **v** = d**r**/dt (Figure 3.1).

Figure 3.1 **The trajectory of the body is contained in the plane defined by the position and velocity vectors, r and v, respectively**

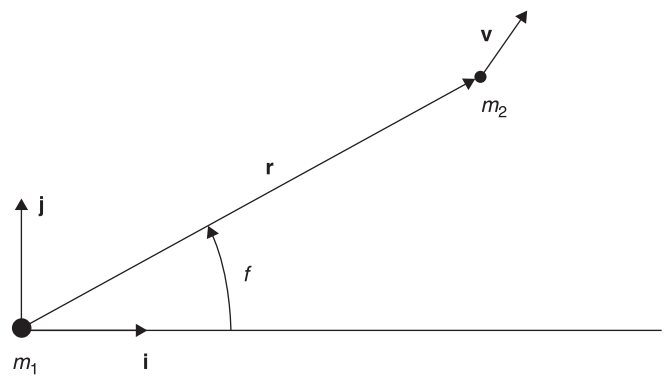

Key: m_1 and m_2, masses of the bodies; **i**, **j**, reference system; *f*, angular position of **r**.

Figure 3.2 Main parameters of an ellipse

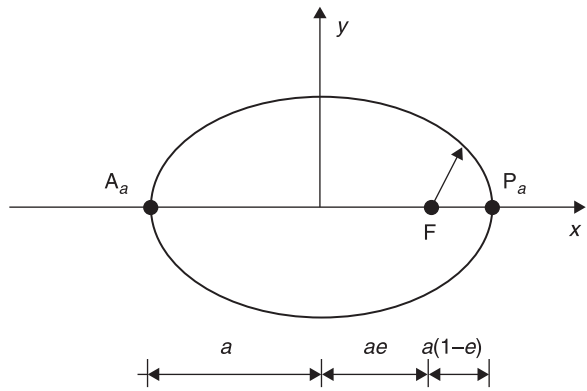

Key: A_a, apoapsis; P_a, periapsis; a, semi-major axis; F, focus; e, eccentricity.

Integration of (3.5) leads to

$$r = \frac{a(1-e^2)}{1+e\cos f}. \tag{3.6}$$

This equation represents a conic section, which can be classified by the value of the eccentricity e in the following curve types: ellipse ($0 \leq e < 1$), parabola ($e = 1$), and hyperbola ($e > 1$). A special case is $e = 0$ (circle). In the case of an ellipse, f is the angular position of **r**, so-called true anomaly, and a the semi-major axis. For more details see Roy (1988).

The point closest to the focus of the ellipse, the periapsis (P_a in Figure 3.2), appears at $f = 0$, at a distance $r = r_{Pa} = a(1 - e)$.

3.1.1 Characteristic velocities

Depending on the type of mission, the spacecraft must obtain a given energy level, or speed. These velocity levels are defined in terms of the so-called cosmonautic characteristic

velocities: circular velocity, escape (or parabolic) velocity, and hyperbolic velocity.

The circular velocity, $v_C = (\mu/r)^{1/2}$, is the speed of a body in a circular orbit at a distance $a = r$ from the primary. It is the speed that a spacecraft should travel at, in the direction perpendicular to the position vector (when the spacecraft is at a distance r from the primary), for the spacecraft to follow a circular orbit.

The escape (or parabolic) velocity, v_P, that a body has at a given distance r from the primary, is appropriate for following a parabolic trajectory. In this trajectory the body travels away from the primary towards the infinite, where its speed would be zero; that is, the body has the exact energy to escape from the gravitational field of the primary, $v_P = (2\mu/r)^{1/2} = 2^{1/2}v_C$. In the case of a body that has escaped from the terrestrial orbit, with regard to the Sun it can be considered that the body is moving along the same orbit as the Earth, at the same orbital speed, and close to the same orbital position, but outside the gravitational field of the Earth.

The hyperbolic velocity, v_H, is the speed of a body which follows a hyperbolic trajectory at a given distance from the primary. In this case, the body has energy greater than that necessary to escape from the gravitational field of the primary. Therefore, it does not only go very far from the primary, but it escapes from the orbit followed by the attracting body.

3.1.2 Orbit transfers

The transfer between orbits is the set of operations needed to change the orbit of a body from an initial to the final one. This change is performed by imposing on the body several impulsive actions. These impulsive actions are a modellization of the thrust generated by a rocket motor, which generally is a relatively large force, and of short duration.

Actually, the calculation of trajectories is greatly simplified if the thrust action is applied instantaneously; that is, the velocity vector is changed without a noticeable change in the position vector. Although this is not possible (the duration of the thrust during the firing of the rocket is finite, not infinitesimally small), if the thrust is large enough and the firing time short, this is a good approximation.

The simplest cases of orbit transfer are the in-plane Hohmann transfer, and the orbit plane inclination change.

Hohmann transfer

A body following an initial circular orbit, *I*, around a primary, *P*, can be placed in another circular final orbit, *F*, both in the same plane, by using an elliptical transfer orbit, *T*, or Hohmann transfer orbit, as shown in Figure 3.3.

To perform the transference, an impulse is given at the instant when the body reaches point A, which is translated into a velocity increment Δv_A in the instantaneous direction of motion. This velocity increment leads to an increase in body energy, changing its trajectory to the transfer ellipse *T*. Then, as it reaches point B, a second impulse is imparted to the body, in this case producing a velocity increment Δv_B, increasing the energy again, to obtain the circular velocity, corresponding to the radius of the final orbit.

This method can also be used to analyse the interplanetary transfer orbit of a spacecraft which has escaped from a planet in the solar system, travelling towards its capture by another planet.

Orbit plane inclination change

The orientation in space of the plane that contains the orbit can be changed by producing an impulse directed along the perpendicular to this plane. Thus, the final angular

Figure 3.3 Hohmann transfer

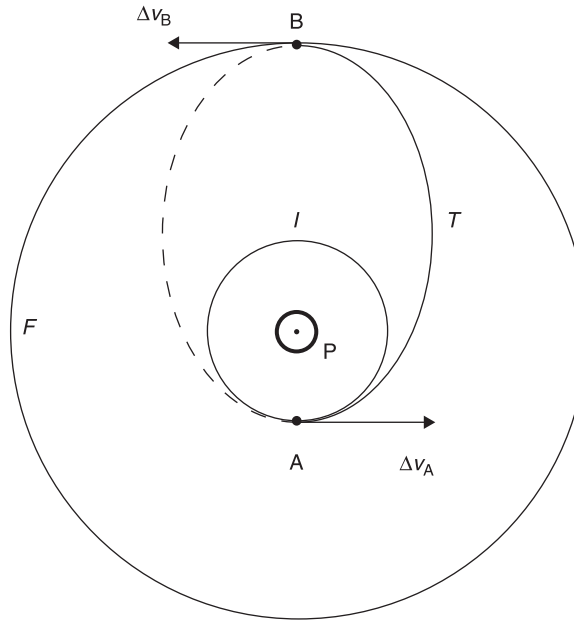

Key: *I*, initial orbit; *F*, final orbit; *T*, transfer orbit; Δv_A, Δv_B, impulsive velocity increments applied at points A, B, respectively; P, primary.

momentum $\mathbf{h}_F = \mathbf{r} \wedge (\mathbf{v} + \Delta\mathbf{v})$ will have a component perpendicular to the original orbit plane normal vector.

If the impulse only gives rise to a velocity increment contained in the orbit plane, it would not change the orientation of the angular momentum, which is the case of in-plane transfer manoeuvres.

As is shown in Figure 3.4, the change in the inclination of the orbit plane Δi consists of the rotation of the orbit plane around the axis defined by the spacecraft and the primary by an amount $\Delta i = \Delta v/v$ in the case $\Delta v << v$. As the velocity increment Δv needed to achieve a given inclination increment Δi is proportional to the spacecraft speed at the instant of the manoeuvre (firing of the rocket motor), this operation should be performed at the apoapsis (where the speed v is a minimum).

Figure 3.4 **Orbit plane inclination change Δi generated by an impulse $\Delta \mathbf{v}$ perpendicular to the initial orbit plane *I***

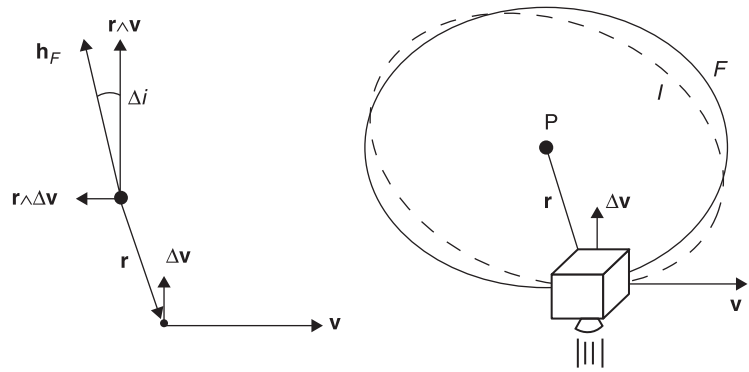

Key: *F*, final orbit; $\mathbf{h}_F$, angular momentum (perpendicular to the final orbit); **v**, initial velocity; **r**, position of the spacecraft with regard to the primary, P.

3.2 The orbit in space

When it is necessary to define the orbit and the position of a body along it, in space technology the description of the orbit as used in astronomy is usually employed. This is based on six quantities called the orbital elements. The first three (inclination, right ascension of ascending node and argument of periapsis) define the orientation of the orbit with regard to an inertial reference system; another two are the type and size of the orbit (given by the eccentricity and semi-major axis); and the last is the position of the body along the orbit (true anomaly).

The inclination, *i*, is the angle between the orbit plane and a reference plane, which contains the barycentre (Figure 3.5). The most often used reference planes in space technology are the equatorial plane for Earth-based missions, and the ecliptic (the plane of the orbit about the Sun) for interplanetary missions.

Figure 3.5 Orbital elements for an Earth's orbit

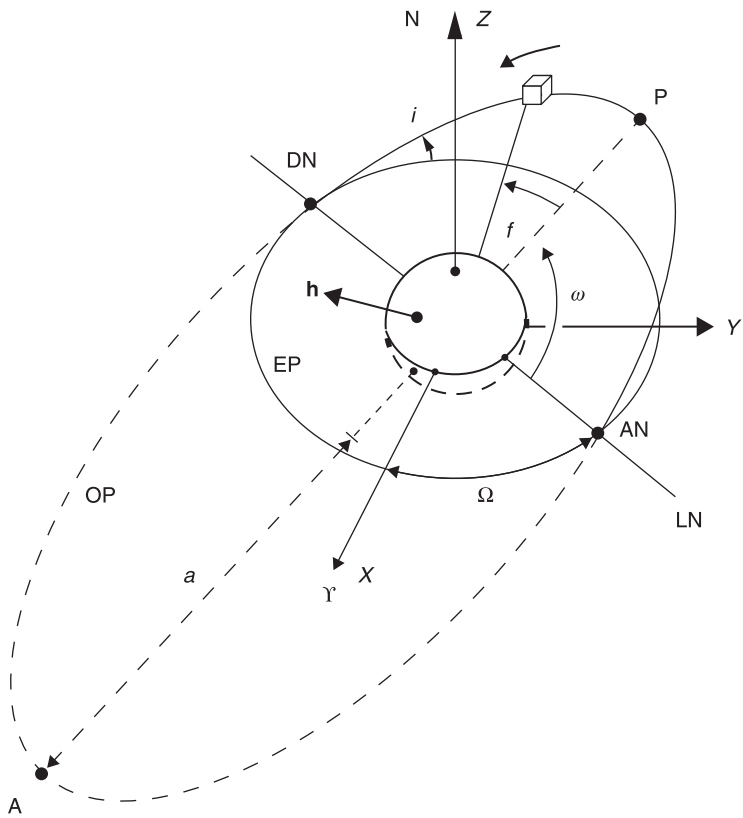

Key: EP, Earth's equator plane; N, North Pole; LN, line of nodes; AN, ascending node; DN, descending node; OP, orbit plane; P, perigee; A, apogee; *a*, ellipse semi-major axis; γ, vernal equinox; Ω, right ascension of the ascending node; ***i***, inclination; ω, argument of perigee; *f*, true anomaly; **h**, angular momentum, perpendicular to the orbit plane; *X, Y, Z,* inertial reference frame. The dashed segment of the orbit is below the equatorial plane.

The line of nodes is the intersection of the orbit plane and the reference plane, which goes through the centre of mass. In the case of an Earth satellite, the point of its orbit where the satellite crosses the equatorial plane going from south to north is called the ascending node. The

descending node is the opposite point in the line of nodes, where the satellite crosses the equatorial plane from north to south.

The right ascension of the ascending node, Ω, is the angle in the equator plane taken from the First Point of Aries γ to the ascending node of the orbit (in counter clockwise direction, or eastwards).

The ecliptic, as already said, is the plane that contains the orbit of the Earth about the Sun. The intersection of the ecliptic and the Earth's equator plane in the vernal equinox is the First Point of Aries, and the intersection angle is called the obliquity of the ecliptic, $\varepsilon_E = 23°\,27'$.

The rotation of the orbit within the orbital plane is measured by the argument of perigee, ω, which is the angle at the Earth from the ascending node to perigee. The position of a satellite in orbit is given by the true anomaly, f, which is the angle at the Earth measured between the perigee point and the satellite.

The accurate description of the trajectory of a satellite (or of some of its characteristics) as required for some applications, can be quite a challenging problem because it may require the use of methods more sophisticated than the Keplerian orbits. However, it is possible to cover the needs of most of the accuracy requirements in the mission design process by using approximate methods based on the assumption that the satellite trajectories can be considered Keplerian orbits whose elements change as a result of additional perturbations. This change over time is produced by the actions not fully covered by the usual assumptions considered by Keplerian orbit modellization (e.g. gravitational interaction with additional bodies, the lack of sphericity or homogeneity of the primary, additional non-gravitational actions such as radiation pressure, residual atmospheric drag, etc. . . .).

3.3 Orbit perturbations

Orbit perturbations are the deviations of the true orbit from the reference orbit due to several reasons. The main causes are: non-gravitational forces, third-body interactions, and non-homogeneous mass distributions or non-spherical shape (non-spherical mass distributions).

3.3.1 Non-gravitational forces

Non-gravitational forces are:

- Aerodynamic forces (drag atmospheric friction, opposite to the velocity vector, and lift, perpendicular to the velocity vector). They are proportional to the density, and therefore more relevant in low Earth Orbits, at the perigee, as density decreases exponentially with altitude. This effect (mainly drag) reduces the energy of the orbit and therefore produces the reduction of the apogee height, reducing the eccentricity (orbital decay). The atmospheric density fluctuates considerably depending on solar activity, and therefore the estimations of the spacecraft lifetimes are only approximations, whose margin of error can be wide (between 10% and 50%).
- Drag due to solar wind.
- Solar radiation pressure (important for spacecraft with large solar panels).
- Drag due to the interaction of induced current at the spacecraft and the Earth's magnetic field (only significant in case of tethers), which could be useful in the future to remove spacecraft from Earth orbits.

3.3.2 Non-spherical mass distributions

The shape of the Earth can be approximated by an oblate spheroid, as would be formed by a rotating fluid, with smaller deviations from this oblate shape.

The effects of oblateness over short times (short period variations, which affects the semi-major axis, a, eccentricity, e, and inclination, i) average to zero over an orbit. The long-term effects produce cumulative secular variations in the line of nodes (the right ascensions of ascending nodes), the line of apsides (the argument of perigee), and the mean angular motion.

The regression of the line of nodes can be used to change the orientation of the orbit one rotation per year in the inertial reference frame, an amount of 0.986 degrees/day in such a way that the orientation of the orbit plane remains fixed relative to the Sun (Sun-synchronous orbits).

The regression of the line of apsides, or secular variation of the argument of perigee, ω, obviously applies to orbits with $e \neq 0$ (non-circular). It is positive for equatorial orbits (it rotates in the direction of motion), is negative for polar orbits (it rotates in the opposite direction of motion), and at $i = 63.4°$ it becomes zero, and therefore it remains fixed. This property has applications such as in the so-called Molniya orbits.

These interactions decrease as orbit altitude increases.

3.3.3 Interactions with third bodies

For an Earth satellite, as the distance from the Earth increases, the perturbations coming from the Earth's oblateness decreases, and the gravitational forces of the Sun and the Moon start to become dominant. In some cases the influence is so great that it defines the motion, as is the case with

satellites placed in the Lagrange libration points (where the gravity effects of the bodies forming the system are compensated). In satellite applications, these interactions mainly affect satellites in geostationary orbits.

3.4 Lighting conditions

Of particular interest for thermal control are the situations where spacecraft are illuminated by the Sun or affected by eclipse conditions. In Figure 3.6 these situations are shown. To define the different concepts involved, the relative positions of the planet, the observer, and the spacecraft, have to be taken into account. Thus, transit refers to the case when the observer sees the satellite pass in front of the disc of the planet, and occultation when it passes behind the disc of the planet.

Figure 3.6 **Definition of the shadows of the planets in the solar system**

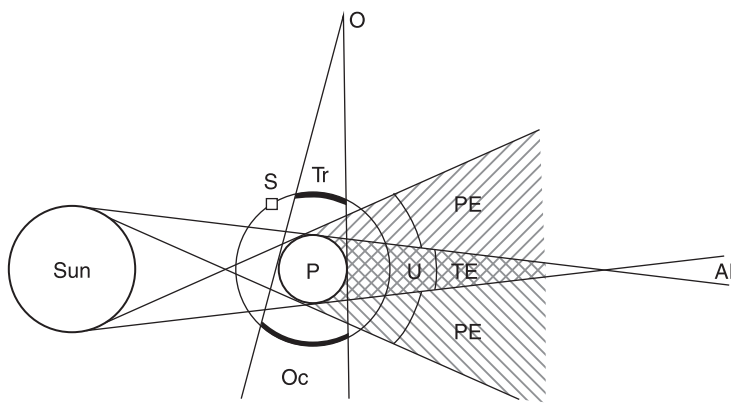

Key: P, planet; S, satellite; O, observer; Tr, transit; Oc, occultation; U, umbra; TE, total eclipse; PE, partial eclipse; AE, annular eclipse.

The shape of the shadows of the planets in the solar system can be sketched as shown in Figure 3.6. Due to the relative size of the objects in the solar system (the Sun is the largest object) it produces a conical region behind the planet, called the umbra, where the Sun cannot be seen, because the planet completely blocks the view. Around the umbra, only a portion of the Sun view is blocked and the illumination on objects is reduced with regard to the full Sun illumination.

3.5 Types of orbits

Several typical orbits can be considered.

Low Earth orbit (LEO) sun-synchronous orbit. The orbit plane maintains the orientation with regard to the Sun as the Earth moves in its orbit; at a given point on the Earth's surface the pass of the satellite is always at the same hour of the day (same local time). In this way, lighting conditions will be nearly the same, at a given point, which allows changes in surface features to be identified. The inclination of the orbit (for circular orbits) and altitudes between 400 km and 1000 km, is in the range of 97° to 99°. Therefore, they are also quasi polar orbits, which allow the whole surface of the Earth to be covered, even passing several times a day over the same point.

One particular parameter, which is very useful for the thermal analysis of a spacecraft, mainly in low Earth orbits, is the so-called orbit beta angle, β (Figure 3.7), which describes the relative orientation of the orbit with regard to the Sun, and is defined as the minimum angle between the orbit plane and the solar vector.

When $\beta = 90°$ (dawn/dusk orbit), the orbit plane is placed perpendicular to the Sun's rays, and there are no eclipses, regardless of the altitude. The albedo loads are near zero.

Figure 3.7 **Orbit orientation with regard to the Sun**

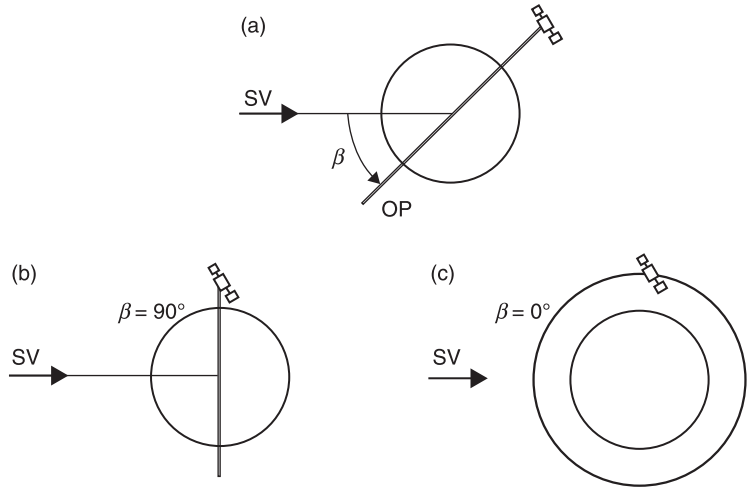

Key: β, orbit beta angle; SV, solar vector; OP, orbit plane. (a) definition, (b) polar orbit (dawn/dusk injection), (c) polar orbit (local noon or midnight injection).

This configuration is very advantageous from the point of view of the power subsystem, due to the absence of eclipses (reduced need for batteries) and reduced aerodynamic drag (solar panels oriented along the direction of the motion). But it is not appropriate for visible light Earth observation because shadows of the objects (mountains, trees, etc.) are too long.

When $\beta = 0°$ (local noon or local midnight), the orbit plane is parallel to the direction of solar rays and the orbit appears edgewise to the Sun. The subsatellite point passes over the sub-solar point on the Earth, which has several implications. From the thermal design point of view, on the one hand, albedo loads are greatest, but, on the other hand, the longest eclipses periods happen (the orbit passes through the shadow of the full diameter of the Earth). From the observation point of view, shadows can be very short (which leads to images with low definition), and also the sensors may experience specular reflections from seas and oceans.

The choice of orbit is the result of a trade-off in which these factors are taken into account, and finally, a compromise is adopted.

Molniya orbits (Subsection 3.3.2). They are highly elliptical (perigee altitude 500 km, apogee 38 900 km) with the appropriate inclination (i = 62°) to avoid the regression of apoapsis (thus maintaining the apogee at the most northerly position possible with regard to the Earth), providing good coverage of the northern hemisphere, including polar regions (which are not observable from the geostationary orbit). Also, as the satellite travels at low speed near the apogee, it maintains a good view of the polar region about 8 hours out of 12, which is the orbit period. Continuous coverage of the northern hemisphere can be obtained by using three satellites, organized in a constellation, much in the same way as in the case of geostationary orbits.

Geostationary orbit. The geostationary orbit was first proposed by Arthur C. Clarke in 1945. Its main characteristic is that the subsatellite point remains fixed in longitude (with null latitude), and therefore, it does not need dynamic tracking from ground stations. That is, communications can be maintained with antennae pointing in a fixed direction. This characteristic is achieved by choosing the altitude of the orbit in such a way that the period of the orbit coincides with the Earth's sidereal rotation period, semi-major axis a = 42 200 km, eccentricity close to zero to keep the motion of the satellite along the orbit constant, and in the equatorial plane to avoid latitude changes. In this way, a satellite placed in the geostationary orbit can provide communications between any points placed in the beam of its antennae. With a constellation of three satellites placed in the geostationary orbit, global communications coverage can be supplied.

The mission to be accomplished determines the orbit or trajectory of the spacecraft. It should be recalled that one of the main reasons for space missions is the privileged spatial position with regard to a planet's surface (concerning observation, remote sensing, communications) which allows global coverage, at a relatively low cost, and with relatively little infrastructure. Therefore, the orbit plays a crucial role.

However, a large number of scientific missions are not accounted for in the previous paragraphs since their aims are more widely distributed, and, generally speaking, the requirements imposed on the orbit design are also very mission-specific.

As is generally accepted, the relationship between missions and type of orbits employed can be summarized as in Table 3.1. It should be noted that the type of orbit required to accomplish a given mission has a large influence on the spacecraft design, as is explained in Chapter 1.

Table 3.1 **Mission and type of orbit**

Mission	Type of orbit
Astronomy	Several orbits
Climate, weather forecast	LEO, GEO
Communications	GEO (low latitude), Molniya (high latitude)
Earth observation	GEO, LEO, global coverage
Global positioning, navigation	LEO, MEO, global coverage
Military	Several LEO orbits
Space environment	Several, including sounding rockets
Space station	LEO
Technology development	Several orbits

Note: Low Earth orbit (LEO), medium altitude Earth orbit (MEO), geostationary orbit (GEO).

In the case of the geostationary orbit, the propulsive requirements derived from the need to reach a high-altitude orbit are very restrictive, leading to a dry mass (spacecraft without propellant) which is a modest fraction of the total spacecraft mass. This situation enforces the design towards a minimization of mass, leading to a configuration which is only appropriate in a short range of parameters, or, which is the same thing, a narrow range of possibilities for the payloads (and therefore of missions).

The large distance between the spacecraft and the ground station implies that communications require relatively high power. Although, as the spacecraft is continuously in view from the ground station, the health of the spacecraft and the status of the mission can be continuously monitored, thus reducing the need for spacecraft autonomy and the complexity of the data handling system.

Low Earth orbit missions are quite different. Communications with the spacecraft are more complex due to the intermittent nature of the contacts with the ground station. The power subsystems for these missions are also very different. The main characteristic is the fraction of time that the spacecraft spends in eclipse and in illumination periods. In Low Earth orbits, the eclipse fraction is large, and therefore the solar panels should be oversized to charge the batteries for the energy needed during the eclipse duration, and the number of charge/discharge cycles to be performed every day requires the oversizing of the batteries (to allow for a low depth of discharge).

In the case of geostationary orbits, there are eclipse periods only during a small part of the year and during relative short eclipse times (less than 70 min.) but the depth of discharge should be large.

A detailed description of the thermal control design in the case of a satellite for geostationary orbit can be found in Agrawal (1996).

3.6 References

Agrawal, B. (1996) *Design of Geosynchronous Spacecraft*, Prentice Hall, Englewood Cliffs, New Jersey, USA.

Roy, A.E. (1988) *Orbital Motion*, Adam Hilger, Bristol, UK.

4

Conductive heat transfer

Abstract: This chapter summarizes the basics of heat conduction necessary to understand and apply the heat balance equation to a space vehicle. Starting from the one-dimensional steady-state case, Fourier's law and the heat diffusion equation for an elemental volume are written for the three main coordinate systems: Cartesian, cylindrical and spherical. The main physical property related to heat conduction, the thermal conductivity, is defined and its values for space-used materials are presented.

Key words: Fourier's law, thermal conductivity, conductive shape factor.

4.1 Introduction

In this chapter and in the following, some basic concepts about heat conduction and thermal radiation heat transfer are presented. The aim of this short review is to make the reader familiar with the concepts and notation that will be used in the following chapters. For more detailed information about heat transfer in general, a number of general text books on heat transfer, such as Incropera et al. (2007), Holman (2010), Çengel (2007), etc. are available in the literature. For more specific information about thermal radiation, the reader is referred to Howell et al. (2011) and Modest (2003).

4.2 Fourier's law

Heat conduction is the transfer of thermal energy between regions of matter due to a temperature gradient. The physical mechanism is related to the transfer of free electrons from areas with higher energy (higher temperature) to areas with lower energy (lower temperature) and to lattice vibration. Thus, heat conduction requires the presence of matter; it is not possible in a vacuum, and also takes place within fluids: liquids and gases.

The equation that governs heat conduction is Fourier's law. It allows the calculation of heat fluxes for a given temperature field. Temperatures are calculated from the principle of energy conservation.

Fourier's law is an empirical law derived from experimental evidence and observation. Consider a wall of thickness Δx and area A, as shown in Figure 4.1. Let the temperature be uniform over the area A on both wall surfaces. Assume that

Figure 4.1 **One-dimensional heat conduction, $\dot{Q}$, across a solid wall of thickness, Δx, whose surfaces are at temperatures T_1 and T_2 ($T_1 > T_2$), respectively**

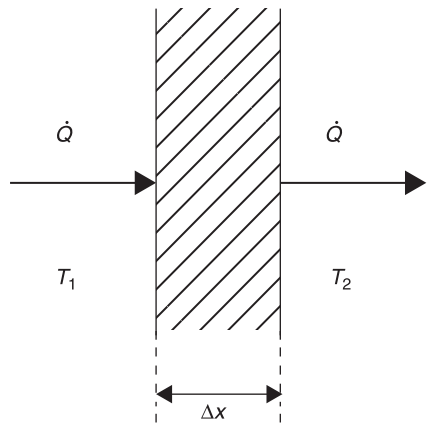

the temperature on the left face of the wall is higher than on the right face.

Fourier's law states that the rate of heat flux, $\dot{Q}$, through a uniform material is directly proportional to the area of heat transfer and to the temperature difference, ΔT, in the direction of heat flux, and is inversely proportional to the length of the path flow, Δx. Thus,

$$\dot{Q} \propto A\frac{\Delta T}{\Delta x}. \tag{4.1}$$

The constant of proportionality is the so-called thermal conductivity. Hence,

$$\dot{Q} = kA\frac{\Delta T}{\Delta x}. \tag{4.2}$$

Thermal conductivity, k, is a physical property, a characteristic of the materials, which measures how fast heat flows in the materials. It is measured in W/(m·K) in SI units.

Thermal conductivity of different materials varies over a wide range. Thus, there are up to four orders of magnitude of difference between the thermal conductivity of gases and that of conductive metals. Table 4.1 shows a list of thermal conductivities for several materials used in space applications.

Evaluating equation (4.2) in the limit $\Delta x \to 0$, the heat rate is given by

$$\dot{Q} = -kA\frac{\mathrm{d}T}{\mathrm{d}x}. \tag{4.3}$$

Note that the negative sign in the previous equation indicates that the transfer of heat occurs from higher to lower temperatures. Differentiating equation (4.3) with respect to the area gives the heat flux density or the heat flux per unit of time and area, q, whose SI units are W/m^2:

$$q = -k\frac{\mathrm{d}T}{\mathrm{d}x}. \tag{4.4}$$

Table 4.1 **Thermal conductivity, k, of various materials of space use at room temperature**

Group	Material	Chemical composition	k [W/(m·K)]
Aluminium and Al alloys	Aluminium (ISO Al 99.5)	99.5% Al	230
	Aluminium-copper alloy (ISO AlCu4Mg1)	4.5% Cu, 1.5% Mg, 0.6% Mn, remaining Al	150 to 180
	Aluminium-magnesium alloy (ISO AlMg2)	1.7% to 2.4% Mg, remaining Al	155
	Aluminium-magnesium-silicon alloy (ISO AlMgSi)	0.4% to 0.9% Mg, 0.3% to 0.7% Si, remaining Al	197 to 201
	Aluminium-zinc alloy 7075	5.6% Zn, 2.5% Mg, 1.6% Cu, 0.3% Cr, remaining Al	134
	2219 Aluminium-copper-manganese alloy (ISO AlCu6Mn)	Cu 5.8% to 6.8%, Mn 0.2% to 0.4%, remaining Al	116 to 170
Copper and Cu alloys	Copper (Oxygen-Free High-Conductivity, OFHC)	99.95% Cu	394
	Beryllium-copper (CDA 170)	1.8% Be, 0.3% Co + Ni, remaining Cu	84 to 150
	Brass (α-β) leaded	40% Zn, 2% Pb, remaining Cu	117
	Phosphor bronze (CDA 510)	5% Sn, 0.2% P, remaining Cu	75
Titanium and Ti alloys	Timetal 35A (IMI 115)	Commercially pure Ti	16
	Ti 6Al 4V (IMI 318)	6% Al, 4% V, remaining Ti	6
	Ti 4Al 4Mo – Si (IMI 550)	4% Al, 4% Mo, 2% Sn, 0.5% Si remaining Ti	8

Stainless steels	Stainless steel A286	25% Ni, 15% Cr, 2% Ti, 1.5% Mn, 1.3% Mo, 0.3% V, remaining Fe	23.7
	Stainless steel AISI 304L	8% to 12% Ni, 18% to 20% Cr, 2% Mn max, 1% Si max, 0.03% C max, remaining Fe	16.2
	Stainless steel AISI 316L	12% Ni, 17% Cr, 2.5% Mo, 2% Mn, 1% Si, 0.03% C max, remaining Fe	16
Miscellaneous metallic materials	Magnesium-aluminium-zinc alloy	8.5% Al, 0.5% Zn, remaining Mg	90
	Magnesium-aluminium-zinc-manganese alloy	3% Al, 1% Zn, 0.2% Mn, remaining Mg	84
Adhesives, coatings and varnishes	Araldite AV138/ HV998 (100/40 pbw)	Epoxy	0.35
	D.C. 93500	Silicone	0.146
	Eccobond 'solder' 56C	Epoxy-silver-loaded	5.8
	RTV S 691	Silicone, filled	0.39
	RTV S 695	Silicone	0.21
	Epo-tek 930	2-part epoxy, boron nitride filled	4.1
Potting compounds, sealants and foams	D.C. 340	Silicone compound, filled	0.55
	RTV 566	Silicone (methyl, phenyl)	0.3
	Stycast 1090	Epoxy	0.167
	Stycast 2850FT	Epoxy	1.44
	Upilex foam	Polyimide	0.03
Reinforced plastics	Makrolon GV 30	Polycarbonate/glass	0.16

(*Continued*)

Table 4.1 **Thermal conductivity, *k*, of various materials of space use at room temperature (*Continued*)**

Group	Material	Chemical composition	*k* [W/(m·K)]
Rubbers and elastomers	Eccoshield SV-R	Metal-filled silicone	4.3
Thermoplastics (non-adhesive tapes and foils [MLI])	Sheldahl 146368	Fluorocarbon (FEP), silver and Inconel coated	0.194
	Sheldahl 146372	Fluorocarbon (FEP), aluminized	0.194
	Sheldahl 146633	Polyimide Kapton HN, aluminium and ITO coated	0.155
	Sheldahl G423020	Fluorocarbon (FEP), aluminized and ITO coated	0.194
	Dunmore DE291	Polyimide (Kapton HN), aluminized with protective coating on both sides	0.028
	Dunmore DM100	Polyimide (Kapton HN), aluminized/acrylic adhesive	0.0155
	Dunmore DE 028	Polyethylene terephthalate/PETP, aluminized	0.61
	Dunmore DE 320	Polyimide (Kapton HN), aluminized	0.155
	Dunmore TM05564	Fluorocarbon (FEP–Type C), aluminized	0.194
	Kapton H, HN	Polyimide	0.155
	Hostaform C9021	Acetal copolymer	0.31
	PETP (Mylar, Melinex, Terphane, . . .)	Polyethylene terephthalate	0.61

	PTFE (Teflon, Halon, Fluon, Hostaflon)	Polytetrafluoroethylene	0.25
	Sheldahl 146401 (previously G401500)	Fluorocarbon (FEP), silver and Inconel coated	0.194
	Sheldahl 146383 (previously G400900)	Fluorocarbon (FEP), aluminized	0.194
	Sheldahl 146631 (previously G425120)	Polyimide (Kapton H), ITO/aluminized	0.155
	UPILEX S	Polyimide	0.29
Thermoset plastics	Rexolite 1422	Polystyrene, cross-linked	0.146

Source: after ECSS-Q-70-71A rev. 1 (2004).

Fourier's law has been introduced under restricted and simplified conditions (one-dimensional, steady-state conduction in a plane wall). Therefore, the temperature distribution can straightforwardly be deduced to be linear. However, Fourier's law also applies to multidimensional and transient conduction in complex geometries. In these cases, the temperature field is not evident. Thus, a more general form of Fourier's law for a three-dimensional case can be written as:

$$\mathbf{q} = -k\nabla T = q_x\mathbf{u}_x + q_y\mathbf{u}_y + q_z\mathbf{u}_z =$$

$$-k\left(\frac{\partial T}{\partial x}\mathbf{u}_x + \frac{\partial T}{\partial y}\mathbf{u}_y + \frac{\partial T}{\partial z}\mathbf{u}_z\right), \tag{4.5}$$

where $\mathbf{u}_x$, $\mathbf{u}_y$, $\mathbf{u}_z$ are unit vectors of a Cartesian reference frame. Note that the heat flux, $\mathbf{q}$, is a vector quantity, and $T(x,y,z)$ is the scalar temperature field. It is implicit in

equation (4.5) that the heat flux vector **q** is perpendicular to the isothermal surfaces.

Coming back to the one-dimensional case, sometimes, mainly in the field of thermal modelling, it is useful to write Fourier's law in terms of the thermal resistance, R_{th}, measured in K/W in SI units, a magnitude that depends not only on the material but also on the geometry. It is defined as $R_{th} = d/(k \cdot A)$, in this case d being the heat path length, and A the area of heat flux. Insertion of this definition in equation (4.2) yields

$$\dot{Q} = \frac{\Delta T}{R_{th}}. \tag{4.6}$$

This means that a heat flux $\dot{Q}$ can be analysed in a similar way to an electric current. In Ohm's law, $\dot{Q}$ is equivalent to the intensity, the temperature difference ΔT corresponds to the electrical voltage, and the thermal resistance R_{th} to the electrical resistance.

4.3 The heat diffusion equation

Fourier's law described in the previous section allows the heat fluxes for a given temperature field to be calculated. However, one of the major objectives in a conduction analysis is to determine the temperature field in a domain, as a result of the conditions imposed on its boundaries. Heat fluxes would then be calculated from this temperature field.

To do this, the energy balance equation is applied to a differential element. In the following, this is done for the three most common systems of coordinates: Cartesian, cylindrical and spherical.

4.3.1 Cartesian coordinates

The energy balance equation for an elemental volume, such as the one depicted in Figure 4.2 is (Incropera et al., 2007):

$$\frac{\partial}{\partial x}\left(k\frac{\partial T}{\partial x}\right)+\frac{\partial}{\partial y}\left(k\frac{\partial T}{\partial y}\right)+\frac{\partial}{\partial z}\left(k\frac{\partial T}{\partial z}\right)+\dot{q}_v=\rho c_p\frac{\partial T}{\partial t}, \qquad (4.7)$$

where $\dot{q}_v$ is the rate at which energy is generated per unit volume of the medium and $\rho c_p \partial T/\partial t = \dot{E}_v$ is the time rate of change of the internal energy of the medium per unit volume, where ρ is the medium density and c_p the specific heat. If the thermal conductivity is constant, equation (4.7) can be simplified and written in the form

$$\frac{\partial^2 T}{\partial x^2}+\frac{\partial^2 T}{\partial y^2}+\frac{\partial^2 T}{\partial z^2}+\frac{\dot{q}}{k}=\frac{1}{\alpha}\frac{\partial T}{\partial t}, \qquad (4.8)$$

where $\alpha = k/(\rho c_p)$ is the thermal diffusivity. Other

Figure 4.2 Differential element for energy equation in Cartesian coordinates

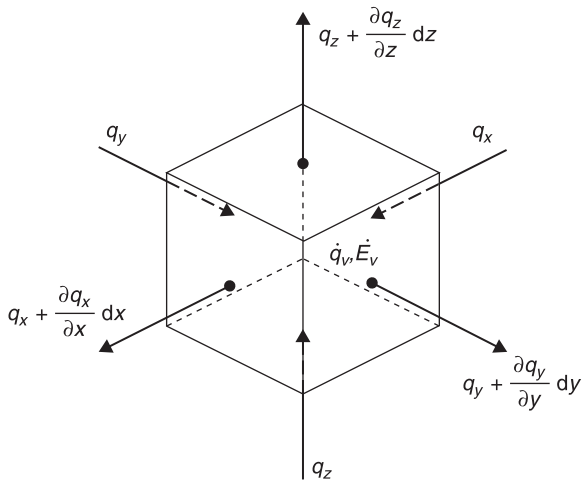

simplifications can be obtained if equation (4.7) is written for the steady-state case. Hence,

$$\frac{\partial}{\partial x}\left(k\frac{\partial T}{\partial x}\right)+\frac{\partial}{\partial y}\left(k\frac{\partial T}{\partial y}\right)+\frac{\partial}{\partial z}\left(k\frac{\partial T}{\partial z}\right)+\dot{q}_v=0. \tag{4.9}$$

4.3.2 Cylindrical coordinates

When the operator ∇ of equation (4.5) is expressed in cylindrical coordinates, the general form of Fourier's law is

$$\mathbf{q}=-k\nabla T=q_r\mathbf{u}_r+q_\phi\mathbf{u}_\phi+q_z\mathbf{u}_z=$$
$$-k\left(\frac{\partial T}{\partial r}\mathbf{u}_r+\frac{1}{r}\frac{\partial T}{\partial \phi}\mathbf{u}_\phi+\frac{\partial T}{\partial z}\mathbf{u}_z\right), \tag{4.10}$$

where $\mathbf{u}_r$, $\mathbf{u}_\varphi$, $\mathbf{u}_z$ are unit vectors of the cylindrical reference frame. The heat diffusion equation obtained from the energy balance applied to a differential element is

$$\frac{1}{r}\frac{\partial}{\partial r}\left(kr\frac{\partial T}{\partial r}\right)+\frac{1}{r^2}\frac{\partial}{\partial \phi}\left(k\frac{\partial T}{\partial \phi}\right)+\frac{\partial}{\partial z}\left(k\frac{\partial T}{\partial z}\right)+\dot{q}_v=\rho c_p\frac{\partial T}{\partial t}. \tag{4.11}$$

4.3.3 Spherical coordinates

Fourier's law for the spherical coordinates is

$$\mathbf{q}=-k\nabla T=q_r\mathbf{u}_r+q_\theta\mathbf{u}_\theta+q_\phi\mathbf{u}_\phi=$$
$$-k\left(\frac{\partial T}{\partial r}\mathbf{u}_r+\frac{1}{r}\frac{\partial T}{\partial \theta}\mathbf{u}_\theta+\frac{1}{r\sin\theta}\frac{\partial T}{\partial \phi}\mathbf{u}_\phi\right), \tag{4.12}$$

where $\mathbf{u}_r$, $\mathbf{u}_\theta$, $\mathbf{u}_\phi$ are unit vectors of the spherical reference frame. From the energy balance applied to a differential element the following general form of the heat equation is obtained:

$$\frac{1}{r^2}\frac{\partial}{\partial r}\left(kr^2\frac{\partial T}{\partial r}\right)+\frac{1}{r^2\sin^2\theta}\frac{\partial}{\partial \phi}\left(k\frac{\partial T}{\partial \phi}\right)+ \frac{1}{r^2\sin\theta}\frac{\partial}{\partial \theta}\left(k\sin\theta\frac{\partial T}{\partial \theta}\right)+\dot{q}_v=\rho c_p\frac{\partial T}{\partial t}. \tag{4.13}$$

4.4 Boundary and initial conditions

To determine the temperature field in a medium it is necessary to solve the heat diffusion equation, written here for different coordinate systems (equations (4.7), (4.11) and (4.13)). To do this, it is necessary to know some physical conditions on the boundaries. These can be given as temperatures, heat fluxes, or a combination of both. If the problem is time dependent, conditions existing in the medium at some initial time also have to be provided. Mathematically, the heat diffusion equation is a differential equation that requires integration constants in order to have a unique solution. Boundary conditions are in fact the mathematical expressions or numerical values necessary for this integration.

4.5 Conductive shape factors

In two- or three-dimensional conduction problems where only two temperature levels are involved, a conduction shape factor can be defined in such a way that the heat transfer rate may be expressed as

$$\dot{Q}=Sk\Delta T. \tag{4.14}$$

The conduction shape factor S has been obtained analytically for numerous two- and three-dimensional systems. The values can be found in Holman (2010) for some simple configurations.

4.6 Numerical methods in heat conduction

The equations shown in the previous sections can be solved by analytical methods only in certain particular cases. These solutions are available in the literature for different geometries. When it is not possible to obtain an exact mathematical solution, the best alternative is often to use numerical techniques. As explained in Chapter 19, numerical solutions allow temperature determination only at discrete points of a system, unlike analytical solutions, which allow the temperature field to be known all over the medium. The most widely used numerical methods for heat conduction are the finite-difference, finite-element, and boundary-element methods. For thermal control purposes, lumped capacitance models are used. To apply numerical methods, the system has to be divided into regions where temperature is assumed to be uniform, the temperature value being the average temperature of the region. Generally, in order to assign properties, the centres of these regions are used as reference points, which are called nodes. The meshing of the system,

Figure 4.3 **Example of mesh and node distribution in a typical discretization of a satellite surface for a preliminary thermal control analysis (the nodes are indicated by black dots)**

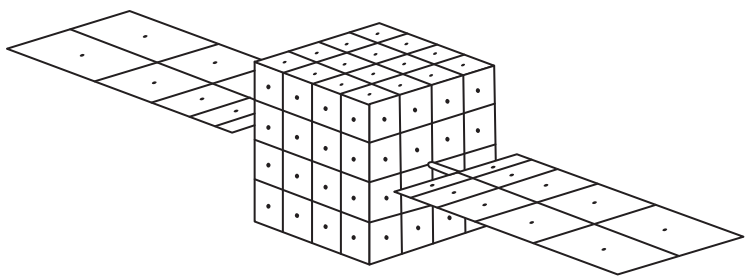

that is, selection of nodes, is done arbitrarily. The accuracy of the calculations depends strongly on the number of nodes, their sizes, and their locations. The higher the number of nodes, the more accurate the results, but the procedure is more time consuming. Figure 4.3 shows a typical discretization of a satellite surface with the nodes indicated on it.

4.7 References

Çengel, Y.A (2007) *Heat and Mass Transfer: A Practical Approach*, McGraw-Hill, New York, USA.

ECSS-Q-70-71A rev. 1 (2004) *Space product assurance. Data for selection of space materials and processes*, ESA Publications Division, ESTEC, Noordwijk, The Netherlands, June 2004.

Holman, J. (2010) *Heat Transfer*, McGraw-Hill, New York, USA.

Howell, J.R., Siegel, R. and Menguc, M.P. (2011) *Thermal Radiation Heat Transfer*, CRC Press, Boca Raton, Florida, USA.

Incropera, F.P., DeWitt, D.P., Bergman, L.T. and Lavine, A.S. (2007) *Fundamentals of Heat and Mass Transfer*, John Wiley and Sons, New York, USA.

Modest, M.F. (2003) *Radiative Heat Transfer*, Academic Press, Amsterdam, The Netherlands.

5

Thermal radiation heat transfer

Abstract: This chapter presents the basics of thermal radiation necessary for the thermal modelling of spacecraft. The nature of thermal radiation is briefly described while the concept of blackbody and the Planck's distribution, describing the spectral emissive power of a blackbody, are presented. The thermo-optical properties of a surface, emissivity, absorptance, transmittance and reflectance, are defined, and the equations necessary to determine the radiation exchange between diffuse, grey surfaces are obtained and written in terms of thermal resistances to apply the electrical analogy.

Key words: Planck's distribution, emissive power, irradiation, radiosity, blackbody, emissivity, absorptance, transmittance, reflectance, view factor.

5.1 Nature of thermal radiation

Thermal radiation is electromagnetic radiation emitted from all matter that is at a non-zero temperature in the wavelength range from 0.1 μm to 100 μm. It includes part of the ultraviolet (UV), and all of the visible and infrared (IR). It is called thermal radiation because it is caused by and affects the thermal state of matter. Figure 5.1 shows the regions of the electromagnetic spectrum with the thermal radiation range indicated on it. The spectrum of the solar irradiation can be found in Figure 2.2.

Figure 5.1 **Electromagnetic spectrum classification according to radiation wavelength λ, showing the wavelength range corresponding to thermal radiation**

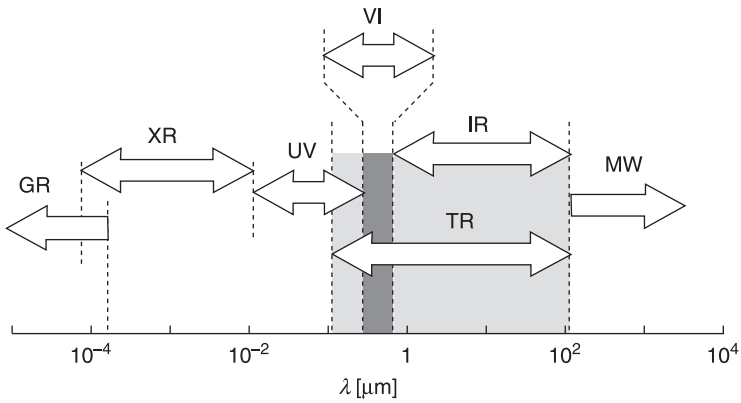

Key: GR, gamma rays; XR, X-rays; UV, ultraviolet; VI, visible; IR, infrared; TR, thermal radiation; MW, microwaves.

Thermal radiation does not require a material medium for its propagation. Although in the context of spacecraft thermal design the interest of radiation is mainly focused on solid surfaces, emission may also occur from liquids and gases. The mechanism of radiation emission is related to energy released as a result of oscillations or transitions of the electrons that constitute matter. These oscillations are sustained by internal energy, and therefore, the temperature of the matter.

All forms of matter emit radiation as they are at a non-zero temperature. For gases and semi-transparent matter, thermal radiation is a volumetric phenomenon. This can be of interest when studying the behaviour of lenses, for instance, as part of optical devices.

Since thermal radiation is electromagnetic radiation, the properties of the propagation of electromagnetic waves can be applied. The most relevant ones are the frequency ν and

the wavelength λ, which are related through $\lambda = c/\nu$, where c is the speed of light in the medium. In the case of propagation in a vacuum, $c = c_o = 2.998 \times 10^8$ m/s.

The spectral nature of thermal radiation is one of two features that make its study quite complex. The second feature is related to its directionality. A surface may have certain directions with preferential emission; therefore the distribution of the emitted radiation is directional. When the radiative properties do not depend on the direction, the surface is termed diffuse.

As already said, all surfaces emit thermal radiation. This emitted radiation will strike other surfaces and will be partially reflected, partially absorbed, and partially transmitted. Figure 5.2 shows the different thermal radiation interactions on a body's surface. The symbol Φ in the figure stands for the radiant energy per unit time, measured in W in the SI system. As can be seen, the surface emits Φ_e, receives the incident radiation Φ_i, out of which Φ_a is absorbed, Φ_r is reflected and Φ_t is transmitted.

Figure 5.2 Thermal radiation interactions on a surface

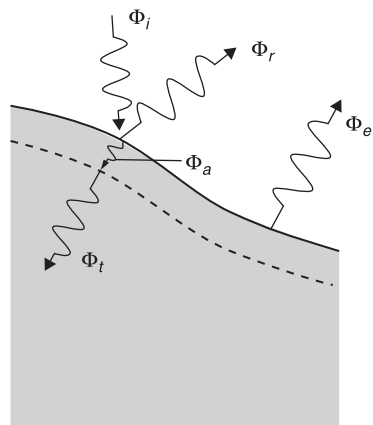

Key: Φ_e, emitted radiation; Φ_i, incident radiation; Φ_a, absorbed radiation; Φ_r, reflected radiation; and Φ_t, transmitted radiation.

The intensity of emitted radiation, $I_{\lambda,e,}$ is defined as the rate at which radiant energy, $\delta\dot{Q}$, is emitted at the wavelength λ in the (θ,ϕ) direction, per unit area of the emitting surface normal to this direction, per unit solid angle $d\omega$ about this direction, and per unit wavelength interval $d\lambda$ about λ, as indicated in Figure 5.3. Thus, the spectral intensity is

$$I_{\lambda,e}(\lambda,\theta,\phi,T) = \frac{\delta\dot{Q}}{dA\cos\theta d\omega d\lambda}. \tag{5.1}$$

In order to obtain the thermal interactions in all directions and wavelengths the intensity of radiation is successively integrated. Thus, the spectral hemispherical emissive power E_λ, measured in W/(m^2·μm) in the SI, is the rate at which radiation of wavelength λ is emitted in all directions from a

Figure 5.3 **Intensity of emitted radiation, $I_{\lambda,e}$, in the (θ,ϕ) direction. dA is the emitting differential area (contained in the xy plane), and dω the solid angle unit about this direction**

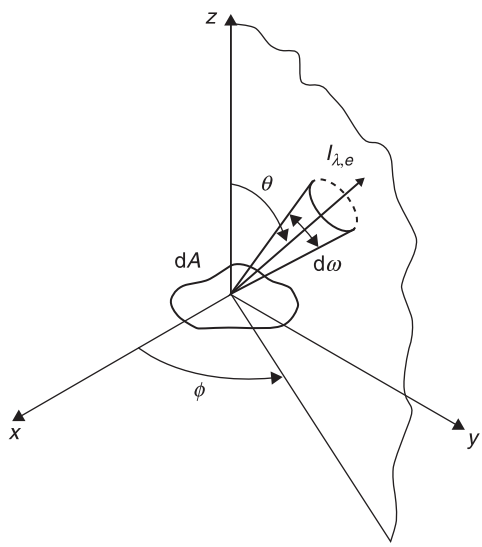

surface per unit wavelength interval dλ about λ and per unit surface area. It has the form

$$E_\lambda(\lambda,T) = \int_0^{2\pi}\int_0^{\pi/2} I_{\lambda,e}(\lambda,\theta,\phi,T)\cos\theta\sin\theta\,\mathrm{d}\theta\,\mathrm{d}\phi, \qquad (5.2)$$

where the solid angle dω has been written as d$\omega = \sin\theta\,\mathrm{d}\theta\,\mathrm{d}\phi$, according to the spherical coordinates defined in Figure 5.3.

Finally, integrating equation (5.2) over all wavelengths, the total emissive power, E, measured in W/m^2 in the SI system, is obtained as

$$E(T) = \int_0^\infty E_\lambda(\lambda,T)\,\mathrm{d}\lambda$$

$$= \int_0^\infty\int_0^{2\pi}\int_0^{\pi/2} I_{\lambda,e}(\lambda,\theta,\phi,T)\cos\theta\sin\theta\,\mathrm{d}\theta\,\mathrm{d}\phi\,d\lambda. \qquad (5.3)$$

The previous definitions, given by equations (5.1), (5.2) and (5.3), refer to the radiation emitted by a surface. Analogous definitions and mathematical expressions can be established for the incident radiation on a surface, called irradiation G, and for all the radiation leaving a surface (sum of the reflected radiation and the emitted radiation), called radiosity J. Both can be defined at spectral and directional levels, at spectral hemispherical level and as total magnitudes integrated over all directions and all wavelengths.

5.2 Blackbody radiation

A blackbody is an ideal surface that absorbs all incident radiation, at all wavelengths and all directions. Therefore, it is the perfect absorber. As a consequence of this definition, the blackbody has three properties: (a) it is the surface that emits most for a given temperature and wavelength, (b) blackbody radiation does not depend on the direction, that is, blackbody radiation is diffuse, and (c) total blackbody radiation in a

vacuum depends only on temperature. Since the blackbody is the perfect absorber and emitter, it will be used as a reference to compare the radiative properties of real surfaces.

The spectral emissive power of a blackbody at a temperature T was obtained by Planck as

$$E_{b,\lambda}(\lambda,T)=\frac{2\pi hc^2}{\lambda^5\left(\exp\left(\frac{hc}{\lambda kT}\right)-1\right)}, \tag{5.4}$$

where h is the Planck constant ($h = 6.6261 \times 10^{-34}$ J·s), $c = 2.9979 \times 10^8$ m/s the speed of light in a vacuum, λ the wavelength, and in this case k is the Boltzmann constant ($k = 1.3807 \times 10^{-23}$ J/K). The subscript b stands for blackbody. This expression is the Planck distribution, and the graphical representation of constant temperature lines, Figure 5.4, provides valuable information.

Looking at the figure, one can see that for a given wavelength the emitted radiation increases with temperature. Each constant temperature line has a maximum. This maximum moves towards longer wavelengths as the temperature decreases. If equation (5.4) is derived to obtain the wavelength where the maximum emissive power occurs, what is obtained is the so called Wien's displacement law given by $\lambda_{max}T = C_3$, where $C_3 = 2898$ μm·K. Furthermore, as temperature decreases it is not only the maximum but also the region where radiation is concentrated which moves towards longer wavelengths. Plotting the line for Sun radiation, equivalent to a blackbody at about 5800 K, one can see that the visible part of the spectrum is included on it. For temperatures of about 300 K, radiation is concentrated in the infrared part of the spectrum.

Equation (5.4) represents the spectral emissive power of a blackbody. It can be integrated to obtain the total emissive

Figure 5.4 **Spectral emissive power of a blackbody, $E_{b,\lambda}$, versus wavelength, λ, according to expression (5.4)**

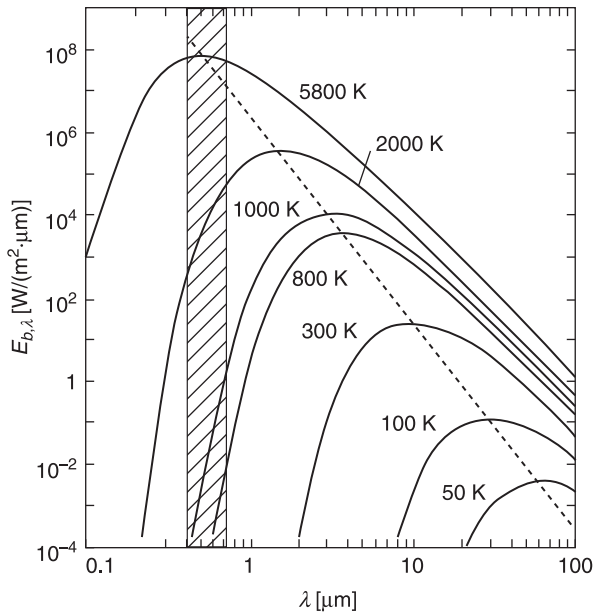

Note: Figures in the curves indicate the blackbody temperature, *T*. The striped area indicates the visible spectral region.

power of a blackbody, giving

$$E_b(T) = \int_0^\infty E_{b,\lambda}(\lambda, T)\mathrm{d}\lambda = \sigma T^4, \tag{5.5}$$

where $\sigma = 5.67 \times 10^{-8}$ W/(m^2·K^4). This result, $E_b = \sigma T^4$, is known as the Stefan-Boltzmann law, and can be used to obtain the energy emitted by a blackbody in all directions and all wavelengths.

When it is necessary to know the fraction of energy emitted by a blackbody at a temperature T within the bandwidth contained between λ_1 and λ_2, it can be calculated from

$$F_{\lambda_1 \to \lambda_2} = \frac{1}{\sigma T^4} \int_{\lambda_1}^{\lambda_2} E_{b,\lambda}(\lambda, T)\mathrm{d}\lambda. \tag{5.6}$$

The quantity, $F_{0\to\lambda}$, that is, the fraction of energy emitted by a blackbody between 0 and the wavelength λ, only depends on the product λT. It can be found tabulated in the references on heat transfer and thermal radiation mentioned above.

5.3 Properties of real surfaces

The blackbody has been defined as an ideal surface to be used as a reference to describe the behaviour of real surfaces. Since the blackbody is the perfect emitter, any real surface will emit less than the blackbody at the same temperature, same wavelength, and same direction. Thus, the spectral directional emissivity is defined as the ratio between the real emission, $I_{\lambda,e}$, and the blackbody emission for the same temperature, wavelength, and direction, $I_{b,\lambda}$, that is

$$\varepsilon(\lambda,\theta,\phi,T)=\frac{I_{\lambda,e}(\lambda,\theta,\phi,T)}{I_{b,\lambda}(\lambda,T)}. \tag{5.7}$$

The spectral hemispherical emissivity is defined as the ratio

$$\varepsilon(\lambda,T)=\frac{E_{\lambda}(\lambda,T)}{E_{b,\lambda}(\lambda,T)}. \tag{5.8}$$

When the surface is diffuse, the spectral hemispherical emissivity has the same value as the spectral directional emissivity. When the properties of the surface depend on the direction, the spectral hemispherical emissivity can be obtained appropriately integrating equation (5.7), according to the definition given in equation (5.8) (Incropera et al., 2007).

The second group of radiant properties is related to irradiation. As previously stated in Section 5.1, a surface will be irradiated by the radiation coming from other surfaces.

This incident radiation will be partially reflected, partially absorbed and partially transmitted (see Figure 5.2). Based on this fact, three radiative properties are defined. First, the spectral directional absorptance is defined as the fraction of the incident radiation, $I_{\lambda,i}$, that is absorbed for a given direction and wavelength, $I_{\lambda,i,abs}$. Thus

$$\alpha(\lambda,\theta,\phi,T)=\frac{I_{\lambda,i,abs}(\lambda,\theta,\phi,T)}{I_{\lambda,i}(\lambda,\theta,\phi)}. \tag{5.9}$$

Second, the spectral directional reflectance is defined as the fraction of the incident radiation, $I_{\lambda,i}$, that is reflected for a given direction and wavelength, $I_{\lambda,i,reflec}$. In this case,

$$\rho(\lambda,\theta,\phi,T)=\frac{I_{\lambda,i,reflec}(\lambda,\theta,\phi,T)}{I_{\lambda,i}(\lambda,\theta,\phi)}. \tag{5.10}$$

Third, the spectral directional transmittance is defined as the fraction of the incident radiation, $I_{\lambda,i}$, that is transmitted for a given direction and wavelength, $I_{\lambda,i,trans}$. Thus

$$\tau(\lambda,\theta,\phi,T)=\frac{I_{\lambda,i,trans}(\lambda,\theta,\phi,T)}{I_{\lambda,i}(\lambda,\theta,\phi)}. \tag{5.11}$$

As has been done for the emissivity, these coefficients can be integrated to obtain their values for all directions and all wavelengths. Therefore, the spectral hemispherical absorptance is defined as

$$\alpha(\lambda,T)=\frac{\int_0^{2\pi}\int_0^{\pi/2}\alpha(\lambda,\theta,\phi,T)I_{\lambda,i}(\lambda,\theta,\phi)\cos\theta\sin\theta\,\mathrm{d}\theta\,\mathrm{d}\phi}{G_\lambda(\lambda)}, \tag{5.12}$$

where

$$G_\lambda(\lambda)=\int_0^{2\pi}\int_0^{\pi/2}I_{\lambda,i}(\lambda,\theta,\phi)\cos\theta\sin\theta\,\mathrm{d}\theta\,\mathrm{d}\phi \tag{5.13}$$

is the spectral irradiance incident on the surface.

The spectral hemispherical reflectance is defined as

$$\rho(\lambda,T)=\frac{\int_0^{2\pi}\int_0^{\pi/2}\rho(\lambda,\theta,\phi,T)I_{\lambda,i}(\lambda,\theta,\phi)\cos\theta\sin\theta\,\mathrm{d}\theta\mathrm{d}\phi}{G_\lambda(\lambda)}, \quad (5.14)$$

and the spectral hemispherical transmittance is defined as

$$\tau(\lambda,T)=\frac{\int_0^{2\pi}\int_0^{\pi/2}\tau(\lambda,\theta,\phi,T)I_{\lambda,i}(\lambda,\theta,\phi)\cos\theta\sin\theta\,\mathrm{d}\theta\mathrm{d}\phi}{G_\lambda(\lambda)}. \quad (5.15)$$

For each of the levels of definition of these coefficients given above (spectral directional and spectral hemispherical), the following relationship verifies

$$\alpha+\rho+\tau=1. \quad (5.16)$$

For opaque surfaces transmittance is zero. Thus in this case $\alpha + \rho = 1$.

Kirchhoff's law establishes that $\alpha(\lambda, \theta, \phi, T) = \varepsilon(\lambda, \theta, \phi, T)$; that is, for each direction and wavelength emissivity equals absorptance. If the surface is diffuse, then from Kirchhoff's law it can be derived that $\alpha(\lambda, T) = \varepsilon(\lambda, T)$.

A surface is defined as grey when its properties are independent of the wavelength, more particularly $\alpha(\lambda,T) = \alpha(T)$ and $\varepsilon(\lambda,T) = \varepsilon(T)$. In the next section the equations of radiation exchange for diffuse grey surfaces are presented. Most real surfaces are not exactly grey, but the equations are still valid provided that the properties do not change with the wavelength in the range of interest, that is, in the range of wavelengths where radiation exchange takes place.

5.4 View factors

The view factor F_{ij} between two surfaces i and j is defined as the fraction of the radiation leaving surface i that reaches

surface *j*. It is also termed the configuration factor or geometrical factor. Mathematically, the view factor between two infinitesimal diffuse surfaces dA_i and dA_j, with uniform radiosity, can be expressed as

$$dF_{ij} = \frac{\cos\theta_i \cos\theta_j}{\pi r^2} dA_j, \tag{5.17}$$

where r is the distance between both elements, and θ_i and θ_j are the angles between the normal vector to each surface and the line of sight between elements, as shown in Figure 5.5.

For finite diffuse surfaces with uniform radiosity, the view factor is (Incropera et al., 2007)

$$F_{ij} = \frac{1}{A_i} \int_{A_i} \int_{A_j} \frac{\cos\theta_i \cos\theta_j}{\pi r^2} dA_i dA_j. \tag{5.18}$$

Figure 5.5 **Magnitudes to calculate the view factor between two elemental surfaces, dA_i and dA_j, placed a distance r apart; n_i, n_j, unity vectors normal to the surfaces**

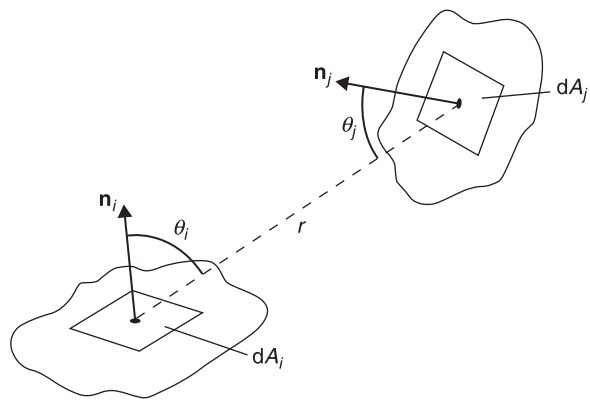

The reciprocity relation can be obtained from the mathematical definition of the view factor, by exchanging the subscripts i and j

$$A_i F_{ij} = A_j F_{ji}. \tag{5.19}$$

This expression is very useful in determining a view factor when the reciprocal is known.

When a set of n surfaces forms an enclosure, the summation rule of view factor applies to any of the surfaces. It is given by

$$\sum_{j=1}^{n} F_{ij} = 1. \tag{5.20}$$

Note that the term F_{ii}, the view factor of a surface with respect to itself, may be non-zero if the surface is concave, that is, if the surface can see itself.

View factors for a number of geometrical configurations have been calculated and are available in the literature (Howell et al., 2011).

5.5 Radiation exchange between opaque, diffuse, and grey surfaces in an enclosure

Consider an enclosure formed by n surfaces. All surfaces are opaque, diffuse, and grey. Each surface i is isothermal and the incoming irradiation on it, G_i, and the outgoing radiosity, J_i, are both uniform and unknown. The aim of this section is to determine the net radiation exchange on surface i, $\dot{Q}_i$, if the temperatures are known, or to obtain the temperatures if the net radiation exchange is known. To do this, the relevant equations are considered in the following.

The term $\dot{Q}_i$ is the net radiation exchange on surface *i*. It is positive when it leaves the surface, and takes into account all radiation exchanges, that is, the emission from its own surface, multiple reflections from the emissions of other surfaces, the absorption of the surface, etc. Therefore, in steady conditions, it can also represent the heat flux that has to be supplied to the surface by other means to maintain it at a constant temperature.

Starting from the radiative balance $\dot{Q}_i = A_i\,(J_i - G_i)$, and given that the radiosity can be written as $J_i = \varepsilon_i E_{bi} + \rho_i G_i$, and that the relationships between the radiative coefficients for opaque diffuse grey surfaces are $\alpha + \rho = 1$ and $\alpha = \varepsilon$, substitution gives

$$\dot{Q}_i = \frac{E_{bi} - J_i}{\dfrac{1-\varepsilon_i}{A_i\varepsilon_i}}. \tag{5.21}$$

Taking into account that the irradiation on a surface can be written as the sum of the radiosities leaving the rest of the surfaces multiplied by the relative view factor, then

$$A_i G_i = \sum_{j=1}^{n} A_j F_{ji} J_j. \tag{5.22}$$

Applying the properties of the view factors described above, one obtains

$$\dot{Q}_i = \frac{E_{bi} - J_i}{\dfrac{1-\varepsilon_i}{A_i\varepsilon_i}} = \sum_{j=1}^{n} \frac{J_i - J_j}{\dfrac{1}{A_i F_{ij}}}. \tag{5.23}$$

Equation (5.23) enables the radiant net heat fluxes or temperatures in an enclosure to be determined. It is written in this form based on the analogy with an electrical network that can be established, as is shown in Figure 5.6. Thus, the terms $E_{bi} - J_i$ and $J_i - J_j$ represent the voltage, the heat flux represents the intensity, and the denominators in equation (5.23) the

Figure 5.6 Electrical analogy for the radiation network approach

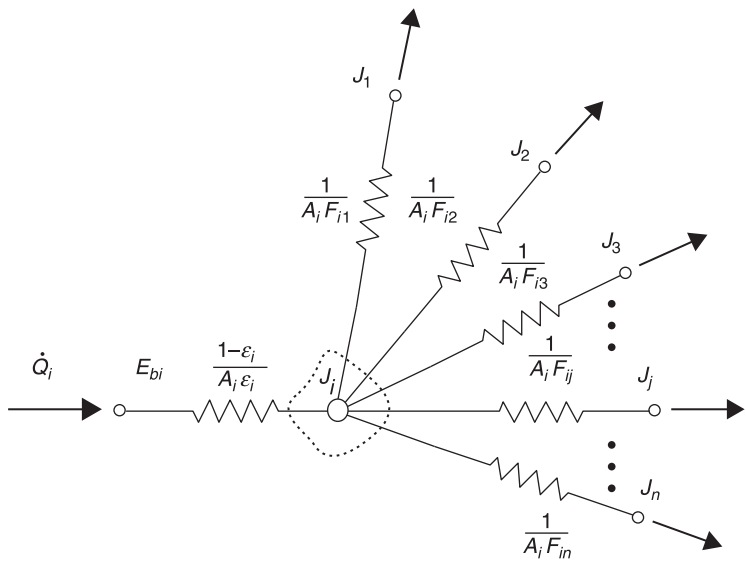

Key: A_i, area of surface *i*; ε_i, emissivity of surface *i*; J_i, radiosity of surface *i*; E_{bi}, total blackbody emissive power of surface ***i*** *at temperature* T_i; F_{ij}, view factor between surfaces *i* and *j*.

resistances. It constitutes a linear system of equations that can be solved just by matrix inversion obtaining the radiosities J_i and the blackbody emissive power E_b. Temperatures are obtained from the Stefan-Boltzmann law, $T = (E_b/\sigma)^{1/4}$.

5.6 References

Howell, J.R., Siegel, R. and Menguc, M.P. (2011) *Thermal Radiation Heat Transfer*, CRC Press, Boca Raton, Florida, USA.

Incropera, F.P., DeWitt, D.P., Bergman, L.T. and Lavine, A.S. (2007) *Fundamentals of Heat and Mass Transfer*, John Wiley and Sons, New York, USA.

6

Thermal control surfaces

Abstract: This chapter describes the effect of thermal control coatings on the spacecraft thermal behaviour, as well as the different types of coatings available for space use. The behaviour of the coatings is characterized through the values of the thermo-optical properties: solar absorptance and infrared emissivity. Depending on the value of these coefficients, the coatings are classified into four groups: solar reflectors, solar absorbers, total or flat reflectors, and total or flat absorbers. The effect of the environment on the values of the thermo-optical properties, mainly on the solar absorptance, is described.

Key words: thermo-optical properties, surface thermal finish, coatings.

6.1 Introduction

A satellite just outside the atmosphere of the Earth is in an extreme situation with respect to its temperature control. Conduction and convection are absent, and therefore, radiative exchange alone determines the heat fluxes to and from the spacecraft. Intense solar irradiation, radiative cooling to outer space, and internal heat generation, determine the equilibrium temperature of a spacecraft. The balance between the solar absorption and thermal emissivity

of the surface is therefore crucial, in particular for autonomous parts directly exposed to solar radiation and thermally insulated from the main thermal mass of the spacecraft.

The thermal radiation from the satellite is characteristic of its temperature, which is ideally close to room temperature, where the maximum intensity of the blackbody radiation is at wavelengths just short of 10 μm. The solar spectrum at 1 AU, according to ECSS-E-ST-10-04C (2008), and the blackbody spectrum at room temperatures, obtained from Planck's equation (see Section 5.2), are shown in Figure 6.1. The most important feature of thermal radiation, as illustrated in Figure 6.1, is that solar radiation is concentrated in the short wavelength range, whereas room temperature emission is concentrated in the long wavelengths. Therefore, the wavelength gap between the maxima of the incoming and outgoing radiation offers a possibility to use optical selectivity for temperature control.

As already explained in Section 5.3, Kirchhoff's law for diffuse surfaces states that $\alpha(\lambda, T) = \varepsilon(\lambda,T)$, that is, for each wavelength and temperature absorptance equals emissivity. However, for convenience, the term solar absorptance, α, is used for the value of the coefficient at short wavelengths, and the term infrared emissivity, ε, is used to name the coefficient in the infrared band. Thus, in space engineering, radiation properties of a surface are characterized by its total solar absorptance, α, and total hemispherical infrared emissivity, ε. These properties are the so-called thermo-optical properties of a surface and, as explained below, their ratio drives the equilibrium temperature of the surface.

In a general sense, a coating consists of a layer (or layers) of any substance upon a substrate. Optical coatings have been used to control the temperature of spacecraft since the first successful orbital flight, in 1957. Since then, coating materials have been developed to the point where reasonably

Figure 6.1 Emissive power E versus wavelength λ

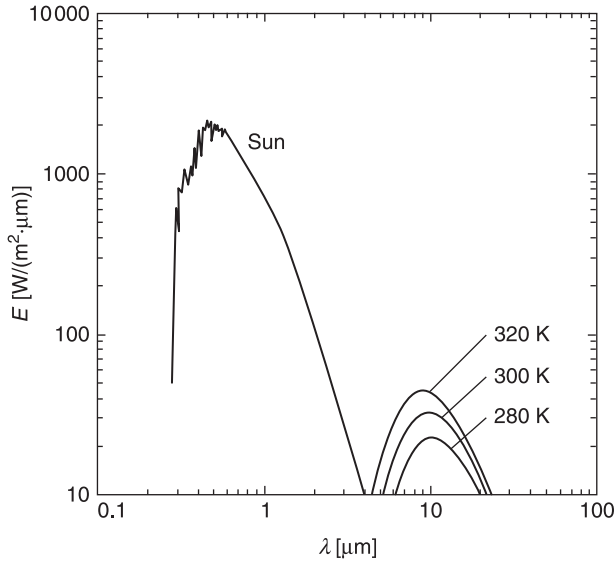

Note: The curves correspond to the solar spectral irradiance (Air Mass Zero, according to ECSS-E-ST-10-04C, 2008), and to the blackbody radiation spectrum at different temperatures, as given by expression (5.4).

stable coatings are available, which give any desired value of the hemispherical infrared emissivity, ε, between 0.05 and 0.95, for any desired value of the solar absorptance, α, between 0.05 and 0.95.

6.2 Thermal control coatings

From the point of view of physical arrangement, according to Touloukian et al. (1972) three types of coatings can be identified:

1. Pigmented coatings which are mixtures of a pigment and a solvent.

2. Contact coatings, formed by layers of a substance coated on a substrate without a chemical reaction occurring between the coating material and the substrate.
3. Conversion coatings which are layers of compounds formed by a chemical reaction of the substrate with another material.

However, when optical properties are considered (absorptance and emissivity), thermal control surfaces are classified into four basic types: solar reflector, solar absorber, total or flat reflector, and total or flat absorber. A plot of solar absorptance, α, versus hemispherical total emissivity, ε, is represented in Figure 6.2. In this plot the above-mentioned four types of coating are identified, and the boundaries corresponding to several values of the ratio α/ε are depicted. For each one of these straight lines, the equilibrium temperature, T_{sc}, for an isothermal sphere at 1 AU, as explained in Subsection 2.4.1, is

$$T_{sc} = \left(\frac{G_s \alpha}{4\sigma\varepsilon} \right)^{1/4}. \tag{6.1}$$

Solar absorbers absorb solar energy while emitting only a small percentage of infrared energy. Therefore, this class of thermal coatings is characterized by the highest values of the α/ε ratio. Such materials absorb moderate amounts of solar energy striking their surfaces but emit very small amounts of infrared radiation (see Figure 6.3). These materials are not very common, but high values of α/ε can be achieved by using certain polished metal surfaces, such as polished beryllium, metal films, or thin films of metal oxides.

Flat absorbers absorb throughout the spectral range, and have relatively high solar absorptances and high emissivities

Figure 6.2 **Solar absorptance, α, versus hemispherical total emissivity, ε**

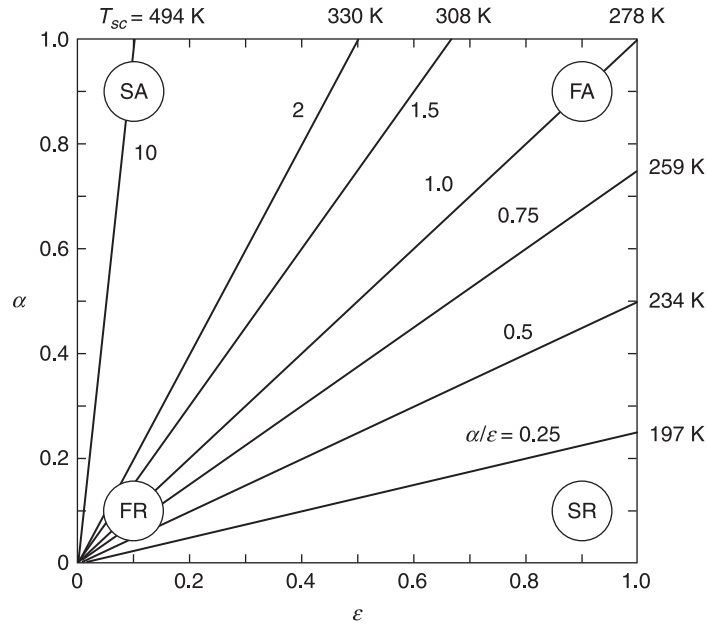

Note: In this plot basic types of thermal control coatings are shown: SA: solar absorbers, FA: total or flat absorbers, FR: total or flat reflectors, and SR: solar reflectors. The lines from the origin correspond to different values of the ratio α/ε, and for each line the equilibrium temperature, T_{sc}, of a coated isothermal sphere at 1 AU is given.

Source: After Touloukian et al. (1972).

(see Figure 6.3). Paints which are flat absorbers can be made from black pigments such as the oxides or mixed oxides (e.g. Cr_3O_4, $Fe_2O_3{\cdot}NiO$, Fe_3O_4, or $Mn_2O_3{\cdot}NiO$). The pigments are ground and dispersed in silicone elastomers or alkali metal silicate vehicles and applied to the base structure. These paints are the so-called black paints because their behaviour is very close to the blackbody. Typical black paints' α values are in the order of 0.95, while typical ε values are about 0.88. An alternate approach is to plate the

substrate material with metals, such as copper or nickel, followed by oxidation of the coating. Because the base materials are often alloys of aluminium or magnesium, experimental work is also being carried out with anodizing. Through anodizing one can achieve protection from corrosion as well as a coating with the desired optical properties. The interior of many spacecraft is finished black because it helps to distribute heat, and provides uniform temperatures.

Flat reflectors, the third class of optical surfaces, differ from flat absorbers in that they reflect energy throughout the spectral range (in both the solar and infrared spectral range). Materials having these optical properties are not common, and flat reflectors are presently obtained with highly polished metals or with paints pigmented with metal flakes. These surface treatments are used to thermally decouple a part of the spacecraft.

Solar reflectors are characterized by small values of the ratio α/ε. Solar reflectors reflect most incident solar energy while absorbing and emitting infrared energy. Typical materials belonging to this type are white paints, with α values in the order of 0.20, and ε values in the order of 0.90, and optical solar reflectors (OSR) or second surface mirrors (SSM), such as fused silica mirrors or silvered Teflon tapes, used where lower α values are needed, in the order of 0.10, with ε values in the order of 0.90. These surfaces are useful for coatings where low temperatures are needed and are mainly used for radiator surfaces that can be exposed to solar radiation. The nature of the emissivity of these solar reflectors is compared with that of a material considered an ideal solar reflector in Figure 6.3.

The range of properties available for different types of materials is summarized in Figure 6.4. The problem of selecting the specific coating for a given α/ε is

Figure 6.3 **Representative spectral emissivity curves of the four basic passive-control surfaces. Variation with the wavelength, λ, of the emissivity, ε, of actual substances and ideal materials**

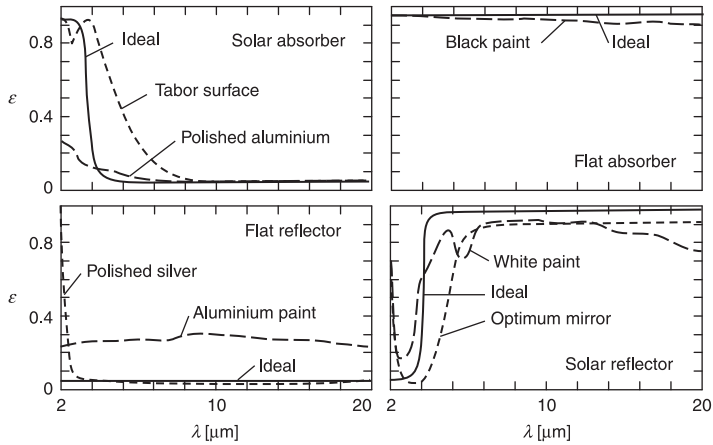

Source: After Lawrence and Bowman (1971) and Gilmore (2002).

somewhat circumvented by the combination of two or more coatings in a checkerboard or stripe pattern to obtain the desired combination of average absorptance and emissivity.

The basic requirement for a coating to be used in spacecraft is its long-term space stability, for periods of months or even years. However, in many instances this objective has not yet been achieved.

Radiation properties of a large number of suitable materials for spacecraft thermal control can be found in Henninger (1984), and extended lists of coatings are presented in Gilmore (2002) and Kauder (2005). The relative position on the absorptance–emissivity plane of the different coatings reported in Gilmore (2002) and Kauder (2005), is depicted in Figure 6.5.

Figure 6.4 **Ranges of solar absorptance, α, and hemispherical total emissivity, ε, covered by different thermal control coatings**

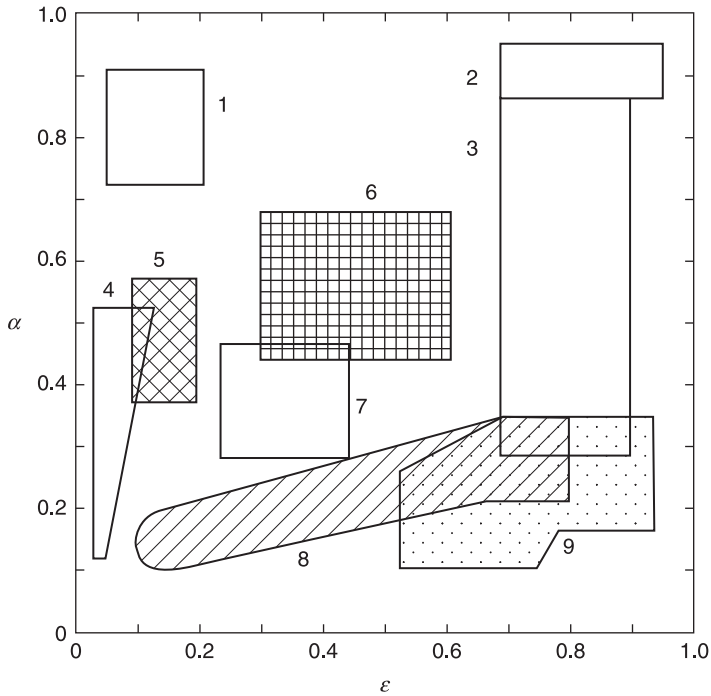

Key: 1 – selective black; 2 – black paints; 3 – grey and pastel paints; 4 – polished metals; 5 – bulk metals (unpolished); 6 – sandblasted metals and conversion coatings; 7 – metallic coatings; 8 – dielectric films on polished metals; 9 – white paints, second surface mirrors, metallized polymers.

Source: After Touloukian et al. (1972) and Gilmore (2002).

Additional coatings are listed in Tables 6.1 to 6.10, although only coatings from sources published after 1998 are included in these tables. Each table contains data from only one source of data, and they are ordered according to the year of publication. The relative position on the absorptance–emissivity plane of the coatings included in Tables 6.1 to 6.10 is presented in Figure 6.6 (p. xx).

Figure 6.5 **Relative position on the absorptance–emissivity (α-ε) plane of the different coatings reported in Gilmore (2002) and Kauder (2005)**

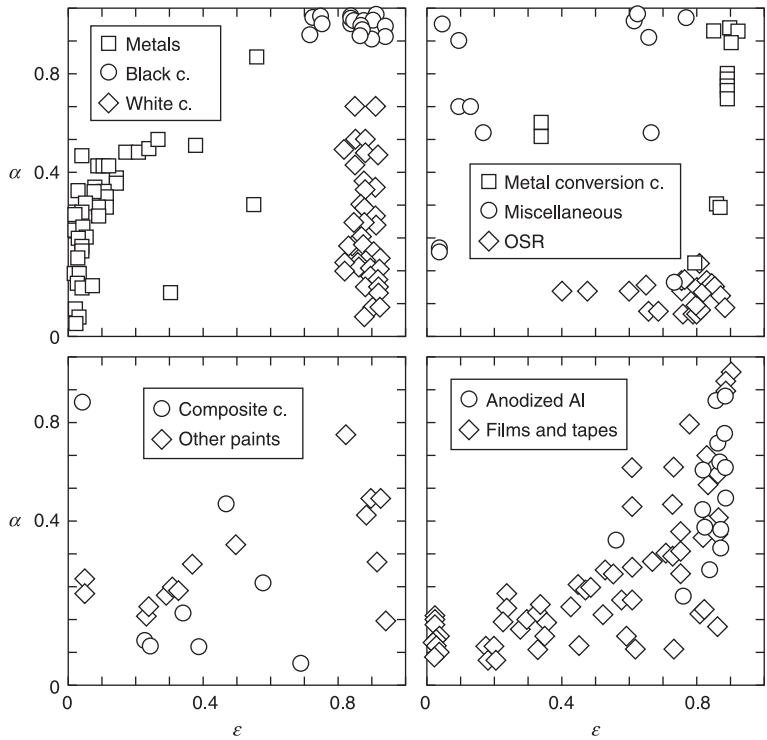

Note: The symbols identify the type of coating according to the keys defined in the different plots.

Table 6.1 **Typical beginning of life design values of absorptance, α, and emissivity, ε, of several anodized coatings**

Treatment	Material	α	ε
Sulphuric acid Anodic coatings	2219-T851 0.25–0.26 in., plate	0.49	0.87
	2219-T852, hand forged	0.48	0.86
	2219-T87 0.25–0.26 in., plate	0.49	0.86
	6061-T6, sheet	0.55	0.85
	6061-T65 I 0.25–0.26 in., plate	0.38	0.82
	7075-T6, clad sheet	0.25	0.84
	7075-T6, sheet	0.48	0.88
	7075-T73, sheet	0.52	0.88
	7075-T7351, bar, cold finish, machined surface	0.43	0.85
	7075-T7351, 0.25–0.26 in., plate	0.46	0.83
	7075-T73511, sheet extruded shape	0.50	0.84
Duranodic™ D 300	7075-T6, clad sheet	0.93	0.81
Black anodize	7075-T7351, 0.25–6 in., plate	0.81	0.79
Colour dyed sulphuric acid anodize	6061-T6, sheet, yellow	0.62	0.82
	6061-T6, sheet, red	0.69	0.82
	6061-T6, sheet, blue	0.67	0.81
	6061-T6511, extruded shape, yellow	0.50	0.81
	7075-T73511, extruded shape, yellow	0.59	0.82
	7075-T7351, 0.25–0.26 in., plate, yellow	0.59	0.82

Source: After Babel et al. (1996).

Table 6.2 **Observed radiation properties (absorptance, α, and emissivity, ε) of multilayer coatings deposited in alternating layers over reflecting silver layer**

Multilayer composition	α	ε
100 nm of SiO_2 and 350 nm WO_3	0.198	0.059–0.069
366 nm of WO_3 and 100 nm of SiO_2	0.155	0.093–0.100
64 nm WO_3, 50 nm SiO_2, 120 nm WO_3, 50 nm SiO_2, and 180 nm WO_3, each on 100 nm Ag	0.228	0.048–0.080

Source: After Jaworske (1998).

Table 6.3 **Absorptance, α, and emissivity, ε, of aluminium substrates coated with lacquer and then coated with a thin film of metal: vapour deposited aluminium (VDA), vapour deposited gold (VDG), and silver composite coating (Ag composite)**

Material	α	ε
VDA over lacquer on aluminium substrate	0.09	0.02
VDA over lacquer on aluminium honeycomb substrate	0.09	0.02
VDG over lacquer on aluminium substrate	0.18	0.07
Ag composite coating over lacquer on aluminium substrate	0.01	0.69

Source: After Peters et al. (2000).

Table 6.4 **Radiation properties (absorptance, α, and emissivity, ε) for different sputtered $Ti_xAl_yN_z$ films deposited for a deposition time, t, with a nitrogen flow, q, on different targets consisting of differently sized titanium and aluminium sectors**

N_2 flow, q [ml/min]	Composition $Ti_x/Al_y/N_z$	Deposition time, t [min]	Film thickness, h [nm]	α	ε	α/ε
1.0	12/56/32	30	600	0.597	0.287	2.08
1.6	–	20	–	0.727	0.413	1.76
1.6	–	30	–	0.728	0.456	1.60
1.6	–	40	–	0.714	0.425	1.68
1.8	14/47/40	30	505	0.751	0.513	1.46
1.4	10/51/39	30	535	0.668	0.343	1.94
1.4[A]	16/43/41	–	840	0.723	0.392	1.84
1.0	20/46/34	30	738	0.654	0.259	2.53
1.4	16/43/41	30	670	0.726	0.435	1.67
1.4[B]	16/43/41	30	690	0.699	0.357	1.96
1.4	16/43/41	–	650	0.750	0.499	1.50
1.6	–	30	970	0.796	0.319	2.50
1.6	–	25	810	0.782	0.275	2.84
1.6	–	35	1100	0.796	0.451	1.76
1.6	–	10	530	0.758	0.131	5.81
1.6	–	15	640	0.780	0.208	3.74
1.0	26/32/42	30	–	0.625	0.238	2.63
1.4	20/31/49	30	–	0.739	0.379	1.95
1.6	–	30	640	0.782	0.397	1.97
1.8	21/26/53	30	–	0.785	0.337	2.33
1.0	30/26/44	30	452	0.643	0.228	2.83
1.4	28/31/41	30	680	0.705	0.332	2.12
1.8	21/26/53	30	360	0.723	0.333	2.17

[A] deposited on TiAl-alloy.
[B] deposited on glass.
Note: A dash indicates that the corresponding magnitude has not been measured.

Source: After Brogren et al. (2000).

Table 6.5 Radiation properties (absorptance, α, and emissivity, ε) of aluminium and steel under different testing conditions

Material	α	ε	α/ε
Aluminium (6061-T6), as received	0.379	0.035	10.95
	0.379	0.039	9.64
Aluminium (6061-T6), polished	0.200	0.031	6.45
	0.200	0.034	5.88
Steel (AM 350), as received	0.567	0.267	2.12
	0.567	0.317	1.79
	0.567	0.353	1.61
	0.567	0.375	1.51

Source: After Brown (2002).

Table 6.6 Absorptance, α, and emissivity, ε, of solar selective coatings before and after heating at 953 K

Material		α	ε
Ni/$A1_2O_3$, cermet coatings	before heating	0.92	0.20
	after heating	0.64	0.17
Ti/$A1_2O_3$ cermet coatings	before heating	0.93	0.09
	after heating	0.93	0.10
Pt/$A1_2O_3$ cermet coatings	before heating	0.83	0.08
	after heating	0.75	0.08

Source: After Jaworske and Shumway (2003).

Table 6.7 **Radiation properties (absorptance, α, and emissivity, ε) of polymer films coated with a thin layer of a suspension of single-walled carbon nanotubes and tetrahydrofuran (anhydrous) sprayed onto polyimide films**

Polyimide	*m* [mg]	*h* [μm]	α	ε
LaRC™ CP2	0.0	38	0.06	0.52
	0.2	41	0.07	0.52
	0.5	41	0.07	0.54
	1.0	38	0.09	0.56
	2.0	38	0.10	0.56
TOR-NC	0.0	38	0.05	0.60
	0.5	38	0.06	0.58
	1.0	38	0.09	0.60
	2.0	36	0.12	0.62
PPO-6FDA	0.0	38	0.05	0.54
	0.5	38	0.08	0.60
	1.0	36	0.09	0.60
	2.0	38	0.10	0.60

Note: In the table, *m* indicates the amount of single-walled carbon nanotubes in tetrahydrofuran sprayed onto 1.0 g of polymer, and *h* the film thickness.

Source: After Watson et al. (2005).

Table 6.8 **Experimental values of absorptance, α, and emissivity, ε, for aluminium substrates coated with plasma sprayed alumina**

Surface condition	α	ε
As sprayed	0.301–0.318	0.801–0.810
Coated surface 800-grit ground	0.243–0.250	0.795

Source: After Li et al. (2006).

Table 6.9 **Absorptance, α, and emissivity, ε, of different thermal control coatings tested on MISSE (Materials on International Space Station Experiments) campaigns**

Material[A]	α	ε
03-W-127A	0.23	0.91
ELT	0.25	0.91
Zero-VOC	0.31	0.91
1% leafing aluminium added to A-276	0.30	0.84
5% leafing aluminium added to A-276	0.31	0.78
10% leafing aluminium added to A-276	0.33	0.72
15% leafing aluminium added to A-276	0.30	0.69

[A] *X*% leafing aluminium refers to *X*% by volume in the coating mix.

Note: In the table the results corresponding to the baseline coating 03-W-127A and two derivatives, the Deft Extended Life Topcoat (ELT) and Deft Zero Volatile Organic Compound (VOC) are shown. Also the results obtained by adding leafing aluminium to the white polyurethane coating A-276 are included.

Source: After Finckenor et al. (2008).

Table 6.10 **Absorptance, α, and emissivity, ε, of unstructured and structured (by anisotropic etching), mono-crystalline silicon wafers coated with sputter deposited aluminium and chemical vapour deposited silicon dioxide**

Material		α	ε	α/ε
Unstructured silicon	native oxide	0.463	0.034	13.61
	2 µm SiO_2	0.548	0.370	1.50
	200 nm Al	0.097	0.019	5.10
	200 nm Al, 2 µm SiO_2	0.132	0.423	0.31
5 µm-grooves	native oxide	0.572	0.276	2.07
	2 µm SiO_2	0.664	0.548	1.21
	200 nm Al	0.175	0.042	4.17
	200 nm Al, 2 µm SiO_2	0.278	0.496	5.60
25 µm-grooves	native oxide	0.603	0.390	1.55
	2 µm SiO_2	0.675	0.650	1.04
	200 nm Al	0.171	0.396	0.43
	200 nm Al, 2 µm SiO_2	0.242	0.642	0.38

Source: After Böhnke et al. (2008).

Figure 6.6 **Relative position on the absorptance–emissivity (α-ε) plane of the different coatings presented in Tables 6.1 to 6.10**

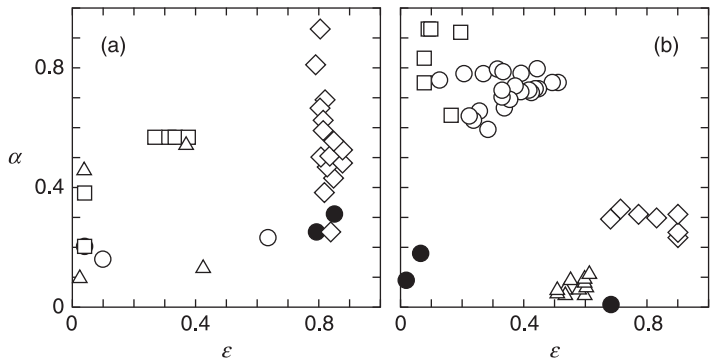

The symbols identify the sources of data according to the following key:

	Symbol	Coating	Table
(a)	Black circles	Plasma sprayed alumina on aluminium substrates	6.8
	Rhombi	Anodized coatings	6.1
	Squares	Aluminium and stainless steel	6.5
	Triangles	Unstructured and structured Al and SiO_2 coatings	6.10
	White circles	Multilayer coatings	6.2
(b)	Black circles	Al, Au or Ag on aluminium substrates	6.3
	Rhombi	03-W-127A and A-276 coating and derivatives	6.9
	Squares	Solar selective coatings	6.6
	Triangles	Coated polymer films	6.7
	White circles	Sputtered titanium-aluminium films	6.4

6.3 Thermal coating degradation

In space, thermal control finishes are subjected to various very destructive effects, such as thermal loads, mechanical loads (vibration, acceleration, shock), general spacecraft contamination (contaminant films that deposit on almost all spacecraft surfaces), radiation, atomic oxygen (in low Earth orbits), and micrometeorites and space debris, as described in Chapter 2. In addition, the loads created during on-ground operations at atmospheric conditions (assembly operations, testing, integration, transport and storage) also have to be taken into account for the design of thermal coatings.

Because of these effects, coating materials can suffer irreversible degradation of the physical characteristics (optical, thermal, electrical and mechanical) which these materials were designed to have. The general result of these processes is an increase in solar absorptance with little or no effect on infrared emissivity. This increase in solar absorptance becomes of paramount importance in the thermal control design of a spacecraft because spacecraft radiators have to be sized to account for the substantial increase in absorbed solar energy that occurs due to degradation throughout the mission. Leaving apart thermal and mechanical effects, in the next paragraphs the effects on thermal coatings of the above-mentioned contamination effects are briefly described.

In many cases the major contributor to optical degradation of thermal control finishes is spacecraft-generated contamination, which can be due to outgassing products from the spacecraft, thruster-generated contaminants or particles released with the spacecraft (particles that can travel to space within the launcher fairing).

Volatiles outgassed from spacecraft materials like plastic films, adhesives, foams, lubricants, and paints, can be especially detrimental to thermal coatings (as well as to optical

instruments and solar cells), because these surfaces may be obscured by condensed outgassing products. The condensation of contaminants on surfaces can be produced at a greater rate if these surfaces are illuminated by the Sun, because ultraviolet radiation enhances chemical binding processes.

In addition, local clouds of outgassed materials may be formed around the spacecraft that can affect sensitive instrument readings (for example, ultraviolet astronomy is effectively impossible in the presence of even trace amounts of water vapour). Finally, in polymeric or other volatile materials, the nature and extent of outgassing can lead to serious changes in the basic material properties. Contamination affects almost any surface finish, but varies with the temperature of, proximity to, and shape factor of the contamination source.

Outgassing is usually dealt with by selecting, in advance, those materials where it is less likely to be a problem. In fact, the screening of space materials is performed in Europe according to ECSS-Q-ST-70-02C (2008) or ASTM E 595–07 (2007) standard procedures.

Another source of degradation is the result of the corruption of thermal coatings due to their exposure to ultraviolet radiation and to high-energy charged elementary particles. The Sun is the dominant source of ultraviolet radiation within the wavelength range between 115 nm to 300 nm (Figure 2.2). In this range, two different regions are usually distinguished: one is the so-called vacuum ultraviolet radiation, with wavelengths below 200 nm, which is only transmitted in the vacuum of the space (atmospheric gases absorb these shorter wavelengths); the second is ultraviolet radiation with wavelengths longer than 200 nm. Longer wavelength radiation remains relatively constant throughout the solar cycles, whereas vacuum ultraviolet radiation fluctuates with solar activity and can increase by up to a factor of 3 as peak solar activity occurs (Gilmore, 2002).

Because of ultraviolet radiation, glasses become brownish, an effect known as solarization. Optical coatings like antireflection coatings and interference filters can also exhibit serious degradation effects (a shift of the spectral absorption characteristics, for instance). In addition to glasses and coatings, optical cements can also show serious degradation effects due to ultraviolet irradiation. Measurements performed on cemented plane plates show effects such as severe discolouration, disintegration of cement layers, or cracks in glass induced by cement shrinkage (Czichy, 1994).

The high-energy particle radiation in space consists of trapped radiation, quiet Sun radiation, solar flare radiation, and low-energy plasma.

Trapped radiation consists of charged particles, mainly electrons up to 7 MeV, and protons, which are trapped by the Earth's magnetic field in the Van Allen's belts (Tribble, 2003, chapter 5). For electrons, two flux maxima exist, one of them at a distance from the Earth's centre of 8920 km and the second maximum is at 28 670 km. For protons, only one maximum exists at a distance of 10 830 km.

Quiet Sun radiation (apart from visible and near ultraviolet radiation) consists of extreme ultraviolet to soft X-rays, from a 4 nm to 200 nm wavelength. Solar flare radiation is a transient type of radiation depending on solar activity, which has a mean cycle of 11 years. The low-energy plasma consists of protons and electrons.

The interaction of high-energy particle radiation with optical materials can cause various types of radiation damage. The basic damage mechanisms are radiolysis by ionization, displacement damage, and electron rearrangement. All these mechanisms lead to local structure defects, and depending on the total dose received and radiation type, this is manifested as transmission degradation (solarization), refractive index change, and dielectric breakdown (spacecraft charging effects).

Degradation of absorptance due to exposure to ultraviolet radiation and bombardment by charged particles seems especially pronounced in polyimide films (Kapton) and white paints with organic binders.

As an example, Figure 6.7 shows the increase over time in solar absorptance of fused silica mirrors on several spacecraft. The probable cause of the solar absorptance degradation contamination is the photo-deposition of contaminant films on fused silica mirrors, because these surfaces are usually sunlit for a significant fraction of time. According to Jaworske

Figure 6.7 **Variation over time in orbit, *t*, of the increase in solar absorptance, $\Delta\alpha$, of fused silica second-surface silver mirrors flown on several satellites**

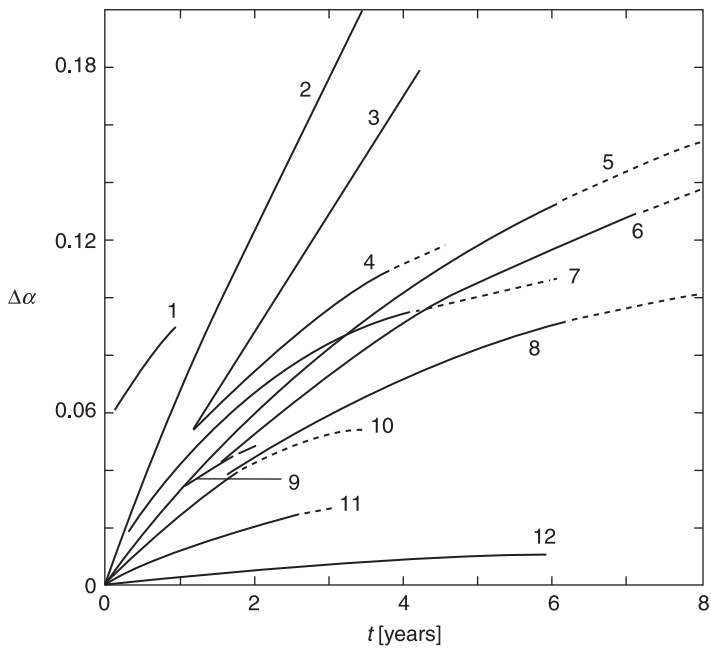

Key: 1 – DSCS III; 2 – GPS NAVSTAR; 3 – SDS; 4 – OTS-2; 5 – INTELSAT IV A; 6 – INTELSAT IV; 7 – FLTSATCOM F-1; 8 – DSP AVG; 9 – FLTSATCOM F-2; 10 – COMSTAR; 11 – DSP FLT-10; 12 – SCATHA.

Source: After Stewart et al. (1990).

and Klein (2008), the absorptance degradation in orbit due to ultraviolet radiation, outgassing contamination, and bipropellant deposition, of Z-93P white paint on the International Space Station (ISS), is expected to increase from $\alpha \cong 0.18$ at the beginning of life to $\alpha \cong 0.33$ after 30 years in orbit.

As described in Chapter 2, atomic oxygen is a major damaging element of the low Earth orbit space environment. It can severely erode externally applied, hydrocarbon-type, thermal-control materials. In low Earth orbit (150 km to 600 km altitude), highly reactive atomic oxygen is the most abundant constituent. Atomic oxygen is formed by the ultraviolet photolysis and dissociation of molecular oxygen in the upper atmosphere. The concentration of atomic oxygen varies inversely with an increase in altitude between 100 and 1000 km, and directly with solar activity, as a result of the increased vacuum ultraviolet component of solar irradiance.

Spacecraft in low Earth orbit, travelling at about 8 km/s, experience surface collision of an atomic oxygen beam with the effective energy of about 5 eV and the flux of 10^{14}–10^{15} atom/(cm^2·s). Atomic oxygen attacks can cause severe damage to polymer materials, such as changes in optical, mechanical, electrical, and chemical properties, and mass loss. Erosion of spacecraft materials in orbits above 1000 km is not a concern because there is negligible atomic oxygen at these higher altitudes, but erosion may be a factor while the vehicle is in a parking orbit. For most widely used polymers or polymer-based composites, such as polyimides (like Kapton) and polyurethane paints, their atomic oxygen erosion yield rate is in the order of 10^{-24} cm^3/atom. Other coatings, like silicone paints, are considered to be stable in the atomic oxygen environment, because when the exposed hydrocarbon components of the silicone polymer are eroded, a dense silicate surface layer is produced on the surface that resists

further oxidations. However, atomic oxygen attacks result in the loss of methyl groups in the silicones, which causes shrinkage of the surface skin. The influence of atomic oxygen on metals (aluminium, beryllium, magnesium, stainless steel and titanium) is negligible, although some degradation of metallic optical coating materials flown in the Long Duration Exposure Facility has been reported (Herzig et al., 1993).

In order to improve the atomic oxygen erosion resistance of polymer materials, these materials can be either silverized or aluminized, or coated with appropriate paints (various kinds of inorganic and organic protective coatings have been developed).

6.4 References

ASTM E 595–07 (2007) *Standard Test Method for Total Mass Loss and Collected Volatile Condensable Materials from Outgassing in a Vacuum Environment*, American Society for Testing and Materials (ASTM).

Babel, H.W., Jones, C. and David, K. (1996) Design properties for state-of-the-art thermal control materials for manned space vehicles in LEO, *Acta Astronautica*, **39:** 369–79.

Böhnke, T., Kratz, H., Hultåker, A., Köhler, J., Edoff, M. et al. (2008) Surfaces with high solar reflectance and high thermal emissivity on structured silicon for spacecraft thermal control, *Optical Materials*, **30**: 1410–21.

Brogren, M., Harding, G.L., Karmhag, R., Ribbing, C.G., Niklasson, G.A. and Stenmark, L. (2000) Titanium-aluminium-nitride coatings for satellite temperature control, *Thin Solid Films*, **370**: 268–77.

Brown, C.D. (2002) *Elements of Spacecraft Design*, AIAA Education Series, J.S. Przemieniecki Ed., American

Institute of Aeronautics and Astronautics. Inc., Reston, Virginia, USA.

Czichy, R.H. (1994) Optical design and technologies for space instrumentation, *SPIE*, **2210**: 420–33.

ECSS-E-ST-10-04C (2008) *Space engineering. Space environment*, ESA Requirements and Standards Division, ESTEC, Noordwijk, The Netherlands, November 2008.

ECSS-Q-ST-70-02C (2008) *Space product assurance. Thermal vacuum outgassing test for the screening of space materials*, ESA Requirements and Standards Division, ESTEC, Noordwijk, The Netherlands, November 2008.

Finckenor, M., Pippin, G. and Frey, G. (2008) 'MISSE thermal control materials with comparison to previous flight experiments', Ninth International Space Conference – Protection of Materials and Structures from the Space Environment, Toronto, Canada, 20–23 May 2008.

Gilmore, D.G., Ed. (2002) *Spacecraft Thermal Control Handbook, Vol. I: Fundamental Technologies,* 2nd ed., American Institute of Aeronautics and Astronautics, Inc., The Aerospace Press, El Segundo, California, USA.

Henninger, J.H. (1984) *Solar Absorptance and Thermal Emissivity of Some Common Spacecraft Thermal-Control Coatings,* NASA Reference Publication 1121.

Herzig, H., Toft, A.R. and Fleetwood Jr., C.M. (1993) Long-duration orbital effects on optical coating materials, *Applied Optics*, **32**: 1798–1804.

Jaworske, D.A. (1998) Correlation of predicted and observed optical properties of multilayer thermal control coatings, *Thin Solid Films*, **332**: 30–3.

Jaworske, D.A. and Klein, S.E. (2008) *Review of End-of-Life Thermal Control Coating Performance,* NASA/TM-2008-215173.

Jaworske, D.A. and Shumway, D.A. (2003) 'Solar selective coatings for high temperature applications', Space

Technology and Applications International Forum-STAIF 2003, Albuquerque, New Mexico, 2–5 February 2003, M.S. El-Genk, Ed., American Institute of Physics, *AIP Conference Proceedings*, 654.

Kauder, L. (2005) *Spacecraft Thermal Control Coatings References*, NASA/TP-2005-212792, NASA Center for AeroSpace Information, Hanover, Maryland, USA, December 2005.

Lawrence, R.M and Bowman, W.H. (1971) Space resources for teachers. Optical surfaces for temperature control of spacecraft, *Journal of Chemical Education*, **48**: 605–7.

Li, R.M., Joshi, S.C. and Ng, H.W. (2006) Radiation properties modeling for plasma-sprayed-alumina-coated rough surfaces for spacecrafts, *Materials Science and Engineering B*, **132**: 209–14.

Peters, W.C., Harris, G., Miller, G. and Petro, J. (2000) Tailoring thin-film/lacquer coatings for space applications, *High Performance Polymers*, **12**: 105–12.

Stewart, T.B., Arnold, G.S., Hall, D.E., Marvin, D.C., Hwang, W.C. et al. (1990) *Photochemical Spacecraft Self-Contamination: Laboratory Results and Systems Impacts, Aerospace Report No. TOR-0090(5470–01)-3*, The Aerospace Corporation, El Segundo, California, USA.

Touloukian, Y.S., DeWitt, D.P. and Hernicz, R.S. (1972) *Thermal Radiative Properties. Coatings, Thermophysical Properties of Matter*, Vol. 9, IFI/Plenum, New York, USA.

Tribble, A.C. (2003) *The Space Environment, Implications for Spacecraft Design*, Princeton University Press, Princeton, New Jersey, USA.

Watson, K.A., Ghose, S., Delozier, D.M., Smith Jr., J.G. and Connell, J.W. (2005) Transparent, flexible, conductive carbon nanotube coatings for electrostatic charge mitigation, *Polymer*, **46**: 2076–85.

7

Insulation systems

Abstract: This chapter describes the two main insulation systems used for spacecraft thermal control: multilayer insulation (MLI), also called thermal blankets, and foams. Multilayer insulation systems are used to insulate the spacecraft from the environment or when different temperature levels are required. They consist of layers of closely spaced, highly reflecting shields separated with non-metallic spacers to avoid direct contact between layers. The different ways of modelling the thermal behaviour of multilayer insulation as well as the equations used to do it are presented.

Key words: multilayer insulation, thermal blanket, foam.

7.1 Introduction

A common design philosophy for the thermal control subsystem of most spacecraft is based on the insulation of the spacecraft from the environment. In order to reject to space the heat from dissipating devices, some radiators (see Chapter 8) are appropriately sized and located on the outer surface of the spacecraft. Compensation heaters (see Chapter 13) are then sized for the worst cold case scenarios to avoid sub-cooling of the equipment. This insulation design philosophy diminishes the impact of the highly variable environmental conditions, and of the cold external radiative

sink, on the spacecraft equipment. The power needed for the compensating heaters is thus minimized. Insulation systems are also needed when different temperature levels have to be simultaneously reached within the spacecraft. This is, for instance, the case of cryogenic devices (Chapter 16), which run at extremely low temperatures, whereas their corresponding proximity electronics work at room temperature. Another example is the engines which run at very high temperatures while the equipment nearby has to be insulated to avoid excessive heating. In this section the two main insulation systems, multilayer insulations and foams, are described.

7.2 Multilayer insulations

A multilayer insulation (MLI), also called a thermal blanket, consists of several layers of closely spaced, highly reflecting shields, which are placed perpendicular to the heat flow direction. Each internal layer is a very thin layer (from 7 μm) of material, typically Kapton or Mylar, coated with vapour deposited aluminium (VDA) on both sides. This mirror-like aluminium finish makes the sheets highly reflective and of low emissivity, which leads to a high resistance to radiative heat transfer between layers (Chapter 5). The outer cover is usually thicker (from 125 μm) than the internal ones to increase its mechanical strength. This external layer is usually aluminized only on its internal face, because aluminium degrades when it is exposed to ultraviolet radiation. The external layer can be just bare Kapton or can be painted, for instance, with a black carbon paint to avoid undesired reflections. When better mechanical properties are needed, for example to protect it from micrometeoroids, more resistant materials, such as beta-cloth, can be used for

this outer layer. In any case, since the outer cover can be exposed to solar radiation, its compatibility with ultraviolet radiation has to be carefully checked.

To avoid direct contact between shields, and therefore heat conduction between sheets, low-conductivity, non-metallic spacers are used. In order to minimize the contact they are usually in the form of a mesh. Typical materials for this netting spacer are Dacron and Nomex. Figure 7.1 shows a typical cross-section of a multilayer insulation.

The pile of layers is stacked together by stitches sewn with special non-metallic thread that has to be free of volatile components. Small Kapton pieces can be used to prevent the blanket from tearing due to thread tension. To close the lateral gaps and avoid the degradation of the internal layers, the outer cover is folded back on the internal layer. This continuity between the external and the internal covers degrades the performance of the blanket in a small area close to the edges and seams. The blankets are attached to the spacecraft structure with hook-and-pile (Velcro) fasteners and pins.

Figure 7.1 **Sketch of a typical multilayer insulation (the mid zone of the multilayer insulation consists of 15 to 20 reflector/spacer layers)**

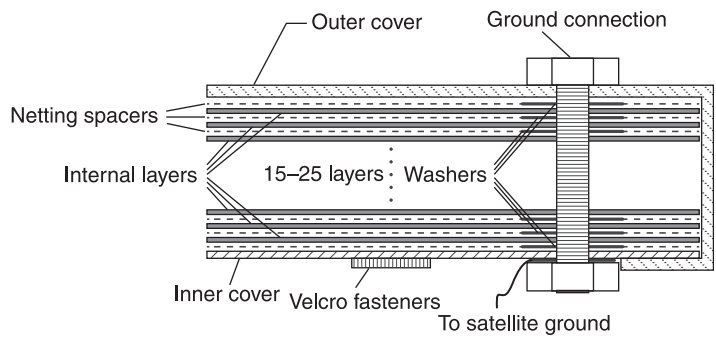

Proper venting of the multilayer insulation should be provided to avoid undue pressure loads on the shields during the ascent flight (Sanz-Andrés et al., 1997). Otherwise, the blanket would billow out like a balloon and the dynamic pressure could detach it from the spacecraft. Thus, to allow for the proper venting of the blanket, the sheets are perforated. The size and separation of the perforations depend on the type of mission. Typical values can be 0.8 mm holes every 6 mm. Some studies have been carried out to obtain the influence of the perforations on the performance of the multilayer insulation (Li and Cheng, 2006). Another option to enable the venting of the blanket is to leave part of the edges unsealed. In this case, gas will flow through these openings. Venting may also be necessary in long-term in-orbit missions to allow for the outgassing of the materials, although bake out is usually performed before launch.

In order to prevent electrostatic charge and the resultant discharges, all the layers of the blanket have to be grounded to the spacecraft structure. A bolt passing through the blanket with washers touching each layer can be used for this purpose. The bolt is then connected to the spacecraft structure with a copper cable. Another option to ground the multilayer insulation is the use of a metallic strip, folded in such a way (like an accordion) that it touches all the layers of the blanket.

Detailed information about multilayer insulation materials, assembly, and performance, can be found in STCDD (1989), Finckenor and Dooling (1999), and Gilmore (2002).

Conventional multilayer insulations were developed in the 1960s and 1970s. Current efforts are now devoted to the development of high-temperature multilayer insulations, such as those necessary for missions to Mercury (BepiColombo), or solar missions such as Solar Probe (Choi, 2007) or the Solar Orbiter. One-dimensional heat transfer testing has shown (Figure 7.2) that, for a given mass, an evacuated multilayer

Figure 7.2 **Effective thermal conductivity, k_{eff}, of multilayer insulations as compared with other insulation materials**

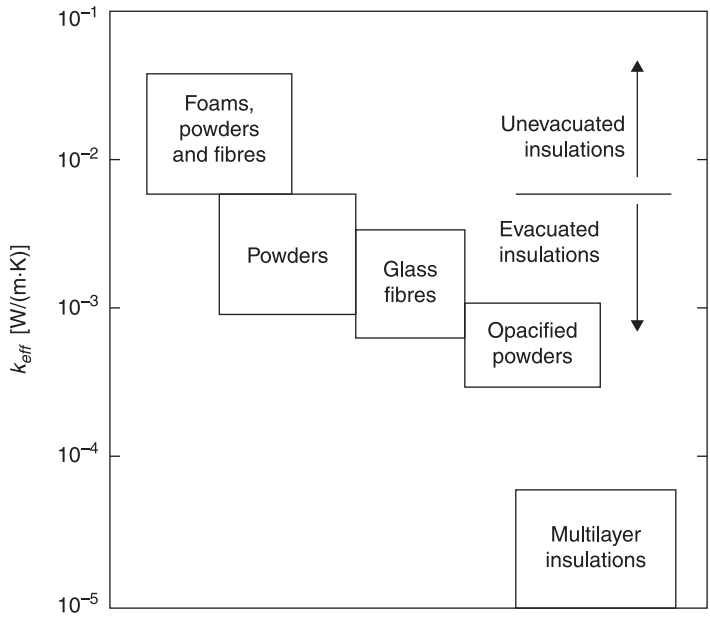

Source: After STCDD (1989).

insulation provides insulation which is orders of magnitude greater than that offered by more conventional materials, such as foams and fibreglass batting (STCDD, 1989).

Prediction of the thermal performance of multilayer insulations is difficult because their properties are anisotropic, discontinuous, and subjected to variations due to manufacture, handling, and use. The main variables that account for the thermal performance of a blanket are: the number of shields, N; the total thickness, t; the thermo-optical properties of the layers; the applied compressive load; the size and number of perforations to permit venting; the size of the blanket; and number of seams, etc. Some empirical relationships for the performance of multilayer insulations

are available in the literature where all these factors are taken into account (Krishnaprakas et al., 2000; Gilmore, 2002). In order to quantify the performance of the multilayer insulations and characterize them for thermal modelling, two methods are commonly used. The first is based on the definition of 'effective conductivity', and the second is based on the definition of 'effective emissivity'. Thus, let the temperatures of the cold and warm boundaries be T_C and T_H, respectively. Most of the available data concerning heat transfer through multilayer insulations are based on a Fourier's law type 'effective conductivity', k_{eff}. Hence, the heat flux through a multilayer insulation of area A is

$$\dot{Q} = k_{eff} A \frac{T_H - T_C}{t} \tag{7.1}$$

where t is the thickness of the blanket. It should be noted that k_{eff} can be used only when comparing the qualities of various insulators, and should not be considered as an average property of the materials constituting the insulation. Typical values between 10^{-4} and 10^{-5} W/(m·K) can be reached. Less often, the performance of multilayer insulation systems is given in terms of a 'heat transfer coefficient' or 'effective thermal conductance', h_{eff}, defined as $h_{eff} = k_{eff}/t$. The use of effective thermal conductance, h_{eff}, is recommended in those cases where the thickness cannot be easily measured.

The second method used to characterize the performance of a multilayer insulation is based on the definition of 'effective emissivity', ε_{eff}. This enables different blankets to be compared. The heat flux through the multilayer insulation is then calculated from

$$\dot{Q} = A\sigma\varepsilon_{eff}(T_H^4 - T_C^4), \tag{7.2}$$

where $\sigma = 5.67 \times 10^{-8}$ W/(m^2·K^4) is the Stefan-Boltzmann constant. Note that the definition of this 'effective emissivity'

is somehow contrived because the hot and cold shields cannot see each other. It is merely a mathematical expression used to compare multilayer insulations and their thermal modelling.

The following relation between the above-mentioned magnitudes can be used:

$$k_{eff} = h_{eff} t = 4\sigma\varepsilon_{eff} tT^3, \tag{7.3}$$

where T is the characteristic temperature of the insulation system, given by the expression:

$$T = \sqrt[3]{\frac{T_H^4 - T_C^4}{4(T_H - T_C)}}. \tag{7.4}$$

The heat transfer rate between two infinite parallel grey planes with N non-touching parallel shields of emissivities ε_1 and ε_2 on each side, inserted between the two boundaries at T_C and T_H can be written as (STCDD, 1989):

$$\dot{Q} = \sigma \frac{1}{\frac{1}{\varepsilon_1} + \frac{1}{\varepsilon_2} - 1} \left(\frac{1}{N+1}\right) A(T_H^4 - T_C^4). \tag{7.5}$$

Hence, the effective emissivity can be written as

$$\varepsilon_{eff} = \frac{1}{\frac{1}{\varepsilon_1} + \frac{1}{\varepsilon_2} - 1} \left(\frac{1}{N+1}\right). \tag{7.6}$$

And the effective conductivity is

$$k_{eff} = \frac{(\dot{Q}/A)/t}{(T_H - T_C)} = \frac{\sigma t}{(N+1)\left(\frac{1}{\varepsilon_1} + \frac{1}{\varepsilon_2} - 1\right)} \frac{T_H^4 - T_C^4}{T_H - T_C}. \tag{7.7}$$

The effective thermal conductivity of a multilayer insulation is, roughly, inversely proportional to the number of radiation

shields per unit thickness, N/t, while the effective emissivity is inversely proportional to N. However, measurements indicate that the real behaviour of most multilayer insulations deviates from the ideal one when N/t increases, due to increased thermal conduction between adjacent layers. The typical number of layers used is between 15 and 25. More layers do not improve the performance of the multilayer insulation. Typical values of effective emissivity range from 0.01 to 0.05. The real performance depends not only on the number of layers, but on layer size, number and positions of the seams, grounding connections, etc. In general, seams and edges are a drawback, in that they increase heat transfer; therefore the larger the multilayer insulation the better its performance.

These features (real thermo-optical properties, heat transfers due to heat conduction between layers, manufacturing implementation) give rise to uncertainties in the final performance of the multilayer insulation, which has to be considered in the thermal mathematical models (Chapter 19). One of the objectives of the thermal testing (Chapter 20) is the reduction of these uncertainties.

Blankets should be manufactured and handled in clean rooms, with a humidity range between 40% and 60%, and a temperature range between 288 K and 300 K. Those handling the blankets and associated material must wear normal clean-room clothing and flint-free gloves. For transportation purposes, the blankets should be wrapped in welded plastic bags containing silica gel packages.

7.3 Foams

Foams are commonly used as insulating materials in building, storage vessels, sports equipment, and spacecraft. They are commonly used as insulators under atmospheric conditions.

Because of their cellular structure of discrete or interconnected voids, a large percentage of foam volume is air, or whatever gas is used as the expanding agent. Therefore foams are lightweight and have very low thermal conductivity, which can be decreased even further by evacuation. Foam density is of the order of 10 kg/m^3 and its thermal conductivity depends on the type of foam. According to their chemical composition, they can be classified as inorganic or organic, and depending on their structure, they can be open-cell or closed-cell.

Thermal conduction through a foam combines solid conduction, gas conduction, and radiation. Although the effective thermal conductivity, in the Fourier-law sense, can be measured with relative ease analytical models are also available for predicting the thermal conductivity and the heat flow through candidate foam materials to be used as thermal insulators (STCDD, 1989). Experiments have shown that, for open-cell foams, gas conduction is the main contributor to heat transfer through the foam at ambient pressure (Gilmore, 2002). As expected, foam conductivity decreases substantially as gas pressure does. Typical values of foam thermal conductivity at ambient pressure are between 0.01W/(m·K) and 0.03 W/(m·K).

Three basic problems should be considered regarding the application of organic foams as thermal insulators, namely: thermal conductivity, thermal expansion and contraction, and flammability and explosion hazards.

7.4 References

Choi, M.K. (2007) 'Thermal testing on high temperature MLI and sunshields for Solar Probe sun-viewing instruments', Paper AIAA 2007–4824, 5th International

Energy Conversion Engineering Conference and Exhibit (IECEC), St. Louis, Missouri, USA, 25–27 June 2007.

Finckenor, M.M. and Dooling, D.D. (1999) *Multilayer Insulation Material Guidelines*, NASA/TP-1999-209263, April 1999.

Gilmore, D.G., Ed. (2002) *Spacecraft Thermal Control Handbook, Vol. I: Fundamental Technologies,* 2nd ed., American Institute of Aeronautics and Astronautics, Inc., The Aerospace Press, El Segundo, California, USA.

Krishnaprakas, C.K., Narayana, B.K. and Dutta, P. (2000) Heat transfer correlations for multilayer insulation systems, *Cryogenics*, **40**: 431–5.

Li, P. and Cheng, H. (2006) Thermal analysis and performance study for multilayer perforated insulation material used in space, *Applied Thermal Engineering*, **26**: 2020–6.

Sanz-Andrés, A., Santiago-Prowald, J., and Ayuso-Barea, A. (1997) Spacecraft launch depressurization loads, *Journal of Spacecraft and Rockets*, **34**: 805–10.

STCDD (1989) *Spacecraft Thermal Control Design Data Handbook*, ESA PSS-03-108, Issue 1.

8

Radiators

Abstract: Radiators are systems which take the waste thermal energy from a heat source and reject it by radiation to outer space, generally by using radiating surfaces with high infrared emissivity and low solar absorptance. Radiators can be classified as passive radiators and active radiators, depending on how the heat is transferred from the source to the radiating surfaces. In passive radiators the connection between the heat source and the radiating surface is made either by direct contact or by means of heat pipes. In this chapter the main characteristics of passive radiators are outlined.

Key words: passive cryogenic radiant cooler, staged radiators, V-groove radiators.

8.1 Introduction

The thermal control of a satellite in orbit is usually achieved by balancing the thermal energy dissipated by the internal electronic equipment and the energy absorbed from its environment with the energy emitted by the satellite. Because convection heat transfer does not exist in a space environment, the heat transfer mechanisms that control this balance are conduction and radiation. The temperature ranges in which satellite components operate are usually narrow; therefore

more heat is transferred by conduction through the spacecraft structure than transferred by radiation inside the compartments. Hence, conduction heat transfer is the most effective means of thermal control of electronic equipment aboard satellites.

Electronic equipment, such as infrared (IR) sensors and charge-coupled device (CCD) cameras, usually operate at cryogenic temperature levels. Because of their operating temperature, they require good thermal decoupling while maintaining good mechanical coupling to the satellite structure. This type of attachment can be achieved by means of low-conductance supports or variable thermal resistance devices (heat switches). Additionally, thermal control devices that provide the required cooling for these devices are needed.

In some space missions (such as planetary missions), radioisotope thermoelectric generators (see Section 13.3) instead of solar panels are used to provide electrical power for both the spacecraft platform and the science payload. Usage of a radioisotope thermoelectric generator allows for a large amount of almost constant electrical power to be continuously generated for all mission conditions. For instance, in the Mars Science Laboratory mission, the basic architecture of the thermal system utilizes the waste heat produced by a radioisotope thermoelectric generator to maintain the temperature of the rover within its limits on the surface of Mars (Bhandari et al., 2005), but during cruise, this waste heat needs to be dissipated safely to protect the sensitive components in the spacecraft and the rover.

Spacecraft waste heat is ultimately rejected to space by radiators, which are systems which take the waste thermal energy from a heat source and reject it by radiation to the exterior, through radiating surfaces. Although spacecraft radiators may adopt very different forms (from simple flat-plate radiators mounted on the side of the spacecraft, to

radiating panels deployed after the spacecraft is in orbit), whatever the configuration, all radiators reject heat by infrared radiation from their surfaces. Thus, the radiating power depends on the emissivity and temperature of the radiating surfaces. Obviously, the radiator must reject the spacecraft waste heat, but also any radiant heat loads from the environment or other spacecraft surfaces that are absorbed by the radiator. Most radiators are therefore given surface finishes (see Chapter 6) with high infrared emissivity ($\varepsilon > 0.8$) to maximize heat rejection, and low solar absorptance ($\alpha < 0.2$) to limit heat loads from the surroundings.

As is well known, the net heat leaving a radiator surface per unit time (assuming a view factor of 100% to space) is given by the simple expression

$$\dot{Q}_{\text{rad}} = A\varepsilon\sigma\left(T^4 - T_0^4\right) \cong A\varepsilon\sigma T^4, \tag{8.1}$$

where A is surface area, ε the infrared emissivity, σ the Stefan-Boltzmann constant ($\sigma = 5.67 \times 10^{-8}$ W/(m^2·K^4)), T the absolute radiator temperature, and T_0 the deep space temperature ($T_0 << T$). According to this expression, it is clear that the radiating capability largely increases with the temperature, $\dot{Q}_{\text{rad1}}/\dot{Q}_{\text{rad2}} \cong (T_1/T_2)^4$. This fact is of paramount importance when cryogenic temperatures are considered, because, according to the fourth power temperature law, an 80 K radiator has a heat-rejection capability 200 times smaller than that of a 300 K room temperature radiator, ($\dot{Q}_{\text{rad1}}/\dot{Q}_{\text{rad2}} \cong (80/300)^4 \cong (1/200)$. This characteristic makes cryogenic radiators extremely sensitive to environmental heating and heat leaks through insulation and supports, and leads to special design considerations.

Depending on how the heat is transferred from the source to the radiating surfaces, radiators can be classified as passive radiators and active radiators. In the former the connection

between the heat source and the radiating surface is made either by direct contact or by means of heat pipes (phase change capacitors are also used), whereas in the latter the thermal link is established by means of fluid loops or by means of fluid loops plus heat pipes.

Active radiators require power to pump the fluid responsible for the heat convection. This fluid is pumped from the source either to the radiating surfaces or just to their root. In this latter case, heat pipes should be used to increase the thermal conductivity of the radiating surfaces.

In the case of active radiators with the heat source connected to the radiating surfaces by means of fluid loops (see Chapter 14), the fluid exchanges heat with the radiating surfaces while it is being cooled (Figure 8.1). Generally, the working fluid is a two-phase fluid entering into the radiator-tube panel in the vapour phase and leaving as a liquid which has been condensed while passing through the tubes of the radiator. Because of their large capacity to remove heat loads, these active radiators are normally used to dissipate the waste heat in spacecraft power systems.

Figure 8.1 **Sketch of a typical configuration of radiator (R) with fluid loop (FL) and heat pipes (HP)**

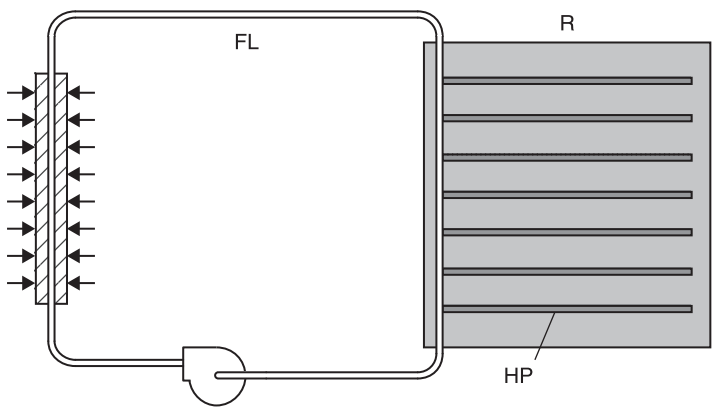

Because of the potential for failure of mechanical pumps, active radiators using mechanically pumped fluid loops are mainly employed in crewed systems that either have short mission durations or are massively redundant and serviceable by astronauts (examples are the Space Shuttle and the International Space Station), whereas passive radiators are normally used in unmanned spacecraft, usually designed for long-duration missions with no servicing. However, because of the increase of the reliability of mechanical pumps and the continuous increase of the available power in unmanned spacecraft, mechanically pumped loop cooling systems may at some point demonstrate a significant weight advantage over competing passive (heat pipe) systems. This is the case of the Mars Science Laboratory mission, where mechanically pumped fluid loops are used to both harness the radioisotope thermoelectric generator heat during surface operations, as well as to reject it to space during cruise phase.

When a heat pipe is used in addition to a pumped fluid loop, the working fluid of the fluid loop carries the heat from the source to the root of the radiating surfaces, while a system of heat pipes distributes the heat along these surfaces. The evaporators of the heat pipes are braced to the fluid loop, and the condensers to the radiating surfaces. In passive radiators, the radiating surfaces are connected to the heat source by thermal conduction through the walls of the heat source, by radiation, or by both.

The main advantage of these passive radiators is their simplicity, and although they have been mainly used to cool lenses and infrared detectors in the range of cryogenic temperatures, there is no reason to overlook possible applications at higher temperatures, provided that the required size does not exceed reasonable limits.

Since directly connected radiators can be tailored to the system to be cooled, it is difficult to define standard

configurations. When passive radiators connected to the heat source with heat pipes are used, the evaporators of the heat pipes are placed close to the heat source, and the condenser zones are placed on the radiating surfaces.

Another possibility explored in the past has been the use of radiators where heat transfer through the radiator is controlled by a phase change material, which melts during the high heat dissipation periods, and freezes again when the temperature decreases (thus absorbing heat during periods of high heat loads and rejecting it when the heat loads are lower). However, radiators with energy storage have rarely been used because of concerns about poor heat transfer through the phase change material due to their low thermal conductivities, and to the lack of theoretical models to accurately predict their performance, although some attempts have been made recently to provide a theoretical basis for the design of space radiators with energy storage (Roy and Avanic, 2006).

In the following sections the main characteristics of passive radiators are outlined.

8.2 Passive cryogenic radiant coolers

A method of obtaining cryogenic temperatures in space is to take advantage of the low-temperature sink of deep space through a passive radiant cooler. This concept is potentially attractive since such a system is completely passive, requires no power, and is capable of high reliability for extended periods. Passive radiant coolers have been developed for the cooling of charge-coupled devices, infrared cameras, and X-ray telescopes, among many other types of electronic equipment, to temperatures in the range from 70 K to 200 K.

Passive cryogenic radiators can have one stage (single-stage), or more than one stage (multi-stage). The efficiency of these coolers is primarily a function of the thermal decoupling from the spacecraft temperature, and the degree of insulation from external radiant fluxes. In the case of multi-stage coolers, the efficiency is also based on the thermal insulation between the successive stages by means of multilayer insulations and low-conductance supports, which minimize the heat exchange by radiation and by conduction, respectively. Furthermore, low-conductance supports can also provide high mechanical coupling needed during the launch/ascent phase of the mission.

In multi-stage radiant coolers each intermediate stage intercepts the parasitic heat leakage from the insulation below and radiates it to space, thus allowing the successive radiator stages to achieve colder temperatures. The lowest temperature stage is called the radiator cold stage, which dissipates the waste thermal energy. Usually, the radiator stages are shielded from environmental heat sources, such as solar radiation, terrestrial infrared, and albedo radiation, by means of a Sun shield. The Sun shield reflects back the environmental heat load into space, thus providing insulation for the radiator cold plate, as shown in Figure 8.2.

Many parameters must be considered for the design of passive cryogenic radiators. Besides those relative to the type of orbit, the orbit altitude, the orientation of the spacecraft relative to the Earth and Sun, and the location of the radiator aboard the spacecraft, other parameters to be considered include the thermo-optical properties of the radiator stages and of the multilayer insulations, the thermal properties of the insulating materials, the heat load applied to the radiator cold plate, and the geometry. Passive radiator coolers also present potential problems relative to the contamination of

Figure 8.2 **Sketch of the Meteosat Second Generation SEVIRI radiant cooler**

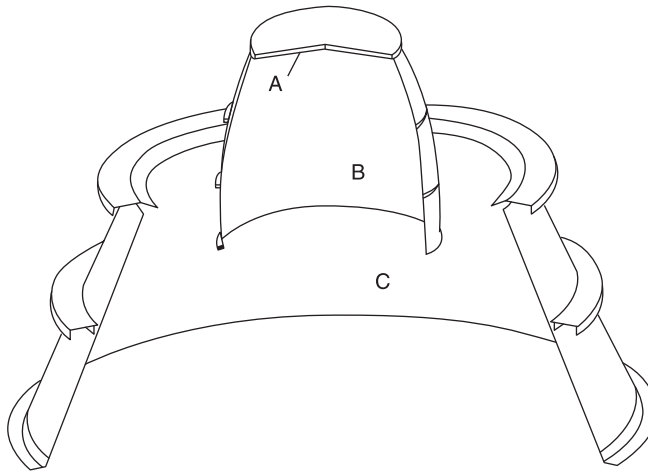

Key: A, radiator second stage; B, radiator first stage; C, Sun shield.

Source: After Jamotton et al. (1999) and ESA BR-153 (1999).

cold surfaces by outgassing from either the spacecraft or the radiator itself.

Passive radiator configuration varies according to mission constraints. As already stated, in general, radiant coolers have several stages, the thermal performance of such coolers almost being maximized with just three stages, although in some cases two stages are enough to meet heat rejection requirements (additional stages provide negligible thermal improvement and add considerably complexity to the design).

The radiator area needed for a given cooling power at a given temperature, as well as the overall geometry of the passive radiant cooler, depend on the orbit of the spacecraft on which the passive radiator is mounted. Therefore, the design of passive coolers is adapted to the orbit. According to Doornink et al. (2008), most existing passive radiators

can be classified into three geometrical designs corresponding to three different types of orbit: (1) low Earth orbit,(2) geostationary orbit, and (3) halo-orbit around Sun–Earth Lagrange point 2.

Thermally, the main difference between these orbits is in the Earth flux levels. The warm part of the spacecraft and the solar fluxes have to be shielded from the cooler in all cases, but the closer the spacecraft is to Earth, the more effort has to be put into the shielding of Earth fluxes as well.

The main characteristic of low Earth orbits is that there is a considerable view factor from the spacecraft to the Earth. The Earth emits infrared radiation and reflects sunlight, both of which have to be blocked. In low Earth orbits the spacecraft has a constrained orientation with respect to the Sun, and in such a case there is a permanently Sun-shadowed side of the spacecraft suitable for mounting a passive cooler (as occurs in Sun-synchronous orbits). In other cases, it is necessary to periodically perform orbit manoeuvres to achieve and maintain permanently shadowed areas of the spacecraft. Passive radiators for low Earth orbits usually have two radiation shields: one of them blocks solar fluxes, whereas the second shield blocks the Earth's radiation from the radiator patch. All this shielding reduces the view of the radiator of cold space. In most cases, the Sun and Earth shields simultaneously act as a reflector, enhancing the view factor of the radiator patch to cold space.

Although there is not a unique geometry for low Earth orbit passive coolers, a typical example of these radiant coolers can be found in the SCIAMACHY two-stage cooler (Kamp et al., 2000), a passive radiant cooler including a cold bus for the SCIAMACHY Instrument on board of Envisat (Figure 8.3). The two-stage cooler has a parabolic reflector to provide coupling to space for the cold stages and to reflect Earth fluxes over the edge of the radiator area. A deployable

Earth shade door shields Earth fluxes and reflects solar flux away (the Earth shield is the part in the front, D, whereas the Sun shield is the curved part on the top, A). The first-stage radiator is the rectangular surface in the centre, C. The second-stage radiator is a black corrugated surface underneath the Sun shield, B, which on the inside is a parabolic reflector. This radiator patch is oriented in a plane that is just over the Earth's horizon. The bus has two cryogenic heat pipes connecting the second stage to the low-temperature detectors, which are supported by glass fibre spikes to a thermal shield that is connected to the first stage of the cooler.

Another typical design of a radiant cooler for low Earth orbit spacecraft is the cooler of Landsat Thematic Mapper, flown at the beginning of the 1980s. This two-stage cryogenic radiator was designed to provide a 90 K environment for the infrared detectors of the Thematic Mapper (Blanchard and Weinstein, 1980). The radiative cooler consists of a specular

Figure 8.3 **Sketch of the SCIAMACHY (SCanning Imaging Absorption SpectroMeter for Atmospheric CHartographY) two-stage cooler**

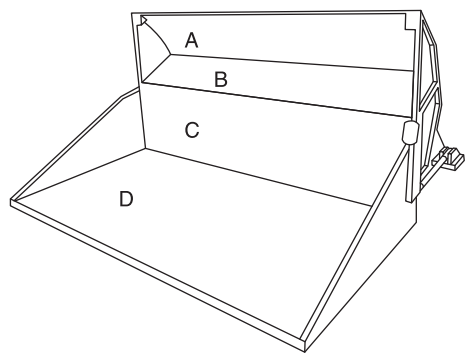

Key: A, Sun shield; B, second-stage radiator; C, first-stage radiator; D, deployable Earth shield.

parabolic shield (A), a cold-stage radiator (B), an intermediate-stage radiator (C), and a specular planet shield (D), as sketched in Figure 8.4. Both cold and intermediate cooling stages employ open-faced honeycomb for the radiator emitting surfaces and the radiators are shielded from direct view of the Sun, Earth, or spacecraft appendages. The cold-stage radiator sees only cold space and infrared emissions from a cooled radiation shield mounted on the intermediate stage. Earth energy is shaded from the radiators of both stages by a deployable Earth shield which also serves as a door. Diffusely reflected solar energy and infrared emissions from the Earth shield fall only on the intermediate stage radiator.

Many other geometrical designs have been used in cryogenic radiators for low Earth orbit spacecraft. For instance, the two-stage radiator used in ABRIXAS,

Figure 8.4 **Sketch of the cryogenic cooler of the Landsat Thematic Mapper**

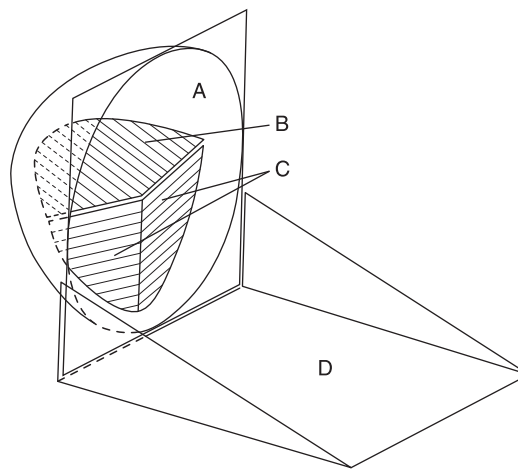

Key: A, intermediate-stage radiation shield; B, cold-stage radiator; C, intermediate-stage radiator; D, deployable Earth shield/door.

Figure 8.5 Arrangement of the ABRIXAS cryogenic cooler

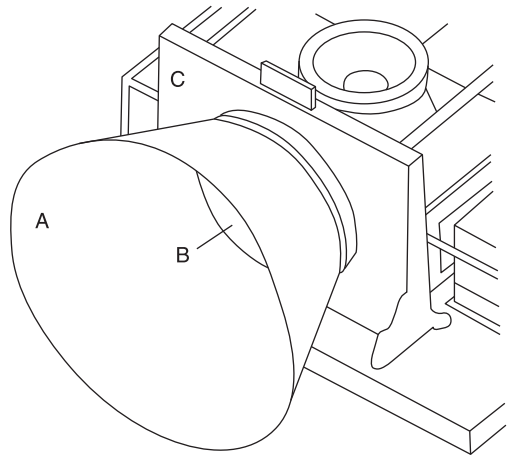

Key: A, conical baffle; B, primary radiator; C, secondary radiator.

Figure 8.5, consists of: a circular primary radiator (B) with a 0.4 m diameter, covered with a white thermal paint; a conical baffle (A) of 0.4 m length and 23° opening, with a highly reflective inner surface to minimize Earth radiation on the primary radiator; and a rectangular secondary radiator (C), covered with the same white paint, integrated into a structural frame which carries the entire radiator module (Brand and Schlitt, 1997).

The requirements of cryogenic radiators for geostationary orbit spacecraft are considerably different from those for low Earth orbit. First, in geostationary orbits the blocking by the Earth of the radiator cold space view is considerably less and, second, the Earth fluxes are much lower. In any case, a shield/reflector combination needs to prevent the Earth's and the Sun's radiation from reaching the radiator patch, while maintaining a view to cold space as large as possible. Nevertheless, here the shield/reflector is somewhat simpler than the low Earth orbit equivalent. An example of

a passive cooler for geostationary orbit is that used on the Meteosat Second Generation SEVIRI (Figure 8.2). This cooler is axisymmetric because the Meteosat Second Generation is a spinning spacecraft. The reflector (internal cone) is elliptical. The advantages of this shape include the complete rejection and sharp cut-off of all radiation entering the reflector beyond a specific acceptance angle from the axis, and the rejection of almost all parasitic radiation originating from the reflector's interior surface, except by a direct view. Therefore, the secondary flux on the second-stage radiator is already minimized. The Sun shield is used to avoid direct solar fluxes on the first and second-stage radiator of the radiator assembly.

When axisymmetry is not needed, the cooler design can be simplified to some extent. This is the case of the radiant cooler flown on the Indian satellite KALPANA-1, shown in Figure 8.6 (Rastogi et al., 2010). In this cooler, the patch (C) is made of an aluminium honeycomb core coated with

Figure 8.6 Sketch of KALPANA-1 radiant cooler

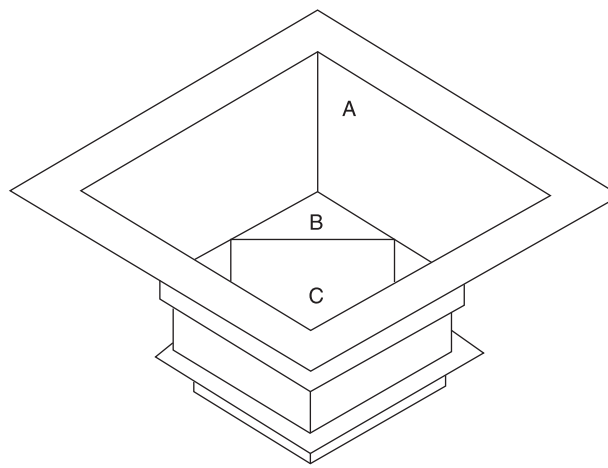

Key: A, Sun shield; B, radiator second stage; C, patch.

conductive black paint. The intermediate stage (B) is co-planar with the patch and the radiator surface facing space is coated with low solar absorptance and high-emissivity white paint. The rear surfaces of the patch and radiator are gold-plated to minimize radiative input to the patch while the Sun shield assembly (A) consists of four trapezoidal panels.

Of course, there are many other missions that require orbits different from low Earth or geostationary orbits, each one with their special requirements and constraints. Examples of these are planetary probes or spacecraft in orbit around Sun–Earth Lagrange points. In most cases, the spacecraft has a fixed orientation with respect to the Sun, and the passive cooler is mounted on the anti-Sun side, allowing the cooler to have an unobstructed view to cold space. The shielding of solar fluxes and blocking of parasitic heat flows from the spacecraft are the main design issues here. Compared to low Earth or geostationary orbits, better radiator performance can be achieved. Examples of spacecraft missions around the 2nd Lagrangian libration point L2 (Subsection 3.3.3), that is, approximately 1.5 million kilometres away from the Earth in the anti-Sun direction, are the Darwin and Planck missions. In both cases V-groove radiators are used (see Section 8.4).

8.3 Thermal efficiency

Thermal efficiency of passive radiant coolers is primarily a function of the thermal decoupling from the spacecraft temperature and the degree of insulation from external heat loads. Thermal efficiency of passive radiators, η, is defined as

$$\eta = \frac{\dot{Q}_L}{\sigma A T^4}, \tag{8.2}$$

where $\dot{Q}_L$ is the heat load from the devices to be cooled, A the detector stage (patch) area, T the patch temperature, and σ the Stefan-Boltzmann constant.

The energy balance on the radiator expresses that the radiant power is equal to the sum of the detector heat load, $\dot{Q}_L$, and the parasitic loads, $\dot{Q}_E$. Thus, according to equation (8.1),

$$\dot{Q}_L + \dot{Q}_E = A\varepsilon\sigma(T^4 - T_0^4) \cong A\varepsilon\sigma T^4, \tag{8.3}$$

where ε is the emissivity of the detector stage surface. The introduction of this last expression into equation (8.2) gives the radiator thermal efficiency:

$$\eta = \frac{\dot{Q}_L \varepsilon}{\dot{Q}_L + \dot{Q}_E}. \tag{8.4}$$

This equation indicates that in order to increase the efficiency η it is desirable to minimize the parasitic heat loads, $\dot{Q}_E$, as well as to maximize the patch emissivity, ε. Reductions in $\dot{Q}_E$ can be achieved through high thermal insulation from the satellite and shading from the external flux. Potential heat sources affecting the cooler are listed in Table 8.1.

Expression (8.3) gives the minimum theoretical effective area required as a function of the parameters involved (the detector heat load, the parasitic heat load, and the patch temperature and emissivity). Obviously, the complete assembly is larger because of the shielding system and the structure. For a 0 K heat sink, rearranging expression (8.3) yields

$$\frac{A}{\dot{Q}_L} = \frac{1}{\varepsilon\sigma T^4 - \dfrac{\dot{Q}_E}{A}}, \tag{8.5}$$

where $A/\dot{Q}_L$ is the area needed to evacuate a power unit, so-called specific radiator area. Expression (8.5) gives the

Table 8.1 Potential heat sources affecting radiant coolers

Direct radiant heat flux	Direct solar energy Earth albedo Earth emitted thermal energy Lunar albedo Lunar emitted thermal energy Spacecraft emitted thermal energy
Indirect radiant heat flux	Direct radiant heat flux reflected onto the radiator by the spacecraft assembly Direct radiant heat flux reflected onto the radiator by the cooler assembly surface Radiator emitted or reflected heat flux reflected back by the cooler or spacecraft surfaces Radiative heat leaks through insulation
Conducted and generated heat flux	Heat flux through supports Heat flux generated on the radiator surface by electrical resistance losses

specific radiator area, $A/\dot{Q}_L$, as a function of the detector stage temperature and the ratio $\dot{Q}_E/A$. The ratio $\dot{Q}_E/A$ is estimated to range from 1.60 to 3.20 W/m^2 of radiator surface. Taking into account expression (8.4), equation (8.5) can be rewritten as

$$\frac{A}{\dot{Q}_L} = \frac{1}{\sigma T^4 \eta}. \tag{8.6}$$

The variation of the specific radiator area, $A/\dot{Q}_L$, with the detector stage temperature, T, and the radiator thermal efficiency, η, is shown in Figure 8.7. In this plot the performance of several radiant coolers (measured in terms of specific radiator area, $A/\dot{Q}_L$, versus cold-stage temperature, T, is also shown).

Figure 8.7 **Variation of the specific radiator area with the detector stage temperature for several values of the radiator thermal efficiency**

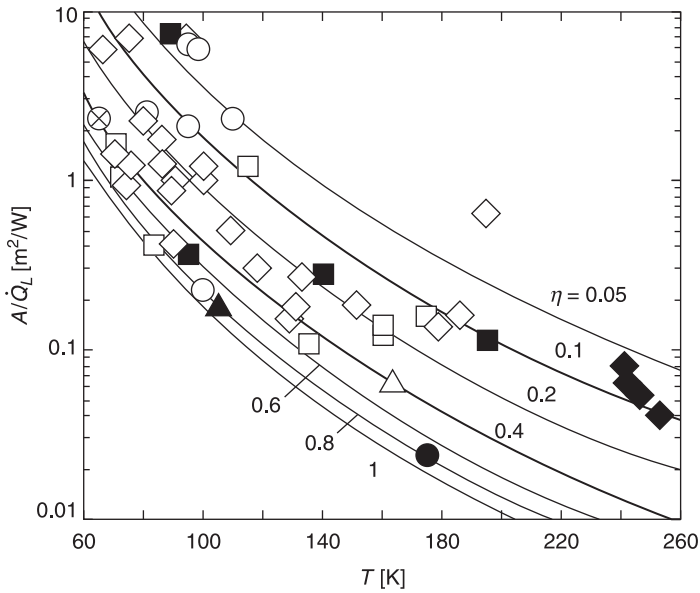

Note: Symbols identify the source of data as indicated in the following. When a radiator is quoted in more than one source, the older source of data is listed.

Symbol	Reference	Symbol	Reference
White triangles	Rastogi et al.(2010)	Black triangles	Van Es and Bsibsi (2006)
White squares	Donabedian (2003)	Black squares	Couto et al. (2002)
White rhombi	Collaudin and Rando (2000)	Black rhombi	Choi (2000)
White circles	STCDD (1989)	Black circle	Brand and Schlitt (1997)
Crossed circle	Bard (1987)		

Some applications of passive radiant coolers require the detector temperature to be stabilized within some limits, so that the radiometric sensitivity of the optical system remains constant. This stability can be achieved by bonding a strip heater and temperature sensor onto the insulated side of the patch. A heater control circuit is used to maintain a constant temperature.

The control heater can also be used to prevent icing of the patch during the initial cool down and outgassing periods. Once the outgassing has subsided, the heater can be switched to a control mode, and the patch cools to its normal operating temperature.

In addition, flight data indicate that passive radiant coolers can suffer from contamination of their thermal control surfaces. This contamination, which is due to outgassing from the satellite, changes the optical properties of the surfaces and tends to raise the patch temperature with a corresponding decrease in detector sensitivity. In this case, heaters can be provided to reverse the contamination.

8.4 V-groove radiators

As pointed out in equation (8.4), the thermal efficiency of a passive radiator depends on the parasitic thermal loads, which must be reduced as much as possible to increase the efficiency. Therefore, since the thermal insulation on the cold payload can be transmitted either through radiative or conductive links, great efforts have been made to drastically reduce such parasitic loads.

To reduce the radiative links between the spacecraft and the cold payload, the common solutions are the use of thermal insulation of the payload with multilayer insulation blankets, and of V-groove shields.

Multilayer insulation is the conventional approach, and is used in most existing passive cooler configurations such as Meteosat Second Generation or Envisat. When this technology is used, the typical effective emissivity of the blanket is in the order of 0.015 (see Section 7.2), giving a heat flow of more than 6 W/m^2 between 50 K and 300 K (Collaudin and Passvogel, 1999).

The V-groove concept is similar in principle to multilayer insulation, as it consists of several shields, but with an open angle between each shield. Larger V-groove cavities are created by arranging adjacent shields with an angle of a few degrees expanding outwards from the cold stage, giving each shield a view factor to space (Bard, 1987). The shields intercept radiation from the warm spacecraft and instrument, and by multiple reflections direct the energy out of the openings towards space. This system allows an efficient heat rejection to space, resulting in excellent insulation efficiency. The radiation can escape easily from the shields, rather than being trapped, as is the case for the multilayer insulation. Parasitic conductive heat leaks are reduced by the use of low-conductance structural supports.

If ε is the emissivity of each layer, the equivalent emissivity of the V-groove shields assembly will be near ε^2, compared to ε/n for an n-layer multilayer insulation. This becomes very efficient for very low-emissive surfaces, such as aluminium (ε = 0.05) or gold (ε = 0.02) coatings. In addition, the predictability of this design with such a shield is good, as the geometry and the coatings are well known. The drawbacks of the V-groove shields are the constraints on the geometry, and the integration.

An example of the use of V-grooved radiators can be found in the Planck spacecraft, a satellite of the European Space Agency, devoted to cosmic microwave background research. A sketch of the Planck satellite is shown in Figure 8.8. Planck

Figure 8.8 **Sketch of Planck satellite showing the V-groove radiator**

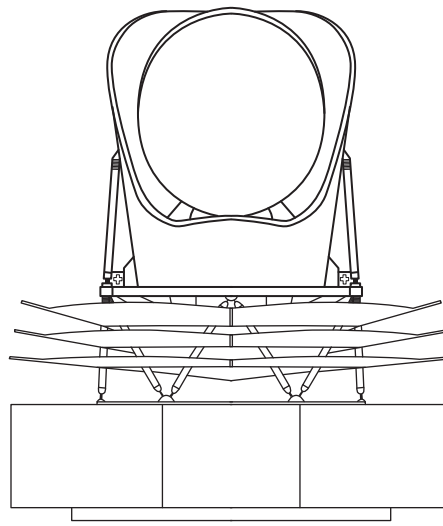

Source: After Tauber et al. (2010).

Figure 8.9 **Sketch of EPIC with the four-shield V-grooved radiator deployed**

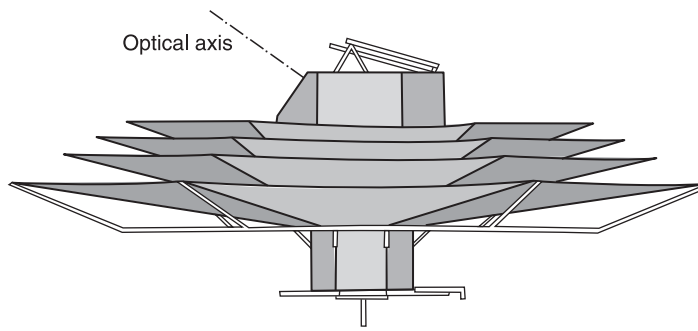

Source: After Chui et al. (2010).

is equipped with three V-groove radiators. The final V-groove is required to achieve between 45 K and 60 K at the same time providing the required cooling power for the instruments (Tauber et al., 2010). A similar design, following in the footsteps of the Planck mission, is considered in the Experimental Probe of Inflationary Cosmology (EPIC), an implementation of NASA's Einstein Inflation Probe mission. A sketch of EPIC with the four-shield V-grooved radiator design is depicted in Figure 8.9. Each shield is a double-layered shield, which is needed to mitigate the risk of micro meteorites puncturing the shield.

8.5 References

Bard, S. (1987) Development of a high-performance cryogenic radiator with V-groove radiation shields, *Journal of Spacecraft*, **24**: 193–7.

Bhandari, P., Birur, G., Pauken, M., Paris, A., Novak, K. et al. (2005) 'Mars Science Laboratory thermal control architecture', Paper 05ICES-196, 35th International Conference on Environmental Systems, Rome, Italy, 11–14 July 2005.

Blanchard, L.E. and Weinstein, O. (1980) Design challenges of the Thematic Mapper, *IEEE Transactions on Geoscience and Remote Sensing*, **18**: 146–60.

Brand, O. and Schlitt, R. (1997) 'Low temperature radiator design for the ABRIXAS X-Ray Satellite', 6th European Symposium on Space Environmental Control Systems, Noordwijk, The Netherlands, 20–22 May 1997, ESA SP-400.

Choi, M.K. (2000) 'Thermal considerations of SWIFT XRT radiator at -350 C or colder in low Earth orbit', Paper

AIAA-2000–2906, 35th Intersociety Energy Conversion Engineering Conference, Las Vegas, Nevada, USA, 24–27 July 2000.

Chui, T., Bock, J., Holmes, W. and Raab, J. (2010) Thermal design and analysis of a multi-stage 30 K radiative cooling system for EPIC, *Cryogenics*, **50**: 633–7.

Collaudin, B. and Passvogel, T. (1999) The FIRST and Planck 'Carrier' missions. Description of the cryogenic systems, *Cryogenics*, **39**: 157–65.

Collaudin, B. and Rando, N. (2000) Cryogenics in space: a review of the missions and of the technologies, *Cryogenics*, **40**: 797–819.

Couto, P., Mantelli, M.B.H., Marotta, E. and Fuller, J. (2002) Parametric analysis of heat transfer on multistage cryogenic radiator, *Journal of Thermophysics and Heat Transfer*, **16**: 313–23.

Donabedian, M., Ed. (2003) *Spacecraft Thermal Control Handbook, Vol. II, Cryogenics*, The Aerospace Press, El Segundo, California, USA.

Doornink, D.J., Burger, J.F. and ter Brake, H.J.M. (2008) Sorption cooling: A valid extension to passive cooling, *Cryogenics*, **48**: 274–9.

ESA BR-153 (1999) *Meteosat Second Generation, The Satellite Development, European Space Agency*, ESA Publications Division, ESTEC, Noordwijk, The Netherlands.

Jamotton, P., Cucchiaro, A., Demaret, D. and Balbeur, H. (1999) Cryogenic testing of several parts of the meteosat second generation payload, *Cryogenics*, **39**: 167–74.

Kamp, A., Dobber, M. and van der Linden, R. (2000) SCIAMACHY, ready for launch, *Acta Astronautica*, **47**: 289–96.

Rastogi, S.C., Prasad, M., Basavaraj, S.A., Santram, M., Selvan, T. et al. (2010) Optical polishing for development of highly specular sunshield for radiant coolers of

meteorological satellites of ISRO, ISRO-ISAC-TR-0908, Issue No. A, Rev. 00, 2010.

Roy, S.K. and Avanic, B.L. (2006) Optimization of a space radiator with energy storage, *International Communications in Heat and Mass Transfer*, **33**: 544–51.

STCDD (1989) *Spacecraft Thermal Control Design Data Handbook*, ESA PSS-03-108, Issue 1.

Tauber, J.A., Mandolesi, N., Puget, J.L., Banos, T., Bersanelli, M. et al. (up to 96 authors) (2010) Planck pre-launch status: the Planck mission, *Astronomy and Astophysics*, **520**: A1 1–22, DOI: 10.1051/0004–6361/200912983.

van Es, J. and Bsibsi, M. (2006) Variable effective surface radiator. Executive summary, VARES-TN-010-NLR-Issue 01, Nationaal Lucht- en Ruimtevaartlaboratorium, Amsterdam, The Netherlands.

9

Louvers

Abstract: In this chapter a description of louver systems, their components and their performance is presented. Louver systems are mechanical devices consisting of a frame with an array of highly reflective blades, used to modify the effective emissivity of a radiator, by blocking its view of outer space. They are used when the environmental conditions or the power internally dissipated change considerably throughout the different mission phases in order to decrease the power need for compensation heaters. Most louver actuators are passive, based on bimetallic helicoidal springs, which allow them to work without any power consumption.

Key words: louvers, blades, bimetallic springs.

9.1 Introduction

The thermal control subsystem of most spacecraft is based on the thermal insulation of the spacecraft from space, and the appropriate sizing of radiators located on its outer surface whose aim is to reject to space both the power internally dissipated and the absorbed environmental heat fluxes (see Chapter 2). In this way, the effect of the highly fluctuating environmental thermal loads on internal equipment is damped. The sizes of the radiators are calculated for the worst hot operational case, that is, for the case when the

spacecraft is exposed to the maximum environmental thermal loads and the power internally dissipated is the maximum. The most suitable thermal finish to be used on radiators requires a high emissivity, thereby minimizing the area, and therefore, the mass of the radiator. If the radiator is exposed to solar radiation, a low solar absorptance value is also required. Thus, white paints or optical solar reflectors are typical radiator finishes. For the cold cases, compensation heaters are used to maintain the devices above the lower limit.

On some occasions the environmental conditions change considerably throughout the different mission phases, or the spacecraft electrical heating power is limited, and therefore there is not enough power available for the thermal subsystem. This is, for instance, the case of ESA's Rosetta mission, whose mission includes several Earth flybys and a long period of deep space hibernation. In these cases, one way of maintaining the spacecraft temperature above a minimum is to diminish the emissivity of the radiators, to decouple the spacecraft from outer space and minimize the electrical power used for the heaters. Although currently research is being carried out regarding electrochromic emissivity modulators for space use (Demiryont and Moorehead, 2009; Bannon et al., 2010), over the last few decades the flight-proven devices most widely used to modify the effective emissivity of a radiator have been thermal louvers.

Louvers have been used since early space missions. Thus, Mariner 2, the first successful mission that flew by a planet other than Earth, Venus, was launched in 1962, and used louvers as part of its thermal control system (Dumas et al., 1963). In this mission, the effective emissivity ranged from 0.08 to 0.72, as described by Gram (1964). Since then, louvers have been used very often, and although over the years their designs have evolved, mainly aimed at improving

the performance and diminishing the mass of the system, current concepts are very similar to the old ones both mechanically and functionally.

9.2 Description of louvers

Louvers are mechanical devices that consist of a frame which contains an array of highly reflective blades, usually specular, which can pivot about their longitudinal shafts by means of some actuators, similarly to a Venetian blind, as shown in Figure 9.1. The ends of the shafts are attached to the frame by bearings. This assembly is fitted over the spacecraft radiator. When the temperature of the radiator increases, the actuators rotate the blades towards their open position, normally perpendicularly to the radiator surface, in such a way that the radiator has the maximum view of outer space.

Figure 9.1 Typical louver design (Venetian blind type)

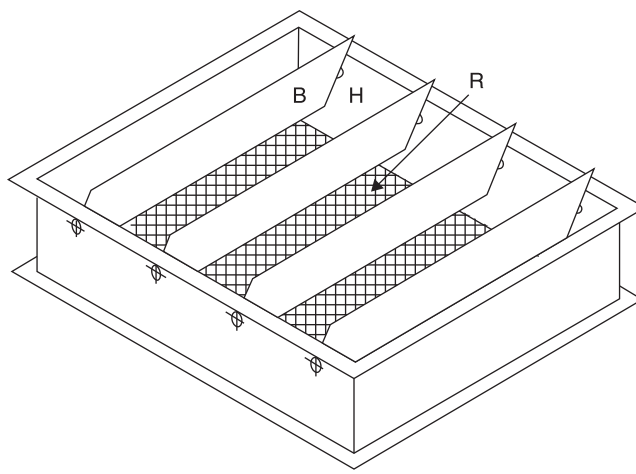

Key: R, radiator; H, housing; B, blades.

When the temperature of the radiator decreases, the actuators move the blades towards the closed position, totally blocking the radiator's view of outer space. The highly reflective, and therefore low-emissive, finish of the blades lowers the energy radiated to space.

The physical effect of the louvers is the blockage of the radiator area by means of the blades, but in order to measure its performance, and for comparison purposes, an effective emissivity is defined, as will be explained below.

The two most important and sensitive louver system components are the blades and actuators, elements which are described in more detail in the following subsections.

9.2.1 Blades

Although for each application louver blades have different sizes and thicknesses, the principles of design are common to most commercial louvers. Thus, louver blades are usually thin, rectangular, aluminium pieces made from one or two individual sheets. If two are used, they are bonded along their longitudinal edges and to a hollow central aluminium shaft. The thickness of the blades is in the order of 0.3 to 0.5 mm. The louver system has to withstand high vibration loads, a fact which constrains the design.

The surface thermal finish of the blades has to be highly reflective. Traditionally, highly specular finishes have been used. Thus, polished aluminium was used for Mariner 2 (Dumas et al., 1963), whereas VDA (vapour deposited aluminium) Kapton tape was more recently used for Rosetta (Domingo and Ramírez, 2003; Härtel et al., 2000). If the louver system is sunlit, a radiation shield has to be used to avoid solar radiation becoming trapped between the blades.

Some studies have been carried out to find out which highly reflective blade surface performs better: specular or

diffuse. Butler et al. (1967) came to the conclusion that, on average, during the maximum dissipation periods, diffuse blades reject less energy than specular ones, but they also absorb less energy.

Among the initiatives to reduce the mass of louver systems, Buna (1984) proposed the concept of a flexible louver made of flexible blades (e.g., aluminized Kapton film) built into a single deformable assembly.

9.2.2 Actuators

Louver actuators are the devices that move the blades, allowing or impeding the view between the radiator and the surroundings. They vary the angle of their blades depending on the temperature of the radiator, according to previously calibrated values. In principle, the actuators can act passively or actively, but in the latter case electrical power is needed. However, most of the louvers flown are actuated by means of bimetallic helicoidal springs formed by two bonded strips of materials with different coefficients of thermal expansion. These bimetallic actuators are located within a housing that provides thermal insulation from the environment, and good thermal coupling with the radiator surface, so that they can react to changes of temperature of the radiator without any power consumption. Each blade is moved by its own actuator, which allows for the control of local effects.

Instead of the traditional bimetallic actuators, novel trimetallic actuators with an intermediate copper layer were used for the louver systems fitted over the radiators of the Rosetta spacecraft (Domingo and Ramírez, 2003). In this way, the coil thermal conductivity was multiplied by a factor of 15 when compared to a conventional bimetallic one. The tasks carried out to design this new actuator included the estimation of the friction torque against which the actuator

has to open the louvers (the torque was obtained from a rig test on the ground as a conservative approach), and the definition of the nominal range of temperature.

Another type of actuator is bellows, a thin-walled, circumferentially corrugated cylinder. An inner to outer pressure difference causes a change in the bellows' length. If one end is clamped and the other is free, the bellows can work as an actuator. In this case the blades are actuated by a temperature-sensing element containing a vapour–liquid mixture. The Nimbus satellites, the second generation of spacecraft used for meteorological research, used bellows with Freon 11 and Freon 114 (London, 1967).

More recently, Matovic and Reichenberger (2010) have proposed shape memory alloys to replace bimetallic actuators. The principle of operation of these 'smart materials' is based on solid-to-solid phase transformations from the martensite phase to the austenite phase induced by temperature or stress.

9.3 Performance of louvers

The performance of louvers is based on two factors: mass and thermal behaviour.

The mass parameter used to compare louvers is the ratio of mass to footprint area. Although for Mariner 2 this ratio had a value of 8.6 kg/m^2, shortly after, the design for Mariner C practically halved this value (Gram, 1964).

The values of the mass parameter for current spacecraft depend on the louvers' geometry and accommodation. Typical values range from 3.2 kg/m^2 for the Global Positioning System (GPS) satellites, to 5.4 kg/m^2 for the Mars Global Surveyor (Gilmore, 2002; ORBITAL, 2011). Reducing the mass of louvers is currently a target. However, according to

Karam (1998), current Venetian blind louvers are themselves the result of great efforts made to cut back on mass. A major concern in mass reduction is a reduced frame rigidity, which can lead to distortions and the binding or hindering of the blades' movement.

The thermal behaviour of louvers has been widely studied over the last decades since the flight of Mariner 2 (Plamondon, 1964; Buskirk and Parmer, 1965; Karam, 1979; Furukawa, 1979; Eby and Karam, 1987; Furukawa, 1993). Detailed information about louver thermal models for performance prediction, transient behaviour, Sun shielding modellization and effects, as well as experimental data can be found in Karam (1998).

The main parameter, already mentioned, used to measure the thermal behaviour of louver systems is the effective emissivity, ε_{eff}. It is defined as the ratio of net heat transfer, $\dot{Q}$, from a louvered surface to the energy that would be radiated from an equivalent black area, A, at the same temperature, T, but in the absence of louvers. Thus,

$$\varepsilon_{eff} = \frac{\dot{Q}}{A\sigma T^4}, \tag{9.1}$$

where $\sigma = 5.67\times10^{-8}$ W/(m^2·K^4) is the Stefan-Boltzmann constant.

It should be mentioned that real louvers also involve heat conduction along the frame and the blades. The effective emissivity thus defined includes these effects, and has to be experimentally determined by measuring the physical magnitudes involved in equation (9.1).

According to Eby and Karam (1987), typical values of effective emissivity, ε_{eff}, when the blades are open are ε_{eff} = 0.62 when the radiator finish is an optical solar reflector (with ε = 0.77), and ε_{eff} = 0.70 if the radiator is painted white (with ε = 0.88). Thus, about 20% of emission capacity is lost

due to the blockage of the blades. When the blades are closed, typical values of effective emissivity are between 0.08 and 0.12. The difference or jump in temperature between both operation modes, open and closed blades, is between 10 and 18 K.

9.4 MEMS louvers

During the last decade, smaller spacecraft, nano- and picosatellites, have appeared on the market for educational and technological demonstration purposes. These spacecraft require thermal control subsystems that fulfil the thermal requirements with very limited power and mass budgets. With this aim, solutions based on microelectromechanical systems (MEMS) have been developed (Osiander et al., 2001, 2004). These systems consist of microelectromechanical arrays of gold-coated sliding shutters that can be operated independently to allow the effective emissivity to be digitally controlled. As a part of the qualification process, a microelectromechanical shutter design was flown on the NASA/GSFC Space Technology 5 (ST-5) technology demonstration mission as a variable emissivity coating. ST-5 was successfully launched in March 2006 and the flight thermal data have been reported by Farrar et al. (2007).

9.5 References

Bannon, E.T., Bower, C.E., Sheth, R., Ryan Stephan, R., Chandrasekhar, P. and Zay, B. (2010) 'Electrochromic radiator coupon level testing and full scale thermal math modeling for use on Altair Lunar Lander', Paper

AIAA-2010–6110, 40th International Conference on Environmental Systems, Barcelona, Spain, 11–15 July 2010.

Buna, T. (1984) 'The development of the flexible louver', Paper AIAA-1984–1795, 19th Thermophysics Conference, Snowmass, Colorado, USA, 25–28 June, 1984.

Buskirk, D.L. and Parmer, J.F. (1965) *Thermal Control Aspects of Spacecraft Louvers*, NASA-CR-88876, January.

Butler, H.W., Parmer, J.F. and Stipandic, E.A. (1967) *Thermal Control Characteristics of a Diffuse Bladed Specular Base Louver System*, NASA-CR-95870.

Demiryont, H. and Moorehead, D. (2009) Electrochromic emissivity modulator for spacecraft thermal management, *Solar Energy Materials and Solar Cells*, **93**: 2075–8.

Domingo, M. and Ramírez, J.J. (2003) Mechanical design and test of ROSETTA platform louvres, ESA SP-524, 289–92.

Dumas, L.N., Gram, M.B., Lewis, D.W. and Spehalski, R.J. (1963) Final report on Mariner 2 temperature control, NASA-CR-52463.

Eby, R.J. and Karam, R.D. (1987) 'Louvers for spacecraft temperature control', Paper AIAA-1987-1567, 22nd Thermophysics Conference, Honolulu, Hawaii, USA, 8–10 June 1987.

Farrar, D., Douglas, D.M., Swanson, T., Collins, C., Darrin, A. and Osiander, R. (2007) MEMS shutters for thermal control – flight validation and lessons learned, *AIP Conference Proceedings*, **880**: 73–80.

Furukawa, M. (1993) 'A new method facilitating design calculations of passively or actively movable louvers', Paper AIAA-93-2733, 28th Thermophysics Conference, Orlando, Florida, USA, 6–9 July 1993.

Furukawa, M. (1979) Analytical studies on design optimization of movable louvers for space use, *Journal of Spacecraft and Rockets*, **16**: 412–25.

Gilmore, D.G., Ed. (2002) *Spacecraft Thermal Control Handbook, Vol. I: Fundamental Technologies,* 2nd ed., American Institute of Aeronautics and Astronautics, Inc., The Aerospace Press, El Segundo, California, USA.

Gram, M. (1964) Temperature control louvers for the Mariner Venus and Mariner Mars spacecrafts, NASA Document ID: 19660023664.

Härtel, K., Morgenroth, L., Reichenberger, K., Domingo, M., Pérez, F.J. and Stramaccioni, D. (2000) 'Thermal design and test of ROSETTA platform louvres', SAE Paper 2000-01-2276, 30th International Conference on Environmental Systems, Toulouse, France, 10–13 July 2000.

Karam, R.D. (1998) *Satellite Thermal Control for Systems Engineers, Progress in Astronautics and Aeronautics* Vol. 181, American Institute for Aeronautics and Astronautics Inc., Reston, Virginia, USA.

Karam, R.D. (1979) Temperature distribution in louvered panels, *Journal of Spacecraft and Rockets*, **16**: 92–7.

London, A. (1967) 'Shutter system design for the Nimbus spacecraft,' Paper AIAA-1967-309, Thermophysics Specialist Conference, New Orleans, Louisiana, 17–20 April 1967. In *Thermophysics of Spacecraft and Planetary Bodies – Radiation Properties of Solids and the Electromagnetic Radiation Environment in Space*, Heller, G.B., Ed., Progress in Astronautics and Aeronautics 20.

Matovic, J. and Reichenberger, K. (2010) Two-way SMA actuators for space application: performances and reliability, *Procedia Engineering*, **5**: 1372–5.

ORBITAL (2011) *Thermal Control Louvers*, http://www.orbital.com (retrieved July 2011).

Osiander, R., Champion, J.L. and Darrin, A.M. (2001) 'Micromachined louver arrays for spacecraft thermal control radiators', Paper AIAA-2001-215, 39th Aerospace

Sciences Meeting and Exhibit, Reno, Nevada, USA, 8–11 January 2001.

Osiander, R., Firebaugh, S.L. and Champion, J.L. (2004) Microelectromechanical devices for satellite thermal control, *Sensor Journal*, **4**: 525–31.

Plamondon, J.A. (1964) Analysis of moveable louvers for temperature control, NASA-CR-53046, January 1964.

10

Mechanical interfaces

Abstract: This chapter describes the phenomenon of heat transfer across a mechanical interface, quantified through the thermal contact conductance, which mainly depends on contact pressure, surface finish and mechanical properties, and the presence of interstitial materials. Main models to estimate this parameter are presented as well as experimental results obtained over the last decades, focusing on those that can be applied to thermal modelling of spacecraft. The different types of thermal fillers, materials used to improve the thermal contact conductance are presented.

Key words: thermal contact conductance, thermal contact resistance, bolted joints, thermal filler.

10.1 Introduction

The two main modes of thermal energy distribution within a spacecraft are thermal radiation and heat conduction, as explained in Chapters 4 and 5. Thermal radiation exchanges are managed through thermo-optical properties (see Chapter 6) and heat conduction is driven by the thermal conductivities of the materials, and the type and configuration of the mechanical joints. Thus, the joints can be adapted to the thermal needs of the system: when thermal insulation is needed, bad couplings are sought; however, when it is

necessary to spread heat, good thermal couplings need to be achieved.

When heat has to be evacuated from highly dissipating devices, as in the case of electronics boxes, special thermal hardware may be needed. This thermal hardware can simply be a thermal filler, used to improve the thermal behaviour of mechanical joints just as in ground systems, or can be a bulky material used to transport heat.

In the following section, the phenomenon of the conductive heat transfer at a mechanical joint is presented, and the models predicting thermal contact conductance are reviewed. The special thermal hardware used to modify the thermal couplings in mechanical joints is described in Sections 10.3 and 10.4.

10.2 Thermal contact conductance

When two solids are brought into contact heat is conducted from one to the other. However, at the interface between both solids, a resistance to heat transfer appears caused by the inherent irregularities of the contacting surfaces. All surfaces, no matter how well polished, consist of asperities, a number of peaks and valleys (as can be seen in Figure 10.1), the result of the machining process. Thus, the actual solid-to-solid contact area is only a small fraction of the total apparent contact area. Voids formed by asperities are either empty in a vacuum environment, or filled with gas in the presence of an atmosphere; in this case the gas contributes little to heat conduction. Therefore, the heat flow is almost exclusively constricted to the areas of solid-to-solid contact, and gives rise to a macroscopically observed temperature jump across the interface. This resistance to heat transfer is called joint resistance or thermal contact resistance, and the inverse value is the so-called thermal contact conductance.

Figure 10.1 Schematic representation of two surfaces in contact and heat flow across the interface. Vertical scale has been oversized

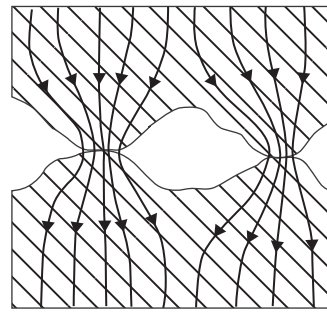

Numerically the thermal contact conductance is quantified as follows. Let us consider two solid rods, A and B, of section A, with their ends kept at different temperatures T_{1A} and T_{2B}, as indicated in Figure 10.2. Their lateral surfaces are thermally insulated so that heat conduction through the rod is one-dimensional. The heat flux is $\dot{Q}$. Macroscopically, in steady-state conditions, a temperature jump ΔT_c is observed at the contact plane. The thermal contact conductance h_c is defined as

$$h_c = \frac{\dot{Q}}{A\Delta T_c}, \tag{10.1}$$

and the thermal contact resistance is the inverse value $R_c = 1/h_c$. When the apparent area of contact cannot be easily identified (as for instance in a bolted joint), the thermal contact conductance is not defined per unit area, but simply as $\dot{Q}/\Delta T_c$.

Thermal contact conductance is a quite complex phenomenon, influenced by many factors. The first factor is contact pressure. As contact pressure grows, the real area of contact grows, and therefore, the resistance to heat flow

Figure 10.2 Temperature distribution of two rods in contact, with the temperature jump at the contact plane, ΔT_c, indicated

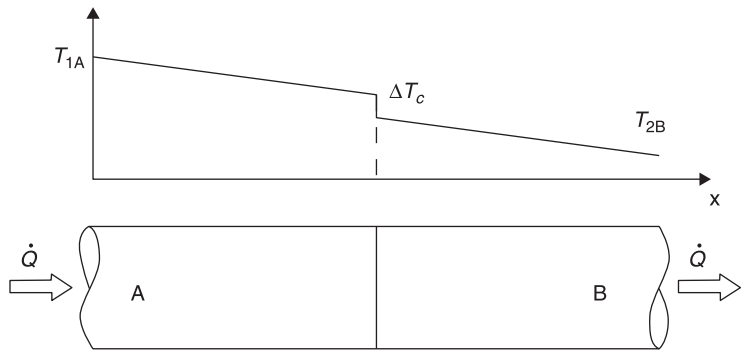

decreases. The second factor is the finish of the surface: the geometry of the asperities and their distribution determines the real contact area. The three properties related to the finish are roughness, waviness and flatness. The third factor is related to the mechanical properties of the contacting solids. When the two bodies come into contact, deformation of the contact surfaces occurs, and this deformation can be either elastic or plastic. If the surfaces undergo plastic deformation, the thermal contact resistance is lowered because the real contact area increases. The mechanical properties related to this factor are the modulus of elasticity when elastic deformation occurs, and hardness when plastic deformation occurs. Finally, the fourth factor is related to the presence of an interstitial material in the contact region. Special materials are commonly used to fill the voids and increase thermal contact conductance. For bare joints, the presence of dust particles or oxide layers can also influence the value of the thermal contact conductance.

The arrangement described above, heat transfer through two solid rods in contact, has been widely studied to define the

thermal contact conductance since the 1950s (Centinkale and Fishenden, 1951) both analytically and experimentally. Some interesting reviews of the problem have been made available in the literature over the years, such as Madhusudana and Fletcher (1986), Sridhar and Yovanovich (1994), Madhusudana (1995) and Yovanovich (2005). A comprehensive review of contact conductance data and models is presented in Gilmore (2002).

The analytical models focus on three aspects of the problem. The first is related to the characterization of the surfaces, that is, the shape and distribution of the asperities. The second is the mechanical problem. When the surfaces are brought into contact deformations occur and the shapes of the asperities change. A real contact area has to be determined as a function of the contact pressure and the mechanical properties of the surface. A deformation model has to be established. Finally, the third element to be studied is the thermal problem for the contact configuration described above. This is a heat transfer problem. The difficulties found over the last few decades in dealing with these three steps have resulted in the problem often being faced experimentally.

Among the different models available for the contact conductance problem, one of the most widely used in later models is that provided by Cooper et al. (1969). These authors solve the thermal problem based on a single flat circular contact. This way they obtain a solution for the temperature field in a single contact. With a model for the distribution of asperities, and therefore contacts, considering the surfaces flat and with random roughness, and assuming that the ratio between the real contact area and the apparent contact area equals the ratio between the contact pressure and the micro-hardness, they obtain the following expression for the thermal contact conductance, h_c which fits quite well with the experimental data then available

$$\frac{h_c}{k}\frac{\sigma}{m} = 1.45\left(\frac{p_a}{H}\right)^{0.985}, \tag{10.2}$$

where $1/k = (1/k_1+1/k_2)/2$ is the harmonic mean of the thermal conductivities of both materials involved in the contact, σ is the equivalent Gaussian variance of the surface profiles heights, $m = |\tan\theta|$ is the mean modulus of the slopes of the asperities, p_a is the apparent contact pressure and H the micro-hardness (in SI units).

Data available in the literature of the thermal contact resistance for aluminium alloys as a function of the contact pressure are shown in Figure 10.3. They have been gathered by Yovanovich (2005), who has also compiled data available in the literature for other materials. The important aspect here is the order of magnitude of the thermal contact conductance,

Figure 10.3 **Contact conductance, h_c, versus contact pressure, P_c, for aluminium alloys obtained by different authors**

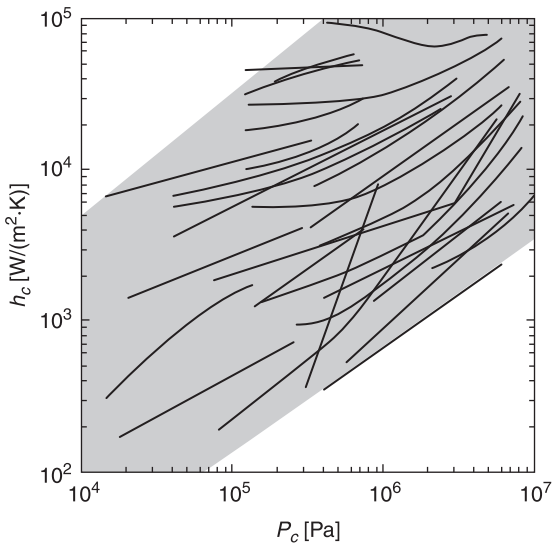

Source: After Yovanovich (2005).

which can range from 10^3 W/(m^2·K) to 10^5 W/(m^2·K) when pressure is applied. As is explained below, these values cannot be directly applied to spacecraft thermal modelling, because the values obtained for real joints are much lower than the ones shown in the figure. Nevertheless, all these studies are really valuable in understanding the phenomenon.

The reason for this lack of applicability to spacecraft joints is that the models and the experimental results are based on the contact configuration described above: two rods in contact, the diameter being in the order of 1 cm. This causes the pressure to be constant over the contact area. However, contact problems in spacecraft deal with larger surfaces where pressure cannot be considered constant. Thus, for instance, most electronics boxes on board spacecraft have a typical dimension ranging from 10 cm to 60 cm, and the mounting systems usually consist of a number of bolts along the perimeter of the mounting base-plate.

One of the first works carried out to improve the prediction of real spacecraft thermal performance of mechanical joints was that of Bevans et al. (1965). They measured the actual thermal contact conductances of bolted surfaces and developed a successful method of correlation for bare mounting joints. In this work two types of joints were studied: components joints and structural ones.

Component joints represent joints such as those appearing when electronics boxes are bolted to a platform. Three configurations with sizes and bolt patterns representative of typical space systems were studied. The influence of the bolts' torques and the power dissipation was analysed. The improvement of the thermal performance of the joint when a thermal filler (a material used to fill voids as will be explained in the next section) is used, was also experimentally quantified. The configurations tested (sizes and bolt patterns) are shown in Figures 10.4 and 10.5.

Figure 10.4 **Component joints configurations (all lengths are in inches)**

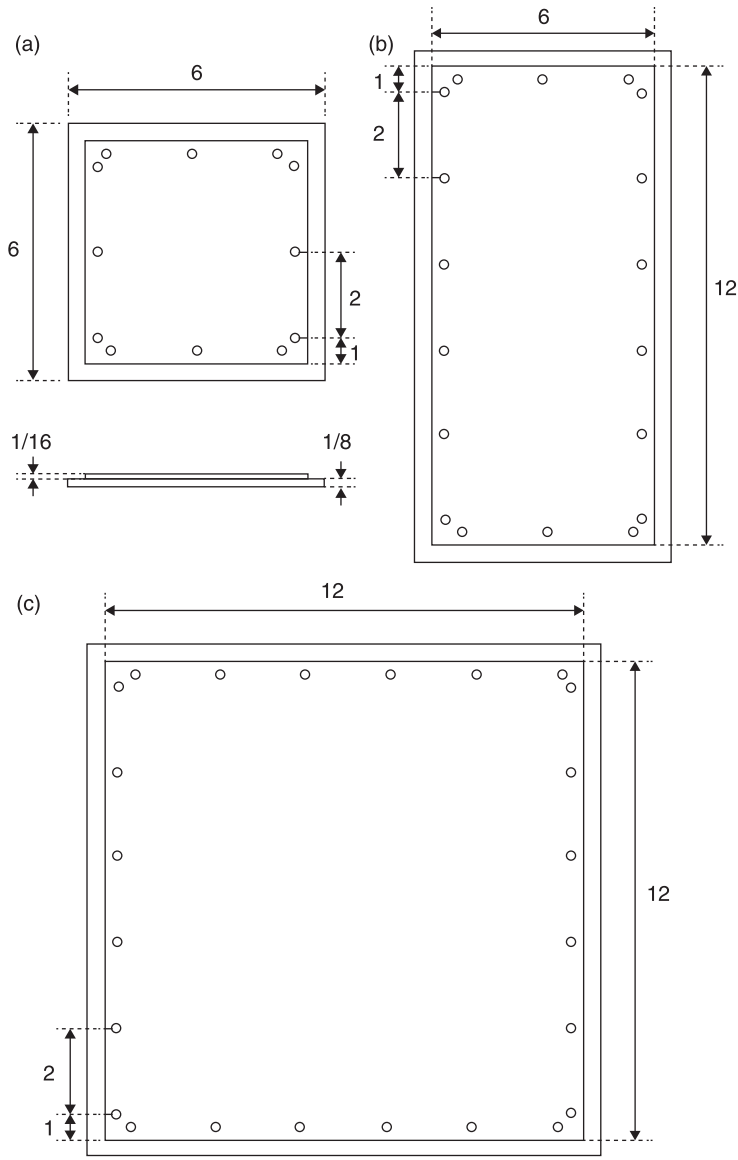

Source: After Bevans et al. (1965).

Figure 10.5 **Structural joints configurations (all lengths are in inches)**

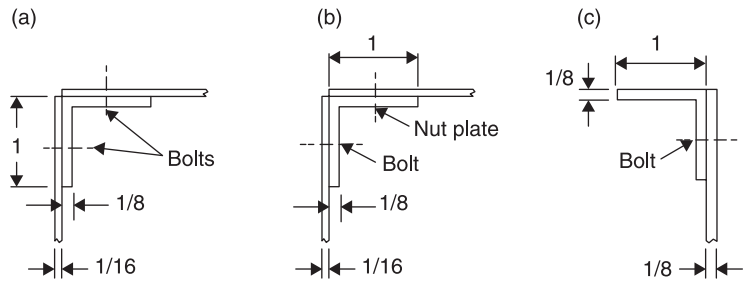

Source: After Bevans et al. (1965).

The results obtained for the bare joints for the three configurations described in Figure 10.4 are shown in Figure 10.6. As expected, the thermal contact conductance measured values are much lower than those obtained for small contacts, such as the ones described at the beginning of this section. Another important issue was the lack of repeatability of the results obtained. This was due to the difference in flatness of the samples tested, which means that, to solve this problem, low tolerances have to be applied during the manufacturing process.

The configurations of the structural joints tested in these experiments are shown in Figure 10.5. The results obtained for the bare joints shown in Figure 10.5 are presented in Figure 10.7.

Roca and Mikic (1972) studied in depth the thermal behaviour of bolted joints. They provided valuable information about the local heat transfer phenomenon across a bolt. However, these results were difficult to directly apply to a thermal design problem. A good compilation of the existing data for thermal resistance of bolts can be found in Gilmore (2002).

Figure 10.6 **Component joints thermal contact conductance, h_c, versus heating power, $\dot{Q}$, for different joint configurations (defined in Figure 10.4); in all cases bolt torque is 2.71 N·m**

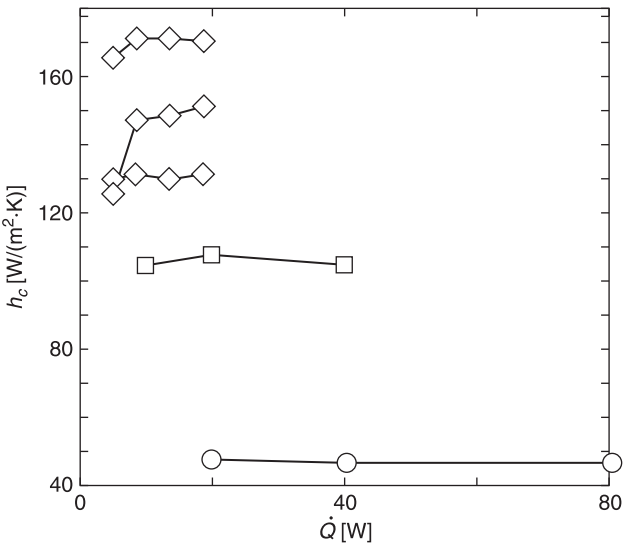

Note: Results correspond to bare joints. Symbols identify the configuration according to Figure 10.4: rhombi (a), squares (b) and circles (c). Different curves correspond to different tested samples.

Source: Data are from Bevans et al. (1965).

Trying to face the real system problem, Costamagna et al. (1991) again dealt with the overall thermal conductance problem of boxes bolted to supporting structures. They derived analytical correlations based on thermal balance tests performed on a number of actual satellites. The correlations correspond to typical configurations of units with aluminium base-plates mounted on aluminium honeycomb plates with M4, M5 and M6 titanium bolts. Two correlations were obtained: one for bare joints and another for joints with a filler material, as a function of the apparent contact area A_c.

Figure 10.7 **Structural joints thermal contact conductance, h_c, versus heating power, $\dot{Q}$, for different joint configurations (defined in Figure 10.5); in all cases bolt torque is 2.71 N·m**

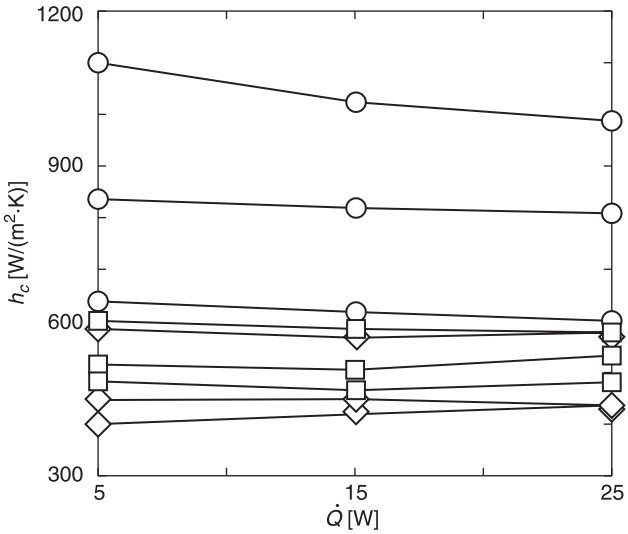

Note: Results correspond to bare joints. Symbols identify the configuration according to Figure 10.5: rhombi (a), squares (b) and circles (c). Different curves correspond to different tested samples.

Source: Data are from Bevans et al. (1965).

Thus, for bare joints

$$h_c = C_{bj} \frac{A_c}{A_0 + A_c}, \tag{10.3}$$

for 0.003 m^2 < A_c < 0.05 m^2, where C_{bj} = 4 W/(m^2·K), A_0 = 0.015 m^2. And for joints where a thermal filler is used the correlation is

$$h_c = \frac{C_{tf}}{A_c^{0.9}}, \tag{10.4}$$

for 0.003 m^2 < A_c < 0.05 m^2, where C_{tf} = 1.99 × 10^8 W/(m$^{1.1}$·K), and a maximum flux through the joint lower than 0.1 W/cm^2.

Note that the applicability of the derived formulae is limited to the contact areas indicated in the expressions.

The prediction of the thermal contact conductance of bolted units is still of great interest. More recently Hakkak and Farhani (2007) proposed a method to measure it. Their main conclusion after this revision is that for applications requiring precision, the only reliable method is to conduct experimental measurements.

10.3 Thermal fillers

Thermal fillers are materials used to fill the voids formed by the surface peaks and valleys appearing in the contact region when two materials are brought into contact. With these materials, the area of the heat transfer path is maximized, and therefore, heat conduction is enhanced. A sketch of how the interface is modified when a thermal filler is used is shown in Figure 10.8. The thermal fillers are usually made of soft materials with high thermal conductivity, and in some cases also high electrical impedance so that they can provide electrical isolation. These thermal fillers are generally used to improve the heat transfer between units with high power dissipation, such as electronics units, and their mounting base-plates.

Figure 10.8 **Effect of a thermal filler in a mechanical joint: (a) before joining the materials, (b) after joining the materials**

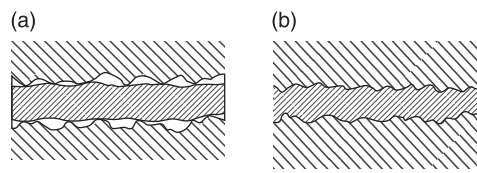

Although nowadays there are a number of thermal materials available in the market, they can be classified into three main types.

The first type of materials are graphite foils, such as Calgraph (Welch and Ruttner, 1989) or Sigraflex (Sigraflex, 2011). They are made of natural graphite flakes with a well-ordered crystalline structure, and are available in different shapes and thicknesses.

The second type of materials are elastomeric thermal fillers, such as the ones produced by Chomerics Co. (Chomerics, 2011). The thermal interface materials are pads that consist of a thermoset elastomeric binder containing a dispersed highly thermally conductive ceramic filler. The elastomeric binder is typically a silicone moulding resin cured at high temperatures and high pressure. Urethane elastomers have been introduced for use where silicone cannot be tolerated due to possible contamination. The ceramic fillers are added to the elastomer to increase its thermal conductivity. Typical fillers are boron nitride, aluminium oxide, and magnesium oxide. This mixture is generally reinforced with fibreglass cloth or with polyimide or polyester dielectric film, which makes the material highly resistant to tearing and cutting.

The main problem with these elastomeric pads is that, at low pressures, contact resistance is high due to the poor fit between surfaces. As pressure is increased, the material begins to flow into the voids and the contact resistance decreases. This may be a problem in the case of large units with a perimeter bolt pattern, where the central area of the box is not in real contact with its mounting base-plate, even with the use of a thermal filler.

The third group of materials that can be used as thermal fillers are the room temperature vulcanizing (RTV) materials. In fact, these materials are 'cure in place'

adhesives that are able to fill all the gaps between the surfaces in contact. This is possible because they form a mould that conforms to the surface profile with voids and peaks.

In 2003, NASA decided to test a number of thermal filler materials against each other to verify which ones performed best. The tests were done only to compare the thermal performance of the materials relative to each other under repeatable conditions, and do not take into consideration other design issues. The materials tested, test apparatus, procedures, and results of these tests, in terms of the ΔT across the contact, can be found in Glasgow and Kittredge (2003).

10.4 Thermal braids and straps

In some applications, the removal of heat of dissipating devices is critical, and cannot be achieved just by radiation and conduction through the mechanical mounting system to the structure. This is, for instance, the case for camera detectors or some cryogenic devices, which require an additional heat transfer path from the heat source to a colder element or radiator.

This additional heat path may simply consist of a piece of a highly conductive material. However, on some occasions, mechanical compliance is also required, which is why flexible thermal straps or braids are used, to avoid the stresses occurring when two materials with different coefficients of thermal expansion are brought into contact. Typical materials that are used to design thermal straps are copper, aluminium, or carbon or graphite fibres.

A typical thermal strap assembly consists of a flexible part attached to two bulky pieces that are bolted to the hot and

Figure 10.9 Typical thermal straps configurations: (a) fibre bundles, (b) multi-foil thermal strap, (c) thermal braids

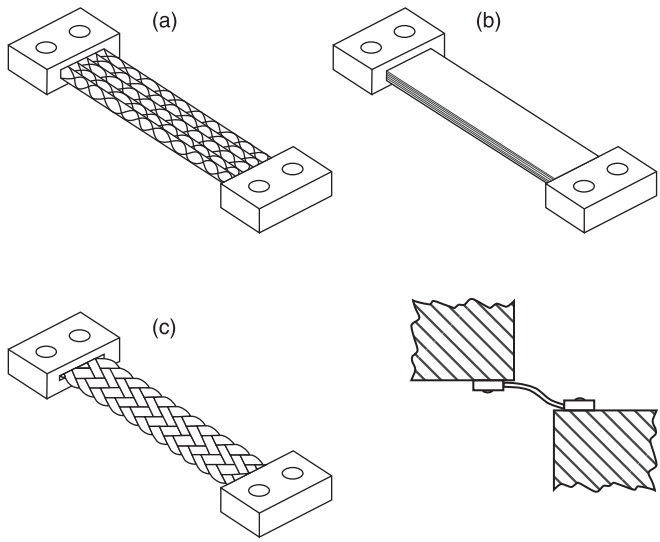

cold surfaces. The flexible part may be one or several braids, a multi-foil pack, or a number of fibre bundles in the case of carbon or graphite fibres. A sketch of the three typical configurations is shown in Figure 10.9.

The performance of the thermal strap is measured through the thermal conductance (or inversely thermal resistance) of the thermal strap. Thus, the strap linear conductance, C, defined as the heat flux passing through the strap divided by the difference of temperature between the ends of the strap may be calculated from $C = kA/L$, where k is the thermal conductivity of the material, A the cross-sectional area of the strap and L its length. A thermal efficiency factor, η, is often defined to take into account the losses. It is defined as the ratio of the real to theoretical values, $\eta = C_{real}/C_{theoretical}$, and has to be determined experimentally for each type of strap.

10.5 References

Bevans, J.T., Ishimoto, T., Loya, B.R. and Luedke, E.E. (1965) *Prediction of Space Vehicle Thermal Characteristics*, AFFDL-TR-65–139, Air Force Flight Dynamics Laboratory, USA, August 1965.

Centinkale, T.N. and Fishenden, M. (1951) 'Thermal conductance of metal surfaces in contact', International Conference on Heat Transfer, Institution of Mechanical Engineers, 271–5.

Chomerics CHO-THERM® T500, *Highly Thermally Conductive Elastomer Insulators*, Technical Bulletin 69, http://www.chomerics.com (retrieved July 2011).

Cooper, M.G., Mikic, B.B. and Yovanovich, M. M. (1969) Thermal contact resistance, *International Journal of Heat and Mass Transfer*, **12**: 279–300.

Costamagna, L., Perotto, V. and Sacchi, E. (1991) 'A systematic approach to thermal balance test evaluation and thermal mathematical model correlation for spacecraft thermal design', 4th European Symposium on Space Environmental Control Systems, Florence, Italy, 21–24 October 1991, ESA SP-324, 425–31.

Gilmore, D.G., Ed. (2002) *Spacecraft Thermal Control Handbook, Vol. I: Fundamental Technologies,* 2nd ed., American Institute of Aeronautics and Astronautics, Inc., The Aerospace Press, El Segundo, California, USA.

Glasgow, S.D. and Kittredge, K.B. (2003) *Performance Testing of Thermal Interface Filler Materials in a Bolted Aluminium Interface Under Thermal Vacuum Conditions*, NASA TM-2003–212500, June 2003.

Hakkak, F. and Farhani, F. (2007) 'Thermal resistance in satellite bolted joints', International Conference on Mechanical Engineering, Dhaka, Bangladesh, 27–31 December 2007.

Madhusudana, C.V. (1995) *Thermal Contact Conductance*, Mechanical Engineering Series, Springer, New York, USA.

Madhusudana, C.V. and Fletcher, L.S. (1986) Contact heat transfer – the last decade, *AIAA Journal*, **24**: 510–23.

Roca, R.T. and Mikic, R.E. (1972) 'Thermal conductance in a bolted joint', Paper AIAA 72–282, 7th AIAA Thermophysics Conference, San Antonio, Texas, USA, 10–12 April 1972.

Sigraflex (2011) Products manufactured from flexible graphite foil, http://www.sglgroup.com (retrieved July 2011).

Sridhar, M.R. and Yovanovich, M.M. (1994) Review of elastic and plastic contact conductance models: Comparison with experiment, *Journal of Thermophysics and Heat Transfer*, **8**: 633–40.

Welch, J.W and Ruttner, L.E (1989) 'An experimental and computational analysis of the thermal interface filler material Calgraph', Paper AIAA 89-1658, 24th AIAA Thermophysics Conference, Buffalo, New York, USA, 12–14 June 1989.

Yovanovich, M.M. (2005) Four decades of research on thermal contact, gap, and joint resistance in microelectronics, *IEEE Transactions on Components and Packaging Technologies*, **28**: 182–206.

11

Heat pipes

Abstract: In this chapter the use of heat pipe technology for spacecraft thermal control is summarized, starting with the basic configuration, the types of existing models, and the basic phenomena involved (capillarity, surface tension, contact angle, wettability). Attention is also given to the heat pipe components: working fluids and their properties, the wicks, and their different internal configuration (porous, grooved, arteries). Finally the main concepts are described: constant conductance, variable conductance, thermal diodes, capillary pumped loops and loop heat pipes.

Key words: heat pipes, capillarity, wicks, capillary pumped loops, loop heat pipes.

11.1 Introduction

The heat pipe is a thermal device which allows an efficient transport of thermal energy. It is composed of a closed structure whose internal surface is lined with a thin layer of porous material, usually referred to as a wick. The container may have a cylindrical shape, or any other shape that can be conveniently manufactured. The pores of the wick are filled with a working liquid appropriate to the application, and the vapour of the liquid occupies the remaining internal volume. Therefore, since the liquid and its vapour coexist in

equilibrium, the pressure inside the container is equal to the vapour pressure corresponding to the saturation conditions.

This relatively simple configuration allows for a very efficient heat transfer from one end of the heat pipe to the other, following a quite simple heat transfer mechanism (Figure 11.1). As heat is applied to one end (the evaporator), the working liquid evaporates from the wick, while the removal of heat from some other portion of the surface (the condenser) causes the vapour to condensate on the wick. The pressure gradient resulting from the accumulation of vapour at one end of the heat pipe and its depletion at the other end causes the vapour to flow though the core region of the container (the vapour space). But, as the liquid evaporates, it retreats into the wick pores, then the meniscus there is depressed and the liquid pressure drops below the pressure of the adjacent vapour. At the other end condensation takes place, so that the working liquid fills in the wick, tending to maintain a flat surface without any depression of the pressure in the liquid. Due to capillary forces, the result is a pressure gradient in the liquid that causes the working liquid to flow through the wick towards the evaporator end, in the opposite direction to that of the flowing vapour in the core region, completing the flow circuit (see also Section 11.2).

Figure 11.1 **Sketch of a constant conductance heat pipe**

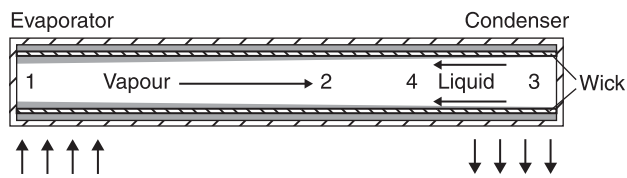

Note: The phenomena involved in the transfer process are the following: 1 – vaporization in the evaporator, 2 – vapour flow in the core region of the container, 3 – condensation in the condenser, and 4 – liquid return to the evaporator by capillary action in the wick.

The pressure variations in the vapour core are normally small and, therefore, the heat pipe temperature is almost uniform and close to the saturated vapour temperature corresponding to the vapour pressure (heat transfer through a heat pipe is virtually isothermal because the vapour pressure drop is usually of the order of 1% or less). Therefore, the heat pipe can be considered an extra-high thermal conductivity device, with reference to Fourier's law, as the effective thermal conductivity along the direction of heat transport is generally at least four to five orders of magnitude greater than the thermal conductivity of copper.

Yet another interesting heat pipe property is the capability of converting or transforming the surface heat flux (heat transfer rate per unit surface area) at the heat input zone to a higher or lower heat flux at the heat output zone. Since the heat flow rate is the same in both zones, the transformed heat flux varies inversely to the ratio of the surface areas. Thus, to reduce the heat flux by a factor of ten, the area of the heat output zone should be ten times that of the heat input zone (Silverstein, 1992).

There is a great variety of heat pipes in terms of their geometry, function, and methods used to transport the liquid from the condenser to the evaporator. The above-described heat pipe, consisting of a working fluid, a wick structure, and an envelope, is the most basic type of heat pipe, and it is known as a constant conductance heat pipe. There are other more sophisticated heat pipe designs, namely: variable conductance heat pipes, thermal diodes, pulsating (oscillating) heat pipes, micro-heat pipes, rotating heat pipes, sorption heat pipes (SHPs), magnetic fluid heat pipes, loop heat pipes, and capillary pumped loops (LHPs and CPLs, respectively). The distinction between these two last types is historical and controversial, because, coming from different heritages, they were associated with different

design philosophies. Some of these types are presented in Section 11.5.

Created almost three decades ago for space applications, heat pipes are now extensively and successfully applied to electronics and microelectronics cooling, bio-medical devices and many other applications. The absence of moving components, and their simple operation, makes heat pipes a very attractive, reliable and cost effective technology. Consequently, many companies in the space sector are working on developing these devices (Figus et al., 2003; Hoa et al., 2003; Swanson and Birur, 2003, Vasiliev, 1998; Wang et al., 2008). Figure 11.2 gives an overview of the status of two-phase transport technologies in which the heat transport is driven by capillary forces. Transport capacity parameter C_{QL} measures the capacity of the system to transfer a heat load $\dot{Q}$ a distance L.

Figure 11.2 **Comparison amongst several heat transport technologies. Transport capacity, C_{QL}, versus system mass, M, plane**

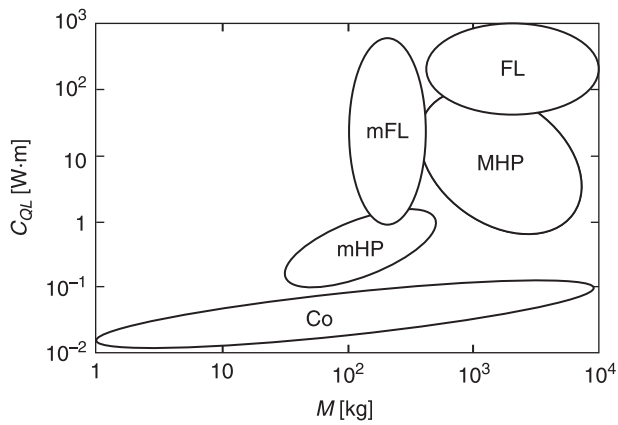

Key: FL, classical fluid loops; mFL, mini fluid loops; MHP, macro heat pipes; mHP, mini heat pipes; Co, conduction.

Source: After Figus et al. (2003).

In the next section a brief review of the basic phenomena involved in capillarity is presented. A review of the working fluids usually used in heat pipes is outlined (Section 11.3). Section 11.4 is devoted to heat pipe components, mainly wicks, and in Section 11.5 the main heat pipe types are described.

11.2 Capillarity

Capillarity refers to surface tension driven phenomena appearing at fluid–fluid interfaces. It is a macromolecular description of the different molecular forces acting between the molecules of a fluid located at its interface with either another fluid or a solid.

Molecules in a liquid attract one another. Therefore, a molecule in a liquid is attracted by the molecules surrounding it, and, on average, a molecule in the bulk of the fluid does not experience any resultant force. This situation is not valid in the case of a molecule at or near the surface of a liquid, because there the forces of attraction are no longer balanced, and the molecule experiences a resultant force inwards. Because of this effect, the liquid tends to take up a shape having minimum surface area (in the case of a drop under microgravity conditions this would be a sphere). Microgravity conditions can be reached not only in gravity-free environments, such as in spacecraft or in free-falling conditions, but also in normal gravity conditions. In this case capillary forces, which are proportional to the surface area, become dominant compared to the volume forces, which obviously are proportional to the volume, provided the size of the liquid sample (e.g. a drop of liquid) is small enough.

Due to this spontaneous tendency to contract, a liquid surface behaves rather like a rubber membrane under tension.

In order to increase the surface area, work must be done on the liquid. The energy associated with this work is known as the free surface energy, and the corresponding free surface energy per unit surface area is the surface tension, σ_S.

Since latent heat of vaporization, or enthalpy of vaporization, h_v, is a measure of the forces of attraction between the molecules of a liquid, it can be expected that surface tension be related to the latent heat of vaporization, which is the case. Solids also have a free surface energy, and, in terms of magnitude, it is found to be similar to the value for the same material in a molten state.

When a liquid is in contact with a solid surface, molecules in the liquid adjacent to the solid experience forces from the molecules of the solid, in addition to the forces from other molecules in the liquid. Wettability refers to the tendency of a liquid to spread over the surface of a solid. In general, a drop of liquid placed on a surface will partially deform, producing a contact angle ϕ with that surface. The value of the contact angle depends on the relative magnitudes of forces of cohesion and adhesion. According to Silverstein (1992), cohesion refers to the tendency of the liquid phase molecules to remain together, while adhesion refers to the tendency of the liquid phase molecules to bind to the solid phase molecules.

A liquid is said to wet when the adhesive forces predominate over the forces of cohesion. The contact angle is then less than 90° (see Figure 11.3). When the cohesive forces predominate, the liquid is said to be non-wetting to the solid. The contact angle is then greater than 90°. Extreme examples of these are oil and mercury on glass.

In a heat pipe, since capillarity is responsible for the circulation of the heat pipe fluid, strongly wetting fluids are preferred (normally, a liquid that acts as an effective solvent will have good wettability characteristics on hard surfaces

such as glass or metal). The wettability of a given surface by different liquids varies with their surface tension. As the surface tension increases, the contact angle increases, and wettability decreases.

The capillary pressure jump across a fluid–fluid interface, Δp, is proportional to the surface tension, σ_S, and to the radius of curvature:

$$\Delta p = \sigma_S \left(\frac{1}{R_1} + \frac{1}{R_2} \right), \tag{11.1}$$

where R_1 and R_2 are the radii of curvature of the intercepts of the surface by two orthogonal planes containing the normal to the surface. R_1 and R_2 must be regarded as quantities with the appropriate sign, taking into account that the contribution to the equivalent pressure in the surface is directed towards the centre of curvature in each case (Batchelor, 1967).

Since the interface has zero mass, a curved interface can be in equilibrium only if the effective pressure due to surface tension is balanced by an equal and opposite difference between the pressures in the fluids on the two sides of the interface. Thus, at any point of the interface there must be a jump in the fluid pressure of magnitude given by expression (11.1) when passing toward the side of the surface on which the centre of curvature lies.

Capillary pressure jump explains the basic driving force for the wicked heat pipe. Consider a configuration like the one shown in Figure 11.3, where a part of a heat pipe is represented. Assuming the configuration to be two-dimensional, and the shape of the different menisci to be arcs of circumference (e.g., $R_1 = R_j$ and $R_2 \rightarrow \infty$), the pressure jump across the interface is

$$\Delta p_j = p_{v,j} - p_{l,j} = \frac{\sigma_j}{R_j}, \tag{11.2}$$

where p_v and p_l are the pressure on the vapour side and on the liquid side, respectively, and the subscript j indicates the position along the heat pipe of the meniscus ($j = e$ for the evaporator and $j = c$ for the condenser). Note that, as stated above, according to the plot in Figure 11.3, the pressure increases when passing from the liquid phase to the vapour phase. Under normal operation, the fluid condenses at the condenser, so that the amount of liquid increases there and the meniscus radius of curvature increases. Therefore, the pressure jump decreases, which, according to expression (11.2), means that the pressure in the liquid increases. At the evaporator the process is the opposite, the liquid evaporates, then the amount of liquid diminishes and the meniscus depletes. Consequently, the radius of curvature of the meniscus decreases, the pressure jump increases, and then the pressure in the liquid phase diminishes.

Figure 11.3 **Sketches of (a) wetting and non-wetting liquids, and (b) a heat pipe showing the different magnitudes involved in fluid motion due to capillary actions**

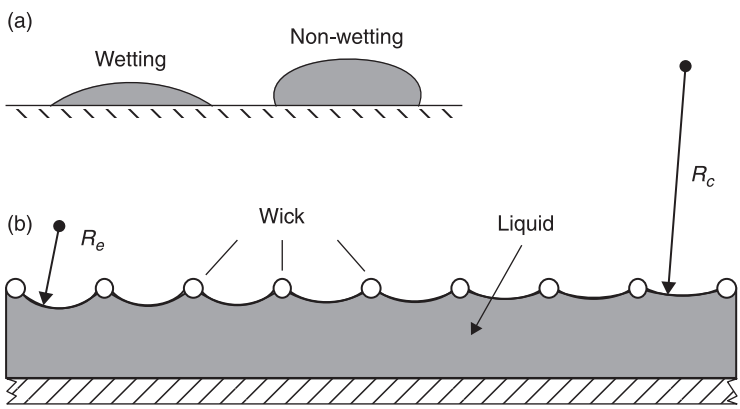

Note: R_e, R_c, radii of curvature of the liquid–vapour interface at the evaporator, and the condenser, respectively.

Source: After Reay and Kew (2007).

Hence, a longitudinal pressure gradient along the wick is created, which forces the liquid to flow from the condenser towards the evaporator.

11.3 Working fluids

A wide variety of fluids ranging from cryogens to liquid metals have been used as heat pipe working fluids. The choice of a working fluid for a heat pipe application is dictated to a large extent by several physical properties of the fluid, one of the most relevant being the temperatures of the desired operating range, and by the chemical compatibility of the fluid with the container and the wick. The operating range for a heat pipe working fluid is limited at one end by a temperature which is somewhat above its triple point, and at the other end by a temperature which is below its critical point. If the triple point is approached too closely, the temperature drops in the vapour flow increase, while if the critical point is approached, the distinction between liquid and vapour blurs, and the surface tension drops to zero. Also, the pressure that the envelope has to withstand increases significantly.

The physical properties to be considered in the selection of a heat pipe working fluid are: on the one hand, the vapour pressure, latent heat of vaporization, and surface tension; while on the other hand, the density, dynamic viscosity, and thermal conductivity of both the liquid and vapour phases. Some of these properties for different working fluids can be found in STCDD (1989), Silverstein (1992) appendix C, and in Reay and Kew (2007) appendix A. The requirements which should be taken into account when selecting a heat pipe working fluid are: a large latent heat of vaporization, high thermal conductivity, low viscosity, high surface tension,

high wetting ability, and a boiling point suited to the required operating temperature.

To compare the relative performance of heat pipe working fluid within a particular temperature range, the so-called liquid heat transport parameter, merit number, 0-*g* figure of merit, or simply figure of merit, *N*, can be used. This parameter has dimensions of heat flux (W/m^2), and is defined as

$$N = \frac{\rho_l h_v \sigma_S}{\mu_l}, \tag{11.3}$$

where ρ_l is the density of the liquid phase, h_v the latent heat of vaporization, σ_S the surface tension, and μ_l the dynamic viscosity of the liquid phase. The dependence on the temperature of the figure of merit of different suitable liquids is shown in Figure 11.4.

Each one of the curves plotted in this figure is limited between the reasonable bounds imposed by the limiting values of the heat pipe working pressure. The upper limit, purely structural, is approximately 50×10^4 Pa, while the lower limit is either 0.3×10^4 Pa, or the saturation pressure of the working fluid at freezing point, whichever is greater.

Other elements, such as lithium, zinc, magnesium, cadmium, sodium, etc., have even higher operating temperature ranges and higher figures of merit.

Working fluids used in heat pipes range from helium at 4 K up to lithium at 2300 K. For temperatures below 450 K water is superior over the range from 300 K to 400 K, where the alternative organic fluids tend to have considerably lower figures of merit. At slightly lower temperatures, between 200 K and 300 K, ammonia is a desirable fluid, although it requires careful handling to avoid contamination, whereas acetone and alcohols are alternatives which have lower vapour pressures. These fluids are commonly used in heat pipes for space applications. Water and methanol, both

Figure 11.4 **Figure of merit, *N*, as a function of temperature, *T*, for several heat pipe working fluids**

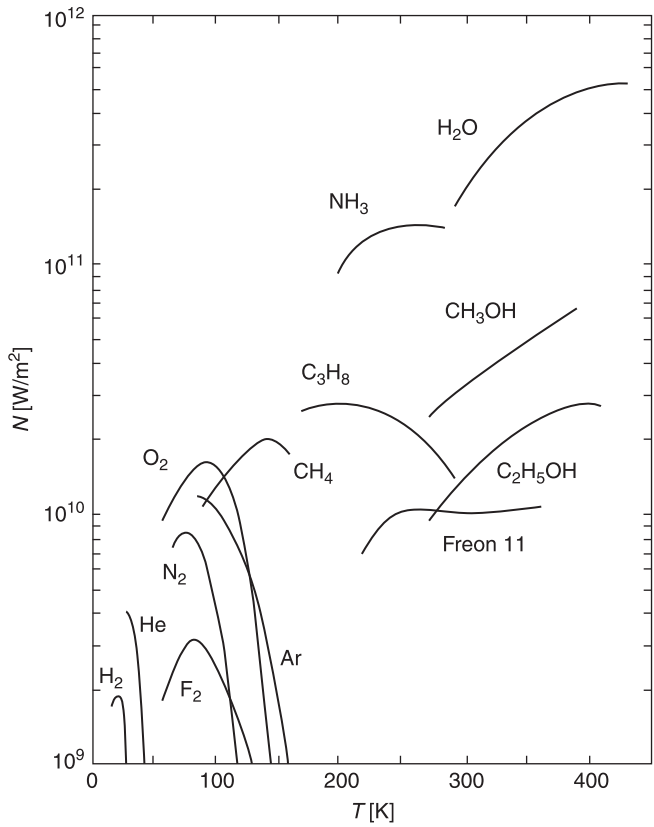

Note: For each curve, the range of temperature variation is bounded between the largest and smallest operating pressures.

Source: After STCDD (1989).

compatible with copper, are often used for cooling electronic equipment (Reay and Kew, 2007).

Temperature ranges of heat pipes for space applications are usually in the low or room temperature region in Figure 11.4. However, high-temperature applications of heat pipes are also envisaged in spacecraft technology, and the use of alkali metal heat pipes has been proposed for cooling wing

leading edges in hypersonic vehicles as well as for rocket nozzle cooling (Buffone et al., 2003).

11.4 Wicks

The operation of heat pipes is based on capillary-induced fluid flow, instead of on gravitational or mechanical work. The primary requirement for a heat pipe wick is that it acts as an effective capillary pump. That is, the surface tension forces arising between the fluid and the wick structure should be sufficient to overcome all viscous and other pressure drops in the pipe, while still maintaining the required fluid circulation.

In addition to the operating characteristics, several mechanical features must be considered: the wick must be mechanically stable and rigid enough to avoid the change of flow properties in response to wick sagging or stretching, and the wick material must be compatible with the working fluid used. Selection of a particular type depends on the design requirements of the specific application.

A wide variety of wicks have been successfully employed in heat pipes (some of them are depicted in Figure 11.5, p. 175), and research in this area still plays a significant role in heat pipe design. Whatever the wick structure, liquid flow channels should be characterized by a relatively coarse pore structure in order to minimize the resistance to liquid flow. However, relatively fine pores are desired to maximize the capillary pressure that balances the liquid–vapour pressure difference throughout the heat pipe. A relatively thick wick structure is also desirable to minimize the axial resistance to liquid flow, whereas resistance to heat flow across the wick increases with thickness (Silverstein, 1992).

Heat pipes are often categorized according to the type of wick structure they use. In situations in which a porous wick

structure is used, the wick may be formed from a variety of small elements, including screens, particles, and fibres. The wick structure may also include grooves cut into the heat pipe wall. The condensed liquid can also be delivered to the evaporator through one or more arteries, which are placed within the pipe where vapour returns to the condenser. Some of these types are described in the following paragraphs.

11.4.1 Porous wicks

Of the wick forms available, meshes, gauzes and twills are the most widely used. The simplest wick consists of several layers of fine mesh screens. Screens have also been used merely as a retaining structure for wicks consisting of various types of beads packed in an annulus between the retaining screen and the pipe wall (Figure 11.5a). Monel, glass, and stainless steel beads of different diameters have been used to produce these wicks. Textile fabrics have also been employed as wicks, as well as many other products covering a wide range of pore size and permeability (metal foams, felts, fibrous materials, sintered powder, etc.).

Many efforts have been devoted to characterizing suitable wick materials, for instance, measured values of pore size and permeability for a variety of meshes and twills can be found in Reay and Kew (2007), and many investigators are nowadays involved in research concerning the capillary pumping performances of wick materials. For example, the thermal hydraulic characterization of some stainless steel wicks (sintered porous media and gauzes) for water heat pipes is reported in Canti et al. (1998); nickel base sintered porous wicks are considered in Mishra et al. (2010); while pure nickel porous wicks are studied in Li et al. (2010). Sintered porous titanium, sintered porous nickel, Monel (high-porous cell structure), and brass (mesh porous

structure), are studied in Kiseev et al. (2010). Ceramic wick structures made of mullite and alumina as raw material, and activated carbon as pore former, are considered in Berti et al. (2011), and the capillary properties of a nickel powder biporous wick are analysed in Yeh et al. (2009).

11.4.2 Grooved wicks

Another simple heat pipe wick design consists of axial grooves in the wall of extruded metallic tubing. Grooves are formed most often in tubes of aluminium, but they can be formed in tubes of other materials, such as stainless steel, copper, or even refractory metals.

Most heat pipes were first designed with rectangular grooves. The extrusion process is well suited to this geometry and sets the limits of the small dimensions such as the open groove width and the groove depth. For instance, a method of forming axial microgrooves by ball-spinning inside a copper heat pipe is described in Li et al. (2008).

Trapezoidal grooves (Figure 11.5b) have been developed because they have shown better performances: the base of the grooves is slightly wider and this increases the liquid flow area. Thus, the pressure loss in the liquid flow decreases and the heat transport capacity is enhanced. Concepts of re-entrant grooves, drop-shaped, and Ω-shaped grooves, have been the subject of new developments of improved heat pipes. Axially grooved heat pipes are flight-proven designs. For example, ALCATEL SPACE has provided more than 5000 heat pipes since 1981, and no failures in orbit have been reported (Hoa et al., 2003).

Although most of the available research on heat pipes with axial microgrooves focus on groove configurations featuring a groove opening of width wider than the groove base, which is the case of the so-called inverted trapezoidal

microgrooves, there have been very few reports on heat pipes with axial microgrooves having a groove opening narrower than a groove base, as is the case of swallow-tailed regular trapezoid, and even of Ω-shaped grooves (Figure 11.5c). It seems that these last devices present some advantages over more traditional designs. According to Chen et al. (2009) and Chen et al. (2010), Ω-shaped grooves, as well as swallow-tailed grooves, combine a high capillary pumping pressure with a low axial pressure drop in the liquid. Meanwhile, the retardation of the liquid flow due to the counter-current vapour flow over the liquid–vapour interface is minimized when compared to other axial groove designs.

11.4.3 Arteries

Arterial wicks are necessary in high-performance heat pipes for spacecraft, where temperature gradients in the heat pipe have to be minimized to counter the adverse effect of what are generally low thermal conductivity working fluids. This class of heat pipe was introduced to minimize viscous losses by using separate fluid flow passages or arteries in combination with fine capillary structures (in order to achieve the full heat transport potential of the arterial wick, the artery must be completely shut off from the vapour space). Therefore, arteries provide one or more relatively unrestricted liquid-flow paths in parallel with the longitudinal wick, aimed at obtaining liquid transport along the pipe with the minimum pressure drop.

A further consideration in the design of arterial heat pipes is the vapour or gas blockage of the arteries. These pipes are particularly prone to bubble formation because the liquid in the artery contains dissolved control gas, which tends to come out of solution as the liquid warms during its transit

from the condenser to the evaporator. If a vapour or gas bubble forms within or is vented into the artery, then the transport capability is seriously reduced. Indeed, if the bubble completely blocks the artery then the heat transport capability is dependent on the effective capillary radius of the artery.

The most noteworthy designs among the earliest arterial heat pipes were the so-called pedestal artery and the spiral artery. Cross-sections of some of these wick structures are shown in Figure 11.5. The simplest pedestal arterial heat pipe has a circular cross-section artery with two retainer legs made from a stainless steel mesh (Figure 11.5d). The artery is connected to the pipe wall by these two legs and the heat pipe envelope is aluminium tubing with circumferential screw grooves on the inside surface. Another arterial heat pipe design incorporates two circular cross-section arteries made from stainless steel mesh (Figure 11.5e). These two arteries are spot-welded to a felt-metal bridge wick, which allows the liquid to flow to the circumferential wall grooves from the arteries (Kaya, 2009).

In the lateral tunnel heat pipe (Figure 11.5f), a single artery is formed using a stainless steel mesh by contact spot welding. Circumferential screw grooves on the inside wall are arranged along the entire length of the pipe, which provide the additional capillary structure for liquid transportation from the liquid artery along the circumference of the heat pipe. They also provide a large uniform thin film for evaporation, which helps prevent boiling in the liquid artery. The remaining section of the heat pipe envelope is reserved for vapour flow. As a result, the liquid and vapour flow are separated and the entrainment constraint due to the liquid–vapour counter-current flow is eliminated (Kaya, 2009). A summary of additional arterial heat pipe designs can be found in Kaya and Goncharov (2011).

The spiral arterial heat pipe is also made from aluminium tubing with internal circumferential grooves. The artery is formed by rolling a stainless steel screen mesh with successive gaps around the heat pipe axis (Figure 11.5g), or around a central tunnel (Figure 11.5h). The spiral artery formed is connected to the pipe's inside wall by a three-legged retainer again made from a stainless steel screen.

Figure 11.5 **Sketches of the cross-sections of several heat pipe designs. (a) classic porous wick design; (b) trapezoidal grooved wicks; (c) Ω-shaped; (d) single artery; (e) two arteries; (f) lateral tunnel; (g) spiral artery; and (h) spiral-tunnel design**

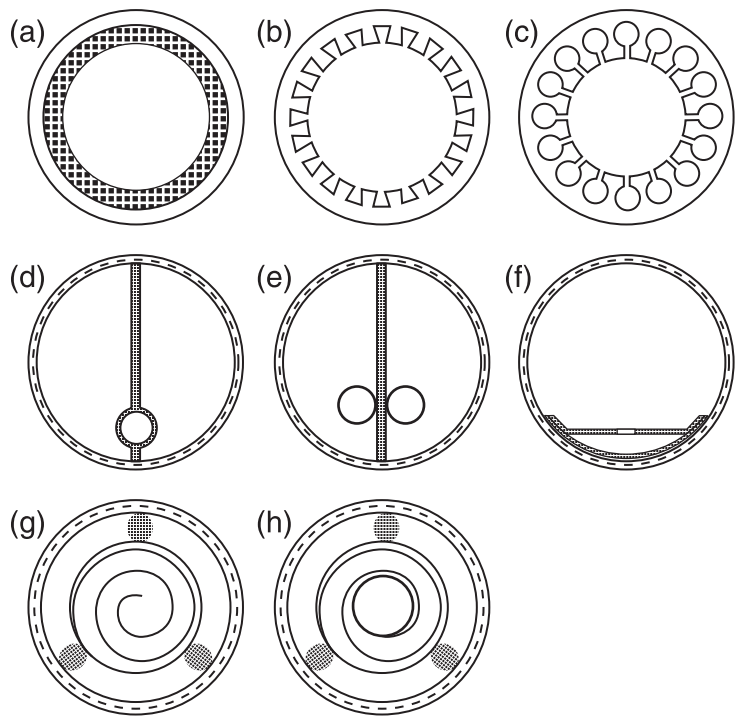

Source: After Gilmore (2002) and Kaya (2009).

11.5 Other capillary heat transfer designs

The heat pipe design depicted in Figure 11.1 represents a constant conductance heat pipe, where, as previously described, heat is transferred along a heat pipe by continuous mass transfer and phase changing of a suitable working fluid. These processes depend exclusively on the surrounding temperature field, and, provided that the heat flow rate is kept below certain limits, in principle, it is impossible to control the heat pipe performance once the heat flow is fixed.

Heat pipes whose performance cannot be varied, so-called constant conductance heat pipes, have a wide range of applications, but there are, however, many other applications in which some control of the evaporation, condensation, or pumping phenomena is needed, and therefore, a more sophisticated heat pipe design has to be used. Some of these designs are presented in subsequent subsections.

Whatever the heat pipe design, the maximum heat transfer rate it produces is limited. The operating limits are due either to a breakdown of the fluid flow, or to any process that fixes a maximum value of the amount of fluid that can be forced through the tube by increasing the heat transfer. Common operating limits are:

- *Capillary*: The liquid evaporates faster than it can be supplied by capillary pumping to the evaporator.
- *Sonic*: The vapour density decreases and simultaneously the vapour velocity increases due to heat addition, until the velocity equals the sound velocity; then the flow in the tube is choked.
- *Entrainment*: The vapour stream shears off droplets from the liquid–vapour interface, carrying them into the condenser.

- *Boiling*: The liquid in the wick boils off and a vapour blanket appears in the capillary structure.

11.5.1 Variable conductance heat pipes

Variable conductance heat pipes (VCHPs) have a unique feature that sets them apart from other types of heat pipe. This is the ability to control the operating temperature of a given component against variations in the heat dissipation of the component and in the environmental thermal conditions. A variable conductance heat pipe allows a device mounted on the evaporator to be maintained at a near constant temperature, independently of the amount of power generated by the device.

Variable conductance heat pipes are now routinely used in many applications. These applications range from the thermal control of components and systems on satellites, to precise temperature calibration duties, or conventional electronics temperature control. An example of the application of variable conductance heat pipes is the Automated Transfer Vehicle (ATV), an expendable vehicle developed by ESA to service the International Space Station (ISS), which uses 40 variable conductance heat pipes located in the avionics bay.

Inasmuch as the heat pipe transfers energy between two points through a continuous fluid circulation, some change in the conductance of the heat pipe may be exerted by controlling the mass flow, which is generally achieved by controlling the condensation rate, normally by using a non-condensable gas which tends to collect in the condenser, partially displacing the condensable gas from the condenser (Figure 11.6). This has been the most widely used technique up to date, although some others have been considered (for example, the interruption of the fluid flow, either the liquid flow in the wick or the vapour flow in the

Figure 11.6 Sketch of a variable conductance heat pipe

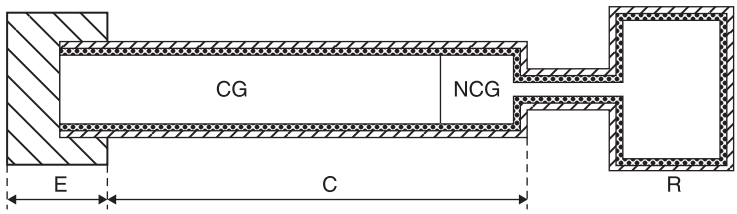

Key: E, evaporator; C, condenser; R, non-condensable gas reservoir; CG, condensable gas; NCG, non-condensable gas.

Source: After STCDD (1989).

core, by means of suitable thermostatically controlled valves).

At the beginning of the process, both condensable and non-condensable fluids are uniformly mixed throughout the pipe. During the start-up period, the heat addition and consequent evaporation at the evaporator induces pressure waves which sweep both condensable and non-condensable gases towards the condenser zone. Capillary pumping through the wick drives back the condensed gas to the evaporator, while there is no driving force for the non-condensable gas which is trapped (diffusion effects apart) at the condenser end, reducing the volume of the active condenser zone. For a given mass of either fluid, the volume of the inactive portion of the condenser depends on the pressure and temperature, which are controlled by the heat input and subsequent evaporation.

Operation of variable conductance heat pipes can be passive and active. In the passive mode of operation, the active condenser length varies in accordance with temperature changes in various parts of the system. An increase in the evaporator temperature causes an increase in the vapour pressure of the working fluid, which causes the gas to compress into a smaller volume, releasing a larger amount of

active condenser length for heat rejection. Conversely, a drop in the evaporator temperature results in a lower vapour surface area. Therefore, when the pressure increases, the interface separating both gases recedes in the condenser, increasing the condenser volume, and thence the heat transfer capability, without requiring external power (see Section 11.1). The opposite occurs when the pressure decreases: the net effect is a passively controlled variable condenser area that increases or decreases heat transfer in response to the heat pipe vapour temperature.

In the active mode of operation it is possible to partially decouple the volume of the non-condensable gas from the heat addition by means of an auxiliary non-condensable gas-heater with a feed-back temperature sensor attached to the heat source. Additional information on variable conductance heat pipes can be found in STCDD (1989).

11.5.2 Thermal diodes

Thermal diode heat pipes operate as conventional heat pipes, but with a high thermal conductance in one direction, and a very low thermal conductance in the opposite direction. They are used in spacecraft for the coupling of equipment to radiators, the surface of which becomes temporarily hotter than the equipment.

The normal fluid flow in a thermal diode is somewhat interfered with when the evaporator side becomes cooler than the condenser. Common techniques employed in thermal diode heat pipes are outlined in Figure 11.7.

In the liquid trap technique, liquid is accumulated in the evaporator when cold. As shown in Figure 11.7a, the heat pipe behaves normally when the heat flows from the condenser to the evaporator. However, if the relative positions of the evaporator and condenser are reversed, then the

Figure 11.7 **Sketches of heat pipe diodes: (a) liquid trap diode, and (b) liquid blockage diode**

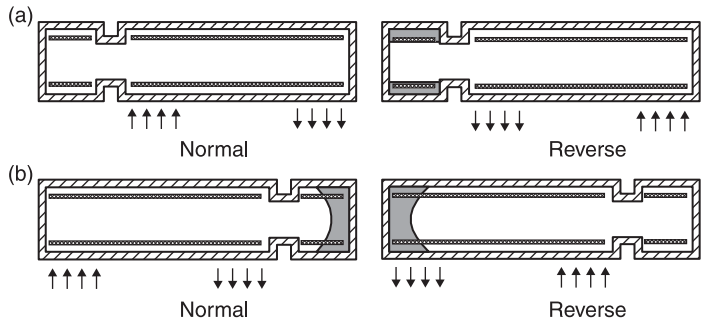

Source: After Reay and Kew (2007).

condensing liquid is trapped in the reservoir whose wick is not connected to the pipe wick on the left-hand side of the diagram, and hence cannot return. The pipe then does not operate and no heat transfer occurs.

Figure 11.7b shows a similar arrangement, but in this case, excess liquid is placed in the pipe. In normal operation, the liquid accumulates in the reservoir at the condensing end and the pipe operates normally. When the positions of the evaporator and condenser are reversed, the excess liquid accumulates as a slug in the coldest portion of the heat pipe. Thus the heat pipe ceases to operate, and heat is then transferred by conduction only.

11.5.3 Capillary pumped loops and loop heat pipes

Because of performance advantages, and operational features, the Western-heritage capillary pumped loops and the Russian-heritage loop heat pipes have rapidly gained

acceptance in the aerospace community. Both passive heat transport technologies have demonstrated that they can be used as primary heat transport devices in thermal control technology. Like heat pipes, capillary pumped loops and loop heat pipes are completely passive systems which have no mechanical moving parts to wear out or that cause unwanted vibrations in the spacecraft.

The heat transport capabilities of capillary pumped loops and loop heat pipes are at least one order of magnitude higher than those of heat pipes. It should be noted that, although initially capillary pumped loops and loop heat pipes were perceived as alternatives to conventional heat pipes at high transport powers, each of these systems has its own application range.

Both capillary pumped loops and loop heat pipes are capable of removing heat quickly from a heat source and transporting it to remotely located heat sinks via small and flexible transport lines. Circulation of the working fluid in both systems is accomplished entirely by capillary action taking place in fine pore wicks. Despite sharing many operational characteristics, capillary pumped loops and loop heat pipes do have differences. Each has its own advantages and disadvantages, often in different areas of operation. For example, a capillary pumped loop provides tight temperature control for the electronics on board a spacecraft, but requires a tedious and sometimes time consuming priming process prior to starting-up. However, a loop heat pipe can start, stop, and re-start, at any time regardless of operating conditions. Unfortunately, temperature control is not always possible with a loop heat pipe, and its effective thermal conductance is not as high as that of a capillary pumped loop (Hoang et al., 2003; Hoang and Ku, 2002). Outlines of these two systems are shown in Figure 11.8.

In both systems heat from the heat source vaporizes liquid in the capillary pump. Vapour travels along the vapour line

Figure 11.8 **Diagrams of a single capillary pumped loop (a), and of a loop heat pipe (b)**

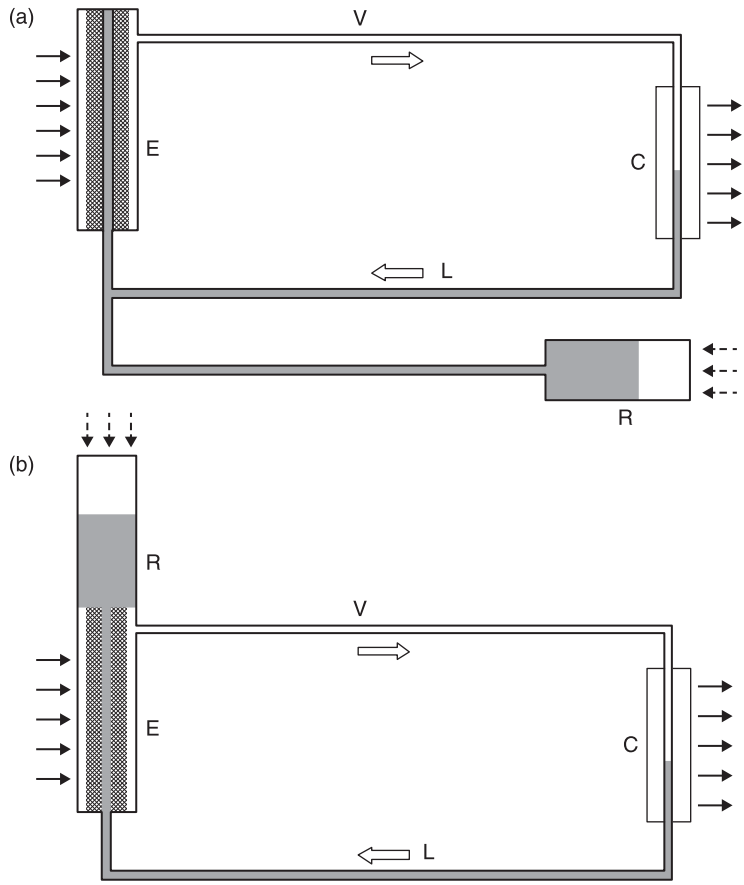

Key: V, vapour line; C, condenser; L, liquid line; R, compensation chamber reservoir; E, evaporator pump.

Source: After Hoang et al. (2003).

to a heat exchanger where it rejects the latent heat to condense vapour back to liquid. Liquid flows back to the capillary pump via the liquid line to complete the cycle. The basic distinction between a conventional capillary pumped loop and a conventional loop heat pipe lies in the fluidic and

thermal links of the compensation chamber reservoir to the evaporator. This distinction has a large impact on the design and operation of the capillary loop, and sets them apart in terms of both operational characteristics and potential usage.

The capillary pumped loop reservoir is employed to control the loop saturation temperature (set point) by regulating the heater power into the reservoir (Figure 11.8a). The capillary pumped loop reservoir is cold-biased so that an active control of the set point is possible. As a result, any vapour bubble formed in the capillary pump liquid core expands and blocks off the liquid supply to the pump wick causing the wick to dry out. To assure that no vapour is present in the pump core before start-up, the loop undergoes a tedious and sometimes time consuming procedure called a priming process. Heat is applied to the reservoir to raise and maintain its temperature at least 5 °C above the rest of the loop for a minimum of 30 minutes. This forces the liquid in the reservoir to completely fill the entire loop volume (including the vapour line), and thereby eliminates all vapour bubbles initially in the loop. Once the priming procedure is complete, the capillary pump is allowed to receive heat from the heat source to commence the loop operation. To prevent excessive heat conduction across the wick (heat leak) that could initiate boiling in the pump liquid core, only porous plastics have been successfully used as capillary pumped loop pump wicks (Hoang et al., 2003). Hence, capillary pumping heads of currently available plastic wicks are limited to 3500 Pa with ammonia as the working fluid. Finally, the return liquid must be kept sub-cooled (more than 5 °C) to make sure that no boiling takes place in the liquid line. This restriction does not allow the capillary pumped loop to operate at a set point far below ambient temperature.

With loop heat pipes, however, the wick does not need to be primed prior to start-up because the reservoir is an integral

part of the capillary pump. As shown in Figure 11.8b, a secondary wick connecting the evaporator pump wick to the reservoir provides the pump wick with a continuous liquid feed (even with vapour in the liquid core). In addition, as a direct consequence of the loop heat pipe vapour tolerance, porous powdered metals (nickel, titanium, stainless steel), whose capillary pumping heads (more than 3.5×10^4 Pa) far exceed those of plastics wicks, have been the mainstays of loop heat pipe wicks. The main drawback of metal wicks is the fact that they allow too much heat conduction (heat leakage) into the liquid core. Even though loop heat pipe pumps do not fail, heat leakage raises the loop operating temperature until it is balanced by the amount of sub-cooling brought back by the return liquid. Hence, the loop heat pipe heat leakage poses two practical drawbacks: first, the loop temperature is not easily controlled, and, second, the heat rejection efficiency of the radiator is greatly reduced because a part of the radiator is needed to sub-cool the return liquid.

Theoretical analyses of different aspects of the operation of loop heat pipes are presented in numerous publications (Ku, 1999; Hoang et al., 2003; Hoang and Ku, 2002; Maydanik, 2005; Launay et al., 2007, amongst others).

Focusing the attention on loop heat pipes, the operation of these devices is based on the same physical processes as those used in conventional heat pipes. However, as explained above, they are organized in a quite different way. A thermodynamic analysis of a capillary two-phase system can help to understand the thermal and hydraulic processes taking place in the loop heat pipe operation.

A pressure-temperature diagram of a working fluid cycle is given in Figure 11.9a. The numbers in the diagram correspond to the physical locations shown in Figure 11.9b. According to the explanation given in Launay et al. (2007), the vapour generated at the evaporator wick outlet (point 1) is at a

Figure 11.9 **(a) Pressure–temperature, *p-T*, diagram for loop heat pipe steady-state operation (capillary controlled mode), and (b) flow schematic of a loop heat pipe**

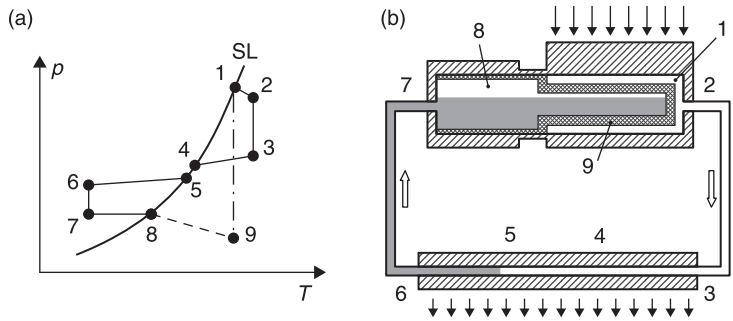

Key: SL, saturation line; 1 – start of vapour channel; 2 – start of vapour line; 3 – start of condenser; 4 – start of condensation; 5 – end of condensation; 6 – end of condenser; 7 – end of liquid line; 8 – compensation chamber; 9 – outer surface of first wick.

Source: After Ku (1999) and Launay et al. (2007).

saturation state. It becomes superheated at the exit of the grooves (point 2) due to heating and pressure losses. Assuming that the vapour line is perfectly insulated, the vapour temperature drop can be neglected. Since the pressure continues to drop along the way, the vapour becomes more and more superheated relative to the local saturation pressure until it reaches the entrance of the condenser (point 3). The vapour releases its sensible heat and begins to condense inside the condenser (point 4). The vapour condensation takes place along the saturation line where both the pressure and the temperature decrease. At point 5, the vapour condensation is complete, and the liquid starts to be sub-cooled inside the condenser until it exits at point 6. The sub-cooled liquid flows along the liquid line, while its temperature may increase or decrease, depending on whether the liquid loses or gains heat from the surroundings. As the liquid

reaches the compensation chamber inlet (point 7), the working fluid is heated up to point 8. The evolution from points 8 to 9 corresponds to the liquid flow through the wick into the evaporation zone. In this way, the liquid may be superheated, but boiling does not take place because it remains in such a state for too short a time. Point 9 determines the state of the working fluid in the vicinity of the evaporating menisci, and the pressure drop between point 1 and point 9 corresponds to the value of the total pressure losses along the whole loop.

11.5.4 Sorption heat pipes

The sorption heat pipe is a device that combines heat pipes and sorption cooling (in this case adsorption, like in solid adsorption cooling systems, which are well-known in the air-conditioning field), by combining the enhanced heat and mass transfer in conventional heat pipes with sorption phenomena in the sorbent bed. A sorption heat pipe consists of a sorbent system (adsorber/desorber and evaporator) at one end, and a condenser plus evaporator at the other end. It can be used as a cooler/heater and be cooled and heated as a heat pipe (Vasiliev and Vasiliev, 2004, 2005).

The schematic of a sorption heat pipe evaporator is shown in Figure 11.10. A simplified explanation of the operation of a sorption heat pipe is as follows:

Phase 1. At the beginning it is necessary to desorb the sorption structure (2), applying a heater. During desorption, the vapour (1) of a working fluid is released from the porous media (2) and condensed in the evaporator/condenser (3). Due to the pressure drop, part of the liquid between the hot side of the heat pipe and the evaporator is filtrated through the porous valve (5) and enters the evaporator (6). The other

Figure 11.10 Sorption heat pipe showing: 1 – vapour channel; 2 – porous sorption structure; 3 – finned heat pipe evaporator/condenser; 4 – heat pipe wick; 5 – porous valve; 6 – heat pipe low-temperature evaporator wicked; 7 – working fluid accumulated in the evaporator; 8 – cold box

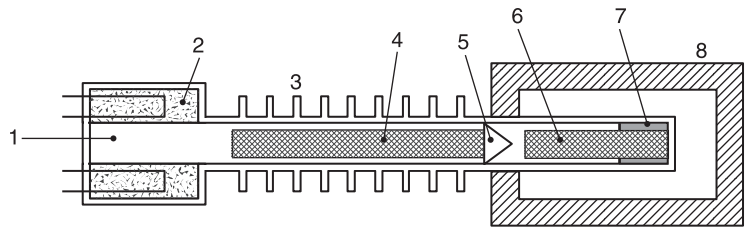

Source: After Vasiliev and Vasiliev (2004, 2005).

part of the liquid returns to the sorbent bed due to the capillary forces of the wick (4) and is used to enhance the heat and mass transfer inside the sorbent material. When the desorption process of the sorbent structure is stopped, the heater has to be switched off, the working fluid is accumulated inside the evaporator and the pressure in the sorbent bed decreases due to its cooling.

Phase 2. When phase 1 is accomplished, the porous valve (5) is opened and the vapour pressure inside the heat pipe is equalised following the process of liquid evaporation inside the porous structure of the evaporator (6). During the process of liquid (7) evaporation, the box (8) is cooled. When the liquid evaporation inside the evaporator is finished and the sorbent bed is saturated with the vapour, the porous valve is closed and then the sorbent bed starts to cool down to the ambient temperature with the help of the heat pipe condenser (3).

11.6 References

Batchelor, G.K. (1967) *An Introduction to Fluid Dynamics*, Section 1.9: Conditions at a boundary between two media, Cambridge University Press, London, UK.

Berti, L.F., Santos, P.H.D., Bazzo, E., Janssen, R., Hotza, D. and Rambo, C.R. (2011) Evaluation of permeability of ceramic wick structures for two phase heat transfer devices, *Applied Thermal Engineering*, **31**: 1076–81.

Buffone, C., Bruno, C. and Sefiane, K. (2003) 'Liquid metal heat pipes for cooling rocket nozzle walls', Paper AIAA 2003–4452, 39th AIAA/ASME/SAE/ASEE Joint Propulsion Conference and Exhibit, Huntsville, Alabama, USA, 20–23 July 2003.

Canti, G., Celata, G.P., Cumo, M, and Furrer, M. (1998) Thermal hydraulic characterization of stainless steel wicks for heat pipe applications, *Revue Générale de Thermique*, **37**: 5–16.

Chen, Y., Zhang C., Shi M., Wu J., and Peterson, G.P. (2009) Study on flow and heat transfer characteristics of heat pipe with axial 'Ω'-shaped microgrooves, *International Journal of Heat and Mass Transfer*, **52**: 636–43.

Chen, Y., Zhu W., Zhang C. and Shi M. (2010) Thermal characteristics of heat pipe with axially swallow-tailed microgrooves, *Chinese Journal of Chemical Engineering*, **18**: 185–93.

Figus, C., Ounougha, L., Bonzom, P., Supper, W. and Puillet, C. (2003) Capillary fluid loop developments in Astrium, *Applied Thermal Engineering*, **23**: 1085–98.

Gilmore, D.G., Ed. (2002) *Spacecraft Thermal Control Handbook, Vol. I: Fundamental Technologies,* 2nd ed., American Institute of Aeronautics and Astronautics, Inc., The Aerospace Press, El Segundo, California, USA.

Hoa, C., Demolder, B. and Alexandre, A. (2003) Roadmap for developing heat pipes for ALCATEL SPACE's satellites, *Applied Thermal Engineering*, **23**: 1099–108.

Hoang, T., Brown, M., Baldauff, R. and Cummings, S. (2003) 'Development of a two-phase heat transport for spacecraft central thermal bus', Space Technology and Applications International Forum-STAIF 2003, CP654, American Institute of Physics, M.S. El-Genk Ed., 49–54.

Hoang, T.T. and Ku, J. (2002) 'Advanced loop heat pipes for spacecraft thermal control', Paper AIAA 2002-3094, 8th AIAA/ASME Joint Thermophysics and Heat Transfer Conference, St. Louis, Missouri, USA, 24–26 June 2002.

Kaya, T. (2009) Analysis of vapor-gas bubbles in a single artery heat pipe, *International Journal of Heat and Mass Transfer*, **52**: 5731–9.

Kaya, T. and Goncharov, K. (2011) Investigation of the thermal performance characteristics of a variable conductance arterial heat pipe, *Frontiers in Heat Pipes*, **2**. DOI: 10.5098/fhp.v2.1.3004.

Kiseev, V.M., Vlassov, V.V. and Muraoka, I. (2010) Experimental optimization of capillary structures for loop heat pipes and heat switches, *Applied Thermal Engineering*, **30**: 1312–19.

Ku, J. (1999) 'Operating characteristics of loop heat pipes', Paper ICES 1999-01-2007, 29th International Conference on Environmental System, Denver, Colorado, USA, 12–15 July 1999.

Launay, S., Sartre, V. and Bonjour, J. (2007) Parametric analysis of loop heat pipe operation: a literature review, *International Journal of Thermal Sciences*, **46**: 621–36.

Li, J., Zou, Y. and Cheng, L. (2010) Experimental study on capillary pumping performance of porous wicks for loop

heat pipe, *Experimental Thermal and Fluid Science*, **34**: 1403–8.

Li, Y., Xiao H., Lian B., Tang Y. and Zeng, Z.X. (2008) Forming method of axial micro grooves inside copper heat pipe, *Transactions of Nonferrous Metals Society of China*, **18**: 1229–33.

Maydanik, Y.F. (2005) Loop heat pipes, *Applied Thermal Engineering*, **25**: 635–57.

Mishra, D.K., Saravanan, T.T., Khanra, G.P., Girikumar, S., Sharma, S.C. et al. (2010) Studies on the processing of nickel base porous wicks for capillary pumped loop for thermal management of spacecrafts, *Advanced Powder Technology*. Doi:10.1016/j.apt.2010.07.011.

Reay, D. and Kew, P. (2007) *Heat Pipes* (Fifth edition), Elsevier (eBook), Doi:10.1016/B978-075066754-8/50006-3.

Silverstein, C. (1992) *Design and Technology of Heat Pipes for Cooling and Heat Exchange*, Taylor & Francis, Washington, DC, USA.

STCDD (1989) *Spacecraft Thermal Control Design Data Handbook*, ESA PSS-03-108, Issue 1.

Swanson, T.D. and Birur, G.C. (2003) NASA thermal control technologies for robotic spacecraft, *Applied Thermal Engineering*, **23**: 1055–65.

Vasiliev, L. (1998) State-of-the-art on heat pipe technology in the former Soviet Union, *Applied Thermal Engineering*, **18**: 507–51.

Vasiliev, L. and Vasiliev Jr., L. (2004) The sorption heat pipe – a new device for thermal control and active cooling, *Superlattices and Microstructures*, **35**: 485–95.

Vasiliev, L. and Vasiliev Jr., L. (2005) Sorption heat pipe – a new thermal control device for space and ground application, *International Journal of Heat and Mass Transfer*, **48**: 2464–72.

Wang, G., Mishkinis, D. and Nikanpour, D. (2008) Capillary heat loop technology: space applications and recent Canadian activities, *Applied Thermal Engineering*, **28**: 284–303.

Yeh, C.C., Chen, C.N. and Chen, Y.M. (2009) Heat transfer analysis of a loop heat pipe with biporous wicks, *International Journal of Heat and Mass Transfer*, **52**: 4426–34.

12

Phase change capacitors

Abstract: The aim of this chapter is to explain the basic physical principle on which the phase change capacitors are based, their applications in a thermal control subsystem, the ways they are used, the main characteristics that the phase change material should have, the relevant physical characteristics affecting these materials, and the main materials selected for space applications. Also, some basic aspects of the technology involved, such as the constituents of the phase change capacitor, bellows or metallic membranes, and materials used as thermal enhancers in powder or foam form, are included.

Key words: phase change material, phase change capacitors, thermal enhancers.

12.1 Introduction

An effective way of storing thermal energy is the use of a latent heat storage system using a phase change material (PCM), which is characterized by a high-energy storage density, and also an isothermal process. The use of a phase change material is an option to be considered when the thermal loads, such as the incident orbital heat fluxes, or the internal equipment heat dissipation, fluctuate widely.

Energy storage is based on the heat absorption or release that occurs when a given storage material undergoes a phase

change. The phase change can be solid to liquid, liquid to gas, or vice versa; and also a solid–solid phase change. These phase changes absorb or release heat at a nearly constant temperature. In space applications, solid–liquid phase changes have been most widely used, because they show smaller volume variation than liquid–gas or solid–gas transitions. Solid–solid phase changes have also been studied (Wirtz et al., 1999), although in space applications they are still in development.

Phase change materials have received much attention over the last few years, due to the applications of these systems in the field of the utilization of renewable energies. Reviews can be found in Sharma et al. (2009) and Zalba et al. (2003). Furthermore, this technique appears as a candidate to solve some thermal design packaging problems in a rapidly developing field such as mobile phone technology (Tan and Fok, 2007).

The phase change material as a thermal control system consists of a container filled with a substance capable of undergoing a phase change. When the temperature of the spacecraft surface increases, either because of external radiation or inner heat dissipation, the phase change material will absorb the excess heat through phase change, and will restore it through the inverse change when the temperature decreases again. Because of the obvious electrical analogy, this thermal control system is also called a phase change capacitor.

Phase change material systems can be used to control the temperature of equipment in several ways. In the case of cyclically operating equipment, the aim is to avoid temperature extremes of modest duration. The phase change material cell is normally sandwiched between the equipment and the heat sink. When the equipment is active and therefore generating heat, the energy is stored in the phase change

material via a phase change. During the off portion of the cycle, the heat of fusion energy is removed via the heat sink.

If the aim of the thermal control system is to protect an element from abnormal heat dissipation peaks, as is the case of equipment that transfers its excess heat to a sink, the phase change capacitor is attached to the equipment but without interfering with the normal heat path.

When insulated equipment is considered, the phase change capacitor may be used as the sole heat sink, provided that the heat transferred during the heating period does not exceed that required to completely melt the material.

Phase change material-based systems have long been used by NASA, for instance for Mars missions' advanced thermal control (Hickey et al., 1996). One of the relevant elements in phase change material storage technology is the high-conductive matrix inside the storage unit, which provides a good conductive path, and can also survive several hundreds of diurnal thermal cycles on the Martian surface for the operation of rovers.

Phase change material was also considered as an option in the thermal control system of the Aerial Regional-scale Environmental Survey (ARES), proposed for the 2007 Mars Scout Mission. This would have been the first mission to fly an aircraft over another planet. After much consideration, it was not selected due to mass and packaging concerns (Gasbarre and Dillman, 2003).

12.2 Characteristics of phase change materials

The characteristics that a phase change material should have are the following:

- Suitable phase-transition temperature. The melting point (in a solid–liquid system) should be within the allowed temperature range of the component being thermally controlled, usually between 260 K and 320 K.
- High latent heat of fusion, or enthalpy of fusion. It is relevant in order to minimize the mass and/or volume of the system.
- Good thermal conductivity. This property helps to reduce thermal gradients and facilitates the charging and discharging of energy storage. As most phase change materials have low thermal conductivity, fillers have to be used to increase the conductivity of the system.
- High density. This allows a storage container of smaller size.
- Small volume change on phase transformation, and low vapour pressure, which help to reduce container design problems.
- Reversible phase-to-phase transition. The chemical compositions of both phases should be the same.
- Long-term reliability and chemical stability during repeated cycles.
- Non-toxic, non-corrosive, compatible with container materials, not a fire hazard.
- No tendency to supercool. This is a troublesome aspect of a phase change material, particularly for salt hydrates. If it is more than a few degrees, it will interfere with the proper functioning of the system.
- Available and cost effective.

Some of the relevant physical characteristics of solid–liquid phase change materials are summarized in the following paragraphs.

12.2.1 Supercooling

Supercooling is the process of cooling a liquid below the solid–liquid equilibrium temperature without solidifying. The best way to reduce supercooling is to ensure that the original crystalline material has not been completely melted. In such a case, the seeds which are present in the melt tend to nucleate the solid phase when heat is removed. Nucleating catalysts are available for many materials. For instance, paraffin does not show supercooling unless it is contaminated, e.g. with water.

12.2.2 Nucleation

Nucleation is the formation of the first crystals (nuclei) capable of spontaneous growth into large crystals in an unstable liquid phase. If nuclei are generated spontaneously from the liquid itself at the onset of freezing, it is called homogeneous nucleation. In this case, the rates of formation and dissociation do not depend on the presence or absence of surfaces, such as container walls or foreign particles. If the nuclei are formed on solid particles already in the system, or on the container walls, it is called heterogeneous nucleation. In this case, supercooling can be considerably reduced, or even eliminated.

12.2.3 Bubble formation

Several types of bubbles are likely to occur during phase change material performance under microgravity: vapour bubbles, cavities or voids from volume shrinkage, and gas bubbles.

In the solidification process, dissolved gases can be rejected at the solid–liquid interface, just like any other solute, and

during melting bubbles previously overgrown in the solid can be liberated and move due to capillary thermal or solutal Marangoni convection. In a one-*g* field, bubble motion is governed by gravity effects, so they are more likely to float to the top and coalesce. Under microgravity, bubbles can be trapped in a frozen solid.

Phase change material operation can be affected by bubbles: thermal conductivity is normally altered; bubbles can cause stirring actions in the liquid phase; and small bubbles in the solid phase can take up some of the volume shrinkage, thereby avoiding the formation of large cavities.

As the most persistent bubbles are those formed by dissolved gases, to reduce the amount of dissolved gases, it is suggested that the phase change material is boiled under reduced pressure.

12.2.4 The effect of gravity

Gravitational forces between molecules are comparatively small relative to intermolecular or interatomic forces. Since phase change is controlled by intermolecular forces, the rate of melting or freezing should be the same under microgravity as it is under normal gravity conditions, provided that thermal and solutal fields are the same. However, phase change happens to be indirectly influenced by gravity due to convection in the liquid phase, which propagates nuclei and enhances heat transfer, also changing the thermal contact conductance between the heated (or cooled) wall and the phase change material.

As no single material can have all the required properties for an ideal thermal storage medium, one has to use the available materials and try to make up for the poor

physical properties by an appropriate system design. For example, metallic fins can be used to increase the thermal conductivity of phase change materials, supercooling may be suppressed by introducing a nucleating agent or a 'cold finger' in the storage material, and incongruent melting can be inhibited by use of suitable thickness (Sharma et al., 2009).

12.3 Materials data

Data concerning the phase change materials used in existing missions can be found in Sharma et al. (2009), STCDD (1989), and Zalba et al. (2003). Information given includes: chemical formula, density, specific heat, surface tension, thermal conductivity, thermal diffusivity, vapour pressure, viscosity, melting and boiling point, heat of fusion, thermal expansion coefficient (and isothermal compressibility), volume change on melting, flash point, autoignition temperature, supercooling, cost and compatibility. All of these phase change materials have reasonably large heat of fusion, e.g. inorganic compounds in the range from 150 kJ/kg to 400 kJ/kg, and both eutectics (organic and inorganic), and organic compounds in the range from 100 kJ/kg to 250 kJ/kg.

Some materials selected for space applications are summarized in Table 12.1 and a comparison between the different materials is shown in Table 12.2.

Two technologies based on paraffin waxes, dodecane (melting point 10.5 °C) and hexadecane (melting point 18.5 °C), have been used in thermal storage capsules to control the battery temperatures in the NASA Mars rovers (Swanson and Birur, 2003).

Table 12.1 Phase change materials

Paraffins	Non-paraffin organics	Salt hydrates	Metallic
1-Heptene	1-Chloro-propane	Barium hydroxide octahydrate	Cerrobend eutectic
2,4-Dimethyl-pentane	Acetamide	Disodium hydroxide heptahydrate	Gallium
N-Dodecane	Acetic acid	Lithium nitrate trihydrate	
N-Eicosane	Elaidic acid	Sodium hydrogen phosphate dodeca-hydrate	
N-Heptane	Ethyl acetate		
N-Hexadecane	Methyl ethyl ketone		
N-Octadecane	Methyl fumarate		
N-Tetradecane	Methyl propyl ketone		
	Myristic acid		
	Oxazoline wax-es-254		
	Oxazoline wax-ts-970		
	Polyethylene glycol 600		
	Tristearin		

Source: Data extracted from STCDD (1989).

12.4 Phase change material technology

A phase change capacitor consists of the following elements: phase change material, container, and fillers or thermal

Table 12.2 **Comparison of organic and inorganic materials for heat storage**

	Organics	Inorganics
Advantages	No corrosives Low or no undercooling Chemical and thermal stability	Greater phase change latent heat
Disadvantages	Lower phase change enthalpy Low thermal conductivity Inflammability	Undercooling Corrosion Phase separation Phase segregation Lack of thermal stability

Source: After STCDD (1989), Zalba et al. (2003).

conductivity enhancers. Containers and thermal conductivity enhancers are summarized in the following paragraphs.

12.4.1 Containers

Containers differ in their outer shape (circular or rectangular), and in the flexible element that is used for compensating the volume variation of the material during the phase change (STCDD, 1989). Amongst flexible elements of the container, the most common are metallic bellows, metallic membrane, or rubber diaphragm.

- *Elastic bellows*. This is placed between the cold plate and the opposite wall, and pre-stressed in tension during the filling process. At the end of this filling process, the bellows exerts a compressive load on the liquid phase change material. When solidification occurs, the bellows contracts

further and still maintains a compressive load on the phase change material. The major advantage of this type of container is that no void or gas volume is left in the container; therefore the heat transfer within the container is not decreased by the presence of such voids.

- *Metallic membrane*. It should be pre-stressed prior to installation and have a negative deflection in the load-free state. The initial deflection of the metallic membrane will depend on the filling level of the phase change material in the container.

If a rigid container is used, it is necessary to provide a void or gas volume for expansion of the phase change material during melting. A significant problem in designing the rigid container is the sizing of the void volume. The inner volume of the container must be large enough to keep the pressure of trapped gases in the void below reasonable limits. Liquid phase containment problems can be avoided by using solid-to-liquid organic phase change compounds, or 'dry' phase change materials, as reported by Wirtz et al. (1999).

12.4.2 Thermal conductivity enhancers

Two types of thermal conductivity enhancers are considered here: fillers and fins. Fillers are used to improve the thermal conductivity of non-metallic phase change materials which have low conductivities. When fillers are not used, the temperature at the heated surface of the phase change capacitor may rise far above its melting point, with solid material still available but thermally insulated from the heated surface. However, when a metal filler is used, thermal gradients in the phase change material bulk are considerably reduced because of the high thermal conductivity of the filler. The fillers which are most widely used, according to reported

tests, are: aluminium (as powder, foam, wool, or honeycomb), copper (as foam), alumina (Al_2O_3, as powder or foam), and graphite (as foam or fibre).

A quite complete review on elements to enhance thermal conductivity, including graphite-based phase change materials, can be found in Fan and Khodadadi (2011). Carbon foam matrices, with different thermal conductivities and porosities (filled with paraffin wax, for thermal protection purposes), have been investigated by Mesalhy et al. (2006). Others under study are carbon nanofibres and carbon nanotubes (Xia et al., 2010).

As regards the reported results in space applications, aluminium honeycomb offers one of the best system improvements compared to other fillers tested (STCDD, 1989). However, the new systems developed for commercial purposes, such as expanded graphite, carbon fibres, or carbon foam matrix impregnated with paraffin, show a six to ten-fold increase in thermal conductivity. Paraffin loaded into graphite blocks can have a thermal conductivity 20 to 130 times higher than the pure phase change material (Xia et al., 2010).

Concerning fins, aluminium fins are used in preference to honeycomb because of the problems associated with the contact conductance between the honeycomb and the cold plate. Aluminium can be welded to the cold plate whereas honeycomb is usually attached to it with epoxy, which may result in an undesirably high contact resistance. There are several types of fins, as summarized in Zalba et al. (2003). A design optimization procedure is reported in Shanmugasundaram et al. (1997).

Containers and fillers of phase change material cells are made of metals to provide a high thermal conductivity to the cell. Four different metals are currently used for this purpose: aluminium, cooper, titanium and stainless steel. The compatibility of phase change materials with these metals is

limited by the corrosion induced by the phase change material itself, or by impurities in it. Chemical corrosion is the primary mode of material corrosion of concern in phase change material technology. Generally, salt hydrates, metallic, and fused salt eutectics are the most corrosive materials. Corrosion can be reduced by appropriate inhibitors (STCDD, 1989) such as oxide films and additives:

- *Oxide films*. The protective layer of oxide, such as those which appear on aluminium, titanium, and stainless steel, is inert to many phase change materials.
- *Additives*. They form protective coatings made up of compounds absorbed directly on to the metal surface, which provides physical protection against corrosive attack. Among these additives, the most widely used are long-chain aliphatic acids and aqueous solutions of sodium bicarbonate and phosphate.

12.5 The performance of phase change materials

In order to make a first estimation of the phase change material container size, a model of the phase change capacitor should be used. This model should take into account the most relevant characteristics of the heat transfer problem, such as: the heat transfer rate from the heat source; the heat rejection rate to the sink; the maximum energy which can be stored in the phase change material package; the time history for heating and cooling; the temperature level; and constraints on size, mass, and material compatibility.

A very simple analytical, one-dimensional model, based on the following assumptions, is developed in STCDD (1989). In this model, the system is controlled by melting, and the

heat capacity is considered negligible compared to the heat of melting. Also, material properties are considered constant, although different from solid to liquid. Non-steady effects are reduced to changes in the position of the melting (or freezing) front. This front is supposed to be planar and infinitely thin. Furthermore, conduction of heat through the phase change material–filler system is produced simultaneously, although separately, through two different paths, one exhibiting the characteristics of the phase change material and the other those of the filler, without any interaction between the two paths. As a first result of the previous assumptions, it is deduced that a linear variation of temperature in both solid and liquid phases should appear.

The system considered in this model is sketched in Figure 12.1, which consists of: (1) the components whose

Figure 12.1 **Sketch of the one-dimensional model for a phase change capacitor**

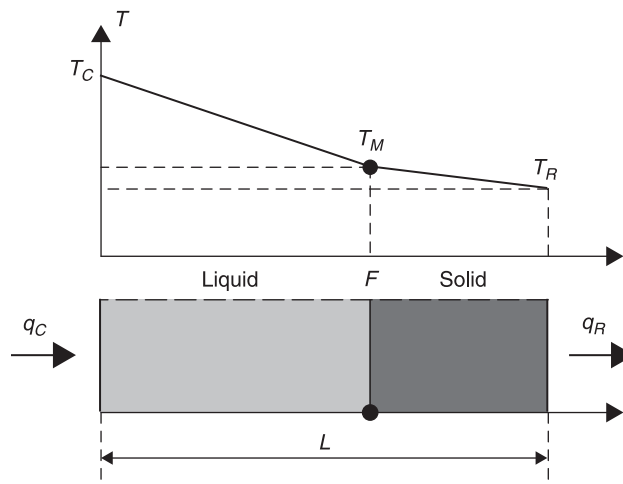

Note: The phase change front, *F,* moves to the right or to the left, depending on whether the heat flux from the component, q_C, is higher or lower than the heat flux dissipated by the radiator, q_R. T_C, T_M, T_R, are the component, melting point, and radiator temperature, respectively. *L* is the thickness of the phase change capacitor.

temperature is to be controlled, (2) a phase change material package, and (3) a radiator. This model allows the required thickness, L, of a given phase change material, to be estimated.

More complex numerical models have been used as a tool for design optimization with aerospace applications (Shanmugasundaram et al., 1997). Reviews of the general thermofluid problem and of the numerical methods of solution can be found in Sharma et al. (2009) and Zalba et al. (2003).

12.6 References

Fan, L. and Khodadadi, J.M. (2011) Thermal conductivity enhancement of phase change materials for thermal energy storage: a review, *Renewable and Sustainable Energy Reviews*, **15**: 24–46.

Gasbarre, J.F. and Dillman, R.A. (2003) 'Preliminary design and analysis of the ARES Atmospheric Flight Vehicle thermal control system', Paper SAE 2003–01–2686, International Conference on Environmental Systems (ICES), Vancouver, Canada, 7–11 July 2003.

Hickey, G.S., Manvi, R. and Knowles, T.R. (1996) 'Phase change materials for advanced Mars thermal control', 26th International Conference on Environmental Systems, ICES-961533, Monterey, California, USA, 8–11 July 1996.

Mesalhy, O., Lafdi, K. and Elgafy, A. (2006) Carbon foam matrices saturated with PCM for thermal protection purposes, *Carbon*, **44**: 2080–8.

Shanmugasundaram, V., Brown, J.R. and Yerkes, K.L. (1997) 'Thermal management of high heat-flux sources using phase change materials: a design optimization

procedure', Paper AIAA 97-2451, 32nd Thermophysics Conference, Atlanta, Georgia, USA, 23–25 June 1997.

Sharma, A., Tyagi, V.V., Chen, C.R. and Buddhi, D. (2009) Review on thermal energy storage with phase change materials and applications, *Renewable and Sustainable Energy Reviews*, **13**: 318–45.

STCDD (1989) *Spacecraft Thermal Control Design Data Handbook*, ESA PSS-03-108, Issue 1.

Tan, F.L. and Fok, S.C. (2007) 'Thermal management of mobile phone using phase change material', 9th Electronics Packaging Technology Conference, Singapore, 10–12 December 2007.

Wirtz, R.A., Zheng, N. and Chandra, D. (1999) 'Thermal management using "dry" phase change materials', 15th annual IEEE, Semiconductor Thermal Measurement and Management Symposium (SEMI-THERM), San Diego, California, USA, 9–11 March 1999.

Xia, L., Zhang, P. and Wang, R.Z. (2010) Preparation and thermal characterization of expanded graphite/paraffin composite phase change material, *Carbon*, **48**: 2538–48.

Zalba, B., Marin, J.M., Cabeza, L.F. and Mehling, H. (2003) Review on thermal energy storage with phase change: materials, heat transfer analysis and applications, *Applied Thermal Engineering*, **23**: 251–83.

13

Heaters

Abstract: In general, spacecraft and their parts and components must be kept within precise operational temperature ranges to assure the fulfilment of the expected performances. In some cases this implies the warming of the item under consideration by using appropriate heaters. When the power needed for this task is compatible with the power budget of the vehicle, electrical heaters are a suitable option. Otherwise other heat sources, such as a radioisotope heater, are needed. The main characteristics of these different heating systems are presented in this chapter.

Key words: electrical heaters, radioisotope heat sources, heat switches.

13.1 Introduction

Reliable long-term performance of most spacecraft components takes place at a specified temperature range. The attainment of some temperature range requires, in many instances, the generation of heat within the spacecraft. In these cases, heaters are sometimes required to fulfil specific requirements such as the protection of components from low temperatures, to provide precise temperature control for devices or components, or to warm up equipment to its operating temperature. For example, heaters are used to warm overboard dump valves for liquids; to keep constant structural temperature on space

telescopes in order to prevent optical misalignment; to maintain the temperature of sensitive gyroscopes and accelerometer guidance platforms; to control the temperature of pressure transducers, other electronics components, and infrared reference sources; to prevent condensation on viewing windows; to keep solar panels warm at night; on catalyst beds of hydrazine thruster engines for spacecraft attitude control; and as shunt resistors, mounted on the skin of a satellite, to dump the excess power of overcharged batteries which would otherwise overheat delicate instruments.

When a local uniform heat source or a profiled heating area is needed, electrical heaters can provide it efficiently due to their versatility, although other types of heaters (chemical or nuclear) are also used in spacecraft. Obviously, the use of electrical heaters requires the availability of a power source. For near-Earth applications, power provided by photovoltaic devices is the preferred option because of the relative proximity of the Sun. However, when spacecraft missions include distances far from the Sun, or in harsh environments (such as the surface of Mars or in certain lunar locations), reliable, long-lived, electrical and thermal power sources independent of the Sun are needed.

In the following sections the main features of electrical heaters, as well as of the auxiliary devices needed for control and regulation, are presented; basic concepts of nuclear heaters are described; and, finally, thermal switches are presented.

13.2 Electrical heaters

Electrical heaters are based on Ohm's and Joule's laws. Ohm's law states that the steady electric current, I, flowing through an electrical conductor is proportional to the constant voltage, V, and to the inverse of the electrical

resistance of the conductor, R, that is, $I = V/R$. According to Joule's law, the heat released per unit time, $\dot{Q}$, by an electrical current, I, is equal to the square of the electrical current, multiplied by the electrical resistance, R: $\dot{Q} = I^2 R$.

Two types of heaters typically used on spacecraft are film heaters (or patch heaters) and cartridge heaters. By far the most commonly used type is the film heater, as due to its flexibility it can be installed on both flat and curved surfaces. These are made of electrical resistance filaments sandwiched between two layers of electrically insulating material, such as Kapton, attached to the leads. The heaters come in various sizes to fit any applications on the spacecraft. They can be custom-shaped to adapt them to specific applications or be simply rectangles of standard dimensions, whereas cartridge heaters consist of a wire-wound resistor enclosed in a cylindrical metallic case.

Typically, the heating power density on the film heaters is limited to less than 0.8 W/cm^2. These are installed on the surface of the particular equipment that needs to be heated using a pressure sensitive adhesive.

For temperature requirements less than 473 K, heaters constructed of Kapton film and FEP Teflon are used, whereas in the case of electrical heaters working in hard conditions, for example temperatures over 473 K, they must be sheathed in metal.

Nearly all heated systems have some type of temperature controller. Unregulated heaters can exhibit large temperature fluctuations when heat demands or ambient temperatures vary.

Often, when the temperature is high, less heating is needed, and when the temperature is low, more is desirable. Heating power can be made to adjust automatically without complicated controls by choosing the heating element material. Nevertheless, the performance of a thermal system is improved by the use of sensors and controllers. Some of

the most significant improvements are the accuracy of the system to maintain the temperature near the set point, the heater life, and the power rating.

The temperature control typically involves a relay that is actuated from the ground (the local control) to enable or disable the power supplied to the heater, a fuse to protect the spacecraft from a short circuit, and usually a thermostat or solid-state controller to turn the heater on and off at predetermined temperatures.

The most common type of control is thermostatic control using a bimetallic mechanical thermostat which opens or closes the heater circuit at a preset temperature. The standard thermostat is a hermetically sealed can containing a switch driven by a snap-action bimetallic actuator (Figure 13.1). The set point at which the thermostat opens can be selected to suit a given application; however, there is a dead band within which the thermostats will close. The dead band chosen for thermostats typically range from 5 °C to 10 °C.

Figure 13.1 **Sketch of a typical thermostat used on spacecraft**

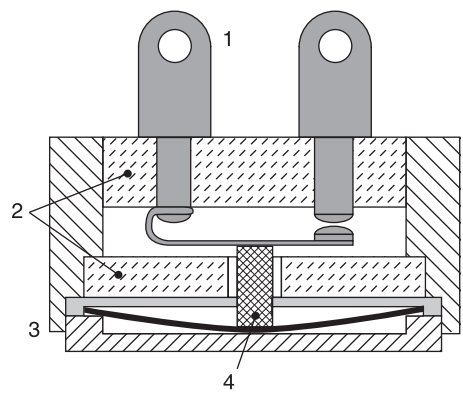

Key: 1 – electric contacts; 2 – electric insulations; 3 – housing; 4 – actuator.

Dead bands less than 4 °C are not recommended because small dead bands have been known to increase the working state in which the thermostat rapidly cycles on and off.

13.3 Radioisotope heat sources

For an Earth-orbiting spacecraft, options for available thermal energy may extend beyond the onboard source (e.g., solar energy), whereas for a deep space mission, these options become more limited. Because the size of solar panels must increase as a function of the distance from the Sun to generate the same power, when designing for a deep space or planetary surface mission, an alternate power source such as a radioisotope power source is generally more effective at generating electrical power than solar energy.

A radioisotope power generator consists of a heat source and a thermoelectric generator (Figure 13.2). The heat is produced from the natural decay of the radioisotope (alpha particles in the case of plutonium-238). With a half-life of 87.7 years, plutonium-238 is an excellent choice for powering long-lived spacecraft. The emitted alpha particles are easily absorbed in the heat source containment system.

The converter in a radioisotope thermoelectric generator consists of an arrangement of thermoelectric couples or elements composed of two legs: a positive-type leg and a negative leg.

Electricity generated at the radioisotope power source can be used to supply power to electrical heaters, although this process of converting the heat in the radioisotope thermoelectric generator to electricity and then back into heat in an electrical-resistance heater is extremely inefficient.

Figure 13.2 Sketch of a generic radioisotope thermoelectric generator

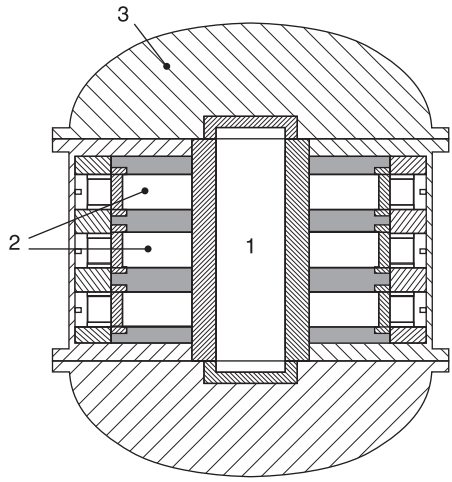

Key: 1 – fuel capsule; 2 – thermoelectric elements; 3 – insulation.
Source: After Bennett (2008).

Since 1961, 41 radioisotope thermoelectric generators have been successfully launched on 23 space missions.These devices have powered the Apollo Lunar Surface Experiments Packages; the Pioneer flybys of Jupiter and Saturn; the Viking Mars Landers; the Voyager flybys of Jupiter, Saturn, Uranus, and Neptune; the Galileo orbital exploration of Jupiter; the Ulysses solar polar explorer; the Cassini orbital exploration of Saturn; and, most recently, the New Horizons mission to the Pluto/Charon system. Increasingly powerful devices have been created since the first flight launched 50 years ago, as illustrated in Figure 13.3.

In addition to the 41 radioisotope thermoelectric generators flown in US spacecraft, one space nuclear reactor was launched in 1965. Furthermore, it is believed that the former Soviet Union has successfully flown radioisotope

Figure 13.3 **Electric power, $\dot{Q}_E$, supplied by radioisotope thermoelectric generators flown in US spacecraft versus launch date, t**

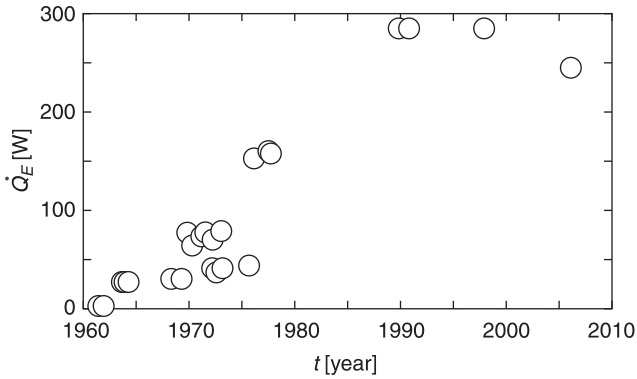

Source: Data are from Rinehart (2001) and Bennett (2008).

thermoelectric generators on two Earth-orbiting spacecraft and on two lunar rovers. Also, most of the Soviet effort was devoted to space nuclear reactors with about 31 (and perhaps 33) thermoelectric reactors used for marine radar observations. The former Soviet Union also launched two experimental thermionic reactors on Earth-orbiting satellites (Bennett, 2008).

Efficiency is improved if the waste heat from a radioisotope power source is recovered by the spacecraft to provide additional thermal control for the avionics and instrumentation without resorting to additional electrical heaters. This leads to the concept of radioisotope heater units. These are devices that place the heat of radioactive decay directly where it is needed. A sketch of this concept is shown in Figure 13.4 (Rinehart, 2001). The heat power of a radioisotope heater unit is around 1 W. There are hundreds of these heating devices flying in US spacecraft.

Figure 13.4 Sketch of a generic radioisotope heater unit

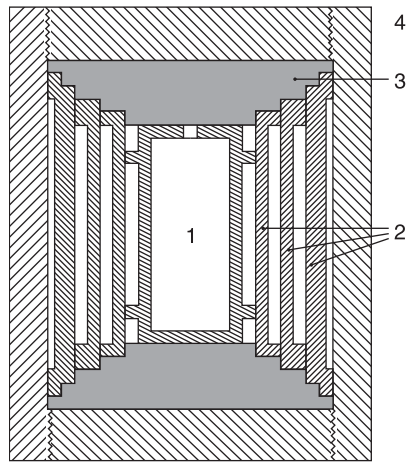

Key: 1 – fuel capsule; 2 – insulator tube nest; 3 – insulation; 4 – housing.
Source: After Rinehart (2001).

13.4 Heat switches

Heat switches cannot exactly be classified as heaters, but their ability to adjust to variations in heat dissipation rates make them an attractive option for temperature control in modern satellites. If a heat switch connects an electronic component to a radiator (Figure 13.5), heat is removed

Figure 13.5 Heat switch between internal components and satellite frame

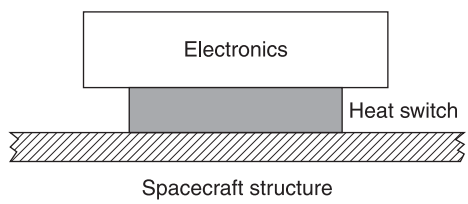

from the device when it is generating large amounts of energy, and conserved when the device is not producing heat, allowing the device to remain in a desired temperature range. Therefore, heat switches can passively control the temperature of warm electronics or instrumentation without the use of thermostats and heaters, thereby reducing power requirements. A list of the relevant properties of available heat switch technologies used in spacecraft is shown in Table 13.1.

In paraffin thermal switches the volume change of paraffin, which expands approximately 15% when it melts, facilitates heat switch operation. Under normal operating conditions, a paraffin heat switch contains a mixture of solid and liquid wax. In addition, a gap exists between the two

Table 13.1 **Summary of available heat switch technologies**

Type	Conductance ratio	Switching time [min]	Advantages	Disadvantages
Paraffin	100:1	~1	Good conductance ratios; well developed	Large physical size, large mass
Gas-gap	700:1 to 2500:1	~5 to 60	High conductance ratios	Slow switching time, large mass
Differential thermal expansion	700:1	~5	High conductance ratios	Requires large temperature differences
Variable thermal layer	70:1	Not available	Flexible approach, active control	Requires power

Source: After Hengeveld et al. (2010).

devices connected by the paraffin heat switch. Due to the vacuum in the gap, heat transfer across the heat switch is limited to radiation across the gap and conduction through the support structure. When heat is added to the heat switch, it is absorbed as latent heat and melts the remaining paraffin solid. The melted paraffin expands and closes the gap that previously separated the hot and cold sides of the heat switch, enabling conduction across the entire heat switch surface. As more heat is added, more paraffin melts and the pressure at the contact between the hot and cold sides increases, causing an increase in conductivity.

The gas-gap heat switch, primarily a cryogenic solution, uses a sorbent bed to control the amount of gas in a gap separating the hot and cold structures. When heat transfer across the switch is desired, the sorbent bed is heated with an electrical resistance heater to release hydrogen gas into the gap. The hydrogen gas enables conduction through the heat switch until the controlling heater is turned off and the hydrogen is again absorbed by the sorbent material.

Differential thermal expansion heat switches provide a more reliable alternative to gas-gap heat switches. This type of heat switch uses two materials with different coefficients of thermal expansion to control contact between the cold and hot sides of the switch.

A recent concept, the variable thermal layer consists of an array of thermoelectric devices embedded in an otherwise insulating matrix. In effect, thermoelectric devices are utilized as individually controllable, bi-directional heat pumps, which provide precise thermal control of the component base-plate (see Chapter 15).

13.5 References

Bennett, L.G. (2008) Mission interplanetary: using radioisotope power to explore the solar system, *Energy Conversion and Management*, **49**: 382–92.

Hengeveld, D.W., Mathison, M.M., Braun, J.E., Groll, E.A. and Williams, A.D. (2010) Review of modern spacecraft thermal control technologies, *HVAC&R Research*, **16**: 189–220.

Rinehart, G.H. (2001) Design characteristics and fabrication of radioisotope heat sources for space missions, *Progress in Nuclear Energy*, **39**: 305–19.

14

Pumped fluid loops

Abstract: The aim of this chapter is to introduce pumped fluid loops, explaining their application in the field of high heat loads, their basic physical principles, and their main types (single-phase, and two-phase flow fluid loops). Both types of fluid loops are outlined, including their main characteristics, the working fluids employed, and their main components (heat exchangers, pumps, additives to reduce pressure loads, evaporators, accumulators). Finally, the description of their operation is provided, as well as flight experiences.

Key words: two-phase flow, frictional analysis, heat exchangers, thermal bus.

14.1 Introduction

If mass expulsion systems are excluded, all energy dissipated on a spacecraft must be transported to an external surface and rejected by radiation. To perform this task, spacecraft thermal control techniques can be classified into two main types: passive thermal control and active thermal control. In passive thermal control techniques, payload components are designed to tolerate large temperature swings and a high operating temperature. Excess heat from these power dissipating components is transferred by conductors and

internal radiation to outer surfaces for radiation to space, which involves the selection of the proper geometrical configurations, insulation blankets, Sun shields, radiating fins, surface thermo-optical properties, thermal coatings, heat sinks, and phase change materials.

When passive thermal control techniques cannot satisfy the requirements of the thermal control design (for example, when environmental extremes are involved or equipment dissipating high power has to be accommodated), active thermal control techniques must be used. Heaters, thermo-electric coolers, cryogenic coolers, and pumped fluid loops are active thermal control techniques which are regularly used in spacecraft design (some of which are described in other chapters of this book).

Traditionally, for relatively small heat loads (say less than 10 kW) and small transport distances, heat pipes have proven excellent options for simple, reliable, and quiet thermal energy transport and temperature control at low to moderate heat fluxes. The common limitation for these devices is a capillary pressure limit, which continues to be extended through the development of higher performance wick materials and geometries. Of course, the capillary driving force is precisely the advantage of the traditional heat pipe in that no pump power and no moving parts are required for the essentially silent operation routinely achieved (see Chapter 11). For high heat loads mechanically pumped loops are arguably unchallenged. Despite a pump power penalty and the drawback of moving parts, mechanically pumped loops have demonstrated their value in many spacecraft thermal control systems.

In both cases heat transfer is achieved through the motion of a fluid, by using capillary forces in the case of a heat pipe, or by using a pumping device, centrifugal or positive displacement pump, normally driven by an electric motor, in

the case of a pumped fluid loop. The process of heat transfer involves the absorption of heat at a relatively steady rate from the component whose temperature is to be controlled, and to transfer it to a heat sink which can be placed apart from the source.

Focusing on pumped fluid loops, they can be categorized as single-phase heat transfer loops (liquid or gaseous), or two-phase fluid loops. A simplified pumped fluid loop is shown in Figure 14.1 (p. xxx). The cooling is accomplished by the use of a coolant as the thermal energy transport agent. The coolant absorbs the dissipated thermal energy from a component and transfers it to a heat sink. The final heat-rejection process depends on whether the coolant is expendable or non-expendable. With expendable coolant, the working fluid is rejected from the space vehicle once it has accomplished its mission. In the case of non-expendable coolant, the working fluid is re-circulated within the system once its thermal energy has been emitted to space via a radiator, as explained in Chapter 8.

In single-phase fluid loops, since only the sensible enthalpy of the circulating fluid is used, the temperature rise in the fluid and the flow rate are directly proportional to the required heat transfer rate. A large temperature rise and high pump power can result from high cooling loads. Low film coefficients in the convective heat exchangers further contribute to the inefficiencies and limit the flux available for special components. In these devices, a liquid or gas phase is used to transfer heat according to the equation

$$\dot{Q} = \dot{m} c_p \Delta T. \tag{14.1}$$

Therefore, in order to increase the heat transfer rate, $\dot{Q}$, either the mass flow rate, $\dot{m}$, or the temperature difference, ΔT, has to be increased for a particular fluid.

For a more effective thermal transport, the single-phase loop can be replaced by a two-phase (liquid–vapour) process. This allows the latent heat of vaporization, or enthalpy of vaporization, to be employed to sharply reduce flow rates, decrease the temperature drops, and increase the heat transfer coefficients. In a typical comparison with a single-phase liquid loop, pump power can be reduced by two orders of magnitude, and heat transfer coefficients can be up to one hundred times higher (Eastman et al., 1984).

14.2 Mechanically pumped single-phase fluid loops

By definition, a mechanically pumped single-phase fluid loop is a system that circulates a working fluid, via routed tubing, to any and all parts of the spacecraft structure. Pumped single-phase fluid loop systems are attractive because they are simple, robust, and have an extensive heritage in terrestrial applications (on Earth, these devices have demonstrated their value in thermal control systems for over 100 years). According to Paris et al. (2004), when compared to other thermal control technologies, the advantages of a mechanically pumped single-phase fluid loop for spacecraft thermal control include:

- Flexibility in locating heat dissipating equipment inside the spacecraft.
- Ability to accept and reject heat at multiple locations.
- Ease of integration into the spacecraft due the use of mechanical field joints in the loop.
- Ease of accommodation with deployable radiators.
- Ability to incorporate late design changes in the spacecraft.

- Ease of predictability of thermal performance.
- Relative immunity to gravitational effects.
- Ease of scalability to meet changes in power dissipation requirements.
- Command of operation.
- Ability to match working fluid to the required thermal environment.

Although mechanically pumped fluid loop systems have some limitations (mainly due to power consumption and reliability concerns for the mechanical pump), they have the potential to greatly increase the capabilities of active thermal management on spacecraft.

While mechanically pumped fluid loop systems are still under development for spacecraft applications, there are several examples of spaceflight heritage. Mechanically pumped fluid loop systems have been used on Earth-orbiting missions such as the Space Transportation System Shuttle and International Space Station (Paris et al., 2004). For deep space missions, mechanically pumped fluid loops were successfully developed and used on both the Mars Pathfinder (Bhandari et al., 2005) and the two Mars Exploration Rover missions (Tsuyuki et al., 2004). Concerning the European Space Agency, a single-phase mechanically pumped fluid loop has been proposed to be flown as a technology demonstrator program on the Alphasat mission (van Benthem et al., 2010).

14.2.1 Analysis of single-phase fluid loops

As sketched in Figure 14.1, the various components within a pumped fluid system (pump, heat exchanger, radiator, etc.) are connected mainly by conduits. As already mentioned, the

Figure 14.1 Schematic representation of a fluid loop showing the main components: 1 – heat exchanger; 2 – pump; and 3 – heat source

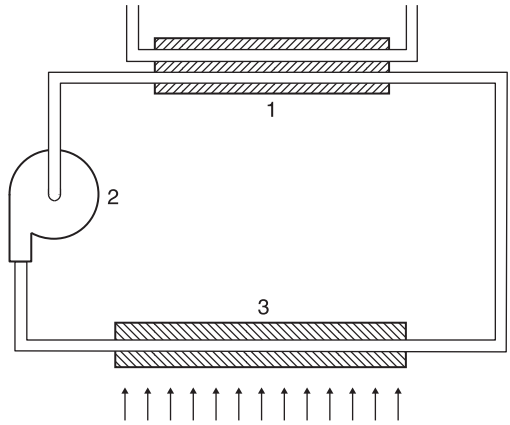

simplest model of a pumped fluid loop consists of a circuit formed by fluid-carrying tubes which connect a heat sink to a heat source. A circulation pump moves the fluid through the loop so that heat is transported from source to sink by forced convection.

The heat source can be an energy dissipating component, such as electronic equipment, an experimental module involving exothermic reactions, or any other heat-producing device. In some applications, the heat source element is mounted on and thermally linked to a cold plate, and the coolant flows through the latter. In this case, the cold plate can be considered as the heat source. The heat sink can be a heat exchanger, where heat is transferred to a cold fluid circulating in another loop (dual loop configuration), or a radiator which rejects the heat directly to space.

To calculate the thermal performances of a fluid loop, it is usually assumed that some input data are known (such as the general layout of the fluid loop, the heat flow rate to be

evacuated, the mass flow rate, and the inlet temperature of the cold fluid), while the expected results are the temperature distribution throughout the loop and the pumping power requirements. All the physical phenomena to be modelled in the analysis of a single-phase pumped fluid loop are well known and established, so that the theoretical basis for such an analysis can be found in available text books dealing with fluid mechanics and heat transfer. However, this is a difficult problem because both thermal and frictional analyses have to be taken into account.

According to STCDD (1989), in the analysis of a single-phase pumped fluid loop, the following magnitudes should be determined:

1. heat transfer areas, free flow areas, and frontal areas (for both the hot side and the cold side of the exchanger);
2. fluid properties (density, specific heat, thermal conductivity, and dynamic viscosity);
3. Prandtl number, Reynolds number, Nusselt number, and the convective heat transfer coefficient;
4. effectiveness of the surface due to fins, if any;
5. overall heat transfer coefficient for each side of the exchanger and number of heat transfer units; and
6. exchanger effectiveness.

Once this last parameter is known, the temperature through the loop can be obtained.

Regarding the frictional analysis, the power which must be supplied to the circulation pump can be expressed as a function of the overall efficiency of the pump, the pressure loss through the loop, the fluid mass flow rate, and the fluid density at the pump location.

It is beyond the scope of this book to present detailed information on the calculation process of single-phase

pumped fluid loops. Extensive descriptions of the theories and methods involved in both the thermal analysis and the frictional analysis can be found in STCDD (1989) and Gilmore (2002), and data concerning pressure losses in ducts are given in Idelchik (1996). Available numerical tools for pumped fluid loop calculations are presented in Gilmore (2002).

14.2.2 Working fluids

Coolant fluids for spacecraft temperatures can be gaseous or liquid (molten metals can be used at higher temperatures). The selection of the coolant is based on the thermal and power requirements for achieving a given cooling duty. In the case of non-expendable coolants, the basic variables are: density, specific heat, thermal conductivity and viscosity, as well as temperature limits, which should be compatible with the desired application.

The above-mentioned properties, however, do not give the complete picture of the problem. Many fluids fulfilling the appropriate thermal and frictional requirements can be aggressive to metallic or elastomeric materials. Several coolants are toxic and their use is to be ruled out when manned operations are envisaged; several others are flammable.

Additional requirements can be defined in particular cases. For instance, good lubricity is desirable for hydraulic functions as well as cooling; dielectric properties become important when single-walled jackets are used and the fluid is in contact with electrical equipment. Concern with vapour pressure, storage temperature, safety, and handling appears in the detailed design of the system.

Relevant properties of suitable liquid coolants can be found in STCDD (1989) and Gilmore (2002). However, the list of fluids already selected for single-phase pumped fluid

Table 14.1 **Working fluids for single-phase pumped fluid loops**

Working fluid	Fluid temperature range	Space application	References
Water, H_2O	+20 °C to +60 °C	International Space Station	Paris et al. (2004)
Ammonia, NH_3	−70 °C to +40 °C		
Freon-21 [A], $CHFCl_2$	–	Space Transportation System Shuttle	
Freon-11[A,B], CCl_3F	−80 °C to +50 °C	Mars Pathfinder, Mars Exploration Rover	Paris et al. (2004), Tsuyuki et al. (2004)
Galden ZT 85 [C]	−10 °C to +70 °C	Alphabus	Matthijssen et al. (2006), van Benthem et al. (2010)

Notes:
[A] Freon is a registered trademark of E.I. DuPont de Nemours & Co., Inc.
[B] Also known as chlorofluorocarbon 11, CFC-11, Refrigerant-11, and R-11.
[C] Manufactured by Solvay Solexis.

loops is very restrictive, and only a few liquids have already been used or their use in the near future is envisaged. Some of these are listed in Table 14.1.

14.2.3 System hardware

As mentioned previously, mechanically pumped fluid loop systems have an extensive heritage in terrestrial applications. Thus, many of the devices used in space systems are the result of a successful adaptation of products already used on Earth

to the unique particularities of space environment. This is the case with heat exchangers and mechanical pumps.

Closed-type exchangers or recuperators are heat exchangers in which hot and cold fluids are separated by a tube wall or some kind of surface. Energy exchange between the two fluids is accomplished by convection from one fluid to a surface of the wall, by conduction through the wall or plate, and then by convection from the wall surface to the second fluid. They are usually classified according to their configuration. The most common types are flat-plate, shell-and-tube, and cross-flow. The last two types are depicted in Figure 14.2.

For most heat transfer surfaces used in heat exchangers, the heat transfer rate per unit of surface area increases with the fluid flow velocity, and this heat transfer rate varies as

Figure 14.2 **Basic types of heat exchanger: (a) shell-and-tube exchangers, and (b) cross-flow exchangers**

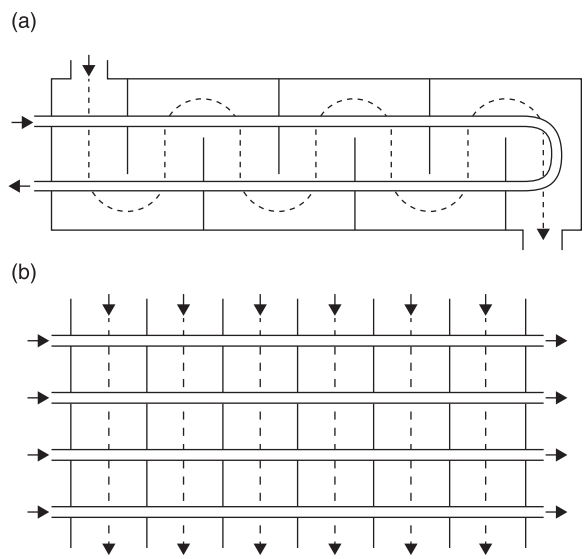

Source: After Gilmore (2002).

something less than the first power of the fluid velocity. The friction power expenditure also increases with fluid-flow velocity, although in this case, the exponent of the velocity dependence varies between two and three.

Therefore, to keep the pumping power within reasonable limits, the designer of the heat exchanger is generally forced to use low velocities, which implies that the heat transfer rate tends to be low, and therefore, large heat transfer surfaces are required. To obtain as much heat transfer in as little space as possible, it is necessary to build exchangers with large surface area densities (surface area density is the ratio of total heat transfer area to total exchanger volume). These are the so-called compact heat exchangers, where multiple passes of one or both fluids are used to obtain as much energy transfer in as little space as possible.

The use of polymeric additives in water for compact heat exchangers, in aerospace and other applications, has been addressed by Fossa and Tagliafico (1995).

Data available in the literature have been confirmed by experimental tests, showing that a great reduction in turbulence is produced by long-chain polymers. For this reason, the use of polymeric additives combined with turbulence-promoting surfaces seems to be inadvisable. However, when the heat transfer enhancement is based on an increase in the exchange area, the use of polymers should offer some benefits in terms of friction factor and pumping power reduction, while still keeping most of the advantages in heat transfer performance. From a general point of view, the use of polymeric additives in heat exchangers with fins or turbulence promoters is not advisable if the benefit expected in pumping power reduction is associated only with the decrease in friction loss in the heat exchanger itself. Notwithstanding, long, single-phase, thermal bus systems can take advantage of the use of polymeric additives due to

the substantial pumping power savings that can be achieved (up to 40%), with only a slight heat transfer performance reduction expected (less than 5%).

Pumps are machines that impart energy to a fluid, in most cases a liquid (compressors, fans, and blowers impart energy to gases rather than to liquids). Space-borne pumps seem to vary enormously in design and principle of action. Nevertheless, they can be divided into two main types: rotodynamic pumps and displacement pumps.

1. A rotodynamic pump imparts energy to a liquid through the work done by a rapidly rotating vaned impeller. Examples of rotodynamic pumps are radial-flow centrifugal pumps, mixed-flow pumps, and axial-flow pumps, or propellers.
2. Displacement pumps, which include reciprocating and rotary pumps, impart energy by a positive displacement action.

For further explanations the reader is directed to STCDD (1989) and Gilmore (2002), where besides the basic theories related to mechanical pumps, typical characteristic curves for different types of pumps are given.

14.3 Mechanically pumped two-phase fluid loops

Though conventional single-phase systems (based on the heat capacity of the working fluid) are simple, well understood, easy to test, relatively inexpensive, and low risk, they carry out proper thermal control with the following characteristics: small temperature drops from equipment to radiator (to reduce radiator size and mass); thick-walled,

large-diameter, heavy lines; and noisy, heavy, high-power pumps, and consequently large solar arrays. Therefore, the main driver for developing alternatives is to overcome these single-phase heat transport system disadvantages. The most promising alternative is the pumped two-phase system, a mechanically pumped loop receiving heat by evaporation of the working fluid at heat dissipating stations (cold plates and heat exchangers), and releasing heat by condensation at heat demanding stations (hot plates and heat exchangers) and at radiators, for heat rejection to space. Such a system relies on the heat of vaporization: it operates almost isothermally and the pumping power is reduced by orders of magnitude, minimizing sizes and masses of radiators and solar arrays (Delil, 2000).

Therefore, mechanically pumped two-phase cooling loops can be considered as an advanced thermal control technology which has emerged as a highly effective means for dissipating large amounts of heat from a small heat transfer area, and providing a robust solution for thermal control design because of its low specific mass, low specific power, high flexibility to load disposition, more precise temperature control, greater heat transport capacity, and better isothermal conditions.

The simplest design of a pumped two-phase fluid loop (Figure 14.3) consists of an evaporator for heat acquisition, a condenser/radiator for heat rejection, a pump for circulation of coolants, and an accumulator serving as a supply reservoir and also as a pressure regulator. The coolants, in a liquid phase, are mechanically pumped into the evaporator where they become wet vapours. In the condenser/radiator, the vapours change into sub-cooled liquids which flow to the pump. A two-phase fluid cycle system is thus formed to achieve the thermal balance.

Figure 14.3 **Schematic representation of a two-phase fluid loop showing the main components: 1 – pump; 2 – evaporator (heat source); 3 – condenser (heat exchanger); and 4 – accumulator**

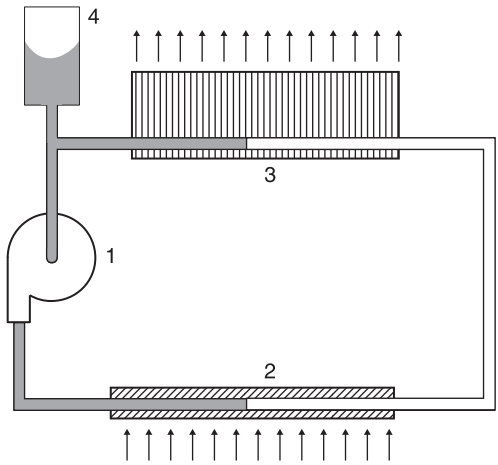

Source: After Furukawa (1997).

The description of the system operation involves many parameters, such as the heat load, the base-plate temperature, the vapour temperature, the liquid temperature, the radiator temperature, the sink temperature, the mass flow rate, the evaporator exit or condenser entrance quality (or dryness fraction), the pump head, the pump speed, and the accumulator pressure. In addition, multiphase flow, that is, the simultaneous flow of the different phases, strongly depends on the level and direction of gravity (Da Riva and Sanz, 1991), since they have an influence on the spatial distribution of the phases, which have different densities. Of great interest for space applications are the more complicated liquid–vapour flows, which are characteristic of spacecraft thermal control systems, life sciences systems, and propellant systems. Especially for liquid–vapour flow in spacecraft

two-phase thermal control systems, the two-phase flow is extremely complicated, because of heat and mass exchange between the two phases by evaporation, condensation, or flashing (Delil, 2001).

However, in spite of such a huge number of difficulties, substantial efforts have been devoted to developing analytical and numerical tools to study two-phase flows under microgravity conditions. For example, a reasonably simple mathematical model of a mechanically pumped two-phase fluid loop, which could be used as a first step in the loop system performance analysis, can be found in Furukawa (1997), and an overview of some of the most popular techniques for multiphase flow computations is presented in Uzgoren et al. (2007).

When, in the thermal control system, there are several heat sources which must be operated simultaneously, the resulting configuration is the so-called thermal bus. This is a pumped fluid, high-capacity heat transport system, serving as a common temperature controlled heat sink or source to more than one payload, usually to several. Such thermal management systems have to transport large amounts of dissipated power (gathered at many dissipating stations) over large distances to the heat sinks, the radiators, where the heat is radiated to the cold space environment.

The basic difference between mechanically pumped single-phase (sensible heat transport by the liquid) and two-phase systems (transport by latent heat of evaporation/condensation) implies important differences in the mode of operation. This leads, for dissipating stations connected in series in a single-phase system, to a temperature increase in the downstream direction of the loop, while for two-phase systems, with evaporators in series, it means an increase of the vapour quality in the downstream direction, associated to a (usually small) decrease of the saturation temperature.

A two-phase thermal bus can serve several modules by extracting heat from them, or dumping heat into them, depending on the operating conditions of any particular module. Components can be coupled to the bus to transfer heat from hot to cold regions. The ordering of modules in the circuit is not important and certainly not crucial.

The stations can be arranged in a pure series (Figure 14.4a), in a pure parallel (Figure 14.4b), or in a hybrid configuration, that is, a combination of parallel and series. When compared to the parallel concept, the series concept has the advantage of simplicity and shorter total piping length. But it has the disadvantage of a greater pressure drop (unless a larger piping diameter is chosen), some (minor) restrictions with respect to the sequence of the stations in the loop, and somewhat more complexity with respect to modularity. The advantage of the parallel concept is the modular approach, in which branches with dissipating stations (evaporators/cold plates) or heat demanding stations (condensers/radiators) can be simply added or removed. But it also has the drawbacks of the tubing length, and of the complex feedback control system to adjust the vapour quality of the two-phase mixture in the exiting line of each cold plate. The latter control system is necessary to keep these mixture qualities close to a certain chosen value in order to guarantee the proper performance of the thermal bus, by preventing system instabilities and oscillations (Delil, 2001).

Two-phase thermal control systems have reached an acceptable level of maturity, and therefore they are becoming more and more accepted as reliable heat transport systems. However, the design of a two-phase flow loop is still rather difficult and cumbersome due to the character of two-phase single-component flow dynamics and heat transfer. In the two-phase lines of mechanically pumped loops and in the

Figure 14.4 **Sketch of a mechanically pumped two-phase thermal bus series configuration (a), and a mechanically pumped two-phase thermal bus parallel configuration (b)**

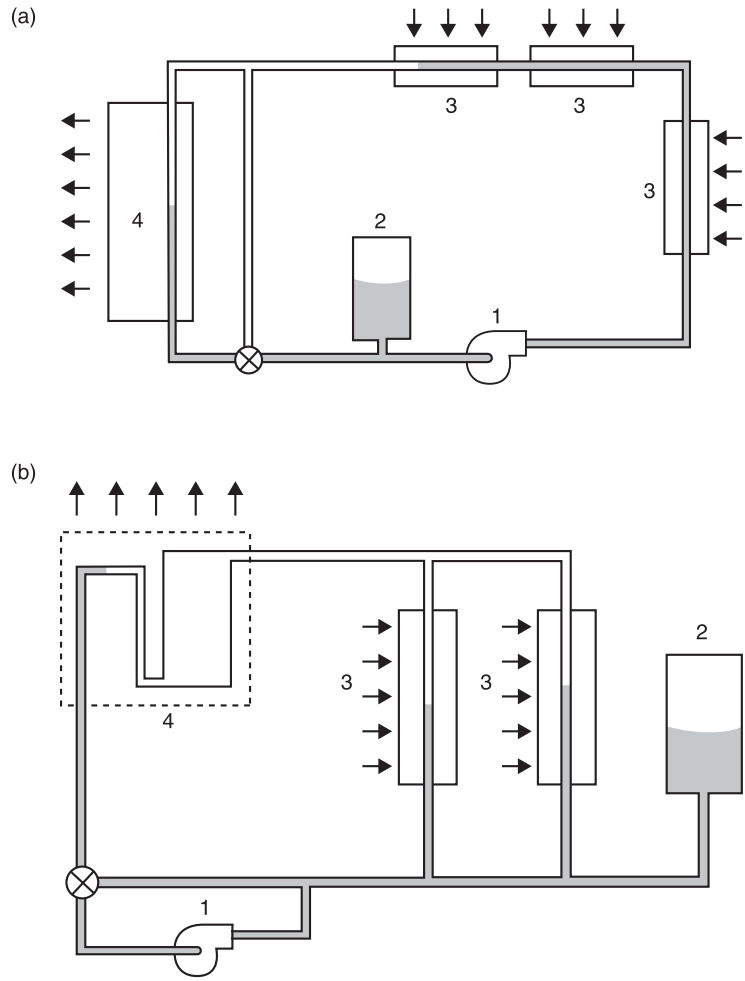

Key: 1 – pump; 2 – accumulator; 3 – heat source; 4 – condenser (radiator).

Source: After Delil (2001).

condenser of any two-phase loop, the flow pattern dependent heat transfer is of great importance for the definition of a particular thermal management system.

14.3.1 Flight experiences

In the last two decades a large amount of work has been devoted to mechanically pumped two-phase systems. In addition to theoretical work, many efforts have been focused on the experimentation and calibration of parts and components of thermal bus devices, and several in-orbit demonstrators have been flown to check their performances in real microgravity conditions. Some of these initiatives are briefly described in the following paragraphs.

Thermo-hydraulic experiments of a pressure-regulated two-phase fluid loop were performed in August 1997 aboard the Space Shuttle (flight STS-85). The fluid loop model, named TPFLEX (Two-Phase Fluid Loop Experiment), used distilled water as a working fluid (Furukawa et al., 1998; Futamata et al., 2002). A sketch showing the operation principles of TPFLEX is shown in Figure 14.5. The evaporator is of a double-piped channel and serves for vapour/liquid phase separation. The inner channel is a circular tube for liquid supply and return, while the outer one takes a semi-circular form as a vapour passage. An annular wall between the two is made of porous materials. A volume of coolant liquid larger than needed is mechanically pumped into the evaporator's inner channel. Only a limited amount of the liquid, proportional to the heat load, is sucked up to the evaporator's outer channel by capillary forces to turn it into vapour. The excess liquid that has not been sucked up is discharged from the inner channel to return to the pump. The vapour then goes to the condenser/radiator, where it is fully liquefied. The condensed (and sub-cooled) liquid flows

Figure 14.5 **Sketch of the Japanese demonstrator TPFLEX (Two-Phase Fluid Loop Experiment), flown on STS-85**

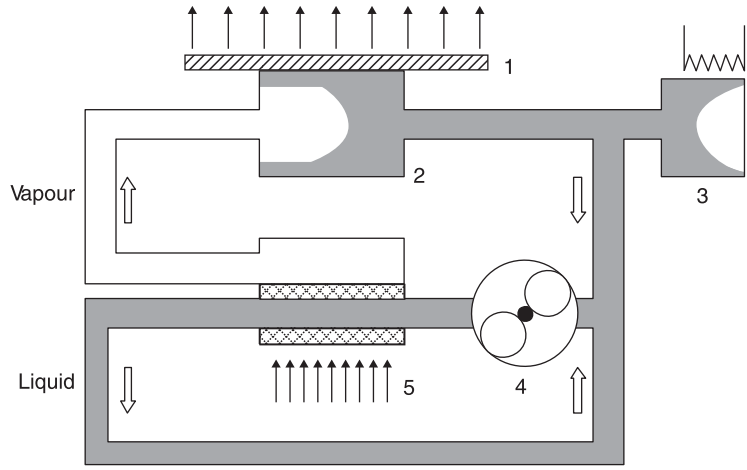

Key: 1 – radiator; 2 – condenser; 3 – accumulator; 4 – pump; 5 – evaporator.
Source: After Furukawa et al. (1998).

out towards the pump inlet to join the oversupplied one. The vapour is in a saturated state, whose temperature can hence roughly be controlled with an accumulator placed at the condenser exit (or at the pump entrance). The accumulator here serves not only as a supply reservoir, but also as a pressure regulator.

Anti-Matter Spectrometer, or Alpha Magnetic Spectrometer (AMS-02), is a particle physics experiment in space to be located on the International Space Station (ISS) truss. The purpose is to perform accurate, high statistics, long-duration measurements of the spectra of energetic (up to multi-TeV) primary cosmic rays in space. Some of the experiment's goals are concerned with dark matter, antimatter, and cosmic rays (Battiston et al., 2005).

Amongst the different subsystems of AMS-02, the AMS Tracker Thermal Control System (TTCS) is a two-phase

cooling system developed by NLR (The Netherlands), INFN Perugia (Italy), Sun Yat Sen University, Zhuhai (China), AIDC Taichung (Taiwan), Massachusetts Institute of Technology (USA), and NIKHEF (The Netherlands). The tracker thermal control system is a mechanically pumped two-phase carbon dioxide cooling loop whose main objectives are to provide accurate temperature control (less than 3 K) and the removal of 140 W heat from the AMS-02 Tracker front-end electronics. The tracker thermal control system requirements, system design, and development status, are described in van Es et al. (2009). A demonstration experiment of this thermal control system (AMS-01) was successfully flown in June 1998 on the Space Shuttle Discovery (STS-91).

The tracker thermal control system is a mechanically pumped two-phase carbon dioxide cooling loop, as shown in Figure 14.6. By following the loop routing, the operation is explained. At the pre-heaters the working fluid temperature is raised to the saturation temperature. The working fluid enters the evaporator with a quality slightly above zero, ensuring a uniform temperature along the complete evaporator.

Due to the widely distributed front-end electronics, the evaporator consists of two parallel branches collecting the heat at both the bottom and top sides of the tracker planes.

With an overall mass flow of 2 g/s, the mean quality at the outlet of the evaporators is approximately 30%. The two-phase flow of both branches is mixed and led through the heat exchanger, where heat is exchanged with the incoming sub-cooled liquid. Behind the heat exchanger, the two-phase line is split into two branches. One branch leads to the condenser at one of the heat pipe radiators, and the other leads to the condenser at the other heat pipe radiator, where the heat is rejected to space. The sub-cooled liquid of both liquid lines is mixed. In principle this flow distribution is

Figure 14.6 Sketch of a tracker thermal control system loop

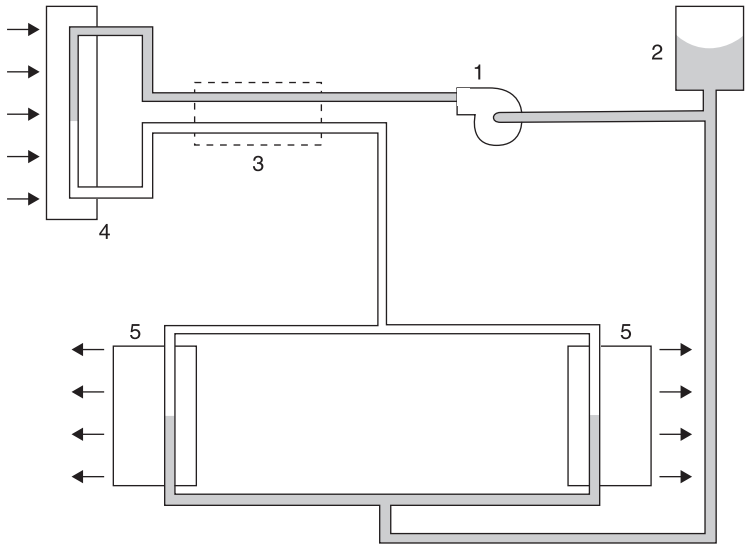

Key: 1 – pump; 2 – accumulator; 3 – heat exchanger; 4 – evaporator; 5 – heat pipe radiator.

Source: After van Es et al. (2009).

self-adjusting. The flow through the branch with the highest quality will induce the largest pressure drop. Hence, a larger part of the condenser flow will be directed to the opposite condenser branch. At the end of the condensers, the fluid is sub-cooled well below the saturation point, so arrives back at the pump in liquid phase.

Downstream from the pump, the sub-cooled liquid is pre-heated by exchanging heat with the returned two-phase flow from the evaporator. In most cases, the heat exchanger increases the temperature of the sub-cooled liquid to saturation. Only in extreme cold orbits, an additional 8 W pre-heater power per branch is needed to create saturation.

The thermal control room of the tracker thermal control system is the accumulator. It is the largest two-phase volume in the loop, and it therefore dictates the saturation (and thus

evaporation) temperature in the loop. The big advantage of this system is that the accumulator can be situated far away from the electronics in the confined tracker area. The accumulator is controlled by heaters and thermoelectric cooling.

Further modifications of this design are under development, aiming to use two-phase carbon dioxide thermal control systems for Earth applications, or to improve the flight performances for future space applications (Liu et al., 2008; Liu and Guo, 2010).

Two accumulator controlled loops have been successfully developed: one CO_2 loop for cooling the AMS-2 particle detector which will study cosmic radiation on board the International Space Station, and a second CO_2 loop for cooling the particle detector of the Large Hadron Collider-Vertex Locator Experiment (LHCb-VELO), at the CERN laboratory in Geneva, Switzerland (Verlaat, 2007).

14.4 References

Battiston, R. (on behalf of the AMS Collaboration) (2005) 'The Anti Matter Spectrometer (AMS-02): a particle physics detector in space', 29th International Cosmic Ray Conference, Pune, India, 3–10 August, 2002, *29th ICRC Proceedings*, **10:** 151–72.

Bhandari, P., Birur, G., Pauken, M., Paris, A., Novak, K. et al. (2005) 'Mars Science Laboratory thermal control architecture', Paper 05ICES-196, 35th International Conference on Environmental Systems, Rome, Italy, 11–14 July 2005.

Da Riva, I. and Sanz, A. (1991) Condensation in ducts, *Microgravity Science and Technology*, IV/3, 179–87.

Delil, A.A.M. (2000) *Research Issues on Two-Phase Loops for Space Applications*, Report NLR-TP-2000-703, Nationaal Lucht- en Ruimtevaartlaboratorium, Amsterdam, The Netherlands.

Delil, A.A.M. (2001) *Tutorial on Single- and Two-Component Two-Phase Flow and Heat Transfer: Commonality and Difference*, Report NLR-TP-2001-538, Nationaal Lucht- en Ruimtevaartlaboratorium, Amsterdam, The Netherlands.

Eastman, R.E., Feidmanis, C.J., Haskin, W.L. and Weaver, K.L. (1984) *Two-Phase Fluid Thermal Transport for Spacecraft*, FWAL-TR-84-3028, Air Force Wright Aeronautical Laboratories (AFSC), October.

Fossa, M. and Tagliafico, L.A. (1995) Polymer solutions in enhanced surface heat exchangers, *Experimental Thermal and Fluid Science*, **10**: 221–8.

Furukawa, M. (1997) 'Static/dynamic analyses for pumped two-phase fluid loop control', Paper AIAA 1997-2468, 32nd AIAA Thermophysics Conference, Atlanta, Georgia, USA, 23–25 June 1997.

Furukawa, M., Mimura, K. and Komori, M. (1998) 'Demonstrative in-orbit operations of a pressure-regulated two-phase fluid loop model', Paper AIAA 1998–2451, 7th AIAA/ASME Joint Thermophysics and Heat Transfer Conference, Albuquerque, New Mexico, USA, 15–18 June 1998.

Futamata, R., Yamamoto, M., Nakagawa, M., Mimura, K. and Komori, M. (2002) Experiment configuration and preliminary results of two-phase fluid loop experiment (TPFLEX)–STS-85 Mission Payload, *Acta Astronautica*, **50**: 217–24.

Gilmore, D.G., Ed. (2002) *Spacecraft Thermal Control Handbook, Vol. I: Fundamental Technologies,* 2nd ed.,

American Institute of Aeronautics and Astronautics, Inc., The Aerospace Press, El Segundo, California, USA.

Idelchik, I.E. (1996) *Handbook of Hydraulic Resistance,* 3rd edition, Begell House, New York, USA.

Liu, J. and Guo, K. (2010) Transient performance investigation of the mechanically pumped cooling loop (MPCL) system, *International Journal of Refrigeration*, **33**: 26–32.

Liu, J., Pei, N.Q., Guo, K.H., He, Z.H., Li, T.X. and Lu, M. (2008) Experimental investigation on mechanical pumped cooling loop for application in future space missions, *Energy Conversion and Management*, **49**: 2704–10.

Matthijssen, R., van Put, P. and van der List, M.C.A.M. (2006) 'Development of an advanced mechanically pumped fluid loop for thermal control of large future telecommunication platforms', 36th International Conference on Environmental Systems, Norfolk, Virginia, 17–20 July 2006.

Paris, D., Bhandari, P. and Birur, G.C. (2004) 'High temperature mechanically pumped fluid loop for space applications–working fluid selection', Paper 04ICES-282, 34th International Conference on Environmental Systems, Colorado Springs, Colorado, USA, 19–22 July 2004.

STCDD (1989) *Spacecraft Thermal Control Design Data Handbook*, ESA PSS-03-108, Issue 1.

Tsuyuki, G.T., Avila, A., Awaya, H.I., Krylo, R.J., Novak, K.S. and Phillips, C.J. (2004) 'Mars Exploration Rover: Thermal design is a system engineering activity', Paper 2004-01-2411, 34th International Conference on Environmental Systems, Colorado Springs, Colorado, USA, 19–22 July 2004.

Uzgoren, E., Singh, R., Sim, J. and Shyy, W. (2007) Computational modeling for multiphase flows with spacecraft application, *Progress in Aerospace Sciences*, **43**: 138–92.

van Benthem, R.C., de Grave, W., van Es, J., Elst, J., Bleuler, R. and Tjiptahardja, T. (2010) *Development of a Mechanically Pumped Fluid Loop for 3 to 6 kW Payload Cooling*, Report NLR-TP-2009–459, Nationaal Lucht- en Ruimtevaartlaboratorium, Amsterdam, The Netherlands.

van Es, J., Pauw, A., van Donk, G., He Sun, Zh., Verlaat, B. et al. (2009) 'AMS02 tracker thermal control system overview and spin-off for future spacecraft cooling system developments', Paper IAC-09.C2.7.1, 60th International Astronautical Congress, Daejeon, Republic of Korea, 12–16 October 2009.

Verlaat, B. (2007) 'Controlling a secondary 2-phase CO_2 loop using a 2-phase accumulator', Paper ICR07-B2–1565, 22nd International Congress of Refrigeration, Beijing, China, 21–26 August 2007.

15

Thermoelectric cooling

Abstract: In this chapter, the thermoelectric cooling technology for space applications is presented, including the main characteristics of space applications (regulation, operation, integration), the scope of its utilization, the basic configuration of a thermoelectric cooler, the connection configuration, the effect of the number of stages, the temperature distribution along the thermoelectric cooler, the performance parameters, and the fundamental effects which explain this phenomena (Seebeck, Peltier, Thomson, Joule and Fourier effects). Finally, some relevant space applications are included.

Key words: thermoelectric cooling, Seebeck effect, Peltier effect, Thomson effect, Joule effect, Fourier effect.

15.1 Introduction

Thermoelectric coolers are solid-state devices that work as small heat pumps, like conventional mechanical heat pumps (refrigerators), absorption refrigerators, and other similar devices involving the transfer of heat. Thus, the behaviour of thermoelectric coolers can also be explained by using the laws of thermodynamics.

The use of thermoelectric cooling in space applications is based on some of the following characteristics:

- A thermal regulation system which is flexible and easy to control, with localized cooling, and the temperature control can operate above or below ambient, heating or cooling, depending on the current direction. The precision of the temperature control can be better than 0.01 K.
- The operation of the system is reliable and easy. It is robust, maintenance free, with solid-state reliability; high resistance to shock and vibration; operation in both low and high *g* levels, with no moving parts, and in any orientation.
- The integration with another spacecraft's subsystems is easy. It is direct-current powered, does not use gases or refrigerant; is small, and lightweight; does not produce electrical or acoustical noise or vibrations.

However, due to its low efficiency it is mostly suitable for localized cooling for temperature control of a single component, rather than a main cooling method for an entire system.

A classic thermoelectric cooler (Scott, 1974; STCDD, 1989) consists of a type N and a type P semiconductor (such as bismuth telluride). A sketch of this device is shown in Figure 15.1. At the surface to be cooled, a junction between these dissimilar semiconductors is formed, and a DC voltage is applied across the other junction, placed at the hot surface, where heat is transferred to the surroundings. The transfer of heat from the cold to the hot junction is produced by the extra electrons in the N type material and the holes left in the P type material (considered as positive charges), which act as heat carriers (Peltier effect).

In order to increase their power handling capacity, thermoelectric elements are usually connected electrically in series, and thermally in parallel, as shown in Figure 15.2.

Figure 15.1 Sketch of a thermoelectric cooling element

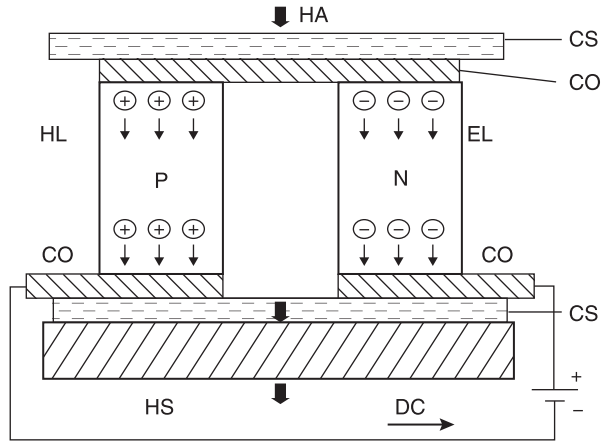

Key: CO, copper plate; CS, ceramic substrate; DC, direct current; EL, electrons; HA, heat absorbed; HL, holes; HS, heat sink. N, P, type N and type P semiconductors, respectively.

Source: After Scott (1974), TE TECHNOLOGY (2011) and MELCOR (2011).

Figure 15.2 Sketch of a typical thermoelectric module assembly

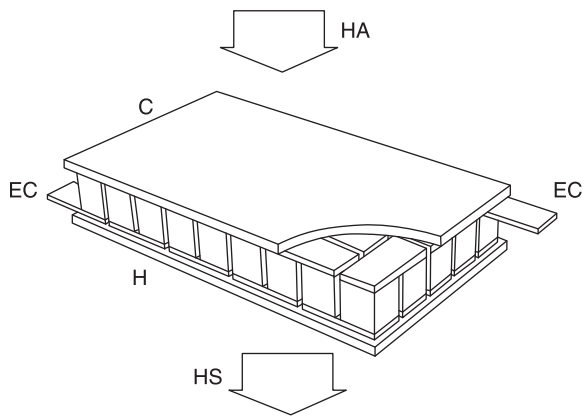

Key: EC, electrical connection; C, cold side; H, hot side; HA, heat absorbed; HS, heat sink.

Source: After MELCOR (2011) and TE TECHNOLOGY (2011).

When a single module does not give the required performance, a multi-stage cascade can be used, which basically consists of two or more single thermoelectric modules, stacked in series. At each successive higher temperature stage, the heat that must be pumped is not only the cold side heat but also the heat dissipated by the lower temperature modules. Thus, at each stage, more thermoelectric couples are needed than at the colder ones. This is the reason for the pyramid shape of the cascade module.

The applied heat load generally determines the maximum temperature difference that can be achieved by the thermoelectric cooler. However, even with zero heat load, regardless of the amount of power applied, every module has a theoretical maximum temperature difference. It depends on the number of stages and the properties of the thermoelectric material, as can be seen in Figure 15.3. Large cooling capacities can be achieved by using several thermoelectric coolers connected thermally in parallel.

Figure 15.3 **The effect of the number of stages, N_s, on the maximum temperature difference ΔT_m**

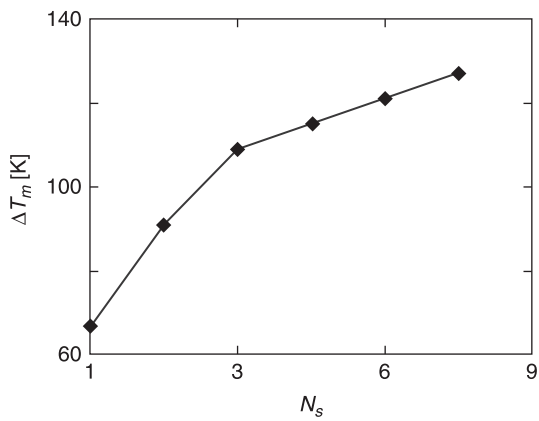

Source: After MARLOW (1998).

The total amount of heat dissipated at the hot side consists of the heat pumped from the cold side plus the electrical power supplied to the thermoelectric cooler. A heat sink is needed to transfer the heat dissipated at the hot side of the thermoelectric cooler to the environment.

To better explain the heat flow, the temperature distribution through a thermoelectric cooler is shown in Figure 15.4. The heat generated by the electronic component to be cooled is first conducted through an insulator (ceramic alumina), and then through a metal contact, which electrically connects the N and P type semiconductor materials. To allow this heat to

Figure 15.4 **Sketch of the temperature distribution, *T*, along a thermoelectric cooling element**

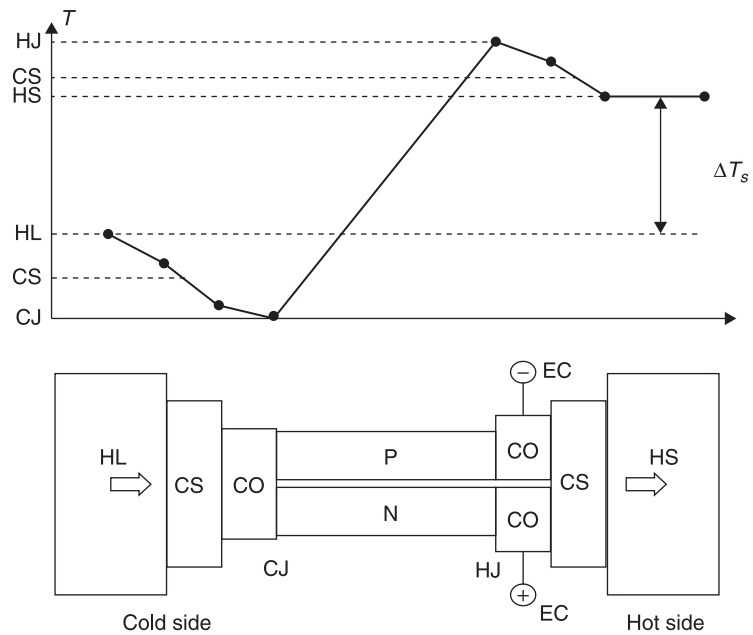

Key: ΔT_s, maximum temperature difference of the system; HL, heat load; CS, ceramic substrate; CO, copper plate; CJ, cold junction; HJ, hot junction; EC, electrical connection; HS, heat sink; N, P, type N and type P semiconductors, respectively.

be conducted from the component to the cold junction, the component has to be hotter than the junction. In fact, the coldest point in the thermoelectric cooling system is the cold junction itself. When the heat is pumped by the electrical current to the hot junction, it is conducted through another metal contact, through another insulator, and then transferred to the surroundings. Therefore, just as the coldest point is at the cold junction, the hottest point is at the hot junction.

The typical performance parameters of thermoelectric devices are I_m, the current which yields the greatest net cooling; ΔT_m, the temperature difference across the cooler at I_m with no applied heat load; $\dot{Q}_m$, the amount of applied heat load necessary to suppress the temperature difference across the device to zero at I_m; and V_m, the thermoelectric cooler voltage at I_m without heat load.

Another parameter of interest is the coefficient of performance (COP), which is defined as the ratio of the heat pumped from the cold to the hot junction, to the power that has to be supplied to operate the module. The coefficient of performance and the heat pumped increase as the temperature difference across it decreases. Typical values of the coefficient of performance of thermoelectric coolers are rather low, about 0.5.

Care should be taken with the mounting arrangements (e.g. clamping to the heat sink instead of soldering or gluing) to avoid stress concentrations that can damage the elements; and also, with the temperature control, using linear or pulse-width modulation instead of on/off controllers, which can cause thermal cycling.

15.2 Fundamentals

The heat flow across a thermoelectric device is the result of five effects (Seebeck, Peltier, Thomson, Joule and Fourier)

that act in combination (Chapter and Johnsen, 1973). While the Seebeck, Peltier, and Thomson effects are reversible thermodynamic phenomena, the Joule and Fourier effects are irreversible.

15.2.1 Seebeck effect

A voltage is created when the two junctions formed by dissimilar conductors or semiconductors are maintained at different temperatures ΔT, resulting in the flow of current. This thermoelectric power generation is the result of the Seebeck effect. The open circuit potential difference ΔV_S is:

$$\Delta V_S = a\Delta T, \tag{15.1}$$

where a is the Seebeck coefficient, measured in V/K in SI units.

15.2.2 Peltier effect

The heat absorbed at the cold junction $\dot{Q}_P$ (measured in W) is pumped to the hot junction at a rate proportional to the carrier current passing through the circuit, as follows:

$$\dot{Q}_P = aTI, \tag{15.2}$$

where T is the absolute temperature at the junction, a the Seebeck coefficient in eq. (15.1), and I is the electrical current. This thermoelectric heat pumping is the result of the phenomenon known as the Peltier effect.

15.2.3 Thomson effect

According to the Thomson effect, when an electrical current, I, flows in a homogeneous conductor, in the direction of the

temperature gradient, dT/dx, it generates a heating or cooling, q_T. The Thomson effect per unit of conductor length (measured in W/m) is given by the expression

$$q_T = \tau I \frac{\mathrm{d}T}{\mathrm{d}x}, \tag{15.3}$$

where τ is the Thomson coefficient (measured in V/K) and q_T is the heat flow per unit of conductor length due to the Thomson effect.

15.2.4 Joule effect

When an electrical current, I, flows along a conductor, a heat $\dot{Q}_J$ is generated within it, by virtue of the Joule effect, which is:

$$\dot{Q}_J = I^2 R, \tag{15.4}$$

where R is the electrical resistance.

15.2.5 Fourier effect

Following eq. (4.3), the conductive heat transfer (so-called Fourier effect) can be expressed as

$$\dot{Q}_F = -kA \frac{\mathrm{d}T}{\mathrm{d}x}, \tag{15.5}$$

where $\dot{Q}_F$ is the heat flow due to Fourier effect, k the thermal conductivity of the material, A the cross-section area, and dT/dx the temperature gradient.

15.3 Space applications

An inherently reliable design is required by planetary probes and space stations. Satellites and spacecraft for long-duration

Figure 15.5 **Active spacecraft thermal control using a thermoelectric device attached to a radiator**

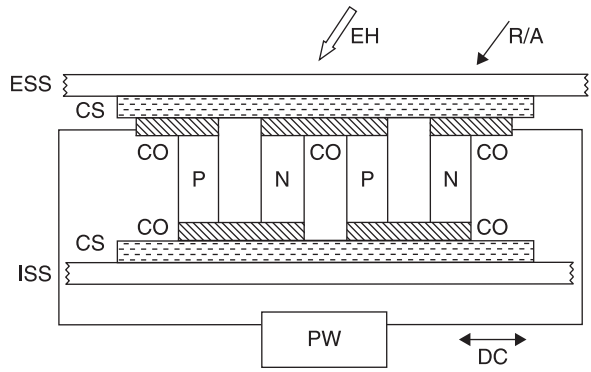

Key: ESS, external spacecraft skin; CS, ceramic substrate; CO, copper plate; ISS, internal spacecraft skin; DC, direct current; EH, environmental heat load; R/A, radiator/absorber; PW, power unit; N, P, type N and type P semiconductors, respectively.

Source: After Chapter and Johnsen (1973).

missions require active thermal control systems. These can be provided by thermoelectric heaters and Peltier effect coolers (Figure 15.5). Variable heat pumping capability between a surface and a spacecraft radiator/absorber can be provided by thermoelectric modules, thus controlling the temperature of critical sensors, such as the temperature controlled quartz crystal microbalances in the Midcourse Space Experiment mission (MSX) (Uy et al., 1999; Wood et al., 1999).

Some of the most common electro-optic applications of thermoelectric coolers in space are: space telescope cameras, thermal viewers, blackbody references, laser gyros for navigation, and cooling of electronic components such as high-resolution charge-coupled device cameras, infrared photo-detectors, high-speed integrated circuits, parametric amplifiers, cold cells and freezers, thermostats, thermocalibrators, step coolers and thermostabilizers.

These devices can also be used in cooling small volumes of air or liquid in a space environment. Such devices include: inertial guidance systems, small forced-air cooling systems, NASA life-science environmental chambers, etc.

A promising new field is being developed, thin film thermoelectric micro-Peltier modules (Kandasamy et al., 2004; NEXTREME, 2011).

As has been mentioned above in relation to active thermal control, the thermoelectric concept can also be used in the opposite sense, generating electrical power (thermoelectric generator devices, Buist and Lau, 1997), see Section 13.3.

15.4 References

Buist, R.J. and Lau, P.G. (1997) 'Calculation of thermoelectric power generation performance using finite element analysis', XVI International Conference on Thermoelectrics, Dresden, Germany, 26–29 August 1997.

Chapter, J.J. and Johnsen, G.W. (1973) Thermoelectric device application to spacecraft thermal control, *Journal of Spacecraft and Rockets*, **11**: 159–64.

Kandasamy, S., Kalantar-Zadeh, K., Rosengarten, G. and Wlodarski, W. (2004) 'Modelling of a thin film thermoelectric micro-Peltier module', IEEE TENCON 2004 Conference, E. Leelarasmee Ed., Chiang Mai, Thailand, 21–24 November 2004, 310–13.

MARLOW (1998) *Design Guide*, Marlow Industries, Inc., Dallas, Texas, USA.

MELCOR (2011) *Thermoelectric Handbook*, Laird Technologies, Trenton, New Jersey, USA.

NEXTREME (2011) *Nextreme Thermal Solutions*, Research Triangle Park, North Carolina, USA.

Scott, A.W. (1974) *Cooling of Electronic Equipment*, John Wiley and Sons, New York, Chap. 8, 215–27.

STCDD (1989) *Spacecraft Thermal Control Design Data Handbook*, ESA PSS-03-108, Issue 1.

TE TECHNOLOGY Inc. (2011) *Technical Information*, Traverse City, Michigan, USA.

Uy, O.M., Cain, R.P., Carkhuff, B.G., Cusick, R.T. and Wood, B.E. (1999) Miniature quartz crystal microbalance for spacecraft and missile applications, *Johns Hopkins APL Technical Digest*, **20**: 199–212.

Wood, B.E., Hall, D.F., Lesho, J.C., Dyer, J.S., Uy, O.M. et al. (1999) 'On orbit Midcourse Space Experiment (MSX) satellite environment flight experiments', Paper AIAA 99–0252, 37th AIAA Aerospace Sciences Meeting and Exhibit, Reno, Nevada, USA, 11–14 January 1999.

16

Cryogenic systems

Abstract: This chapter deals with cryogenic systems, which, from the point of view of spacecraft thermal control, are those concerned with operating temperatures below 100 K. Leaving aside radiators (Chapter 8) cryogenic systems can be classified as open cycle refrigerators (which use stored cryogens, either solid or liquid), and closed cycle refrigerators (including regenerative and recuperative systems).

Key words: stored cryogens, cryogenic recuperative systems, cryogenic regenerative systems.

16.1 Introduction

Systems that work under 100 K are called cryogenic systems. This temperature limit is typical of instruments devoted to Earth observation (infrared detectors), or gamma ray, high-energy or infrared astronomy.

Cryogenic systems for space applications have experienced a long period of development over the last few decades. The increasing reliability of cryogenic equipment, together with larger operational simplicity, has led to its successful use and operation in spacecraft. In parallel, the improvement in performance of cryogenic devices, such as detectors and sensor electronics working at low temperatures, has

dramatically increased their use in space missions, offering new perspectives for new space applications.

The evolution of the lifetime of several cryogenic systems employed in spacecraft is shown in Figure 16.1. The lifetime of these systems has improved steadily over the years.

In the near future, it is expected that cryogenic cooled systems will be used more frequently aiming to increase payload performances. This requires the evaluation of the impact of these devices in the global thermal balance of the spacecraft. To this end, the knowledge of how space cryogenic systems work and how they can be modelled is needed, even in a simplified way, to integrate it within the overall thermal model of the spacecraft and the onboard instruments.

Figure 16.1 **Variation of the lifetime, t_L, with time, t, of several spacecraft-borne systems: stored cryogenics (squares), Stirling and derivatives (circles and triangles), pulsating tubes (rhombi), and Brayton (black circle)**

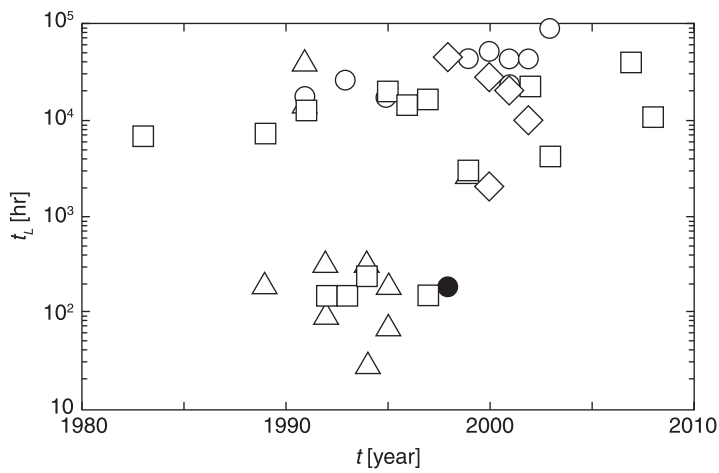

Source: Data from Collaudin and Rando (2000) and Donabedian (2003).

In this chapter, the most relevant basic aspects of space cryogenic systems are analysed, mainly those related to general spacecraft architecture and to several cryogenic cooling systems.

From a general point of view, the spacecraft can be considered as composed of a service module (or satellite bus) and a payload module. This payload module includes one or several instruments processing the signals received from a planet (in the case of a remote sensing satellite, communications from a meteorological satellite) or coming from space in the case of astronomy missions.

Leaving aside the cryogenic liquid fuel reservoirs of the launchers, whose working temperatures are not so low, the most critical cryogenic cooling requirements in spacecraft subsystems come from instruments carrying detectors that have to work at very low temperatures. The relative position of different types of detectors, in the temperature–wavelength (photon energy) plane, is shown in Table 16.1. A detailed review of non-military space missions carrying cryogenic instruments is reported in Collaudin and Rando (2000) and Donabedian (2003), together with a list of current and planned space applications for cryogenic instruments. An overview of the cryogenic systems either for Earth or for space applications already developed or under development in Europe can be found in Ravex and Trollier (2005).

The development process continues, and the availability of cryogenic systems for space use is constantly increasing, even if some of them are still under development. A comparative diagram of the applicability of the several cryogenic cooling systems is shown in Figure 16.2, outlining the region in the cooling power–temperature plane where these systems are placed.

Whatever the cryogenic cooling system employed, it has a relevant impact on the instrument or platform design. In this

Table 16.1 **Temperature range, $T_{min} \div T_{max}$, and dissipation range, $\dot{Q}_{min} \div \dot{Q}_{max}$, of photo-detectors employed in space missions**

Detector type	$T_{min} \div T_{max}$ [K]	$\dot{Q}_{min} \div \dot{Q}_{max}$ [W]	Wavelength
Germanium crystal	50 ÷ 100	0	Gamma
CCD	150 ÷ 300	0.1 ÷ 20	X-ray/Visible
Superconducting Tunnel Junctions (STJs)	0.01 ÷ 1	$10^{-9} \div 10^{-6}$	X-ray-UV-Visible-NIR
Micro-calorimeters	0.05 ÷ 0.3	$10^{-12} \div 10^{-11}$	X-ray
Transition Edge Detectors (TESs)	0.05 ÷ 0.3	$10^{-11} \div 10^{-9}$	X-ray-UV-Vis-NIR
Photo-conductors–Near infrared (NIR)	30 ÷ 100	0.01 ÷ 0.02	NIR
Photo-conductors–Medium infrared (MIR)	2 ÷ 20	0.01 ÷ 0.02	MIR
Photo-conductors–Far infrared (FIR)	1 ÷ 2	0.001 ÷ 0.03	FIR
Sub-millimetre bolometers	0.1 ÷ 0.3	$10^{-9} \div 10^{-8}$	Sub-mm
Superconducting Quantum Interference Devices (SQUIDs)	1 ÷ 4	$10^{-12} \div 10^{-11}$	Read-out / accelerometer

Source: After Linder et al. (2001).

regard, several factors have to be considered (Collaudin and Rando, 2000) when a cooling system (solid or liquid cryogenic material, radiator, mechanical cooler) is to be included in a given design:

- The coolers, of whatever kind, have to have a cooling capacity compatible with the spacecraft size and power availability on board.
- The equipment to work at low temperatures has to be maintained continuously at the required operational conditions, thermally insulated from the platform and protected from direct solar and albedo radiation. Obviously, the lower the operational temperature, the larger is the need for thermal insulation.
- The instrument cold parts (such as detectors, signal wires, temperature sensors, heaters, etc.) have to be accessible,

Figure 16.2 **Operational ranges of several cryogenic systems. Variation of the cooling power capacity, $\dot{Q}$, with temperature, T**

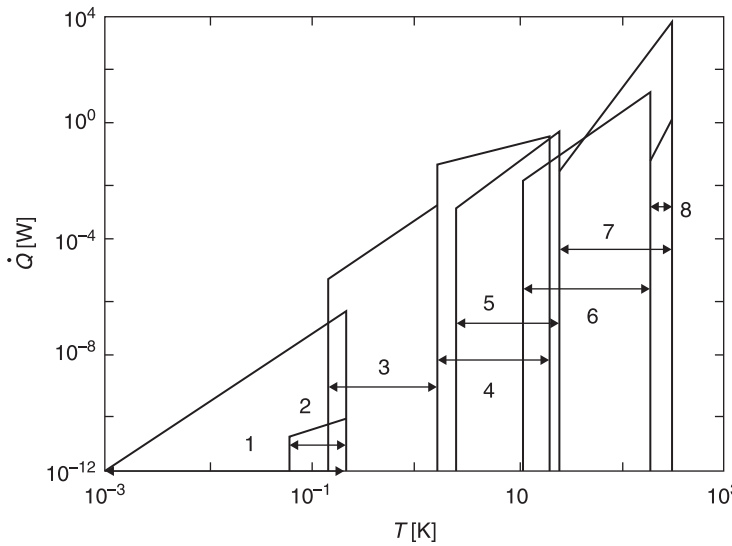

Key: 1 – dilution / adiabatic demagnetization refrigerators; 2 – solid-state coolers based on normal metal-insulator-superconductor; 3 – ^{4}He, ^{3}He sorption coolers; 4 – liquid He, solid H_2 cryogenic tanks; 5 – He, H_2 Joule-Thomson; 6 – Stirling, pulse tube; 7 – radiators; 8 – Peltier.

Source: After Collaudin and Rando (2000).

allowing space for the harness between the cooled payload and the platform (or satellite bus) and also for the signal processing before transmission to the Earth station via telemetry.

- Also included in the design is the cryogenic auxiliary equipment (heat links, thermal switches, filters, and thermometry) needed for cryogenic payload operations.
- The likely impact on the payload architecture of the provisions for testing of the instrument performances and payload cooling system also has to be considered.
- It is important to acknowledge that all the spacecraft parts have to survive the launch mechanical loads. This is an essential requirement with a large impact on the design of the cooling system and the associated instrumentation (e.g. a trade-off between the need for a robust support structure to withstand the launch load and the thermal insulation requirements has to be considered).
- The cooling system has to operate in a space environment, specifically in zero gravity conditions, over periods of several years.
- Materials compatible with both cryogenic and space environments should be employed in the payload design and manufacturing.
- The equipment lifetime (or main time between failures, MTBF) has to be compatible with (and even longer than) the mission lifetime.

Generally speaking, a cooling system provides a heat sink, evacuating this heat from the cool side of the equipment, towards a hot part where heat is dissipated. In the case of a spacecraft, isolated in space, the evacuated energy is radiated to space. Only some basic thermodynamic knowledge is

Table 16.2 **Cooling systems**

Radiators		
Open cycle	Solid cryogens	
	Liquid cryogens	
Closed cycle	Regenerative systems	Stirling
		Pulse tube
		Gifford
	Recuperative systems	Joule-Thomson
		Brayton

needed to describe this cooling process: either the energy is directly radiated to space, or some work is needed to pump energy from a low temperature level to a high temperature level, in order to radiate this energy more easily to space.

In this second case, the heat pumping process can be performed following either a closed loop cycle or an open loop cycle (Table 16.2). Obviously, the final energy transference to space has to be performed using a radiator.

An open cycle involves the use of stored cryogenic materials, liquid or solids. In this case, the work needed is performed on Earth, before the mission, in the liquefaction process (or solidification, as appropriate) of the working fluid. The cold heat sink is generated by the evaporation of cryogenic solids or liquids. In the open cycle system there is no heat radiation, although the gas generated by evaporation has to be evacuated. Thus, the system lifetime is driven by the heat leakages and the cryogenic material stored on board.

In closed cycle systems, mechanical coolers are employed, where work is continuously performed during operations. A closed cycle system typical block diagram is shown in Figure 16.3.

Figure 16.3 Space cooler block diagram

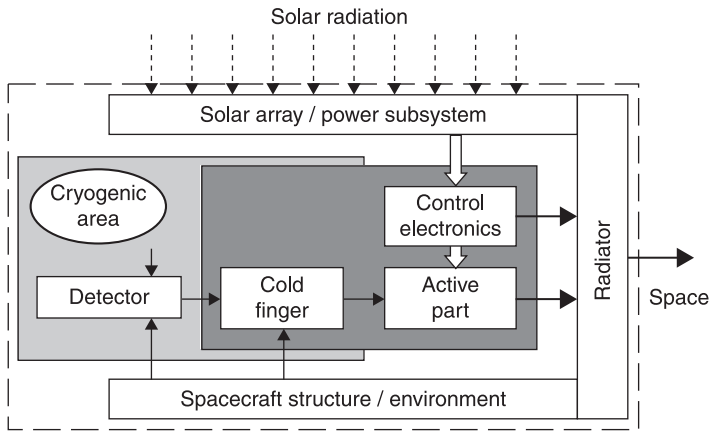

Note: The cold end of the cooler is connected to the detector, whilst the active side and the control elements are connected to the spacecraft structure, and to the radiator.

Source: After Collaudin and Rando (2000) and Linder et al. (2001).

These systems can provide approximately 1 W cooling power in the 50 K to 100 K temperature range (using Stirling or pulse tubes), about 100 mW in the range 15 K to 20 K (two-stage Stirling), and about 1 mW at 4 K (Joule-Thomson). Very low temperature coolers, such as ^3H_e cryo-sorption refrigerators, adiabatic demagnetization refrigerators (ADRs), can achieve even lower temperatures (1 K, 1 mK) if used together with one of the above-mentioned coolers as pre-refrigerators.

Independently of the cooling system employed, some electronics are always required to monitor and control the temperature, to keep it constant, and to drive the internal mechanisms. If the final temperature required is relatively high (higher than 50 K), one cooling stage should be enough. Below this limit, multi-stage coolers or a chain of coolers are required.

16.2 Refrigerating systems

In this section the main features of radiant coolers, open cycle refrigerating systems and closed cycle refrigerating systems are briefly described.

16.2.1 Radiant coolers

Radiant coolers are at present the most widely used systems for cooling at cryogenic temperatures aboard spacecraft. These devices are the most efficient, simplest and most reliable space coolers, and they offer a relatively simple, passive, low-mass technique for cooling space-borne sensors. They present, however, severe limitations with respect to the temperature and the cooling load (see Figure 16.2), as well as on the placement on the spacecraft, and the spacecraft orbit.

They are based (Chapter 5) on the fact that all objects emit infrared radiation proportionally to their area A, emissivity ε, and to the fourth power of their temperature T, and on the fact that the environment temperature (deep space) is very cold (blackbody at $T_0 = 2.73\,\mathrm{K}$). The net cooling power is thus $\dot{Q}_{\mathrm{rad}}, = A\varepsilon\sigma\,(T^4 - T_0^4) \cong A\varepsilon\sigma T^4$, where σ is the Stefan-Boltzmann constant. Radiators are efficient above 100 K, but have limited performance at lower temperatures (where the parasitic loads through the insulation increase) and have limitations related to their size (it is usually difficult to get more than a few square meters on a spacecraft). Additional details on radiant coolers can be found in Chapter 8.

16.2.2 Open cycle refrigerating systems

As already stated, the open cycle corresponds to the use of stored cryogens. These cryogenic systems are passive and not

limited by orbit, spacecraft orientation, or locations within the spacecraft. Cooling is performed in these systems through the sublimation of a solid, or the boiling of a liquid. For 10 K to 90 K detector instrument cooling in space, stored solid cryogen systems offer some advantages over stored liquid systems. Cryogens for this temperature range have enthalpies of sublimation of about 10% to 15% higher than their enthalpies of vaporization. Another difference to be pointed out between solid and liquid cryogens is that for a given volume, the cooling capacity of the stored solid cryogen is larger than that of the stored liquid cryogen, since the solid cryogen densities are 10% to 15% higher than liquid cryogen densities.

In summary, a stored cryogen cooler consists of a cryogen tank, a vacuum vessel (which isolates the cryogen tank before and during launch), filling and venting lines, heat shields and multilayer insulations, plus some interface or volume for instrument accommodation. In the case of liquid-stored cryogens, under microgravity conditions the seepage of the liquid cryogen into the venting tube of the cryogen reservoir (Dewar) must be avoided by all means, otherwise a waste of cryogen will result. Therefore, the fluid needs to be maintained inside the tank by a phase separator (based on capillary forces or fountain effect for superfluid helium), allowing the venting of the vapours through the phase separator while retaining the liquid cryogen.

The usual architecture for ground Dewars consists of an inner cryogen tank which is attached to an external vessel through a neck, which is normally used as a filling and venting line. Dewars for space applications are not compatible with this architecture, due to the dynamic loads present during the launch. In space, a separate venting line is employed to use efficiently the gas enthalpy to cool the shields, as explained below, and to release the gas without applying momentum to the spacecraft (two jets symmetrically

opposed around the centre of gravity). Note that in a spacecraft it is also possible to cool the whole vacuum vessel by radiation to space.

The amount of cryogen required to perform a given mission, and thus the mass of the system, depends not only on the detector cooling load and on the lifetime, but also on the parasitic heat leaks. Therefore, extremely efficient thermal insulations have to be devised to keep these heat leaks to a minimum.

The vapour-cooled-shields Dewars are used both to store cryogens for detector cooling and for long-term storage of cryogenic propellants in space. The main differences between these applications are the temperature level and the geometric scale.

The basic idea of these Dewars consists of using the coldness of the evaporating cryogen to cool the insulation. This is achieved by means of a number of highly conductive metallic shields placed within the insulation – perpendicular to the temperature gradient – and set in contact with the venting ducts conducting the boil-off vapours. The highly conductive shields are placed between the layers of a multilayer insulation extending along the entire container (Figure 16.4).

The advantage of the vapour-cooled-shields system can be understood from Figure 16.5, which represents that part of the insulation close to a venting duct (in this plot it is assumed that the venting tube is normal to the cooled shields, although the vapour-venting duct, in the shape of a cooling coil, can be tangentially soldered or cemented to the metallic foil). The relative amount and the direction of the heat transfer to or from the system is indicated by means of arrows of varying lengths.

According to this sketch, the heat to the outer shield is equal to the heat transferred to the vented gas through the

Figure 16.4 **Sketch of the Infrared Space Observatory (ISO) telescope and cryostat, showing the location of important elements within, and attached to, the cryostat**

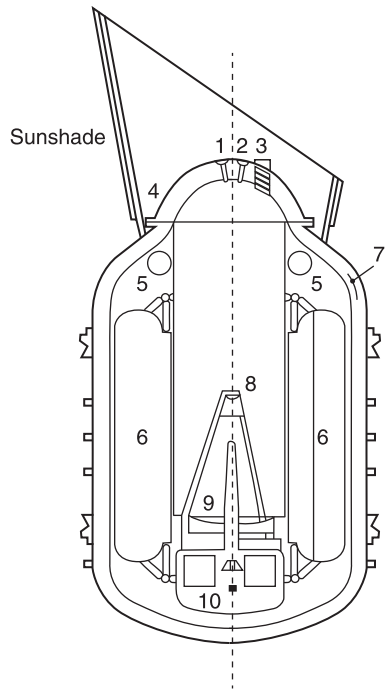

Key: 1 – helium flush outlet; 2 – helium flush inlet; 3 – optical windows and filters; 4 – cryo-cover (released after launch): 5 – ^{3}He tank; 6 – ^{4}He tank; 7 – vapour-cooled shields; 8 – secondary mirror; 9 – primary mirror; 10 – scientific instruments and telescope hardware.

Source: After Kessler et al. (2003).

shield plus the heat which continues through the insulation. This mechanism is repeated at each conductive shield, reducing the heat which would be transferred through a conventional multilayer insulation system.

Since vapours are vented to the vacuum of space, the proper design of the exhaust nozzle allows the regulation of the base temperature (vapour pressure) of the cryogen bath by adjusting

Figure 16.5 **Sketch of a typical vapour-cooled-shields Dewar and of the heat transfer mechanism through a normal attachment vapour-cooled-shields Dewar**

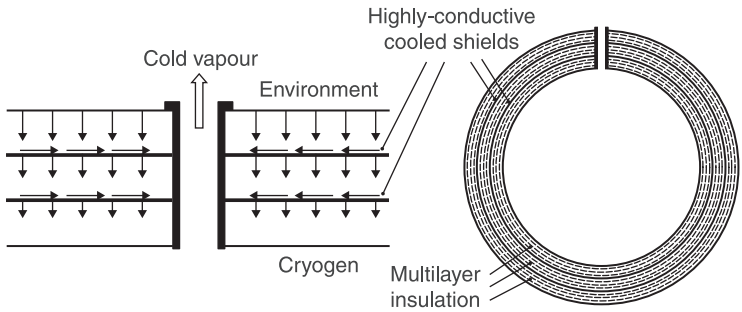

the pressure drop. The volume of cryogen to be carried depends on the mission duration and on the heat input. The choice of the cryogen to be used depends on the base temperature required. The cryogens available do not provide a continuum of temperatures, but rather discrete values in different ranges, as indicated in Table 16.3. The most widely used are superfluid or supercritical helium, solid H_2 and solid Ne. The thermodynamic and transport properties of various cryogens are also indicated in Table 16.3, and an overview of the choices made on different missions is presented in Table 16.4.

Many space-borne applications require cooling in the 1.8 K to 4.2 K temperature range, and in such cases, superfluid liquid helium ^{4}He is well suited to this purpose. Superfluid liquid helium is attractive for space applications because this cryogen has two outstanding properties: the first is its very low density (about 145 kg/m^3 at λ point), and the second, its superfluidity. That means that in the range $T < 2.17$ K ($p <$ 5038 Pa) helium behaves as if it were a mixture of two different liquids. One of these is a superfluid, which is characterized by a given density, zero entropy and zero viscosity. The other is a normal viscous fluid, which is characterized by a different density. No friction occurs

Table 16.3 Properties of several normal cryogens

Cryogen		^{3}He Helium	^{4}He Helium	H_2 Hydrogen	Ne Neon	N_2 Nitrogen	Ar Argon	O_2 Oxygen	CH_4 Methane	CO_2 C. diox
Minimum solid temperature[A]	[K]	–	–	8.3	13.5	43.4	47.8	48.1	59.8	125.0
Boiling temp.[B]	[K]	3.191	4.224	20.38	27.09	77.35	87.29	90.18	111.42	216.55
Melting temp.	[K]	–	–	13.95	24.50	63.15	83.78	54.35	90.66	194.65
Critical point	T [K]	3.324	5.201	33.34	44.40	126.25	150.86	154.77	190.55	304.19
	$p \times 10^{-5}$ [Pa]	1.165	2.275	13.16	26.54	33.96	50.00	50.90	46.41	73.82
	ρ [kg/m^3]	41.3	69.64	31.6	483	304	536	405	162	468
Triple point	T [K]	–	–	13.95	24.57	63.15	83.78	54.35	88.70	216.55
	$p \times 10^{-3}$ [Pa]	–	–	7.20	43.13	12.53	68.75	0.15	10.03	518.00
Gas density[C]	ρ [kg/m^3]	0.1208	0.1624	0.0808	0.81	1.12	1.6	1.28	0.64	1.77

[A] At 13.3 Pa (from Donabedian, 2003).
[B] At 1.013×10^5 Pa.
[C] At 10^5 Pa and 300 K.

Source: Unless otherwise stated, data in this table are from STCDD (1989).

Table 16.4 Characteristics of several cryostats

Launch year	Mission	Type/class[A]	Cryogen[B]	Temp [K]	Lifetime[C] [days]	Volume [dm^3]	Reference
1983	IRAS (NASA, NIVR, SERC)	Satellite	^{4}He	1.8	302	499	Holmes et al. (2002)
1989	COBE (NASA)	Satellite	^{4}He	1.53	306	616	Holmes et al. (2002)
1991	CLAES (NASA)	P/L (STS)	sCO_2+sNe	16	607	302	Holmes et al. (2002)
1992	USMP/LPE (NASA)	P/L (STS-52)	^{4}He	2.2	6		Collaudin and Rando (2000)
1993	SHOOT (NASA)	P/L (STS-57)	^{4}He	1.5	67	180	Holmes et al. (2002)
1994–1997	CRISTA (DARA)	P/L (STS-66/85)	^{4}He	4	10		Collaudin and Rando (2000)
1995	ISO (ESA)	Satellite	^{4}He	1.73	840	2100	Steinz (1997), Kessler et al. (2003)
1995	IRTS (ISAS/NASDA/USEF)	SFU	^{4}He	1.9	35	90	Fujii et al. (1996)
1995	FIRP-IRTS (U. Berkeley/ISAS)	SFU	^{3}He	0.3	10	16.4	Freund et al. (1998)
1996	MSX (BMDO,US)	Satellite	sH_2	10.5	540	410 kg	Donabedian (2003)
1996–1999	XQC (NASA)	Sounding rocket	^{4}He+ADR	1.8	1	4	Porter et al. (2000)

(*Continued*)

Table 16.4 Characteristics of several cryostats (*Continued*)

Launch year	Mission	Type/class[A]	Cryogen[B]	Temp [K]	Lifetime[C] [days]	Volume [dm^3]	Reference
1997	NICMOS (NASA)	Hubble Space T.	sN_2	58	660	110 kg	Schneider (2004)
1997	CHeX (NASA)	P/L (STS-87)	^4He	1.8	12	85	Larson et al. (1999), Holmes et al. (2002)
1999	WIRE (NASA)	Satellite	Dual, sH_2	6.7, 12	120	60 kg	Donabedian (2003)
2000	Gravity Probe-B (GP-B).	Satellite	^4He	1.8	510	2427	Parmley et al.(2003)
2003	Spitzer (NASA)	Satellite	^4He	1.2–1.4	1965	363	Volz et al. (1999)
2003	LTMPF (NASA)	P/L (ISS)	^4He	1.5	38	85	Holmes et al. (2002)
2003	FACET (NASA)	P/L (STS)	$sNe+^4He$	1.9	16	9.5/15	Nash et al. (1999)
2005	Astro-E2 (ISAS/ JAXA, NASA)	Satellite	$sNe+^4He$ +ADR	0.065	730	170/33.4	Shirron et al. (2006)
2006	AKARI (JAXA)	Satellite	^4He+Stirling	1.7	354	170	Shibai (2002), Hirabayashi et al. (2008)
2009	Herschel (ESA)	Satellite	$^4He+^3He$ SC	1.8	1260	2360	Reix et al. (2010)

[A] Acronyms in this column: P/L, payload; STS, Space Transportation System; SFU, Japanese Space Flyer Unit; ISS, International Space Station
[B] "s" stands for solid phase; ADR, Adiabatic Demagnetization Refrigerator; SC, Sorption Cooler
[C] In some cases mass instead of volume is given

between these two parts of the liquid in their relative motion, at least when velocities are small.

Figure 16.6 shows the x-T phase diagram of the ^{3}He–^{4}He mixture at saturated vapour pressure, where x stands for the concentration of the ^{3}He isotope, $x = n_3/(n_3+n_4)$, where n_i represents the number of atoms or moles of each one of the isotopes, and T stands for the temperature. Some important characteristics of this mixture are to be noted. In the dilution of ^{4}He with ^{3}He, the temperature of the superfluid phase transition of the former is lowered and the transition disappears for a concentration of ^{3}He above 67.5%. At such a concentration, and at a temperature of 0.867 K (tricritical point), the λ-line mets the phase separation line. Below this temperature, the two isotopes form a mixture only for certain concentrations, which depend on the temperature, whereas two separated phases are formed along the phase separation line. The grey region in Figure 16.6 is a non-accessible range

Figure 16.6 **Phase diagram for a mixture of ^{3}He–^{4}He at the saturated vapour pressure: temperature, *T*, versus concentration of ^{3}He isotope, *x***

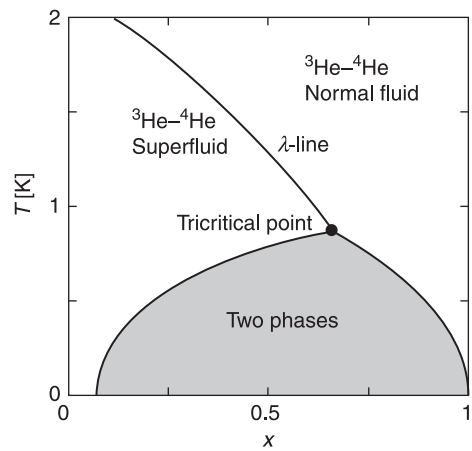

Source: After Ventura and Risegari (2008).

of temperatures and concentrations for helium mixtures (an extensive description of helium properties as well as its use in cryogenic applications can be found in Ventura and Risegari, 2008).

Thanks to superfluidity, helium forms a film that completely covers the walls of the container and guarantees a homogeneous cooling even if most of the liquid does not have a fixed position inside the container (as happens under no gravity conditions). The superfluidity of liquid helium also solves the problem of phase separation in the absence of gravity.

On Earth, gravity keeps the liquid at the bottom of the container, and evaporation takes place at the liquid/vapour interface. Helium vapours flow towards the surroundings or are pumped if temperatures lower than 4.2 K are to be obtained. The situation is rather different in space, where, because of superfluidity, a simple connection to the space vacuum would immediately empty the container. Therefore, the seepage of the liquid cryogen into the venting tube of the Dewar has to be avoided by all means. Otherwise, a waste of cryogen will result. Fortunately, there is a peculiar effect in superfluid helium, the thermo-mechanical effect. In the superfluid state, the ^{4}He viscosity is very low: this property allows the liquid to pass through microscopic holes (superleaks), whereas the gas (viscous) cannot.

The device which allows such a separation is known as a porous plug. It consists of a slab of porous material which separates the container from outer space. This is made of sintered alumina or sintered stainless steel (Parmley et al., 2003; Yu et al., 2005; Ishikawa et al., 2010). The diameter of the pores is quite critical (usually a few microns) and only the superfluid helium is able to pass through the pores. It should be noted that the external surface of the porous plug is colder because of the liquid evaporation and the porous plug is therefore a passive component.

The operating temperature range of a solid cryogen is limited at its maximum by the triple point, and at its minimum by the requirement that the pressure around the sublimating solid be great enough to overcome the pressure losses in the venting tube, allowing the venting of vapours resulting from solid sublimation (Table 16.3). Although the mentioned pressure losses obviously depend on the geometrical configuration of the venting plumbing, the outer pressure, and the mass flow rate, a value in the order of 15 Pa for the pressure losses is appropriate in most cases. For low-temperature systems, in order to optimize the mass of cryogen, use of a bi-cryogen system, such as N_2 and He, or H_2 and He, can be of interest. However, the design is more complex, as all lines and valves have to be doubled. In this configuration the primary cryogen maintains the desired sensor temperature, while the secondary cryogen, which has a substantially higher heat of sublimation than the primary cryogen, intercepts heat from the outer shell and provides a low-temperature environment around the primary stage. A simplified sketch of a dual stage solid cryogen cooler is shown in Figure 16.7.

16.2.3 Closed cycle refrigerating systems

In mechanical coolers, also known as active coolers, refrigerating power is obtained through the mechanical work supplied by the moving parts of the appropriate device. There are several ways to classify these coolers, the most common being to distinguish between regenerative cycles (Stirling, pulse tube, Gifford coolers) and recuperative cycles (Joule-Thomson or Brayton coolers).

Regenerative coolers consist of a compressor (usually mechanical) which generates a pressure wave, and a cold finger, using a mobile (Stirling, Gifford) or a fixed (pulse

Figure 16.7 Sketch of a dual stage solid cryogen cooler

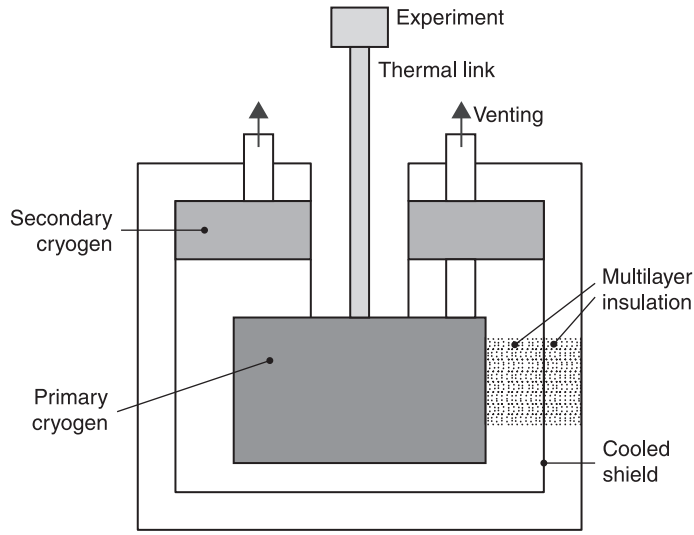

Source: After STCDD (1989).

tube) regenerator. The heat is extracted at the cold end when the gas expands, and rejected at the warm end when the gas is compressed.

Recuperative cycles are based on the enthalpy difference between high- and low-pressure gas. The gas expansion can be produced by using a turbine (Brayton cooler) or expanding it through an orifice to get the desired cooling effect. Because of irreversible effects, Joule-Thomson coolers are less efficient than Brayton coolers, although they are simpler.

A practical Joule-Thomson refrigerator cycle is shown in Figure 16.8, where in a typical application, the working fluid undergoes the following transformations: at the beginning of the cycle the fluid is compressed in a compressor (A to B); once compressed, the gas is cooled and then it passes through a filter in order to remove trace contaminants, which might solidify at cryogenic temperatures (B to C).

Figure 16.8 **Sketches of the Joule-Thomson closed cycle refrigerator and the ideal temperature–entropy (*T*-*s*) diagram**

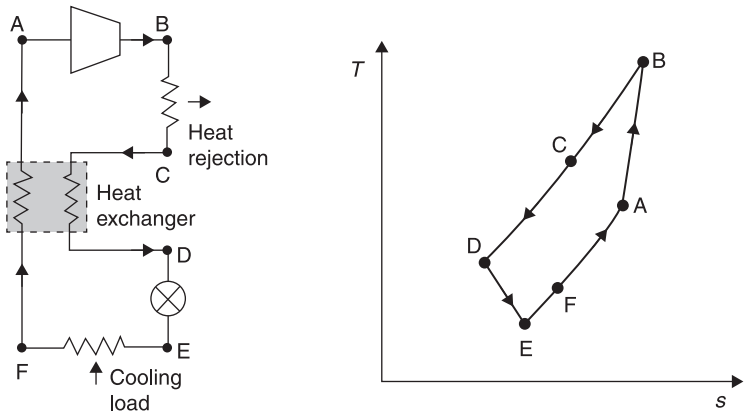

Source: After STCDD (1989).

From C to D the purified high-pressure fluid enters a regenerative heat exchanger where it is cooled by the returning low-pressure gas, and then the high-pressure gas is expanded at the exit of the heat exchanger. This produces a temperature drop which is sufficient to partially liquefy the gas (D to E) and the latent heat of the liquefied fluid is used to provide the main cooling (E to F). Finally, the resulting low-pressure gas, after being used for precooling the incoming gas, returns to the first stage of the compressor to begin a new cycle (F to A).

The major advantage of Joule-Thomson closed cycle coolers is that the compressor module can be located far from the heat sink, and therefore the entire cooling system can be packaged into varied configurations. The primary disadvantage of the Joule-Thomson closed cycle system, from the standpoint of space application, is its relative high power requirements. Another disadvantage is that heat rejection is produced isothermally only at the liquid

temperature of the refrigerant being used, which limits the flexibility of application.

The Stirling system possesses several of the primary requirements of a space-borne refrigerator system, such as low power consumption and small size and mass. Heat evolution takes place in the Stirling cycle by alternately compressing and expanding a given quantity of a gas in a closed cycle. Compression takes place at ambient temperature so as to facilitate heat rejection; the expansion is performed at the required cold temperature.

For the sake of explanation, the Stirling cycle may be split up into four stages, as indicated in Figure 16.9, where the ideal cycle diagram is also sketched.

Figure 16.9 **Sketches of the Stirling cycle refrigerator operation and the ideal temperature–entropy (*T*-*s*) diagram**

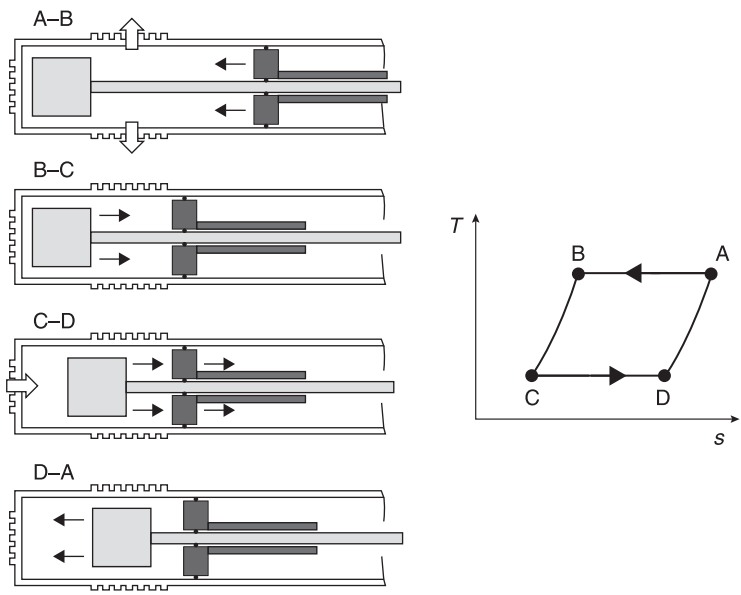

Source: After STCDD (1989).

In position A most of the working gas occupies the so-called ambient end, at ambient temperature. From A to B an isothermal compression is performed: the gas is compressed by inward motion of the compressor piston (this compression takes place at room temperature, the heat being rejected through the ambient heat exchanger).

B to C is the constant volume cooling. The gas is transferred, through the regenerator, from the ambient to the cold end, at constant overall volume, by means of the displacer which usually encloses the regenerator. The gas flowing through the regenerator is cooled to close to the temperature at the cold end. Heat transferred to the regenerator will be rejected in stage D to A.

Isothermal cooling occurs from C to D. The gas is expanded by moving simultaneously both the displacer and the compressor piston. The sensor, or whatever device, is cooled by means of the cooling load heat exchanger.

As already said, constant volume heating occurs from D to A. The gas is displaced from the cold to the ambient end by the displacer. During this transfer, the flowing gas lowers the temperature of the regenerator.

Nowadays, most spacecraft cooling systems are based on Stirling cycles or Joule-Thompson expansion. However, pulse tube refrigerators (PTR) are also considered as an interesting alternative, as this system has no moving parts, which dramatically reduces the vibration level (Tanchon et al., 2010). Some cooling systems, employed in a wide range of space missions, are summarized in Table 16.5.

Another system worth mentioning is the closed cycle hydrogen sorption cooler, which is a vibration-free alternative when a 20 K to 50 K temperature range is needed. Sorption cooling employs a closed cycle Joule-Thomson expansion process to achieve the cooling effect. Sorption cells perform the compression phase in this cycle. At a low temperature

Table 16.5 Cryogenic close cycle space coolers

Launch year	Mission	Type	Cooler	Temperature [K]	Lifetime [years]	Reference
1991	ERS-1 (ESA)	Payload (ATSR)	Stirling	80	2	Collaudin and Rando (2000)
1993–1999	HTSSE I–II (NRL/ USAF)	Payload (ARGOS)	Stirling	70–80	3	Collaudin and Rando (2000)
1995	ERS-2 (ESA)	Payload (ATSR)	Stirling	80	2	Collaudin and Rando (2000)
1999	Terra (NASA)	P/L (MODIS)	Stirling	80	5	Collaudin and Rando (2000)
2001	ENVISAT 1 (ESA)	Payload (MIPAS)	Stirling	80	5	Collaudin and Rando (2000)
2001	ENVISAT 1 (ESA)	Payload (AATSR)	Stirling	80	5	Collaudin and Rando (2000)
2002	INTEGRAL (ESA)	Satellite	Stirling	90	5	Collaudin and Rando (2000)
2002	RHESSI (NASA)	Satellite	Stirling	80	3	Boyle (2004)
2003	Rosetta (ESA)	Probe	Stirling	80	10	Collaudin and Rando (2000)
2009	Herschel (ESA)	Satellite	^{3}He Sorption			Duband et al. (2008)
2009	Plank (ESA)	Satellite	H_2 Sorption	20	2	Bhandari et al. (2004) Borders et al. (2004)
2011	Darwin (ESA)	Satellite	H_2 Sorption He Sorption	14.5 4.5		Doornink et al. (2008) Doornink et al. (2008)

Table 16.5 Cryogenic close cycle space coolers (*Continued*)

Launch year	Mission	Type	Cooler	Temperature [K]	Lifetime [years]	Reference
2013	SXS/Astro-H (JAXA)	Satellite	Stirling, double staged	20	3	Sato et al. (2010)
			^{3}He Joule-Thomson	4	3	Sato et al. (2010)
2018	SPICA (JAXA/ESA)	satellite	Stirling, double staged	20	3	Sugita et al. (2010)
			^{3}He Joule-Thomson	4	3	Sugita et al. (2010)

and pressure, these cells adsorb the working fluid. At a higher temperature, they desorb the fluid and thus produce a high-pressure flow to the expander in the cold stage (Doornink et al., 2008).

Requirements become much stricter when extremely low temperatures (less than 1 K) are needed, as in the case of scientific application satellites. In these cases, closed cycle ^{3}He sorption coolers are employed to achieve temperatures close to 250 mK, and dilution coolers and adiabatic demagnetization coolers to reach 50 mK temperature (Emes et al., 2002).

A detailed description of the different refrigerating systems used in space applications is beyond the scope of this book, so the reader is referred to specific books and papers where such information can be found. A basic and main reference concerning spacecraft cryogenic systems is Donabedian (2003), where the different systems are described in detail. Most of these refrigerating systems are also dealt with in Fereday et al. (2006), where mathematical models of several cooling systems are presented; and a description of some available systems can be found in Ross and Boyle (2006), Reed et al. (2008) as well as in Raab and Tward (2010). Other relevant references related to specific cryogenic systems are listed in Tables 16.4 and 16.5.

16.3 References

Bhandari, P., Prina, M., Bowman Jr., R.C., Paine, C., Pearson, D. and Nash, A. (2004) Sorption coolers using a continuous cycle to produce 20 K for the Planck flight mission, *Cryogenics*, **44**: 395–401.

Borders, J., Morgante, G., Prina, M., Pearson, D. and Bhandari, P. (2004) Optimized autonomous operations of

a 20 K space hydrogen sorption cryocooler, *Cryogenics*, **44**: 565–73.

Boyle, R. (2004) On-orbit performance of the RHESSI cryocooler, *Cryogenics*, **44**: 389–93.

Collaudin, B. and Rando, N. (2000) Cryogenics in space: a review of the missions and of the technologies, *Cryogenics*, **40**: 797–819.

Donabedian, M., Ed. (2003) *Spacecraft Thermal Control Handbook, Vol. II, Cryogenics*, The Aerospace Press, El Segundo, California, USA.

Doornink, D.J., Burger, J.F. and ter Brake, H.J.M. (2008) Sorption cooling: A valid extension to passive cooling, *Cryogenics*, **48**: 274–9.

Duband, L., Clerc, L., Ercolani, E., Guillemet, L. and Vallcorba, R. (2008) Herschel flight models sorption coolers, *Cryogenics*, **48**: 95–105.

Emes, M.R., Hepburn, I.D., Ray, R.J. and Worth, L.B.C. (2002) Structural analysis of a cryogen-free refrigerator for space, *Cryogenics*, **41**: 771–9.

Fereday, J., Bradshaw, T., Crook, M., Orlowska, A., Bhatia, R. et al. (2006) Cryocooler modelling methodology, *Cryogenics*, **46**: 183–90.

Freund, M.M., Duband, L., Lange, A.E., Matsumoto, T., Murakami, H. et al. (1998) Design and flight performance of a space borne ^{3}He refrigerator for the infrared telescope in space, *Cryogenics*, **38**: 435–43.

Fujii, G., Tomoya, S., Kyoya, M., Hirabayashi, M., Murakami, M. et al. (1996) On-orbit thermal behaviour of the IRTS cryogenic system, *Cryogenics*, **36**: 731–9.

Hirabayashi, M., Narasaki, K., Tsunematsu, S., Kimura, Y., Yoshida, S. et al. (2008) Thermal design and its on-orbit performance of the AKARI cryostat, *Cryogenics*, **48**: 189–97.

Holmes, W., Cho, H., Hahn, I., Larson, M., Schweickart, R. and Volz, S. (2002) Performance comparisons of space borne cryostats, *Cryogenics*, **41**: 865–70.

Ishikawa, K., Ezoe, Y., Yamaguchi, H., Mitsuishi, I., Yoshitake, H. et al. (2010) Porous plug and superfluid helium film flow suppressor for the soft X-ray spectrometer onboard Astro-H, *Cryogenics*, **50**: 507–11.

Kessler, M.F., Müller, T.G., Leech, K., Arviset, C., García-Lario, P. et al. (2003) *The ISO Handbook, Volume I: ISO – Mission and Satellite Overview*, SAI-2000-035/Dc, Version 2.0, ESA, November 2003.

Larson, M., Pearson, D., Elliott, S., Petrac, D., Israelsson, U. and Luchik, T. (1999) The confined helium experiment (CHeX). The successful return of the low temperature platform facility (LTPF) to space, *Cryogenics*, **39**: 671–5.

Linder, M., Rando, N., Peacock, A. and Collaudin, B. (2001) Cryogenics in Space – a review of the missions and technologies, *ESA Bulletin*, **107**: 92–105.

Nash, A.E., Shields, P., Jirmanus, M. and Zhao, Z. (1999) Development of the FACET cryostat, *Advanced Cryogenics Engineering*, **45**: 1004–10.

Parmley, R.T., Bell, G.A., Frank, D.J., Murray, D.O. and Whelan, R.A. (2003) Performance of the Relativity mission superfluid helium flight dewar, *Advances in Space Research*, **32**: 1407–16.

Porter, F.S., Almy, R., Apodaca, E., Figueroa-Feliciano, E., Galeazzi, M. et al. (2000) The XQC microcalorimeter sounding rocket: a stable LTD platform 30 seconds after rocket motor burnout, *Nuclear Instruments and Methods in Physics Research*, **A 444**: 220–3.

Raab, J. and Tward, E. (2010) Northrop Grumman Aerospace Systems cryocooler overview, *Cryogenics*, **50**: 572–81.

Ravex, A. and Trollier, T. (2005) 'Recent developments on cryocoolers in Europe', 20th International Cryogenic Engineering Conference (ICEC 20), Beijing, China 127–36.

Reed, J., Perkinson, M.C., D'Arrigo, P., Geelen, K., Hepburn, I. et al. (2008) 300 mK and 50 mK cooling systems for long-life space applications, *Cryogenics*, **48**: 181–8.

Reix, J.M., Passvagel, T., Crone, G., Collaudin, B., Rideau, P. et al. (2010) The Herschel/Planck programme technical challenges for two science missions, successfully launched, *Acta Astronautica*, **66**: 130–48.

Ross Jr., R.G. and Boyle, R.F. (2006) 'An overview of NASA Space Cryocooler Programs – 2006', International Cryocooler Conference, Annapolis, Maryland, U.S.A., 14–16 June 2006.

Sato, Y., Sugita, H., Mitsuda, K., Nakagawa, T., Fujimoto, R. et al. (2010) Development of mechanical cryocoolers for Astro-H/SXS, *Cryogenics*, **50**: 500–6.

Schneider, G. (2004) Highlights from HST/NICMOS, *Advances in Space Research*, **34**: 543–52.

Shibai, H. (2002) ASTRO-F: the Infrared Imaging Surveyor (IRIS) mission, *Advances in Space Research*, **30**: 2089–97.

Shirron, P.J., DiPirro, M.J., Panek, J., Kelley, R., Mitsuda, K. et al. (2006) The Astro-E2/XRS-2 helium insert system, *Nuclear Instruments and Methods in Physics Research*, **A 559**: 666–8.

STCDD (1989) *Spacecraft Thermal Control Design Data Handbook*, ESA PSS-03-108, Issue 1.

Steinz, J.A. (1997) ESA's Infrared Space Observatory (ISO): the development programme, *Acta Astronautica*, **40**: 467–76.

Sugita, H., Sato, Y., Nakagawa, T., Yamawaki, T., Murakami, H. et al. (2010) Cryogenic system design of the next generation infrared space telescope SPICA, *Cryogenics*, **50**: 566–71.

Tanchon, J., Trollier, T., Triqueneaux, S. and Ravex, A. (2010) 20–50 K and 40–80 K pulse tube coolers: two candidates for a low temperature cooling chain, *Cryogenics*, **50**: 55–60.

Ventura, G. and Risegari, L. (2008) *The Art of Cryogenics, Low-Temperature Experimental Techniques*, Elsevier, Oxford, UK.

Volz, S., Schweickart, R., Gause, K. and Pederson, R. (1999) SIRTF cryostat requirements and development, *Cryogenics*, **39**: 975–83.

Yu, X., Li, Q., Li, Z. and Li Qiang (2005) 'Experimental investigation on He II porous plug liquid-vapor phase separator', 20th International Cryogenic Engineering Conference (ICEC 20), Beijing, China, 405–8.

17

Thermal protection systems

Abstract: The aim of this chapter is to describe the thermal problems that a spacecraft encounters when it enters a planet's atmosphere, due to the large amount of energy that has to be dissipated. The main parameters of the problem and their relationship with the thermal protection material and the required thickness are explained. The strategies to re-entry are described, and the main groups of thermal protection materials and main techniques are considered (ablative and radiative systems) together with design examples. Other protection systems are also outlined, such as the heat sinks, the hot structures, and transpiration cooling.

Key words: ballistic entry, lifting entry, ablative systems, radiative systems.

17.1 Introduction

When a spacecraft has to land on a planet's surface at a moderate velocity, the excess kinetic energy the vehicle has when it is in orbit has to be dissipated. The use of fuel to power re-entry is prohibitive from a mass point of view. Thus, the vehicle is slowed down using aerodynamic drag. For example, the Space Shuttle in a low Earth orbit has a velocity of about 7800 m/s. To decelerate to 100 m/s for landing, the kinetic energy, $(1/2)mU^2$ (m being the mass and U the velocity), has to be divided by a factor of 6000.

As a space vehicle enters a planet's atmosphere, it is exposed to a highly changing aerodynamic environment (Fortescue et al., 2003). Initially, the atmosphere's density is very low and free molecular flow occurs around the spacecraft. Then, as the vehicle progresses further into the planet's atmosphere, a transition flow is formed with thick viscous shock waves about the vehicle. Finally, once sufficiently low in the atmosphere, a continuum flow region with velocities still hypersonic is encountered, which causes very large heat fluxes on the spacecraft surface over the relatively short period of re-entry.

The simulation of hypersonic flows over planetary entry vehicles with well-defined uncertainties is critical for the success of solar system exploration, and is still a real concern for researchers in this field (Gnoffo et al., 2010). Thus, the simulation of radiation and ablation coupled to the flow solver continues to be a high priority for planetary entry analyses, especially for return to Earth and outer planet missions. This simulation is quite a complex task because the flow around the vehicle is not only hypersonic, but three-dimensional and reactive, and its interaction with the vehicle's surface may induce chemical reactions.

The thermal protection system (TPS) of a space vehicle is the hardware used to guarantee the structural integrity of the spacecraft and the proper internal temperatures during the entry or re-entry phase of a mission. The peak heat flux determines the selection of the thermal protection material used, whereas the total integrated heat load determines the thickness of the material required. Re-entry into the Earth's atmosphere has been widely studied since the development of the intercontinental ballistic missiles in the early 1950s and the Apollo programme in the 1960s. It is still a subject of research and major concern in the development of new manned vehicles, such as Orion (Kowal, 2011). Entries in

other planetary atmospheres require dedicated analyses and tailored thermal protection systems because each atmosphere has its own composition and characteristics. The first successful entry mission to Mars, Viking I, was launched in 1975. A review of all entry missions to Mars with the current status of the aerothermal models for this planet is presented in Wright et al. (2010). Pioneer-Venus was the first entry mission to Venus, launched in 1978, and Galileo was the first probe to Jupiter, launched in 1989. Galileo was one of the most challenging entry missions ever undertaken by NASA due to the severe thermal environment experienced during entry. In 1995, the probe entered the Jovian atmosphere at a velocity of 47.4 km/s and the peak heating was in the order of 35 kW/cm^2, with a total integrated heat load of 200 kJ/cm^2 (Laub and Venkatapathy, 2003). In 1997, Cassini-Huygens, a joint NASA/ESA/ASI mission, was successfully launched, and after seven years of interplanetary voyage, it reached Saturn's orbit. After separation, the Huygens probe reached Saturn's moon Titan, descending into its atmosphere to the surface.

There are two types of strategies for entering a planet's atmosphere from space. The most widely used is the ballistic entry, based on aerodynamic drag to decelerate the vehicle. Although re-entry capsules are flown with a certain angle of attack to generate some lift to control the trajectory, this lift is generally smaller than the drag force. Depending on the ballistic coefficient, the ratio of the weight of the vehicle to the product of the drag coefficient by a reference area, Earth re-entry times may vary from slightly less than one minute to slightly over three minutes, and the distance between 250 and 340 km. For manned missions, such as the American Mercury capsule or the Soviet Vostok, accelerations can reach up to 8 g_0 (g_0 being the gravitational acceleration at sea level). This fact, together with the high heat peak encountered during ballistic re-entry, motivated the development of a

second type of re-entry strategy: the use of lifting vehicles. In this case, the flight trajectory is controlled by modulating the lift vector. The primary design parameter of these vehicles is the lift to drag ratio. High values of this parameter originate smaller accelerations and lower heat peaks, but the duration of the entries is longer. Thus, although the peak temperatures of a lifting entry are lower than the peak temperatures of a ballistic entry, the total heat load that must be absorbed over the duration of the entry is greater. The American Gemini and Apollo spacecraft, and the Russian Soyuz spacecraft use a lifting re-entry strategy and have a backup ballistic re-entry mode. However, the American Space Shuttle relies exclusively on aerodynamic lift for its re-entry.

In both re-entry options a thermal protection system is needed, and the parameters to be taken into account for its selection, in addition to the heat peak and the duration of the heating period, are the maximum accelerations and the peak dynamic pressure. Therefore, the materials and structures employed have to withstand not only really high temperatures, but also high mechanical loads. They also have to be durable and impact-resistant.

The peak temperatures encountered on the vehicle surface are also related to the shape of the vehicle. Thus, maximum bluntness yields maximum drag, minimum heat loads and minimum mass of the thermal protection system (Allen and Eggers, 1958). However, aerodynamic stability considerations based on shock wave detachment impose an upper limit on bluntness.

Most thermal protection materials can be classified into two groups, depending on the mechanism used to reject energy from the spacecraft. Thus, ablative systems dissipate the incident thermal energy through phase change and loss of material, whereas radiative systems re-emit the energy received from the surrounding environment as thermal

radiation. In the following sections, these two main groups of thermal protection materials are described as well as other techniques employed for thermal protection.

17.2 Ablative systems

Ablative systems have been widely used in most non-reusable entry vehicles due to their high performance. These materials dissipate the incident thermal energy through phase change and mass loss. Basically, the great amount of energy absorbed during the phase change reduces the heat flux experienced by the structure of the vehicle. Thus, an ablative thermal protection system is based on the sublimation, melting, or pyrolysis of the heat shield, and the removal of the products by the outer stream, as can be seen in Figure 17.1, where the

Figure 17.1 **Typical ablative thermal protection system profile, and heat and mass interactions**

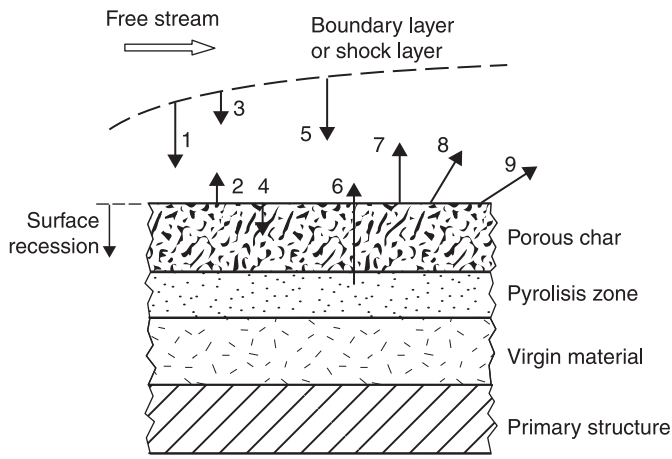

Key: 1 – thermal radiation flux in; 2 – thermal radiation flux out; 3 – convective flux; 4 – heat conduction flux; 5 – chemical species diffusion; 6 – pyrolysis gases; 7 – reaction products; 8 – mechanical erosion; 9 – melt flow.

main layers of the heat shield as well as the heat and mass interactions are indicated.

Most ablative heat shields are made of carbon-based materials due to its properties: good heat sink, high melting point, large enthalpy of sublimation, good radiation properties, and from a structural point of view, low coefficient of thermal expansion. Thus, as described in Laub and Venkatapathy (2003), most materials used for ablative thermal protection systems are reinforced composites with organic resins as binders. When the system is heated, the resin pyrolyses, producing both gaseous and solid products. Gaseous products are mainly hydrocarbons which percolate towards the surface, and are then injected into the boundary layer. The solid carbonaceous residue, called char, deposits on the reinforcement forming a surface layer as indicated in Figure 17.1. The pyrolysis process is endothermic and, furthermore, the gaseous products are heated as they percolate towards the surface, in this way transferring energy from the solid to the surface. The injection of these gases into the boundary layer also causes a reduction in the convective heating. The interaction of the residual gases with the boundary layer gases is quite complex because they may undergo chemical reactions. A result of this ablation process is the consumption of the heat shield material, leading to surface recession. Over the last few decades several models have been developed to predict the behaviour of ablative materials, among them being the ones developed by Lachaud et al. (2008) and Mazzaracchio and Marchetti (2010).

Ablative thermal protection materials are usually classified by density into high density, mid density and low density. The material strength increases with density, but so does the thermal conductivity. This requires a trade-off between mechanical and insulation efficiency, which is different for each mission. For instance, if a high-density material

is used but the heat flux on the vehicle is too low to cause pyrolysis, then the material's high conductivity can allow heat flux conduction into the material, leading to the failure of the thermal protection system.

An undesirable phenomenon that occurs when using ablative materials is a type of mechanical erosion called char spallation. Under the shear stress of the entry flow, the material weakens and some char mass becomes detached from the shield. The main problem is the difficulty in predicting it, although some models are available in the literature (Lachaud and Mansour, 2008). It is known that as the material density increases, the threshold for char spallation moves to higher pressures and heat fluxes. Experimental facilities have been set up to measure spallation, such as the one designed for the Galileo probe (Balakrishnan et al., 1979).

The ablative materials most commonly used in NASA entry missions are (Laub and Venkatapathy, 2003):

- DC-325. A silicone elastomer that is used to fill a fibreglass honeycomb. It was used in the Gemini capsules.
- AVCOAT 5026. An epoxy novolac resin with special additives in a fibreglass honeycomb matrix. It was used in the Apollo missions and is now the base of the thermal protection material for Orion spacecraft, the next generation of crew exploration vehicles.
- SLA-561V (Super Lightweight Ablator). A composite that contains glass and phenolic micro-balloons, glass fibres and chopped cork, with a silicone resin binder in a fibreglass phenolic flexible honeycomb. It has been used in all NASA entry missions to Mars: Mars Viking, Mars Pathfinder and Mars Exploration Rover (MER).
- FM 5055 carbon phenolic. It is a very effective ablative material, but with a high density and therefore bad insulation capacity. It was used in Pioneer Venus, a mission

with high heat fluxes, high pressures, and a relatively modest total heat load, and also in the Galileo mission to Jupiter.

- PICA (Phenolic Impregnated Carbon Ablator). It was the primary thermal protection material used for the Stardust sample return capsule.
- SIRCA (Silicone Impregnated Reusable Ceramic Ablator). It was used on the Backshell Interface Plate (BIP) of the Mars Pathfinder and Mars Exploration Rover (MER) aeroshells.

The ablative materials most commonly used in European entry missions are (Bouilly et al., 2006):

- Norcoat-Liege. Made of hot-pressed cork particles and phenolic resin. It is a very good insulator. Used in Ariane 4 and 5, Beagle 2, and ARD (Atmospheric Re-entry Demonstrator). It is a candidate for the ExoMars descent module.
- Aleastrasil. Produced by high-temperature and -pressure moulding of silica fabric preimpregnated with phenolic resin and cut into a postage-stamp size. Flown in Ariane 4 and ARD (Atmospheric Re-entry Demonstrator).
- AQ60. A felt of phenolic resin reinforced by silica fibres, used by the probe Huygens against the heat of entry into Titan's atmosphere.
- Prosial. Silicone elastomer filled with silica hollow spheres to decrease its density. Flown also in Huygens probe to Titan.
- DO31/SPA. Porous phenolic resin reinforced with ceramic short fibres. Flown in the German re-entry capsule Mirka.
- Picsil. Low-density silicone-based ablator developed within ESA's Manned Space Transportation Program (MSTP).

17.2.1 Design example: Huygens probe

Cassini-Huygens is a joint NASA/ESA/ASI mission launched on 15 October 1997. After seven years of interplanetary journey, it reached Saturn on 1 July 2004. The Huygens probe was separated from Cassini on 25 December 2004, and finally entered the atmosphere of Titan, one of Saturn's moons, on 14 January 2005.

The 320 kg Huygens probe (Lebreton and Matson, 2002) consisted of a Descent Module covered with a hard shell to protect the delicate instrumentation from the extreme temperatures experienced during the descent through the atmosphere. The external shell was a 2.7 m diameter front shield and a back cover. The first entry phase occurred between 350 and 220 km altitude, where Huygens decelerated from about 6 km/s to 400 m/s in less than 2 min. At this velocity, the parachute deployment sequence initiated, starting with a mortar pulling out a pilot chute, which in turn pulled away the aft cover. After inflation of the main parachute, the front heat shield was released to fall from the Descent Module, and the rest of the parachutes and associated mechanisms continued working to bring the Huygens probe down softly to the surface of Titan.

The maximum heat flux on the front face of the heat shield was 1400 kW/m^2 during a period of 20 seconds, and on the rear face the heat flux was between 30 kW/m^2 and 120 kW/m^2. The constituents of Titan's atmosphere are nitrogen (77%), argon (20%) and methane (3%). The main concern during this entry mission was the formation of carbon nitride, CN, due to the dissociation of methane and subsequent combination with nitrogen in the shock layer. The problem with this molecule is the high radiation it generates in a narrow ultraviolet band, from 350 to 400 nm. Thus, in order to evaluate the performance of the thermal

protection materials selected for this mission when exposed to ultraviolet radiation, NASA developed a specific facility based on a high-power Mercury-Xenon lamp with a strong emission in the ultraviolet range (Bouilly, 2006; Powell et al., 2009).

The Huygens probe thermal protection system architecture is depicted in Figure 17.2 (Bouilly, 2006). The 88 kg frontshield was made of a sandwich structure consisting of an aluminium honeycomb with carbon fibre reinforced plastic (CFRP) skins, and of two different ablative thermal protection materials on each face. These materials were developed and produced by EADS-ST. They are:

- AQ60/I tiles were used on the front face. AQ60/I is a felt made of short silica fibres reinforced with phenolic resin. The tiles are bonded on the structure with a silicone glue, also used for the seals between the tiles. As already mentioned, the main concern with this material was its possible transparency in the ultraviolet wavelengths.

Figure 17.2 **Huygens probe thermal protection system architecture**

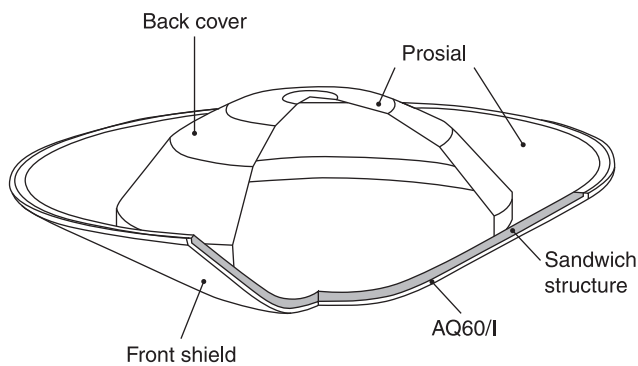

Source: After Bouilly (2006).

- Prosial was used on the rear face (moderate heat flux level). It is a silicone elastomer with excellent thermal properties containing silica hollow spheres to decrease its density. It is sprayed on the surface.

The 21 kg back cover of the external shell was a stiffened aluminium shell also covered with Prosial. It contained a breakout patch, and a door for late access during integration.

17.3 Radiative systems

Radiative systems re-emit the energy received from the surrounding environment in the form of thermal radiation by virtue of a high surface temperature. The heat flux, power per unit area, radiated by a surface at temperature T is $q = \varepsilon\sigma T^4$, where ε is the emissivity of the surface and $\sigma = 5.67 \times 10^{-8}$ W/(m^2·K^4) the Stefan-Boltzmann constant. Therefore, the upper temperature limit of the material largely determines the maximum heat that can be radiated. The applications of these thermal protection systems are then limited to relatively mild entry environments, such as that encountered by the Space Shuttle. Since there is no mass loss, these systems are reusable. A typical profile of a radiative thermal protection system is shown in Figure 17.3. Most of the convective and radiative energy received from the hot boundary layer gases are re-radiated, but part of it can also be conducted into the vehicle. Thus, to minimize heat conduction into the spacecraft a high-emissivity coating as well as the use of a good thermal insulation material is employed.

External insulators can be divided into two classes (STCDD, 1989): rigid and flexible. Rigid insulators can be of

Figure 17.3 **Energy interactions in a reusable thermal protection material**

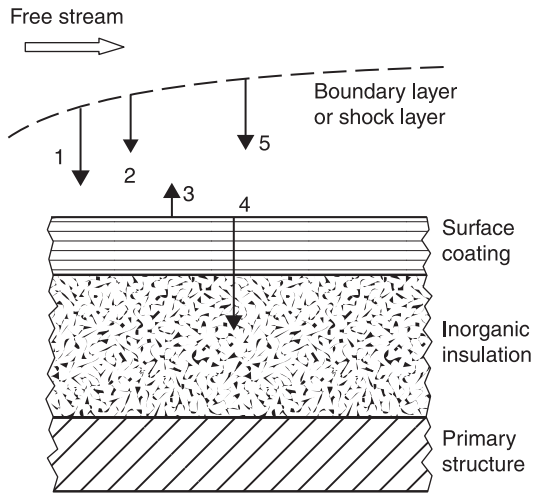

Key: 1 – thermal radiation flux in; 2 – convective flux; 3 – thermal radiation flux out; 4 – heat conduction flux; 5 – chemical species diffusion.

different shapes: tiles, shingles, shells and boxes, and are used to protect the areas exposed to the highest temperatures. Materials used to make rigid insulators can be classified as follows:

- Composites. The main types are carbon-carbon, reinforced carbon-carbon and carbon/silicon carbide.
- Ceramics. The main types are sinterized alumina/silica fibres and sinterized high-purity silica fibres.

Flexible insulators are blankets of different materials consisting of fleeces, felts or threads. The main materials used for flexible insulators are: silica fibres, glass fibres, alumina/silica fibres, alumina/borosilicate fibres, Nomex fibres, alumina fibres plated with rhodium, and nylon.

17.3.1 Design example: Space Shuttle

The Space Shuttle thermal protection system was based on the use of surface materials with a high temperature capability, in combination with an underlying thermal insulation to reduce heat conduction to the interior of the vehicle. The heat from the aerodynamic heating was thereby radiated back into space. Furthermore, the aim of the Space Shuttle thermal protection system was to protect the vehicle not only from the hot re-entry, but also from the extremely cold conditions experienced during the night phase of each orbit. A design life of one hundred missions without major refurbishment was also expected.

Due to the difference of temperature on the surface of the vehicle, ranging from 600 to 1750 K, four different materials were selected (Dotts et al., 1983): reinforced carbon-carbon (RCC), high-temperature reusable surface insulation tiles (HRSI), low-temperature reusable surface insulation tiles (LRSI), and felt reusable surface insulation blankets (FRSI). A map of the distribution of the materials on the vehicle surface is shown in Figure 17.4.

Reinforced carbon-carbon is a light grey all-carbon composite used where the temperature exceeds 1500 K (this is on the leading edges of wings and the nose cap). The reinforced carbon-carbon material is highly resistant to fatigue loads, has sufficient strength to withstand launch and re-entry aerodynamic loads, and a low coefficient of thermal expansion, which provides it with excellent resistance to thermal stresses and shock. Although strong, and capable of withstanding extremely high temperatures, reinforced carbon-carbon is also thermally conductive. This requires the use of insulation blankets and tiles behind the reinforced carbon-carbon panels to protect the vehicle structure and attach fittings from heat radiated from the rear side. Each

Figure 17.4 Space Shuttle thermal protection system

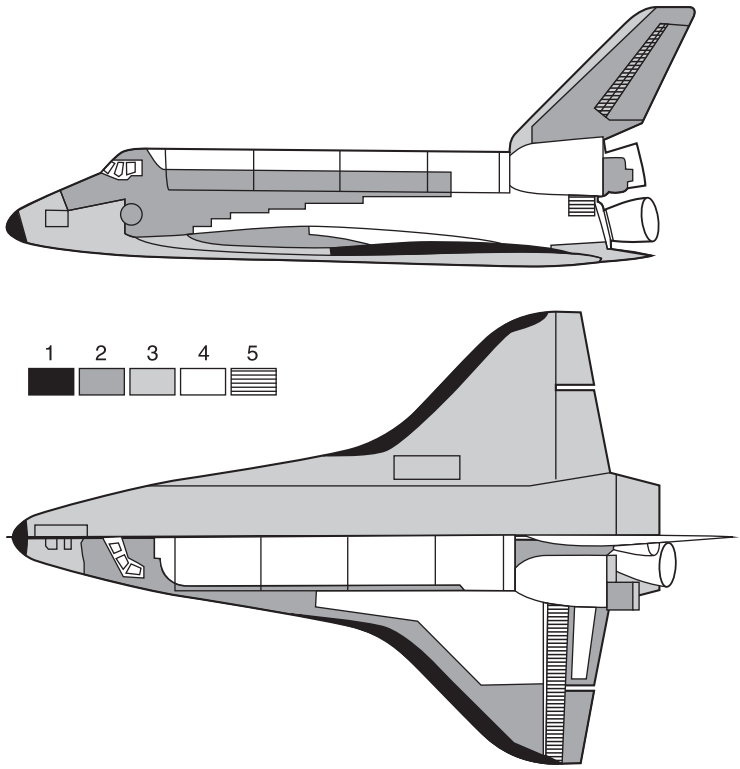

Key: 1 – reinforced carbon-carbon; 2 – high-temperature reusable surface insulation; 3 – low-temperature reusable surface insulation; 4 – coated Nomex felt; 5 – metal or glass.

Source: After Dotts et al. (1983).

wing leading edge had 22 reinforced carbon-carbon panels with Inconel foil-wrapped ceramic insulators protecting the metallic attach fittings. The nose cap was a reinforced carbon-carbon monoconic shell with a combination of Nextel/silica fibre blankets and internal tiles to protect the area behind. Reinforced carbon-carbon was also used in the arrowhead area at the forward external tank attach point, for shock protection during pyrotechnic separation.

The Space Shuttle was equipped with about 24 000 reusable surface insulation tiles. These tiles were used for areas with temperatures ranging from 900 to 1500 K, whereas low-temperature reusable surface insulation tiles were used for areas with temperatures ranging from 650 to 900 K. Both were made of the same base material but with different coatings. Most tiles were made of a material called LI-900, 99.9% pure silica glass fibres. The material was designed to minimize thermal conductivity and weight, which compromised its strength. Thus, for high stress areas, a higher strength version of the material, LI-2200, was used. In 1981, a new material, FRCI-12, with 22% of Nextel fibres, was introduced to replace LI-900 and LI-2200 tiles, and in 1996 NASA introduced a fourth material, the AETB-8 (alumina strength thermal barrier), which improved the properties of the existing materials by adding small quantities of alumina. Other upgrades were the replacement of most low-temperature reusable surface insulation tiles on the upper surface with fibrous insulation blankets (FIB), and the use of toughened unipiece fibrous insulation (TUFI) tiles.

The reaction-cured glass coatings were made from blended glass powders mixed with thickeners and pigments. The coatings were sprayed, dried, and then fired in a kiln at 1200 °C for 90 minutes. The coatings were between 0.25 and 2.5 mm thick. High-temperature reusable surface insulation tiles were coated with a black borosilicate glass coating that provided high emissivity. The low-temperature reusable surface insulation tiles had a white borosilicate glass coating, with a low solar absorptance for in-orbit thermal control.

Felt reusable surface insulation blankets were nylon felt blankets coated with a white silicone rubber. They were used to protect areas exposed at temperatures below 650 K.

17.4 Other thermal protection techniques

17.4.1 Heat sink thermal protection systems

A heat sink is the simplest type of absorptive thermal protection system. Heat sink systems consist of a relatively thick layer of a material with high thermal capacity to absorb a heat input (Glass, 2008), as can be seen in Figure 17.5. When the surface is heated, a part of the energy is radiated away and the remaining energy is absorbed by the structure. If a heat sink structure is heated for a long period of time, the structure can become overheated. Thus, heat sink structures are used with a moderate heat flux for a transient situation. An example is the leading edges of X-15 vehicles.

Materials commonly used as heat sinks are beryllium, beryllium oxide (beryllia) and copper (STCDD, 1989).

17.4.2 Hot structures

Hot structures (Rivers and Glass, 2006) have been developed, among others, for the X-43 and X-37B vehicles, unmanned

Figure 17.5 Heat sink structure concept

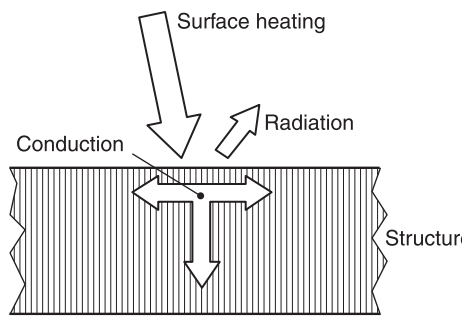

experimental spacecraft for orbital spaceflight missions intended to demonstrate reusable space technologies. These technologies are lighter weight and require less maintenance than those materials attached to a warm or cool substructure. However, the development of hot structures requires a thorough understanding of material thermal and mechanical performance in an extreme environment, operating at temperatures that range from 1500 to 3000 °C, depending on the application. In contrast to heat sink structures, hot structures can be used for a higher heat load and for longer periods, allowing the structure to reach steady-state conditions.

The goal in the development of new materials is to obtain high specific strength at elevated temperature. Two types of materials are used for hot structure applications. The first type is the ceramic matrix composites (CMC), which includes C/SiC material, advanced carbon/carbon (ACC), and SiC/SiC (Lange et al., 2006; Pichon et al., 2006; Glass, 2008). The second type are metallic materials which include metallic matrix composites (MMC), superalloys, and titanium. These all have good specific strength, but only to a temperature of about 1100 °C. Hybrid ceramic/metallic configurations are also studied (Fossati et al., 2006).

Nowadays metallic materials are of great interest as potential thermal protection systems based on hot structures. The use of a titanium-aluminium alloy for the German Ultimate vehicle is reported in Fischer (2006). In Caogen et al. (2008) a superalloy honeycomb thermal protection system panel is studied; this protection system consists of a nickel-based superalloy honeycomb sandwich heat shield, with foil-encapsulated rigid or flexible lightweight ceramic insulation attached to the inner side.

Figure 17.6 Typical transpiration cooling system

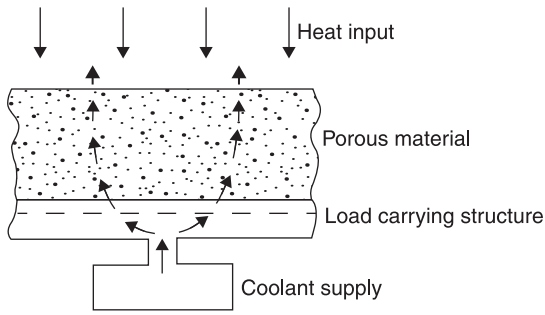

Source: After STCDD (1989).

17.4.3 Transpiration cooling

In transpiration cooling systems a fluid is injected through a porous medium into the boundary layer. The structure is cooled down by means of two basic mechanisms: first, heat is conducted to the coolant as it flows through the structure, and second, when the coolant is ejected it cools down and thickens the boundary layer. The most suitable acceptable coolants are water, ammonia and carbon dioxide. A typical transpiration cooling system is shown in Figure 17.6.

An experimental study on a transpiration cooling thermal protection system using water as coolant is presented in Shuang and BoMing (2010).

17.5 References

Allen, H.J. and Eggers, A.J. (1958) *A Study of the Motion and Aerodynamic Heating of Ballistic Missiles Entering the Earth's Atmosphere at High Supersonic Speeds*, NACA Report 1381, April.

Balakrishnan, A., Nicolet, W., Sandhu, S. and Dodson, J. (1979) *Galileo Probe Thermal Protection: Entry Heating Environments and Spallation Experiment* Design, NASA CR-152334, November.

Bouilly, J.M. (2006) 'Thermal protection system of the Huygens Probe during Titan entry: flight preparation and lessons learned', 5th European Workshop on Thermal Protection Systems and Hot Structures, Noordwijk, The Netherlands, 17–19 May 2006, ESA SP-631.

Bouilly, J.M., Dariol, L. and Leleu, F. (2006) 'Ablative thermal protections for atmospheric entry. An overview of past missions and needs for future programmes', 5th European Workshop on Thermal Protection Systems and Hot Structures, Noordwijk, The Netherlands, 17–19 May 2006, ESA SP-631.

Caogen, Y., Hongjun, L., Zhonghua, J., Xinchao, J., Yan, L. and Haigang, L. (2008) A study on metallic thermal protection system panel for reusable launch vehicle, *Acta Astronautica*, **63**: 280–84.

Fischer, W.P.P. (2006) 'ULTIMATE: Metallic thermal protection system for future RLV's – status of the current development', 5th European Workshop on Thermal Protection Systems and Hot Structures, Noordwijk, The Netherlands, 17–19 May 2006, ESA SP-631.

Fortescue, P., Stark, J. and Swinerd, G. (2003) *Spacecraft Systems Engineering*, John Wiley and Sons Ltd., Chichester, UK.

Fossati, F., Gambacciani, G., De Palo, S. and Langlois, S. (2006) 'Design and manufacturing of a wing hybrid metal/ceramic hot structure', 5th European Workshop on Thermal Protection Systems and Hot Structures, Noordwijk, The Netherlands, 17–19 May 2006, ESA SP-631.

Glass, D.E. (2008) 'Ceramic Matrix Composite (CMC) Thermal Protection Systems (TPS) and hot structures for

hypersonic vehicles', Paper AIAA-2008-2682, 15th AIAA Space Planes and Hypersonic Systems and Technologies Conference, Dayton, Ohio, USA, 28 April–1 May 2008.

Gnoffo, P.A., Johnston, C.O. and Kleb, B. (2010) *Challenges to Computational Aerothermodynamic Simulation and Validation for Planetary Entry Vehicle Analysis*, RTO-EN-AVT-186, NATO Research and Technology Organization.

Kowal, T.J. (2011) 'Orion Flight Test-1 thermal protection system instrumentation', International Planetary Probe Workshop, Portsmouth, Virginia, USA, 6–10 June 2011.

Lachaud, J., Aspa, Y. and Vignoles, G.L. (2008) Analytical modeling of the steady state ablation of a 3D C/C composite, *International Journal of Heat and Mass Transfer*, **51**: 2614–27.

Lachaud, J. and Mansour, N.N. (2008) 'Modeling ablation of fibrous materials from bulk to Knudsen regime', 19th International Symposium on Transport Phenomena, Reykjavik, Iceland, 17–20 August 2008.

Lange, H., Steinacher, A., Handrick, K., Weiland, S., Glass, D. et al. (2006) 'Advanced CMC TPS design concepts for re-usable re-entry vehicles', 5th European Workshop on Thermal Protection Systems and Hot Structures, Noordwijk, The Netherlands, 17–19 May 2006, ESA SP-63.

Laub, B., and Venkatapathy, E. (2003) 'Thermal protection system technology and facility needs for demanding future planetary missions', International Workshop on Planetary Probe Atmospheric Entry and Descent Trajectory Analysis and Science, Lisbon, Portugal, 6–9 October 2003.

Lebreton, J.P. and Matson, D.L. (2002) The Huygens Probe: science, payload and mission overview, *Space Science Reviews*, **104**: 59–100.

Mazzaracchio, A. and Marchetti, M. (2010) A probabilistic sizing tool and Monte Carlo analysis for entry vehicle

ablative thermal protection systems, *Acta Astronautica*, **66**: 821–835.

Pichon, T., Soyris, P., Foucault A., Parenteau J.M., Prel Y. and Guedron, S. (2006) 'C/SiC based rigid external thermal protection system for future reusable launch vehicles: Generic Shingle, Pre-X / FLPP anticipated development test studies', 5th European Workshop on Thermal Protection Systems and Hot Structures, Noordwijk, The Netherlands, 17–19 May 2006, ESA SP-631.

Powell, R.W., Lockwood, M.K., Cruz, J.R., Striepe, S.A., Hollis, B.R. et al. (2009) Cassini/Huygens Probe Entry, Descent, and Landing (EDL) at Titan independent technical assessment, NASA/TM-2009-215732, May 2009.

Rivers, H.K. and Glass, D.E. (2006) 'Advances in hot-structure development', 5th European Workshop on Thermal Protection Systems and Hot Structures, Noordwijk, The Netherlands, 17–19 May 2006, ESA SP-631.

Shuang, L. and BoMing, Z. (2010) Experimental study on a transpiration cooling thermal protection system, *Science China*, **53**: 2765–71.

STCDD (1989) *Spacecraft Thermal Control Design Data Handbook*, ESA PSS-03-108, Issue 1.

Wright, M.J., Tang, C.Y., Edquist, K.T., Hollis, B.R. and Krasa, P. (2010) 'A review of aerothermal modeling for Mars entry missions', Paper AIAA 2010-0443, 48th AIAA Aerospace Sciences Meeting, Orlando, Florida, USA, 4–7 January 2010.

18

Thermal control design

Abstract: This chapter outlines the design objectives and the requirements of the spacecraft components for the different modes of operation, and the tasks to be considered in the design process: the selection of the thermal hardware and the prediction of the temperatures in the spacecraft selected points. The main design philosophy and the flow of the design process are highlighted, the definition of the worst load cases (hot cases, cold cases) and the temperature design margins are presented, and their roles in the design are explained.

Key words: operational modes, mission requirements, thermal hardware, temperature margins.

18.1 Design objectives and requirements

The aim of a spacecraft thermal control system (TCS) is to maintain all the components on board the spacecraft within the allowable temperature limits using the minimum spacecraft resources. Furthermore, it has to guarantee the optimal performance of a component in operational conditions. Thus, when the performance of a component depends on its temperature, as for instance is the case for solar cells, the solution leading to the best performance has

to be adopted. Besides keeping temperatures within ranges, the aim of the thermal control system is to minimize temperature gradients according to specified limits and to guarantee temperature stability for optics, opto-mechanical devices or any other component sensitive to temperature. This has to be done for all mission phases, and the possible degradation that can be caused by in-orbit environment (e.g. atomic oxygen, ultraviolet radiation), wear, and mechanical loads, has to be taken into account during the design process.

The two main tasks under the responsibility of the thermal control system team are the definition of the thermal hardware of the spacecraft and the prediction of the temperatures experienced during the orbit. In addition to this, another important task to be performed during the design of the thermal control system is the identification of the relevant parameters that have influence on the thermal behaviour of the spacecraft in order to find an optimal solution compatible with the limitations given by the spacecraft resources.

The requirements of the components have to be defined for the different modes of operation of the spacecraft. They include operational mode, start-up, and survival conditions. In this last case, the goal of the thermal control system is to avoid damage of the equipment. When the object of study is not a complete spacecraft but only a unit, payload, scientific instrument, or any spacecraft subsystem, thermal requirements in terms of heat fluxes through interfaces also have to be specified in addition to temperature requirements. They are usually defined in terms of the maximum heat flux allowed through an interface.

Some examples of the thermal requirements in operational conditions of common spacecraft equipment are shown in Table 18.1. For a given mission, the thermal requirements of the equipment and platform have to be specified because the

Table 18.1 Thermal requirements

Temperature ranges	T_{min} [°C]	T_{max} [°C]
Electronics (housing)	−10	+50
Batteries	0	+20
Solar arrays	−100	+120
Antenna dish	−65	+95
Hidrazine tank	+10	+50
IR detectors	−223	−173
Inactive structure	−100	+100
Temperature gradients		
Opto-electronic equipment	$\Delta T < 5$ °C	
High-resolution cameras	$\Delta T < 0.1$ °C	
Detectors (CCD)	$\Delta T < 0.01$ °C	
Temperature stability		
Electronics	$dT/dt < 5$ °C/hour	
Detectors (CCD), during observation periods	$dT < 0.1$ °C	

requirements depend on the specific components to be used. Sometimes this is not an easy task, mainly during the early phases of a mission when the flight hardware has not yet been selected.

The thermal control system usually requires specific thermal hardware that has to be taken into account in the corresponding budgets. Minimum mass, power and size have to be used as a baseline criteria for this hardware definition, provided that reliability and safety requirements are fulfilled.

18.2 Design process

The thermal control system design process mainly consists of two tasks. On the one hand, the appropriate thermal hardware for the spacecraft has to be selected. On the other hand, the temperatures of the different parts of the spacecraft have to be calculated for different load cases, verifying that the thermal requirements are met.

There are many types of space missions and payloads (see Chapter 1), which means that the design of the spacecraft, and in particular of the thermal control system, has to be tailored for each type of mission. Hence, most communications satellites in geostationary orbits are based on the same design philosophy, whereas the mission requirements for low Earth orbit satellites or interplanetary spacecraft influence the system design greatly.

Therefore, as stated previously, the first step before starting any thermal design is the compilation of thermal requirements in terms of allowable temperature ranges, maximum temperature gradients, and temperature stability, of all equipment and structural parts of the spacecraft.

The prediction of temperatures is obtained by solving the energy balance equation applied to the spacecraft. Obviously, the temperature distribution strongly depends on the thermal hardware used. Therefore, before carrying out any calculation, it is necessary to define an initial thermal hardware configuration of the spacecraft. This is commonly carried out based on engineering experience. For example, it is common practice to insulate the spacecraft from outer space using multilayer insulations. This helps to lessen the effect of the highly changing environmental conditions on the equipment.

In order to allow the rejection to space of the power internally dissipated, some radiators, located on the outer surface of the spacecraft subjected to lower environmental

loads (facing the deep space as much as possible), are appropriately sized. The thermal couplings between the inner equipment and the radiators are suitably defined to enable heat flux between dissipating devices and radiators. With the initial hardware, based on expertise the temperatures of the spacecraft are determined, and, depending on these results, the thermal hardware is modified until the requirements are met.

The design process is, therefore, an iterative process that has as an output the spacecraft thermal hardware configuration and the spacecraft's temperature predictions. Furthermore, this iterative process involves not only the thermal control system, but also other subsystems of the spacecraft. Indeed, any change in the hardware may have direct implications in the mechanical and structural design, and the need for heaters has direct impact on the power management subsystem, the electronics, and onboard data handling subsystems. Thus, the design of the thermal control system is a complex, iterative process that involves other subsystems of the spacecraft.

The major factors driving thermal control system design are basically:

- the spacecraft environment, which drives the external loads;
- the heat dissipated by the equipment on board the spacecraft;
- the distribution of the thermal dissipation within the spacecraft;
- the temperature requirements of the spacecraft components;
- the configuration of the spacecraft: geometry, materials, mounting systems, etc.

Figure 18.1 Thermal control subsystem design process flowchart

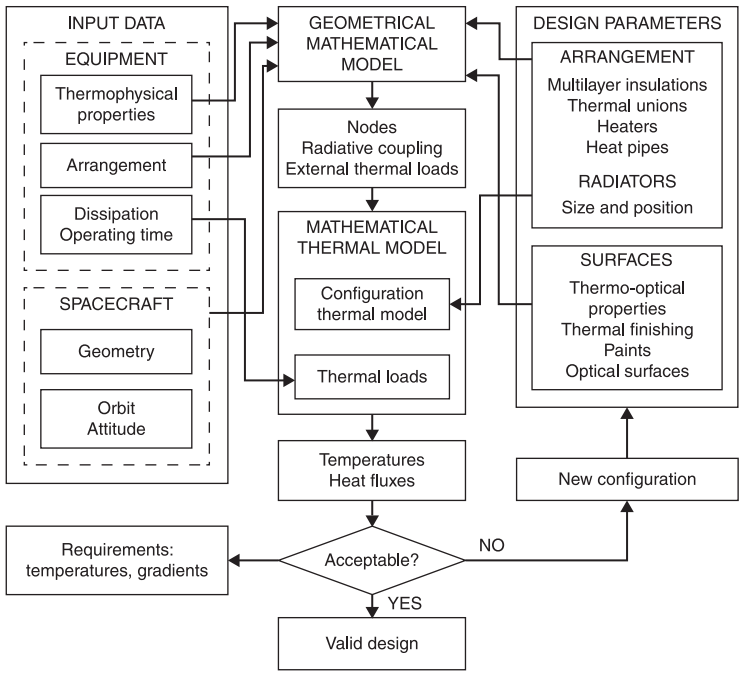

Figure 18.1 shows a simplified scheme of the design process. The parameters in the left box are the main characteristics of the spacecraft with direct influence on its thermal behaviour. Hence, they are the input parameters for the thermal control system activities. The first group of input parameters has the satellite geometry, its orbit, and its attitude or type of stabilization. This will condition the external thermal loads, the maximum sizes of the radiators, and the exchange of radiation between different surfaces, etc. The second group of input parameters are the equipment characteristics and power distribution. Undoubtedly, the properties of the components (mass, shape and thermal

capacity), as well as the modes of operation (the location of the dissipating devices, the periods of time they are switched on and the power they dissipate during these periods), will have a major influence on the thermal behaviour of the system.

The parameters in the right box are the design parameters for the thermal control system, that is, they can usually be modified or appropriately selected for thermal reasons. Thus, the selection of coatings is usually one of the degrees of freedom a thermal engineer has. The solar absorptance, α, and the infrared emissivity, ε, govern the radiation exchanges, either with the environment or between spacecraft surfaces. Other typical thermal hardware used in most spacecraft is the multilayer insulation systems, or thermal blankets. The thermal engineer will select the type and characteristics of the blankets: materials, number of layers, thermal finish, etc. The need for compensation heaters and the power required also have to be estimated.

Another important parameter for thermal design is related to the thermal behaviour of the mechanical joints. Hence, the design of the mounting concepts, bolted joints, etc. can be readapted for thermal reasons. For instance, when insulation is needed, insulation washers have to be used, but when good thermal coupling is needed, highly conductive materials have to be used.

Finally, an important parameter to be determined is the size of the radiators needed to reject to space all the power dissipated by the devices and the power corresponding to the absorbed environmental loads. Usually, this estimation is initially calculated by means of simple analytical calculations, and, as the design progresses, the sizes of the radiators are refined, this time using the complex numerical tools used for thermal calculations. The use of all these thermal hardware elements and of any other one, such as louvers, heat pipes, thermal

straps, etc., have to be determined in order to meet the thermal requirements of the spacecraft platform and equipment.

Once the appropriate thermal hardware has been selected, a geometrical mathematical model and a thermal mathematical model are set up to analyse the design and to determine the temperatures, as explained below. Furthermore, the temperatures have to be obtained for the different dimensioning load cases, which are described in Section 18.3.

The design and development of a space programme is usually organised, according to European Standards (ECSS-E-ST-10C, 2009), into the following phases (see more detailed information in Chapter 1, Table 1.1):

Phase 0: Mission analysis-need identification

Phase A: Feasibility

Phase B: Preliminary definition

Phase C: Detailed definition

Phase D: Qualification and production

Phase E: Operations / utilization

Phase F: Disposal

As stated above, the first loop in the iterative process is based on previous experience. Afterwards, iterations are carried out using basic semi-analytical simulations. This is always done in early phases of the missions, when the concept of the spacecraft is still not completely defined, and detailed geometric information is still not available (phases A and B). In these stages, it is common practice to work in parallel with more than one spacecraft configuration, and trade-offs are necessary to select the final concept. Once the detailed definition phase starts (end of phase B and phase C), thermal calculations are performed with complex

numerical simulations that enable the spacecraft temperature field to be determined. Specific software tools are used for this purpose.

The simulations are affected by several limitations that have to be taken into account when analysing their results. These limitations are mainly related to the numerous uncertainties affecting the parameters used for thermal modelling. Thus, the uncertainties are mainly due to simplifications in the geometry, inaccuracies in the properties of the surfaces and materials, and the estimated or average values used for the determination of the environmental loads (for example albedo coefficients, planetary infrared radiation, etc.). This often makes it necessary to carry out some engineering tests on engineering models of particular equipment, for instance, to determine the thermal couplings of mechanical joints. Moreover, the spacecraft verification plan always includes thermal vacuum tests, at different levels, to verify the design.

The inaccuracies of the design process are also palliated by applying safety margins to the results predicted with the numerical models. Thus, the temperature range predicted with the models is enlarged with a margin that depends on the design phase, and the level of detail of the models. In early phases of the design, a typical uncertainty of ±15 K is applied, but this number may be decreased to ±5 K after having correlated the mathematical models with measured data obtained during the thermal balance tests. The philosophy of margins applied to the calculated temperature range to define the different levels of testing (qualification and acceptance tests), according to ECSS-E-ST-31C (2008), is shown in Figure 18.2.

Figure 18.2 **Temperature margins definition for the thermal control subsystem**

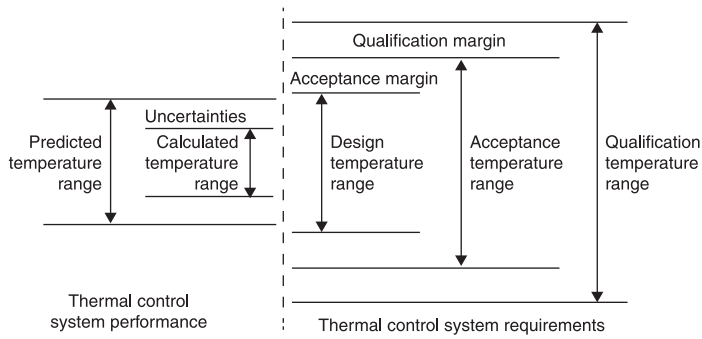

Source: After ECSS-E-ST-31C (2008).

18.3 Load cases

Spacecraft are subjected to highly variable environmental conditions (see Chapter 2). The thermal control system has to fulfil thermal requirements over all mission phases. This includes ground operations (integration, testing, storage and shipping), and flight activities (launch, transfer orbits, cruise, final orbit, etc.). In order to size the thermal control system, the worst case scenarios (those leading to extreme thermal loads) have to be identified. The so-called hot cases and cold cases, for operating, start-up and survival conditions of equipment are defined this way. These dimensioning cases are defined by an appropriate combination of external fluxes (solar, albedo and planetary infrared), material properties, and unit dissipation profiles. Normally, the hot case corresponds to the maximum external loads and maximum internal dissipation. The maximum external loads usually take place at the sub-solar point in a planetary orbit, or during the perihelion in a solar orbit. The cold case usually corresponds to eclipse zones for planetary orbits

and to the aphelion phase for a solar orbit. Modes of operation with minimum dissipation are chosen to assess the cold cases.

A common philosophy in spacecraft thermal control is to design the thermal subsystem for the hot operational case. This implies that the radiators are sized to reject to space the maximum power dissipated by equipment with the maximum external loads, otherwise, the system will not work. Since this hardware, and the radiator sizes selected for the hot case, can lead to extremely low temperatures when the spacecraft is exposed to cold conditions, or the equipment is off, electrical substitution heaters are appropriately sized and located for these cold situations.

The degradation of surface properties, for instance the increase of solar absorptance values (α), due to exposure to solar radiation, also has to be taken into account. End of life (EOL) property values have to be used for thermal calculations corresponding to the hot cases, whereas beginning of life (BOL) property values have to be used to define the cold cases.

Since the dimensioning loads are defined for the worst case scenarios, steady-state calculations under these conditions are carried out. This is a conservative approach that notably simplifies the calculations, and provides the upper and lower limits temperatures can reach. As already said, the study of steady-state hot cases usually allows radiator sizes to be determined, while the study of steady-state cold cases is used to assess the need of heaters, their location and power.

With regard to the different mission phases, the thermal control system is usually designed for the cruise and nominal orbit, making it compatible with ground operations and the ascent phase.

18.4 References

ECSS-E-ST-10C (2009) *Space engineering. System engineering general requirements*, ESA Requirements and Standards Division, ESTEC, Noordwijk, The Netherlands, March 2009.

ECSS-E-ST-31C (2008) *Space engineering. Thermal control general requirements*, ESA Requirements and Standards Division, ESTEC, Noordwijk, The Netherlands, November 2008.

19

Thermal mathematical models

Abstract: The aim of this chapter is to explain the basic principles involved in the development of a thermal mathematical model of a space item, such as a spacecraft, or equipment. The components of the mathematical model are presented: the geometrical mathematical model, the network of nodes, the external thermal loads, the internal power dissipation, and the conductive and radioactive couplings between nodes. The thermal analysis software tools, based on a numerical description of the spacecraft, are presented, together with the modelling procedure.

Key words: thermal mathematical model, geometrical mathematical model, available software tools.

19.1 Introduction

Thermal modelling is the major task in thermal control system design.

The thermal modelling process requires the approximation of the physical system with a mathematical representation, that is, a set of numbers that represent the system from the thermal point of view. The first step in the mathematical procedure (see Figure 18.1) is to set up the so-called geometrical mathematical model (GMM), a representation of the geometry of the system necessary to compute the

external thermal loads on the outer surfaces, and the radiation exchange between different parts of the spacecraft. It is usually a simplified geometry, where non-relevant details from the thermal point of view are excluded.

Once a basic geometry for thermal analysis is defined, this geometry is discretized in a network of nodes. To do this, the basic geometric shapes the geometrical mathematical model consists of are meshed. Each node is an isothermal element characterized by its temperature T_i and its thermal capacitance C_i. This numerical approach is called the 'lumped parameter network' because the continuous parameters of the thermal system have been lumped into the discrete set of the nodes.

The energy equation for each node can be written as

$$C_i \frac{\mathrm{d}T_i}{\mathrm{d}t} = \dot{Q}_{sun,i} + \dot{Q}_{alb,i} + \dot{Q}_{planet,i} + \dot{Q}_{dis,i} + \sum_{j=1}^{n} K_{ij}(T_j - T_i) + \sum_{j=0}^{n} R_{ij}(T_j^4 - T_i^4), \qquad (19.1)$$

where $\dot{Q}_{sun,i}$, $\dot{Q}_{alb,i}$, and $\dot{Q}_{planet,i}$ are the external thermal loads at node i, solar, albedo and planetary infrared, respectively. $\dot{Q}_{dis,i}$ is the power dissipated at node i, and K_{ij} and R_{ij} are the conductive and radiative links or couplings between nodes, respectively. Note that $K_{ij} = K_{ji}$ and $R_{ij} = R_{ji}$. Thus, the term $\sum_{j=1}^{n} K_{ij}(T_j - T_i)$ represents the conduction heat received by node i from the rest of the neighbouring nodes j, and $\sum_{j=0}^{n} R_{ij}(T_j^4 - T_i^4)$ represents the net radiation exchange on node i.

Note that in this last term of equation (19.1), node '0' represents outer space. Thus, a radiative link between the spacecraft and outer space is taken into account, whereas a conductive link is not considered.

In spacecraft thermal control, the main mechanisms of heat transport are thermal radiation exchange and conduction through the materials of the spacecraft. This is why in equation (19.1) these are the mechanisms of heat transfer exchange that are considered. Moreover, every exchange with the environment takes place as a radiative exchange. In the case where fluids are involved in the system, the appropriate convective links should be added to the equation.

When equation (19.1) is applied to all the nodes the spacecraft is divided into, a system of ordinary differential equations is obtained and its solution allows the temperature of such discrete points to be determined. This means that in order to determine the temperature of the satellite, the two matrices of coefficients (conductive and radiative thermal couplings), and vectors (solar, albedo, Earth infrared and internal dissipation thermal loads) in equation (19.1) are needed. These matrices and vectors constitute a mathematical representation of the thermal model of the spacecraft as a set of concentrated thermal capacitance nodes, coupled with a network made of thermal conductors (mainly radiative and conductive). That is why this set of numbers is called the thermal mathematical model (TMM).

For thermal control system dimensioning, as stated above, steady state calculations for the worst case scenarios, hot and cold cases, are performed. This is done by setting the left hand side of equation (19.1) to zero. When it is applied to all the nodes, it constitutes a system of algebraic non-linear equations that can be solved to obtain the temperature distribution for such extreme cases. In fact, what is solved in this case are simple heat flux balances. It is obvious that prior to the resolution of the equation, it is necessary to obtain the thermal loads and the matrices of thermal couplings. These temperatures are the upper and lower limits that could be encountered during the mission. It is important

to point out that the thermal design is usually obtained from these steady calculations whenever there are no strict stability requirements.

Once a feasible thermal control system design based on the previous steady-state calculations is found, transient analyses are performed to determine the changes of temperatures over time, and to verify the fulfilment of requirements. In this case, the system of equations is generally integrated using a Crank-Nicolson method.

A summary of the mathematical procedure to be followed to obtain the temperature distribution of the spacecraft using the nodal network method is as follows:

1. build the geometrical mathematical model based on the spacecraft configuration;
2. discretize the geometry in nodes;
3. calculate the external thermal loads on the nodes (solar, albedo and planet infrared), and the internal ones (equipment dissipation);
4. calculate the conductive and radiative couplings between nodes;
5. solve equation (19.1).

19.2 Thermal analysis software

The main software tool used in spacecraft thermal control design in Europe is ESATAN-TMS, currently supplied by ITP Engines UK, although it was initially developed under ESA responsibility. It is a complete environment for thermal analysis (ESATAN-TMS, 2010a, 2010b). It enables all the radiative and conductive heat transfer calculations for space analysis to be performed, and allows temperatures and heat

fluxes over a previously defined orbit or trajectory to be determined. Other software tools with similar purposes are SINDA, Thermal Desktop, Thermica, Radsol, etc.

The programme is based on a lumped parameter method in which the mathematical model is formulated by dividing the geometric model into a discrete number of elements. Each of these elements, called thermal nodes, is then represented as a point, with its physical properties lumped onto the point. The lumping of the properties of a surface, in particular the temperature, has an important consequence: each node surface is treated as being isothermal. This is very important when one of the aims is to determine the temperature gradients, and the discretization or meshing of the geometry has to be done accordingly. The programme only works with surface elements, or shells, but it allows different thermo-optical properties (solar absorptance and infrared emissivity) on each face of the shell. Once the surfaces are meshed, connections between pairs of nodes to represent conductive and radiative couplings with other parts of the model are established. Therefore, this set of nodes and connections may be viewed as a nodal network, and the system of equations which results is similar to that obtained by applying the finite difference formulation of the problem. This system can conveniently be handled as a set of matrices of coefficients, and is solved by approximate linearization and iterative techniques.

The normal procedure that has to be carried out to set up and run a thermal analysis of a spacecraft with ESATAN-TMS, consists of the following steps:

1. Build the system geometry. The real geometry of the spacecraft and its systems is simplified and represented by a set of shells with the appropriate geometry and thickness. The programme contains a number of primitive

shells, but more complex shells can be created by combining or cutting the primitive shells. If the spacecraft contains an assembly with relative movement between components, for instance a solar panel that automatically re-orientates to always face the Sun, this assembly can also be established when defining the geometry. The thermo-optical properties of the surfaces (solar absorptance and infrared emissivity), and bulk properties (thermal conductivity and specific heat), are also assigned in this step. To verify the geometry model, the graphic interface and the report module can be used.

2. Mesh the geometry with the adequate meshing criteria. Each element, called a node, is considered to be isothermal. Figure 19.1 shows the geometrical model of a typical satellite where the mesh can be observed.
3. Define the environmental conditions (solar constant, planet albedo coefficient, planet blackbody equivalent temperature) necessary for the calculation of the external thermal loads. Define the mission, that is, the orbit or trajectory and attitude of the spacecraft, and the points of the orbit where the thermal loads need to be calculated.

Figure 19.1 ESATAN-TMS geometry and mesh visualization

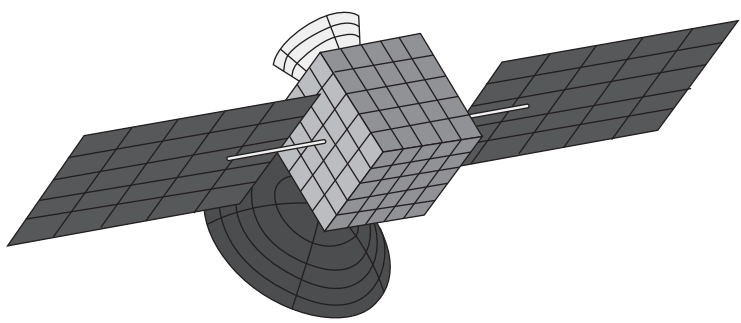

Again, this input can be verified using the graphic interface. The satellite-in-orbit positions, where external heat fluxes need to be determined, are shown in Figure 19.2.

4. Run the so-called 'radiative case'. This way the view factors and radiative exchange factors between thermal nodes, as well as the direct and absorbed external heat fluxes on each node are determined.

Figure 19.2 **Model of the satellite in a circular orbit located in the $z = 0$ plane (the Sun is in the $+x$ direction)**

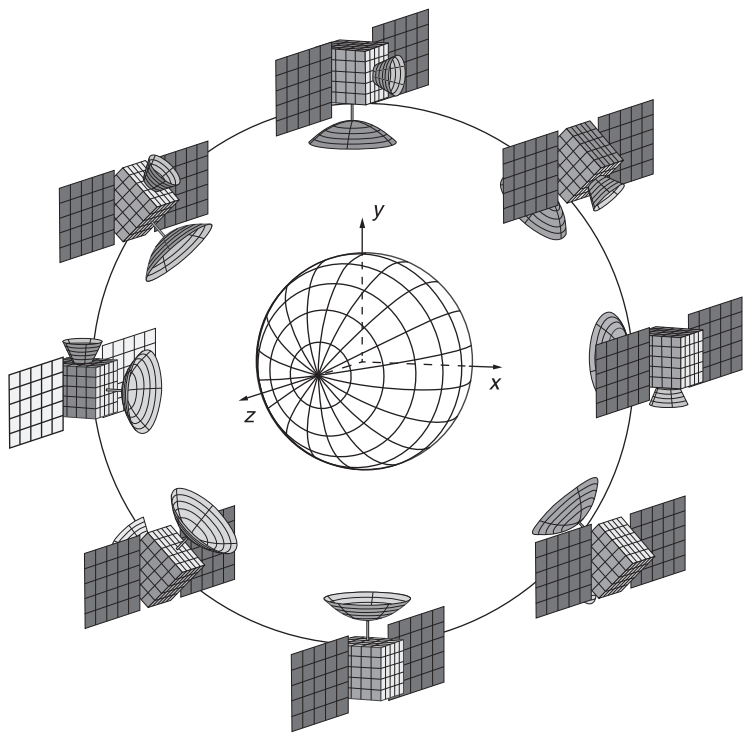

Note: The positions indicate where external heat fluxes are calculated.

5. Define the conductive thermal couplings between nodes. Some of these (corresponding to edges of shells in contact) are automatically calculated by the tool, once the thermal contact conductance of the joint is given, but other conductive couplings, for example those corresponding to an electronics box bolted to a platform, have to be manually introduced into the programme.
6. Define the power dissipation for each node. This depends on the modes of operation of the spacecraft.
7. Define the so-called 'analysis case'. With the radiative results previously obtained, multiple analyses can be carried out: steady-state in particular points of the orbit, steady-state with average values, transients, etc. In this module, the type of analysis and the output data file can be specified, as well as the format of this output. Typical results are the temperatures and the net heat exchange between nodes.

Regarding the accuracy of the results, several sources of uncertainty and/or error have to be taken into account during the modelling process. In what follows, the uncertainties and errors are identified in the order they appear in the calculation process. The first one is related to the simplification of the geometry. Thermal models usually do not include details of the geometry that are not relevant from the thermal point of view, and some elements, such as the harness, are not always geometrically represented. The next source of uncertainty is related to the thermo-optical and bulk properties of the materials. Specific thermal control coatings are well characterized, while other thermal finishes, for instance electronics cards, are not.

Regarding the bulk properties, the main issue is that the model treats the materials as homogeneous, and on many occasions this is not true. An example to be mentioned is

thermal conductivity across a honeycomb. Although there are empirical correlations available in the literature, tests on the specific specimen are necessary. Moreover, even though a material has been experimentally characterized, the use of inserts will change its thermal properties. Another important topic related to the materials is the characterization of the mechanical joints. The values of the thermal contact conductance are usually empirical or estimated values, and therefore a sensitivity analysis to these parameters may be required.

The first mathematical error appears when the surfaces are discretized. Obviously, the finer the mesh, the more accurate the results, but also the more time consuming. A brief analysis and a trade-off to decide the most appropriate mesh size is usually necessary.

Following the calculation procedure, the next source of uncertainty is related to the environmental external loads: average values for the solar constant, albedo coefficients and infrared planetary radiation are typically used. Then, external heat fluxes and radiative exchange factors between surfaces are calculated. To calculate these, a Monte Carlo ray tracing method is used. The accuracy of the results depends on the number of rays randomly launched from each surface. By default, ESATAN-TMS allows the definition of three levels of accuracy (according to the number of rays launched by the programme), depending on the criticality of the surface. Once the thermal loads and thermal couplings between nodes are determined, another numerical error is due to the solution method used to solve the equations. In the case of transient solutions, a Crank-Nicolson method is used. For steady-state cases, linearization techniques are used. The integration time steps, relaxation parameters, maximum number of loops, and other convergence criteria, normally have to be selected by the user.

As a summary, it can be said that the presence of errors in model predictions is due to two factors. The first is related to the uncertainty of physical parameters, and the second is due to the numerical procedure. This explains the need for the margin philosophy shown in Figure 18.2 and the performance of thermal tests to verify the models.

19.3 Reference

ESATAN-TMS (2010a) *Workbench Getting Started Guide*. ITP Engines UK Ltd., Whetstone, Leicester, UK.

20

Thermal control testing

Abstract: In this chapter, the main points concerning thermal control testing are considered. Namely: the phases of a spacecraft project, the objectives associated with the tests performed in the different phases; the types of tests, the main characteristics of these tests, the sources of uncertainty in the tests, the project model philosophy to be considered and the hardware models involved; the test facilities where thermal tests are performed, and their coordination and the effort for standardization of production and testing activities in Europe.

Key words: thermal cycling test, thermal balance test, thermal vacuum test,test facilities.

20.1 Introduction

The development of space systems involves the design, manufacture, assembly, integration and testing (see project phases in Chapter 1) of very complex equipment (and software) by teams composed of large numbers of people, and of several independent organizations. In order to obtain a successful result, a strict prelaunch verification process is required. Failures and repairs become more expensive as the development process proceeds, and are practically impossible after launch. As a result of the design (allocated functions, life cycle profile data, associated manufacturing process, etc.) a baseline for system validation has to be developed, and a validation plan

has to be prepared, with the method of verifying the requirements. Typical validation methods are: inspection, analysis, similarity, test, or simulation. In general, tests are employed to verify the design and manufacturing (qualification tests) and the product verification (acceptance tests). A complete test programme for spacecraft includes development (phase C), qualification (phase D), acceptance (phases D and E), prelaunch validation (phase E), and in-orbit tests (phase F).

20.2 Testing objectives

As mentioned above, development, qualification and acceptance tests are needed as part of the verification process of the spacecraft thermal control system, together with the analysis, using mathematical models, which has been described in Chapter 19.

According to ECSS-E-10-03A (2002), the objective of development testing is to support the design feasibility, to assist in the evolution of the design, and is used to validate new design concepts.

The objective of qualification testing is the formal demonstration that the design implementation and manufacturing methods have resulted in hardware and software which conform to the specification requirements, and demonstrates that the items perform satisfactorily in the intended environments with sufficient margins.

The purpose of acceptance testing is to demonstrate conformance to specifications and to act as a quality control screen to detect manufacturing defects, workmanship errors, the start of failures and other performance anomalies, which are not readily detectable by normal inspection techniques. A typical equipment qualification testing sequence is shown in Figure 20.1, and a space vehicle qualification test

Figure 20.1 Typical equipment qualification testing sequence. After ECSS-E-10-03A (2002)

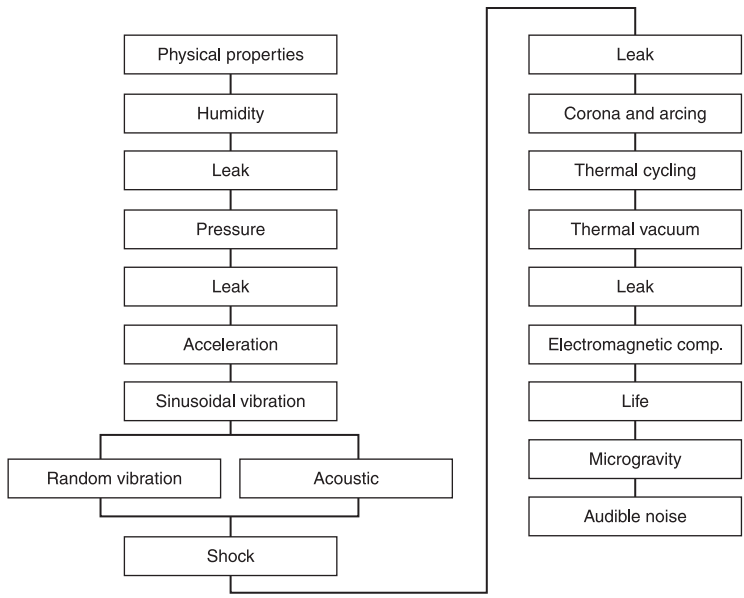

baseline, as defined in ECSS-E-10-03A (2002), is summarized in Table 20.1.

In the case of thermal testing, this testing philosophy is implemented by using three different types of tests: thermal cycling, thermal balance, and thermal vacuum, which cover the following objectives:

- Confirm that the system, subsystem, or element will operate satisfactorily at expected (or more extreme) operating temperatures.
- Evaluate the ability of the thermal control subsystem to maintain the spacecraft thermal environment within established structural, experimental, and subsystem temperature limits.
- Verify the validity of the analytical models.

Table 20.1 Typical space vehicle qualification test baseline

Test	Reference sub-clause	Test	Reference sub-clause
1 Optical alignment	5.3.4.5	14 Random vibration	5.3.3.5.3
2 Functional and performance	5.3.8.1, 5.3.8.2	15 Sinusoidal vibration	5.3.3.5.4
3 Human factors engineering	5.3.9.3	16 Transient	5.3.3.5.5
4 Physical properties	5.3.4.4	17 Ambient pressure temperature cycling	5.3.5.3
5 Pressure	5.3.4.1	18 Thermal balance	5.3.5.2
6 Leakage	5.3.4.2	19 Vacuum temperature cycling	5.3.5.1
7 Boost pressure profile	5.3.4.3	20 Toxic offgassing	5.3.9.1
8 Modal survey	5.3.3.7	21 Aero-thermodynamics	5.3.6
9 Electromagnetic compatibility	5.3.7.1	22 Magnetic field	5.3.7.2
10 Shock	5.3.3.6	23 Life	5.3.8.5
11 Static load	5.3.3.2	24 Mission simulation	5.3.8.3
12 Spin	5.3.3.3	25 End-to-end communication	5.3.8.4
13 Acoustic	5.3.3.4	26 Audible noise	5.3.9.2

Note: Numbers in the 'Reference sub-clause' columns indicate the respective explicative subsection in the standard ECSS-E-10-03A (2002).

The first objective is carried out by means of a thermal vacuum test and a thermal cycling test at an ambient pressure. A thermal vacuum test is similar to a thermal cycling test, but carried out in a vacuum. The other two objectives are allocated to the thermal balance test, which generally consists of two extreme steady (hot and cold) cases. These tests are performed at different stages and at different stress intensities and

durations throughout the development process (development, qualification, and acceptance), and on different levels (equipment, subsystem, spacecraft). According to ECSS-E-ST-31C (2008), conformance to the specified performance has to be demonstrated by carrying out thermal balance, thermal vacuum and/or cycling tests, at all temperature ranges.

For instance, the thermal balance test for vehicle qualification should provide the data necessary to verify the thermal analytical models and demonstrate the ability of the vehicle's thermal control subsystem to maintain the specified operational temperature. The thermal balance test should also verify the adequacy of unit thermal design criteria.

The test levels in thermal balance testing are defined to simulate the external environment (solar radiation and deep space), or to approximate the anticipated energy flux levels at the boundaries of the spacecraft (NASA SP-8105, 1973). These levels are the same as those used in the mathematical model in order to permit a valid comparison with the test.

For thermal vacuum and thermal cycling testing, temperatures are set equal to, or higher than, expected flight temperatures, by some margin. For both types of testing, the component electrical dissipation rates, and duty cycles, are set to values appropriate for the mission mode being tested. In some cases, it may be technically and economically advantageous to perform a combined thermal balance and thermal vacuum test. Test conditions are agreed with the system authority and included in the system test plan. Typical temperature ranges and margins for acceptance and qualification tests are defined in Figure 18.2, and Tables 20.2 and 20.3.

As described in Section 19.2, these margins are a consequence of the uncertainties involved in the environmental parameters (e.g. solar intensity); spacecraft physical parameters (e.g. measurement tolerances, fabrication tolerances in thermo-optical properties); and mathematical

Table 20.2 Qualification test levels and durations, for both equipment and space elements, as defined in table 1, ECSS-E-10-03A (2002)

Test	Levels	Duration
Thermal cycling	10 °C extension of maximum and minimum predicted temperatures	8 cycles
Thermal vacuum	10 °C extension of maximum and minimum predicted temperatures	8 cycles if combined with thermal cycling, 1 cycle if thermal cycling is already performed

Table 20.3 Acceptance test levels and durations, for equipment and space element, as defined in table 2, ECSS-E-10-03A (2002)

Test	Levels		Duration
	Equipment	Space element	Equipment/ space element
Thermal cycling	5 °C extension of maximum and minimum predicted temperatures	Flight temperature	4 cycles
Thermal vacuum	5 °C extension of maximum and minimum predicted temperatures	Flight temperature	4 cycles if combined with thermal cycling, 1 cycle if thermal cycling is already performed

modelling. A comprehensive discussion on temperature limits and uncertainty quantification can be found in Annex B of ECSS-E-10-03A (2002). Another source of uncertainty is the possible errors related to the performance of tests in the test chamber. Chamber errors may result from conduction

transfer from fixtures used in mounting and supporting test articles in the chamber; infrared energy inputs to test articles from the chamber, and reflection from chamber walls and fixtures; monitoring errors (calibration and measurement); thermal losses through wiring; and simulation errors.

In the case of the thermal cycle tests for vehicle qualification, the thermal cycle test should demonstrate the ability of the vehicle to withstand the stressing associated with flight vehicle thermal cycle acceptance testing, with a qualification margin on the temperature range and maximum number of cycles. The thermal cycle test, in combination with a reduced-cycle thermal vacuum test, can be selected as an alternate to the thermal vacuum test (MIL-HDBK-340A, 1999).

In the case of thermal vacuum tests for vehicle qualification, the thermal vacuum test should demonstrate the ability of the vehicle to meet qualification requirements under vacuum conditions and temperature extremes which simulate those predicted for flight plus a design margin, and to withstand the thermal stressing environment of the vehicle thermal vacuum acceptance test plus a qualification margin on temperature range and number of cycles.

The main purpose of qualification thermal vacuum testing is to reveal adverse effects on spacecraft performance that result from weaknesses in the thermal design. The aim of thermal vacuum acceptance testing is to reveal any adverse effects that may result from defects in the materials or workmanship related to thermal design. Both types of testing involve the collection and analysis of spacecraft performance data.

20.3 Model philosophy

As explained in Section 20.1, thermal testing is performed at various stages of the spacecraft's development, according to

the needs of the particular programme. The verification by test is implemented on the selected models chosen for the project, following the model philosophy adopted. The model philosophy is defined by means of an iterative process which combines programmatic constraints, verification strategies, and the integration and test programme, taking into account the development status of the candidate design solution.

According to ECSS-E-10-03A (2002), a test baseline has to be defined, based on the project model philosophy: a prototype approach or protoflight approach. In the prototype approach, the qualification testing can be conducted on one or more qualification models (QMs), and the flight model (FM) has to be subjected to complete acceptance testing. In the protoflight approach, all the qualification tests have to be performed on the same model to be flown, with qualification levels but of a reduced duration. The protoflight model (PFM) should be subjected to a test programme defined on a case-by-case basis, but it has to satisfy the qualification and acceptance objectives.

The qualification, acceptance, or protoflight test activities are shared among the different hardware models. This sharing depends on the model philosophy, project characteristics and model representativeness. The hardware models related to the verification of the thermal control system are described in the following paragraphs (Annex B of ECSS-E-10-02A, 1998).

The hardware thermal model is fully representative of the thermal properties of the end item. It is used for the verification of the thermal design and for the correlation of mathematical models. Generally, the system thermal model consists of a representative structure with thermal dummies of the equipment. It can also include representative thermal parts of other subsystems. This structural-thermal model (STM) can also be a structural model that has been

refurbished, after structural qualification, for thermal verification purposes. However, no potentially destructive structural tests should be performed on the STM in this case.

The qualification models are used for full-level functional and environmental qualification tests. The qualification model fully reflects the end item design in all aspects, but it is not used for flight, because its useful life has been affected by the stressing qualification tests. They are required only for equipment/subsystems of a new design, or elements requiring an incremental (or delta) qualification for adaptation to the project.

The flight model is the flight end item, which has only undergone acceptance tests (ECSS-M-ST-40C, 2009). The protoflight model is the flight end item, but it has been exposed to a partial or complete protoflight qualification test campaign before flight.

20.4 Development tests

ECSS-E-ST-31C (2008) addresses thermal testing at component and system (space vehicle) levels. Besides these two levels, special tests may be necessary at different stages of assembly. In addition, dedicated tests may be required to give confidence in a new design, or to aid in the analysis. One such test is a development test. These tests can provide early data to assist in the design or manufacturing process. Typically, they are used when an old technique is evaluated in a new application, or a new design concept is experimentally assessed. For instance, it is of interest to obtain data to aid the layup and handling of an insulation blanket, or to assess the structural integrity of such blankets under the pressure difference due to venting. Also, heat pipes undergo extensive development tests. Both elements undergo testing at several

levels of assembly. Tests can also be carried out to determine contact conductance along critical heat-flow paths, or the conductance of thermal insulators. Engineering model electronic units are sometimes instrumented and tested in a vacuum environment to verify the thermal analysis. Piece-part temperature predictions may also have to be verified.

20.5 Thermal balance tests

Thermal balance testing is mainly conducted for design verification, while thermal balance testing for design-development is employed to obtain design information on those components for which stringent temperature constraints are imposed, the thermal design is difficult to analyse, or it is necessary to establish the feasibility of the design approach.

Thermal balance testing can be performed at two levels, as a subsystem or at the fully integrated spacecraft level. In the case of subsystem testing, a better understanding of a particular component is obtained than in the testing of the integrated spacecraft, and it also allows for higher quality testing at lower costs, although it cannot reveal interactions among subsystems.

Thermal balance testing at the spacecraft level can be performed on the fully integrated flight spacecraft, a fully integrated prototype, or a thermal-structural model.

More options in test operations and better instrumentation are allowed when a fully integrated prototype or a thermal-structural model is used than if testing is performed on the flight model. Furthermore, design modifications, if needed, can be more easily accomplished at this relatively early stage. Also, a wider temperature range can be applied to the

prototype and thermal structural model, which results in more detailed baseline thermal information.

If a prototype spacecraft is used, the possibility arises that the actual flight spacecraft design will be different from the prototype. In the case of a thermal-structural model, the major disadvantages are differences between the thermal model and the actual flight spacecraft (NASA SP-8105, 1973).

On the one hand, the use of the fully integrated flight spacecraft for thermal balance testing has the following advantages: (a) flight model testing may be the only opportunity to test the complete spacecraft; and (b) major changes are not made before launch except when necessitated by test results. But, on the other hand, it has several disadvantages: (a) the component cannot be tested over a wide enough temperature range to obtain baseline design information because of the temperature range established by mission requirements; (b) it is too late in the development programme for any changes to be made without affecting the schedule and cost; (c) the constraints on test operations and instrumentation to minimize the risk of spacecraft damage may hinder testing; and (d) the testing facility operation may pose the risk that the allowable temperature limits of the spacecraft would be inadvertently exceeded.

As established in ECSS-E-ST-31C (2008), for Thermal Control Subsystem (TCS) items controlled by radiative and conductive heat exchange, a thermal balance test has to be performed in order to: (a) provide data for the verification of the thermal mathematical model as part of the thermal control subsystem qualification; (b) demonstrate the suitability of the thermal control subsystem design; (c) verify the performance of the thermal control subsystem hardware; and (d) provide data about the sensitivity of the thermal control subsystem design with respect to parameter changes, for example heat dissipation. As mentioned above, thermal

balance testing is generally performed on items at high integration levels, such as spacecraft, service module, payload module or instrument. According to this standard, two different steady-state test cases (cold and hot worst cases, see Chapter 18) are to be performed, and also a transient case for items sensitive to dynamic behaviour.

As boundary conditions, the solar environment to be applied for solar simulation and the cases where solar simulation is used have to be carefully considered as representative of the real environment. Generally, this solar simulation is performed when the thermal behaviour is governed by the solar environment, and the analytical verification poses unknown uncertainties, for example items with complex geometry, shape, apertures and with specular reflective coatings. In this test, critical hardware items and interfaces have to be flight representative. Parasitic radiative and conductive heat loads between test items and test surroundings have to be determined, and the influence on the test results analytically verified.

This test is considered successfully accomplished if the following results are obtained: (a) test conditions defined in the test specification and test procedure are met; (b) performance parameters as predicted by analysis for the test are verified (examples of performance parameters are temperatures, temperature levels, gradients, differences, and variations); and (c) resources specified in the thermal control subsystem specification have not been exceeded (for example, heater power, battery energy in an eclipse case).

With the data obtained and the results of the numerical model (see Chapter 19), test correlations are to be performed for the two steady-state cases performed, and the transient case, if any.

A correlation can be declared successful when the following requirements are fulfilled after test correlation: (a) deviations

between measured and predicted temperatures are within specification (this can include temperature gradients, temperature differences and temperature variations); (b) the temperature mean deviation and the temperature standard deviation are as specified; and (c) deviations between measured and predicted heating/cooling power are within specifications.

Typical limit values for the temperature deviation for internal units are 5 K, and for external units 10 K; temperature mean deviation within ±2 K; and temperature standard deviation 3 K.

The thermal balance test should be harmonized with the system thermal vacuum test which, at spacecraft level, generally takes place in sequential order in the same vacuum chamber.

20.6 Thermal vacuum tests

Thermal vacuum testing is usually performed at the component, subsystem, and integrated spacecraft levels. On the component level, the testing is generally performed at the supplier's facility to ensure that the unit meets reliability and quality assurance requirements. On the subsystem level, design qualification tests and flight acceptance tests are carried out (NASA SP-8105, 1973).

The purpose of the design qualification test performed on a prototype component is to prove the component design by checking its performance capability in a vacuum, under temperature stresses more severe than those predicted for the mission. The aim of the flight acceptance test performed on a flight component is to locate latent material and workmanship defects in a component of proven design, by checking its performance capability in a vacuum at the

Figure 20.2 Typical test set-up for equipment thermal vacuum test

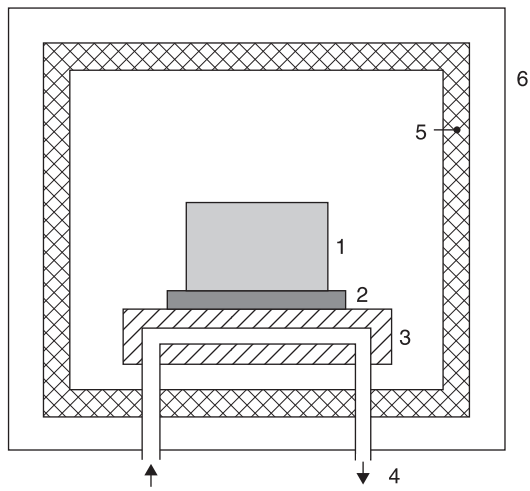

Key: 1 – equipment, 2 – flight type representative thermal interface; 3 – temperature controlled mounting frame or support plate; 4 – temperature controlled fluid loop; 5 – temperature controlled shroud; 6 – thermal vacuum chamber.

Source: After ECSS-E-10-03A (2002).

temperature extremes expected in flight. A typical test set-up for the equipment thermal vacuum test is shown in Figure 20.2. The aim of acceptance testing on the flight model of the spacecraft is to check the interaction between subsystems as well as to ascertain the proper operation of all systems.

To demonstrate that the unit can survive the launch and flight, test durations for acceptance thermal vacuum testing have to be long enough. Test durations for qualification and acceptance thermal tests, according to ECSS-E-10-03A (2002), are given in Tables 20.2 and 20.3. For information purposes, a typical qualification test cycle curve is presented in Figure 20.3.

20.7 Test facilities

A schematic of a thermal vacuum test set-up is shown in Figure 20.2. In thermal vacuum testing, temperature conditioning is usually accomplished by varying the test chamber wall temperature or by monitoring the test article on a temperature controlled base-plate. For thermal balance testing, there are several methods simulating heat flux. Their advantages and disadvantages are presented in Table 20.4.

For thermal cycling tests at an ambient pressure, a wide variety of thermal chambers are available. Nitrogen, or humidity controlled air, is used to prevent water vapour condensation. During heating or cooling, a rapid air or gas flow is required, but a rapid rate of temperature change at the base-plate or case of the component of interest is often difficult to achieve. This is often the major technical challenge faced in thermal cycling testing.

Figure 20.3 **Sequence of a vacuum temperature cycling test at qualification levels**

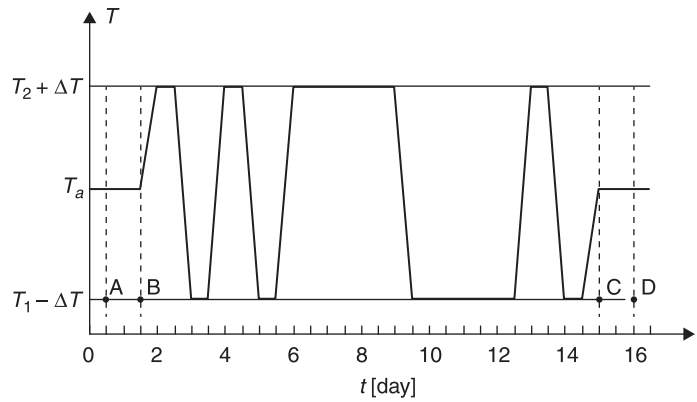

Key: T_a, ambient temperature; T_1, minimum mission temperature; T_2, maximum mission temperature; $\Delta T = 10\,°C$, temperature margin; A–B and C–D, functional tests; t, time.

Source: After NASA SP-8105 (1973) and ECSS-E-10-03A (2002).

Table 20.4 **Comparison of different methods for simulating heat flux in thermal balance testing**

Method	Advantages	Disadvantages
Test chamber wall (temperature adjustment)	Cheapest simulation method	Incident heat flux is uniform over test specimen
Solar simulation	Closest to actual environment	Expensive
Quartz lamps	High heat flux rates attainable	Lack of spatial uniformity of heat flux and spectral simulation
Heater skins	Spatial and temperature variations of absorbed heat flux can be simulated	Complexity of test support equipment prevents verification of energy absorbed by test specimen

Source: From NASA SP-8105 (1973).

Thermal vacuum tests are divided for convenience into two categories depending on the dominant mode of cooling: (1) conduction to a heat sink is the dominant mode, and (2) heat transmission to the surroundings is by both conduction and radiation. The former is the more commonly used. Conduction cooling is usually accomplished by bolting the component to a monolithic, nearly isothermal, heat sink. This is not truly representative of actual component installation, which may, for example, have Delron inserts in an aluminium honeycomb with face sheets. However, it is usually acceptable for component testing, provided that the differences between test mounting and flight mounting are accounted for by analysis, and verified by testing at the system or subsystem level. Occasionally (e.g., where power density is very high), the component is mounted on to a flight-like installation. In both cases, the component is

covered by an insulation blanket to assure that radiation is negligible.

Many components are primarily cooled by radiation, or both radiation and conduction. Such components include control-moment gyroscopes, inertial reference units, and accelerometers. Here, the control of heat-loss paths should be such that radiation and conduction occur in the same proportion as calculated for the flight environment. This is necessary so that module and piece-part temperatures and component-temperature gradients duplicate those that occur in actual usage.

One of the crucial aspects of testing is the development of the appropriate ground support equipment (GSE), mainly when special spacecraft have to be tested, such as those involving cryogenic instruments (e.g. Planck mission). A summary description of the GSE required for thermal testing of the Planck spacecraft can be found in Delrez et al. (2004).

20.7.1 Coordination of test facilities

In order to bring together the efforts of the main European space test centres, ESA has established the Coordinated European Test Facilities (CETeF), a close collaboration of ESA Test Centre (ESTEC, Noordwijk, The Netherlands) with INTESPACE in Toulouse, France, IABG in Munich, Germany and CSL in Liege, Belgium. Contacts are established between CETeF members and the ALCATEL Test Centre in Cannes, France. The coordination of European test facilities has fostered the standardization of procedures and customer interfaces, and has contributed to the exchange of data and improvements concerning quality, reliability, and safety.

A summary of the European environmental test facilities can be found in Stavrinidis (2004). More detailed descriptions

of some of these facilities can be found in Marcé and Pasquet (2001), Deutsch et al. (2001) and Piret et al. (2004).

Another initiative is the EETFI (European Environmental Test Facility Inventory). This is a web-based European inventory of environmental test facilities. Its aim is to provide the European industry with a tool that allows suitable test facilities to be located and identified (Popovitch, 2004). A list of facilities of the USA and Europe can be found in Appendix B in Gilmore (1994).

20.7.2 Test standardization

Standardization is a key aspect of the production activities regarding the optimization of product development and cost. American industries and Government organizations have developed standards such as MIL-, DOD-, or NASA- series standards.

Space activities in Europe were managed by the PSS (Procedures, Specifications and Standards), a set of ESA standards which covered the relevant aspects of these activities, gathering together the common practices and up-to-date approaches. However, an initiative has recently been established by ESA and the national space organizations, named the European Cooperation for Space Standardization (ECSS), which aims to develop a single set of coherent standards for use in all European activities (Giordano, 2004). Also, the International Standard Organization (ISO) has established a Technical Committee (TC20, Aircraft and Space Vehicles) which has appointed a subcommittee (SC14, Space Systems and Operations) with the aim of developing an international standard in this field. The working group WG2 (Interfaces, Integration and Test) of TC20/SC14 has developed the standard ISO/DIS 15864 (2003) 'Space systems – Unmanned spacecraft design, performance and

quality assessment – General test methods for system, subsystem and unit levels'. This standard is similar to the ECSS testing standard.

As regards testing, the relevant ESA standards employed in the past were also included in the Procedures, Specifications and Standards (PSS) series. However, following the implementation of the ECSS initiative, the ECSS standards relevant to thermal testing are:

- ECSS-M-ST-10C (2009), devoted to project planning and implementation.
- ECSS-E-10-03A (2002), devoted to testing.
- ECSS-E-ST-31C (2008), devoted to thermal control general requirements.
- ECSS-Q-ST-70-04 (2008), devoted to thermal testing for the evaluation of space materials, processes, mechanical parts and assemblies.
- ECSS-STQ-70-09 (2008), devoted to measurements of thermo-optical properties of thermal control materials.

In the USA, some of the standards most relevant to testing are:

- MIL-STD-1540D (1999), test requirements for space vehicles.
- MIL-HDBK-340A (1999), test requirements for launch, upper-stage, and space vehicles.
- DOD-HDBK-343 (1986), design, construction, and testing requirements for one-of-a-kind space equipment.

Although the whole development process may seem quite strictly regulated, the standards also have provisions for tailoring the process to the project circumstances. Thus, when a space mission is highly similar to a previous one,

and, therefore, there is a high level of recurrence in the design, or re-use of existing hardware, it is possible to implement new project management practices (so-called 'Flexible Missions' in Europe) in order to reduce the time from original concept to launch, and the cost. These new project management practices involve innovative concepts in the model philosophy and in the environmental test campaigns, including the thermal tests, even if the thermal design is quite different. This was the case for the Venus Express with regard to the Mars Express mission, where the thermal testing had to be tailored to account for these differences. The most relevant were the greater albedo and the solar energy flux (Rustichelli et al., 2004).

20.8 References

Delrez, C., Collin, B., Chisogne, J., Domken, I., Tychon, I. et al. (2004) 'Planck S/C thermal testing mechanical and thermal GSE design and manufacturing', 5th International Symposium on Environmental Testing for Space Programmes, Noordwijk, The Netherlands, 15–17 June 2004, ESA SP-558, 541–8.

Deutsch, G., Kiener, F. and Resch, F. (2001) 'Automation of space simulation/thermal vacuum test facilities', 4th International Symposium on Environmental Testing for Space Programmes, Liège, Belgium, 12–14 June 2001, ESA SP-467, 501–6.

DOD-HDBK-343 (1986) *Military Handbook: Design, construction, and testing requirements for one-of-a-kind space equipment*, DOD, USA, 1986.

ECSS-E-10-02A (1998) *Space engineering. Verification*, ESA Publications Division, ESTEC, Noordwijk, The Netherlands, November 1998.

ECSS-E-10-03A (2002) *Space engineering. Testing*, ESA Publications Division, ESTEC, Noordwijk, The Netherlands, February 2002.

ECSS-E-ST-10C (2009) *Space engineering. System engineering general requirements*, ESA Requirements and Standards Division, ESTEC, Noordwijk, The Netherlands, March 2009.

ECSS-E-ST-31C (2008) *Space engineering. Thermal control general requirements*, ESA Requirements and Standards Division, ESTEC, Noordwijk, The Netherlands, November 2008.

ECSS-M-ST-10C (2009) *Space project management. Project planning and implementation*, ESA Requirements and Standards Division, ESTEC, Noordwijk, The Netherlands, July 2009.

ECSS-M-ST-40C (2009) *Management. Configuration and information management*, ESA Requirements and Standards Division, ESTEC, Noordwijk, The Netherlands, July 2009.

ECSS-Q-ST-70-04 (2008) *Space product assurance. Thermal testing for the evaluation of space materials, processes, mechanical parts and assemblies*, ESA Requirements and Standards Division, ESTEC, Noordwijk, The Netherlands, November 2008.

ECSS-Q-ST-70-09 (2008) *Space product assurance. Measurements of thermo-optical properties of thermal control materials*, ESA Requirements and Standards Division ESTEC, Noordwijk, The Netherlands, July 2008.

Gilmore, D.G., Ed. (1994) *Satellite Thermal Control Handbook*, The Aerospace Corporation Press, El Segundo, California, USA.

Giordano, P. (2004) 'New testing standard for European programs', 5th International Symposium on Environmental

Testing for Space Programmes, Noordwijk, The Netherlands, 15–17 June 2004, ESA SP-558, 385–91.

ISO/DIS 15864 (2003) Space systems – Unmanned spacecraft design, performance and quality assessment – General test methods for system, subsystem and unit levels, ISO/TC 20/SC 14, International Organization for Standardization.

Marcé, J.L. and Pasquet, J.C. (2001) 'Developments in the INTESPACE test centre for the Ariane 5 Launcher', 4th International Symposium on Environmental Testing for Space Programmes, Liège, Belgium, 12–14 June 2001, ESA SP-467, 279–91.

MIL-HDBK-340A (1999) *Military Handbook: Test requirements for launch, upper-stage, and space vehicles*, DOD, USA.

MIL-STD-1540D (1999) *Department of Defense Standard Practice: Product verification requirements for launch, upper stage, and space vehicles*, DOD, USA.

NASA SP-8105 (1973) Spacecraft thermal control, NASA Space vehicle design criteria – Environment.

Piret, G., Checa, E., Dolce, S., Messing, R., and Westera, R. (2004) 'Improvement of the ESA-ESTEC Large Space Simulator: low temperature cooling loops installation and specific test equipment development for the MetOp thermal vacuum tests', 5th International Symposium on Environmental Testing for Space Programmes, Noordwijk, The Netherlands, 15–17 June 2004, ESA SP-558, 531–40.

Popovitch, A. (2004) 'European Environmental Test Facility Inventory', 5th International Symposium on Environmental Testing for Space Programmes, Noordwijk, The Netherlands, 15–17 June 2004, ESA SP-558, 175–6.

Rustichelli, S., McCoy, D., Glorino, T., Pereira, J. and Pendaries, M. (2004) Mars and Venus – the Express way: evolution and heritage in flexi type missions concerning model philosophy and environmental test design', 5th

International Symposium on Environmental Testing for Space Programmes, Noordwijk, The Netherlands, 15–17 June 2004, ESA SP-558, 31–9.

Stavrinidis, C. (2004) 'Test and verification efforts in ESA', 5th International Symposium on Environmental Testing for Space Programmes, Noordwijk, The Netherlands, 15–17 June 2004, ESA SP-558, 269–74.

21

Conclusion

The design of the thermal control subsystem of a spacecraft is an essential element in the design process of space vehicles, aiming to guarantee that all parts of the vehicle are within the appropriate temperature range during all mission phases. The increase over the years in the degree of complexity of the missions has led the thermal control subsystem to be considered one of the main subsystems in the systems engineering design approach.

The thermal control design process consists mainly of two activities. The first is the selection of the specific thermal hardware required to fulfil the thermal requirements of the different parts of the satellite. The second is the prediction of their temperatures over time. It is obvious that both activities depend on each other: the temperature distribution will depend on the thermal hardware used, and the thermal hardware will have to be selected based on the predicted temperatures. The design process is then an iterative one which includes the knowledge of available technology in thermal control (and the knowledge of heat transfer, mainly heat conduction and thermal radiation), as well as the space environment, which the external thermal loads on the satellite strongly depend on.

Following this design philosophy, the book provides the reader with the basics needed to comprehend the thermal control system of a spacecraft and has been structured to cover the subjects mentioned above.

Therefore, in the first part (Chapters 1–3), the basic theory needed for spacecraft thermal control has been reviewed. This part starts with a description of the space mission, which allows the thermal control system to be put into context within a space project, and continues with a description of the space environment. The extreme environmental conditions that spacecraft encounter in orbit are one of the main conditioning factors in their design. Data for other planetary atmospheres are also included, and simple analytical expressions to calculate thermal loads in orbit due to solar, planetary albedo and planetary infrared radiation, are provided. This part finishes with a brief introduction to Keplerian orbits, pointing out the lighting conditions for a spacecraft in relation to the type of orbit, one of the aspects to be analysed when determining the thermal loads.

The second part of the book (Chapters 4–5) presents the basics of heat conduction and thermal radiation necessary to establish the heat balance equations for the thermal modelling of spacecraft. The fundamental equations of heat conduction are presented and the main physical property in this field, the thermal conductivity, is defined. Concerning thermal radiation, prior to deriving the equations for the radiation exchange between grey surfaces, a brief explanation about its nature is given. The thermo-optical properties of a surface such as emissivity, absorptance, transmittance and reflectance, relevant in the thermal behaviour of surfaces in space, are defined.

The third part of the book (Chapters 6–17) is devoted to the technology available for thermal control with up-to-date information collected from technical handbooks, books, and research papers. This part of the book starts (Chapter 6) with a description of the passive techniques used in practically all space projects, from the simplest to the most complex

and continues with the more sophisticated techniques used, where additional resources are needed. Therefore, it begins with a chapter dedicated to thermal control surfaces, describing the effect of thermal control coatings on the spacecraft thermal behaviour, as well as the different types of coatings available for space use. Chapter 7 deals with the two main insulation systems used for spacecraft thermal control: multilayer insulation (MLI), also called thermal blankets, and foams. Typical ways of modelling the thermal behaviour of multilayer insulation, as well as the equations used to do it, are presented. The passive techniques continue with a description of the radiators used to reject to outer space the absorbed thermal loads and the power dissipated by electronics devices, followed by the presentation of louver systems (the mechanical devices used to modify the effective emissivity of a radiator by blocking its view of outer space). The passive system description finishes describing the phenomenon of heat transfer across mechanical interfaces, and how it can be used to modify the thermal behaviour of a system.

When the thermal requirements cannot be met with these purely passive methods, more complex devices are used. The book continues presenting the simplest and most widely used devices over the last decades: heat pipes, giving attention to the basic phenomena involved (capillarity, surface tension, contact angle, wettability), the heat pipe components (pipes materials, wicks, and working fluids) and their different configurations. Chapter 12 includes a description of phase change capacitors and their applicability in spacecraft control systems. Then follows a chapter related to heaters, heat sources used when the temperature requirements cannot be achieved by passive means. After this, the book deals with pumped fluid loops (Chapter 14) and their application for high heat loads, and continues with an explanation of

thermoelectric cooling technology (Chapter 15). For applications involving lower temperatures (below 100 K), Chapter 16 is devoted to cryogenic systems, and the ways to achieve low temperatures in the systems. The technology part finishes with Chapter 17 dedicated to thermal protection systems, necessary for launchers or spacecraft entering a planet atmosphere.

After reviewing the technology available for thermal control, the fourth and last part of the book (Chapters 18–20) is dedicated to the design and verification processes. Chapter 18 describes the common iterative procedures followed in the design of a spacecraft thermal control system over the different mission phases. The usual modelling procedure, based on a geometrical mathematical model and a thermal mathematical model is explained in Chapter 19, as well as the software tools used for this purpose. Chapter 20 is devoted to thermal testing. As a crucial part of the verification phase, thermal vacuum tests and thermal cycling tests have to be performed both to validate the design and verify that the system performs correctly at the expected extreme temperatures.

Summing up, and as already stated in the 'Foreword', this book deals with the different aspects of science and technology needed to understand how the thermal control subsystem of a spacecraft works. The book is a basic guide for aerospace engineering graduate students, for engineers starting their professional careers in the spacecraft thermal control design field, and for engineers or specialists of other space subsystems that want to learn more about spacecraft thermal control.

Index